FINAL REPORT

C^3EO

Competitive CubeSat Constellation for Earth Observation

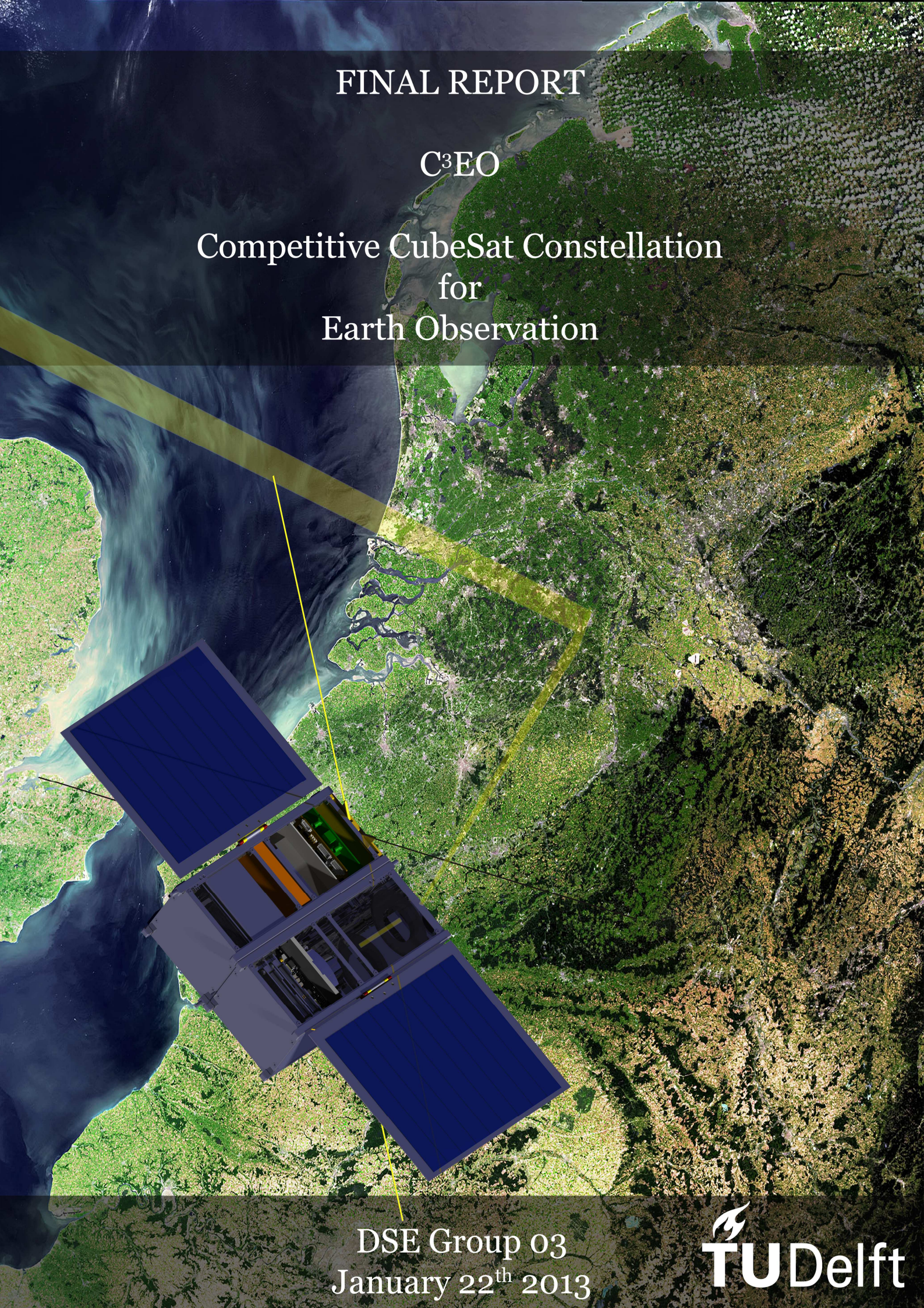

DSE Group 03
January 22th 2013

TU Delft

DSE Group 3

Faculty of Aerospace Engineering

Delft University of Technology

Competitive CubeSat Constellation for Earth Observation

Final report

Authors:

F.L. Bräuer	1544063
F. Dyczynski	1550969
R. van Gijlswijk	1378902
R.H.J. Hartmans	1507087
E. Roebroeks	4024915
C.A.A. Sa	1534556
N. Treffers	1283510
F.G.S. Vicente	4049004
J. Wink	4012305

January 22, 2013

Cover background courtesy of ESA.

Contents

Preface

This report contains the results of the Design Synthesis Exercise (DSE), a third year project belonging to the Aerospace Engineering BSc. at Delft University of Technology. The exercise, handed to us by our tutor Dr.Ir. J.M. Kuiper, gave us the challenge to investigate the possible applications of the ANT-2 and ARCTIC instruments. The project concluded in a constellation for disaster and environmental monitoring. This report describes the design process in detail and presents our ideas and findings during the project. We would like to express our gratitude to Dr. Ir. J.M. Kuiper, Dr. Ir. W. van der Wal and Dr.Ir. A.H. van Zuijlen for their support during the course of this project. Furthermore, we would also like to thank Ir. J. Bouwmeester for providing us with the relevant insight and information on nanosatellites and Dennis Dolkens who advised us on optical design.

Summary

In recent years, growing interest in nanosatellite technology by the space industry has brought about new and exciting possibilities with respect to Earth observation. The possibility of forming nanosatellite constellations promotes cost effective solutions with high temporal resolutions. Secondly, previous DSE assignments have paved the way in Earth observation by designing imaging devices which fit the CubeSat standard. The ARCTIC device excels at high sensitivity thermal infrared imagery, while the ANT-2 TMA and RCC designs, improved versions of the original ANT camera, provide imagery in the visual and near infrared spectrum. In this report the process and results of combining these previously designed cornerstones are presented. The outcome is a constellation named Competitive CubeSat Constellation for Earth Observation (C^3EO).

A market survey on the relevance and requirements of a CubeSat constellation concluded that both high spatial and temporal resolution are important. To provide this, a three segment constellation comprised of 24 ANT-2 RCC platforms at an altitude of 288 km and 27 ANT-2 TMA platforms at 500 km in sun-synchronous orbits and 37 ARCTIC platforms at 443 km in a polar orbit. Together, these segments deliver full Earth coverage in thermal infrared and near full coverage in the visual and near infrared spectrum. Additionally, a temporal resolution of one day with the ANT-2 TMA and ARCTIC platforms is provided alongside a weekly resolution with the ANT-2 RCC platform.

Such a constellation has a wide range of uses, from disaster monitoring to scientific research and environment protection. Both the TMA and RCC variants are powerful tools in oceanography, with the ability to monitor corals and phytoplankton, as well as forestry and agriculture. The ARCTIC camera in combination with its polar orbit allows it to map surface temperatures across the Earth as well as ice extent.

The platforms' technical parameters are very similar to each other, with exception to power systems and propellant mass. The constant lighting of sun-synchronous orbits permit the use of lower efficiency thin film cells in the ANT-2 platforms, while the frequent eclipses in a polar orbit constrain the use of solar cells to high efficiency triple junction cells in the ARCTIC satellites. All satellites possess electrospray thrusters for orbital manoeuvres such as phasing and drag compensation as well as an active attitude control that meets the requirements of the cameras. Furthermore, all subsystems are employed in a 2-by-2U CubeSat structure such that the cameras and antennas can point nadir simultaneously. Finally, data downlink is a main driver in the constellation design, with high data volumes being generated by the RCC platform. All imagery is downlinked by S-band transmitters and a total of eight ground stations are distributed around the Earth. Six of these ground stations are unmanned and especially built for the constellation whereas the other two are commercial ground stations located near the poles.

The economic potential of the C^3EO constellation is exceptional. By selling 2% of all the imagery at a price of 0.1 EUR/km^2, almost an order of magnitude lower than competitors, an estimated return on investment of 20% in the first year of operations and a break even point of five months is expected. The total constellation cost is estimated to be 90M EUR for a two year mission duration and the unit cost of each satellite is 0.2M EUR.

List of Abbreviations and Acronyms

Abbreviations	Description
ADCS	Attitude Determination and Control System
ACS	Attitude control subsystem, part of the ADCS
AM	Amplitude Modulation
DSE	Design synthesis exercise
ANT	Advanced Nano Telescope
ARCTIC	Advanced Remote-sensing CubeSat Thermal Infrared Camera
ASAP	Ariane Structure for Auxiliary Payloads
BER	Bit Error Rate
BEST	Basic Envisat Sar Toolbox
BOL	Beginning Of Life
BRIC	Brazil, Russia, India and China
C^3EO	Competetive Cubesat Constellation for Earth Observation
C&DH	Command and Data Handling
CAGR	Compound Annual Growth Rate
CubeSat	CubeSat unit (1U) is 10 cm x 10 cm x 10 cm
CFD	Communication Flow Diagram
COGS	Cost of goods sold
COTS	Commercial Of The Shelf (components)
CSP	CubeSat Space Protocol
DELFI	TU Delft student satellite
DET	Direct Energy Transfer
DMC	Disaster Monitoring Constellation
DOD	Depth of Discharge
DSE	Design Synthesis Exercise
EIRP	Equivalent Isotropic Radiated Power
EPS	Electrical power system
EO	Earth Observation
ES	Electrospray
ET	Extra Terrestrial
FEEP	Field-Emission Electric Propulsion
FER	Forward Error Control
FM	Frequency Modulation
G/S	Ground Station
GOCE	Gravity field and steady-state Ocean Circulation Explorer
GP	Gross Product
GPS	Global Positioning System
HPB	Half Power Beam-width
HV	High Voltage
ICBM	Inter-Continental Ballistic Missile
IEEE	Institute of Electrical and Electronics Engineers
IR	Infra-red
ISS	International Space station
KSat	Kongsberg Satellite Service

Abbreviations	Description
LEO	Low Earth Orbit
MIT	Massachusetts Institute of Technology
MODIS	MODerate resolution Imaging Spectroradiometer (NASA)
MTBF	Mean Time Between Failure
Nanosatellite	Subset of satellites with a weight between 1 kg and 10 kg
NASA	National Aeronautics and Space Administration
NEST	Next Esa Sar Toolbox
NIR	Near Infrared
OECD	Organisation for Economic Co-operation and Development
OQPSK	Offset Quadrature Phase Shift Keying
PD	Proportional and derivative (refers to control algorithm)
PID	Proportional, integral and derivative (refers to control algorithm)
PPT	Peak Powerpoint Tracking
PPU	Power Processing Unit
PSLV	Polar Satellite Launch Vehicle
PTRX	Primary Transceiver
QPSK	Quadrature Phase Shift Keying
RAMS	Reliability, Availability Maintainability and Safety
RCC	Richy-Chretien Cassegrain
R&D	Research and Development
RGB	Red, Green and Blue band spectrum
ROI	Return on Investment
S/C	Spacecraft
SAR	Synthetic Aperture Radar
SIFT	Scale Invariant Feature Transform
SNAP-1	Surray Nanosatellite Applications Program
SNR	Signal-to-Noise Ratio
STX	S-Band Transmitter
SURF	Speeded Up Robust Features
TIFF	Tagged Image File Format
TNO	Nederlandse Organisatie voor toegepast-natuurwetenschappelijk onderzoek
TT&C	Telemetry, Tracking and Control
TMA	Three Mirror Anastigmatic
UHF	Ultra High Frequency
VHF	Very High Frequency
VIS	Visual band
VLEO	Very Low Earth Orbit
WBS	Work breakdown structure
WFD	Work flow diagram

List of Symbols

Symbol	Description	Unit
a	Semimajor Axis	m
A_{all}	Total surface area imaged in 2 years all cameras	km^2
A_{camera}	Total surface area imaged for each camera layer	km^2
A_{fmh}	Area affected by free molecular heating	m^2
A_{image}	Area imaged per one camera	km^2
A_R	Area of satellite radiating into free space	m^2
A_r	Ram (frontal) area of the satellite	m^2
A_s	Sunlit surface area	m^2
A_{sa}	Total area of solar arrays	m^2
A_{24hrs}	1 day image capacity	km^2
B	Magnetic field strength	$Tesla$
c	Speed of light in vacuum	m/s
c_m	Center of mass	m
c_{pa}	Aerodynamic center	m
c_{ps}	Center of solar radiation pressure	m
C_D	Drag coefficient	$-$
C_{labour}	Labour cost	EUR
C_{nonrec}	Non-recurring cost	EUR
C_{oper}	Operational cost	EUR
C_r	Required capacity for battery	$-$
dc	Duty cycle	$-$
D	Residual dipole moment	Am^2
DOD	Depth of discharge	
$D_{torquer}$	Magnetic moment of magnetorquer	Nm
$f_{imaging}$	Imaging frequency	s^{-1}
F	Viewfactor	$-$
F_d	Drag force	N
GP	Gross profit	EUR
GS	ground station cost	EUR
$H_{max_{wheel}}$	maximum stored angular momentum of the reaction wheel	Ns
H_{orbit}	Orbit Height	m
H_{org}	Original orbit height	m
i	Inclination	deg
$I_{bitdepth}$	Image bit depth	bit
I_d	Inherent degradation	$-$
I_{size}	Raw image size	bit
I_{sp}	Specific impulse	s
I_{wheel}	mass moment of inertia of the flywheel, around z-axis	$kg \cdot m^2$

Symbol	Description	Unit
I_{xx}	mass moment of inertia around x-axis	$kg \cdot m^2$
I_{zz}	mass moment of inertia around z-axis	$kg \cdot m^2$
L	launch cost	EUR
L_D	Total degradation	$-$
L_{eq}	Circumference of Earth at equator	m
M	magnetic constant of the Earth	$Tesla \cdot m^3$
n_{images}	number of images per orbit	$-$
n_{orbits}	number of orbits	$-$
n_{pass}	Number of passes by a satellite	$-$
n_{sats}	Minimum number of satellites	$-$
P	Price per km^2	EUR
P_0	Beginning of life power for solar cells	W/m^2
P_{BOL}	Beginning of life power for solar panel in configuration	W/m^2
P_{EOL}	End of life power for solar panel in configuration	W/m^2
P_{orbit}	Orbital Period	s
P_{input}	Input power for thruster	W
P_{jet}	Jet Power	W
$PlanetIR$	Infra-red radiation of Earth	W/m^2
P_{sa}	Energy produced by solar arrays	W
P_{system}	Energy used by satellite systems	W
P_{S-band}	Energy used by S-band system	W
q	reflectance factor	$-$
Q_{albedo}	Heat added by albedo	W/m^2
Q_{fmh}	Heat added by free molecular heating	W/m^2
$Q_{planetIR}$	Heat added by infrared radiation from planet	W/m^2
Q_{solar}	Heat added by solar radiation	W/m^2
res_{org}	Original resolution	$m/pixel$
res_{target}	Target resolution	$m/pixel$
R	Revenue	EUR
R_{orbit}	Earth radius	km
$S(t_{life})$	total amount of imaged area sold	km^2

Symbol	Description	Unit
T_a	Atmospheric torque	Nm
T_{design}	design torque for ADCS sizing	N
T_{ecl}	Time in eclipse	s
T_g	Gravity gradient torque	Nm
T_m	Magnetic torque	Nm
$T_{max_{wheel}}$	maximum torque of the reaction wheel	N
T_{orbit}	Orbital period	s
T_S	Solar radiation pressure torque	Nm
T_{sun}	Time in sunlight	s
t_{total}	Total time for full coverage with one satellite	s
V	Velocity of the spacecraft	m/s
w_{swath}	Swath width	m
X_b	Path-loss Battery	$-$
X_S	Path-loss Direct	$-$
$\alpha_{max_{wheel}}$	maximum angular acceleration micromotor	rad/s^2
β	Ballistic coefficient	kg/m^2

Symbol	Description	Unit
ΔV_D	ΔV Budget drag compensation	m/s
ΔV_h	ΔV Budget for orbit height change	m/s
ΔV_θ	ΔV Budget for phase change	m/s
ΔV_ω	ΔV Budget for plane change	m/s
ϵ	Emissivity	$-$
η_{power}	Power conversion efficiency	$-$
θ_{FoV}	Field of View angle	deg
θ_{sun}	Angle of incidence to the Sun	deg
θ_{magn}	Angle between Earth's and satellites magnetic field	rad
θ_{grav}	Angle between satellites local vertical and body z-axis	rad
λ	latitude	rad
μ	Gravitational Constant	$m^3 s^{-2}$
ρ	Atmospheric density	kg/m^3
Φ	Solar irradiance	W/m^2
$\omega_{max_{wheel}}$	maximum angular velocity micromotor	rad/s

Introduction

The advent of *CubeSats* brings about a new paradigm in space exploration and Earth observation, no longer bounded by prohibitive costs and high complexity. The exponential advances in commercial-of-the-shelf (COTS) technology over the last decade have only made this transition easier, with universities and research organisations alike developing CubeSats and placing them into orbit. Moreover, large companies like Boeing and NASA have also shown interest in this promising but yet untapped territory.

CubeSats are satellites consisting of one or more cubical units of 10 x 10 x 10 cm each. Due to their small size, this type of satellites often belongs to the category of satellites with a mass between 1 and 10 kg, defined as *nanosatellites*.

The purpose of the Design Synthesis Exercise (DSE) is to design a constellation consisting of CubeSats that can provide competitive near real-time imagery in the visual, near infrared or far infrared spectral bands. Small cameras, especially designed to be fitted into CubeSats, are designed by previous DSE groups and form the cornerstones for the constellation design. This report presents the results of the constellation design. While some preliminary knowledge on space mission and subsystem design is beneficial, this report has been written to be comprehensible for a broader audience.

To provide a clear overview of the design process, this report is divided in four segments; mission design, constellation design, spacecraft design and operational analysis. The mission analysis is presented in segment one. Chapter 1 contains the team organisation and planning that are used to ensure an efficient time and resource allocation during the project. The camera characteristics are listed in chapter 2. In order to create a competitive design, a market survey is made of which the results are presented in chapter 3. Chapter 4 contains definitions of requirements and functions of the system based on the outcome of the market survey. Also technical budgets and an overview of the cameras is given in this chapter. The constellation considerations are presented in segment two. Based on the requirements, a constellation is designed which is presented in chapter 5. Launcher selection and considerations are presented in chapter 6. The spacecraft subsystem designs are presented in segment three. The design of the structural, power, thermal, attitude control, propulsion and command & data handling subsystems are presented in chapters 7, 8, 9, 10, 11 and 12 respectively. Ground stations are elaborated upon in chapter 13. Finally the operational characteristics are presented in segment four. In chapter 14 the process between downlinking the image data and performing useful analysis on it is described. A design assessment including sensitivity analysis, RAMS analysis and risk management can be found in chapter 15. An overview of the cost and the return on investment of the C^3EO mission is presented in chapter 18. The system specifications are summarised in chapter 16 and the production planning is presented in chapter 17. A cost breakdown and image price prediction are shown in chapter 18. Finally, the conclusion and recommendations are formulated in chapter 19.

PART I

MISSION SEGMENT

Chapter 1 | Project organisation

In this chapter the procedure and strategy of how the work has been performed and planned is explained. In the first part the planning of the work packages is done with help of work breakdown and work flow diagrams. These diagrams show what work needs to be performed and in which order. They also include the distribution of the management and technical functions of each team members. This shows how the work described in the diagrams was distributed. In the second part the sustainable development strategy is covered, which indicates how sustainability is taken into account during this project. The aim of this chapter is to allow the reader to understand how the results presented later were developed.

1.1 Organisation

For any project to run efficiently it is important to plan the activities which need to be executed. This planning is done with tools from system engineering, such as work flow, work breakdown diagrams and a Gantt chart, which schedules all activities that need to be performed over time. These diagrams are updated constantly during the project and final versions and corresponding explanations are presented here.

1.1.1 Project phases

This project consists of four phases: project start-up, research, conceptional design and the detailed design phase. In each of these phases different activities are performed. A short overview of these can be found in table 1.1.

Phase	Activities
Project Start-up	During the Project Start-up phase the rest of the project is planned. This includes the initial planning for the activities in form of a work flow, work breakdown diagram and Gantt chart. Furthermore the management position are distributed. The phase is concluded with a project plan.
Research	In the research phase a market analysis as well as a literature study has been performed. The main goal is to familiarise the team members with the topic of CubeSat constellations and platforms. At the end of the phase a set of requirements and design options are derived and reported in form of a baseline report.
Concept Design	In the Concept Design, design options for the constellation are worked out and traded off. With the requirements found in the research phase and additional information gathered the concepts are traded off and the best concept is selected. This phase is reported in a Mid Term Report.
Detailed Design	During the detailed design phase, the selected concept is worked out in greater detail and all findings are reported in form of a Final Report.

Table 1.1: Project phases

1.1.2 Work breakdown structure

The work breakdown structure (WBS) is a useful tool which provides a partitioned view on the tasks that have been performed in the final design phase and all the completed tasks from previous phases, as can be seen in Figure 1.1. These work packages, which are ordered in a hierarchical tree, represent the different phases of the project. At the end of the detailed design phase all work related to it is concluded in the final report. The findings are presented in a final review and at the symposium. Next to the final report, other deliverables such as the executive and jury summary and the poster need to be created.

1.1.3 Work flow diagram

The work flow diagram (WFD), shown in figure 1.2, states the order in which project tasks are performed. The work breakdown structure gives a more detailed breakdown of the various tasks of the project. Changes occurring during the project are incorporated in the final updated diagram. The WFD states the order of how the work needs to performed, while WBS specifies the details of each step. At the end of the project the final report is written and the results are presented during the symposium on the 31^{st} of January.

1.1.4 Gantt chart

The DSE Gantt chart presented in figures 1.3 and 1.4 demonstrates the work flow and its time-line, serving as a basis for monitoring progress of project activities and tasks. The Gantt chart is built up according to work packages in the work breakdown structure, with an update of the actual process during the project. The activities in the work-flow diagram are also included in the Gantt chart and are updated in the final report.

1.1.5 Team organisation

In the project-startup phase of the DSE, the team is distributed into different management functions, with a re-evaluation planned at the of the conceptional design phase. Furthermore, the technical responsibilities for the detailed design phase need to be determined.

Management Tasks

The distribution of the management task proved to be effective. However, as it is expected that quality assuring the final report requires a large amount of time time, the QA-team has been reinforced with two extra people. An overview of the functions of each team member is shown in 1.2 and in the organogram in figure 1.5.

Position	Name	Responsibilities
Chairman	Rian van Gijlswijk	Group motivation, group process monitoring, administration of printing balance, Communication with stakeholders
Secretary	Rick Hartmans	Organisation of digital and printed documents, documentation of meetings with tutors, logbook
Quality Assurance	Fatima Dyczynski Frederico Vicente Constantijn Sa Etteke Roebroeks	Accuracy of technical writing, correct allocation of figures, grammar check, implementation of corrections
Editor-in-Chief	Niels Treffers	Responsible for the layout of documents, creation of template in latex
Systems Engineering	Jeroen Wink Frederik Braeuer	Integration of verification and validation in the project, integration of advice from tutor and coaches
Planner	Etteke Roebroeks Constantijn Sa	Responsible for organisation of deadlines on a daily and weekly basis while making sure that those deadlines are met

Table 1.2: Work distribution

Technical Tasks

For the detailed design phase the general approach of the previous phases of the project is changed to an in-depth design of the system. As a consequence, it is necessary to assign specific technical roles to team members, which can found in figure 1.6. The person mentioned per topic is the main responsible, but to ensure quality of the design and in-depth of the research, people work together in teams.

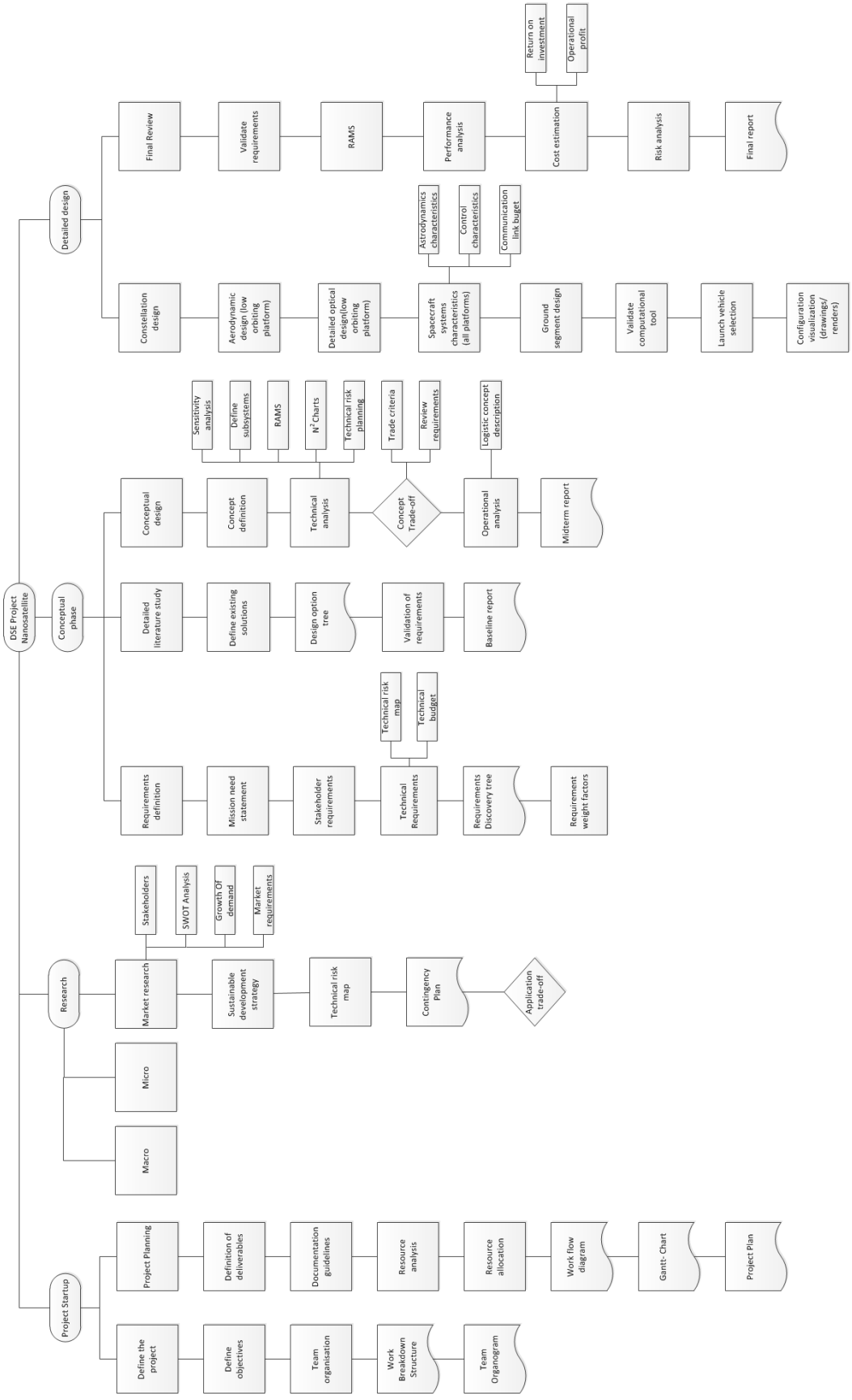

Figure 1.1: Work Breakdown Diagram

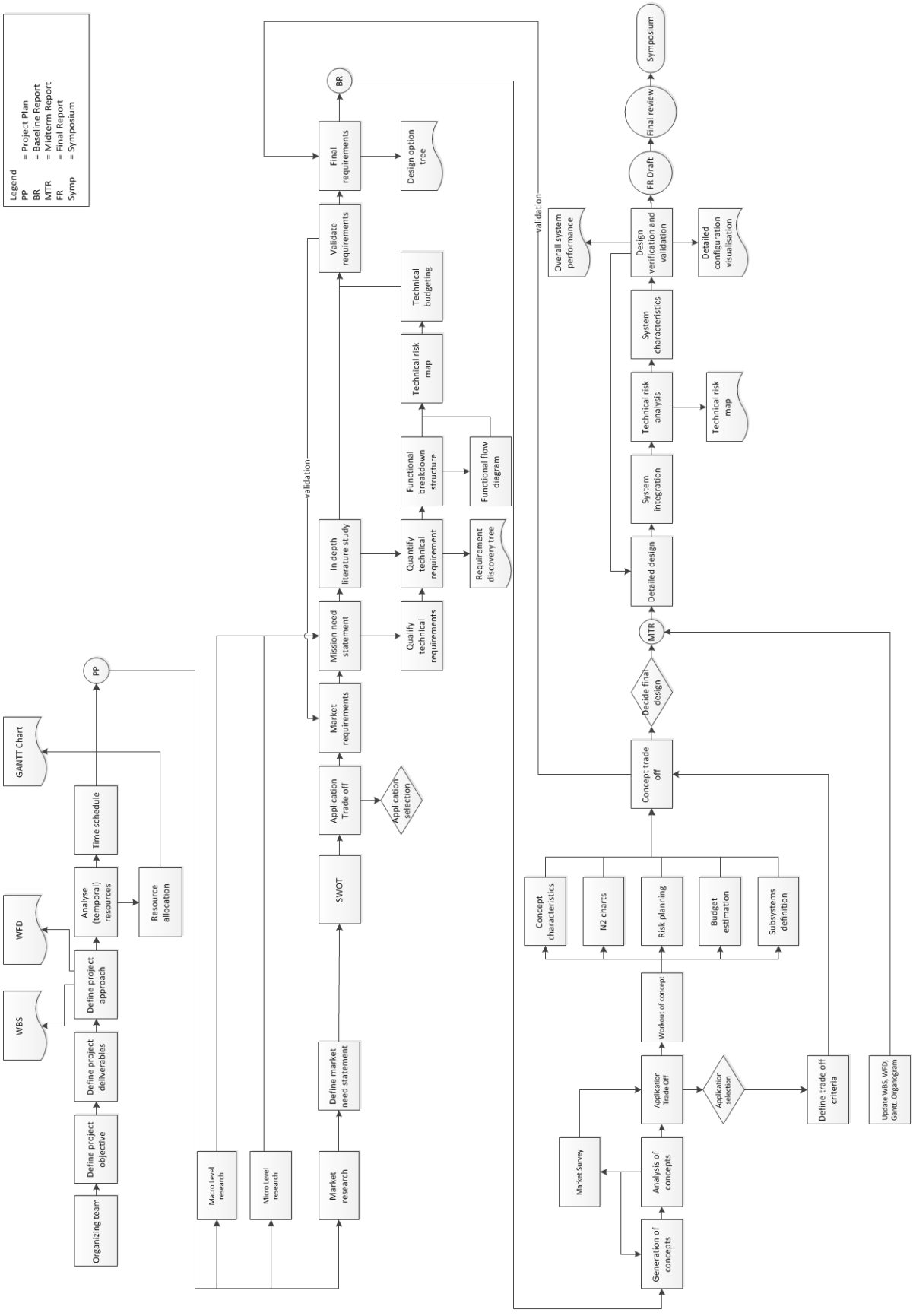

Figure 1.2: Work flow diagram

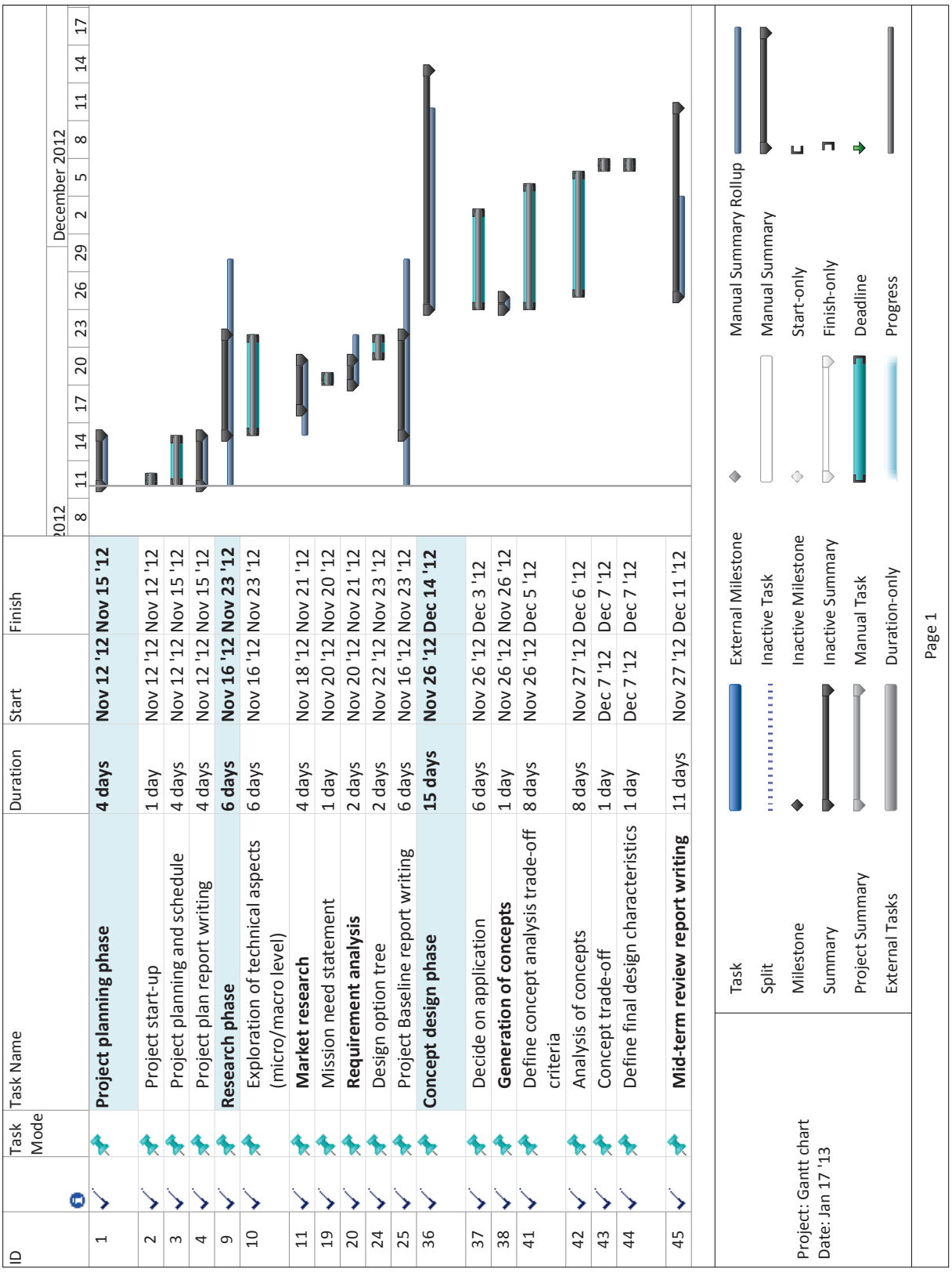

Figure 1.3: Gantt chart Part 1

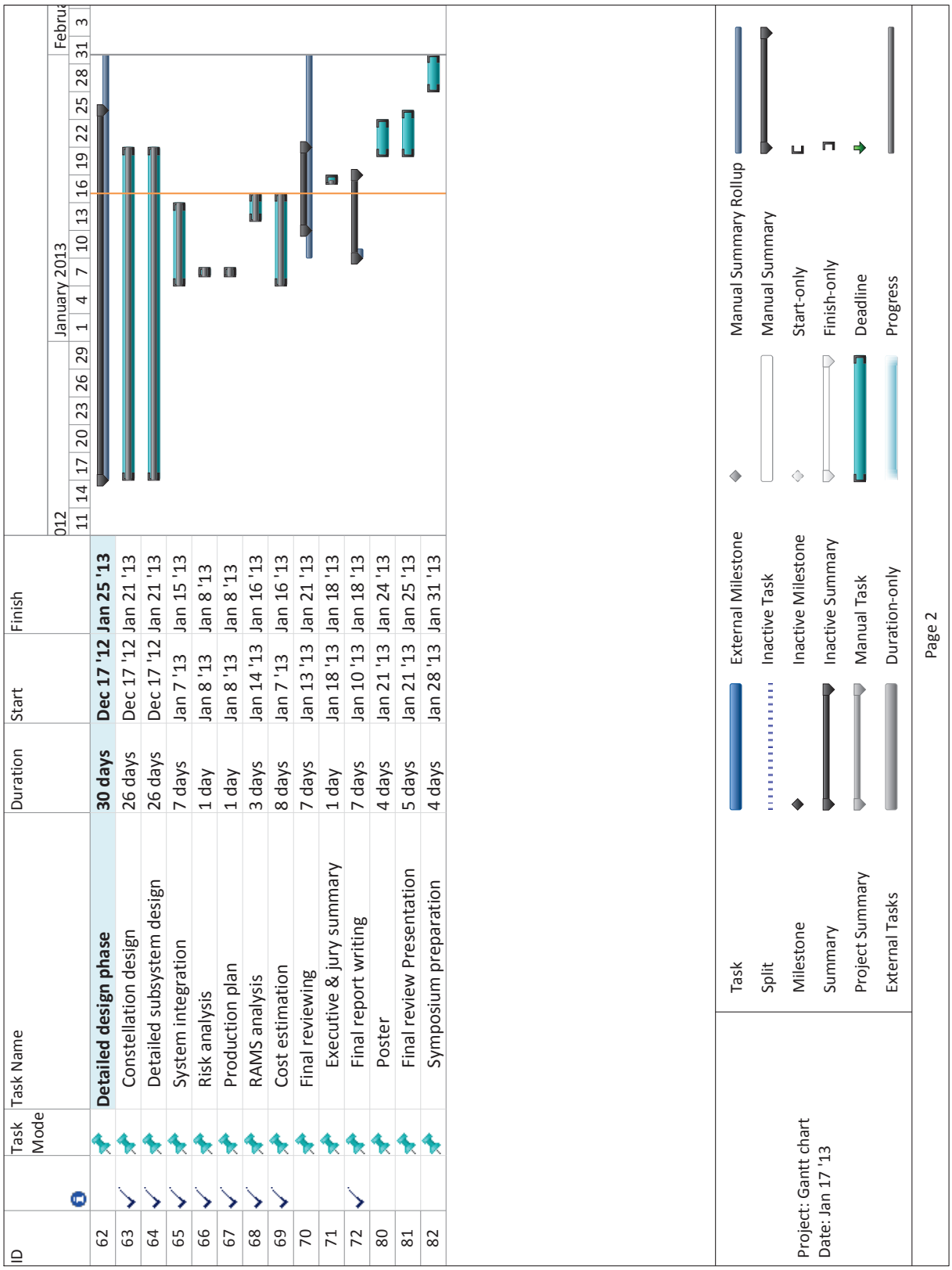

Figure 1.4: Gantt chart Part 2

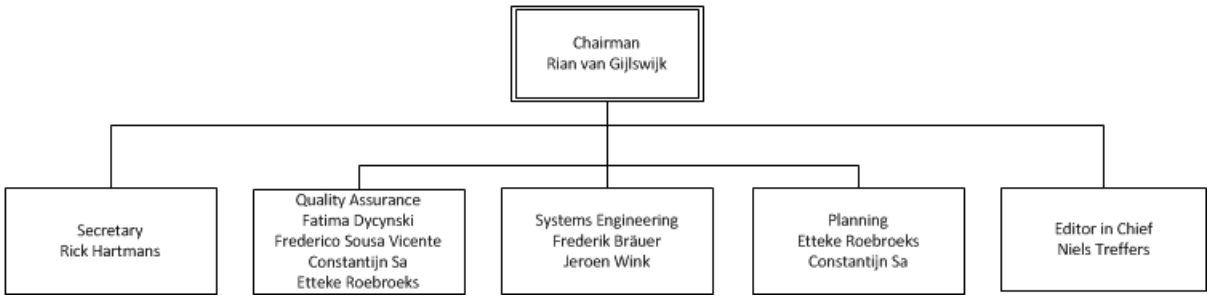

Figure 1.5: Organogram

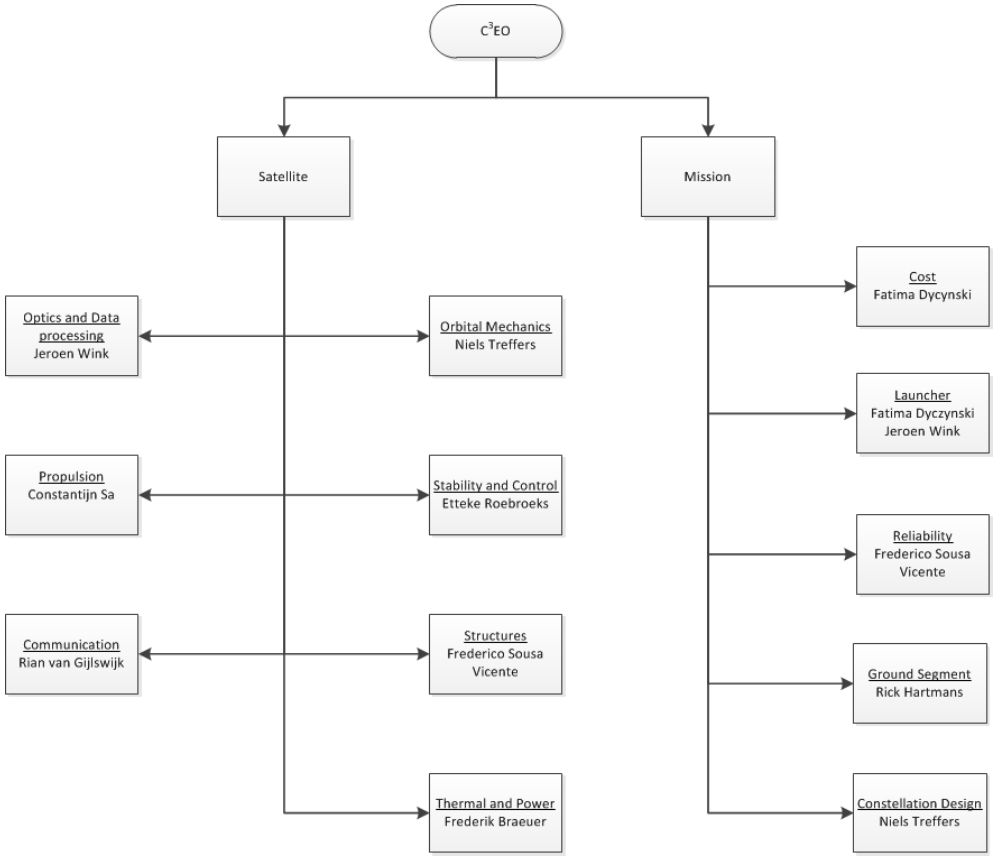

Figure 1.6: Technical functions for the Detailed Design phase

1.2 Sustainable development strategy

The sustainable development strategy is divided into a separate strategy for both the application and the design. The sustainable strategy of the application is related to the use of the generated data for a sustainable future while the design part focuses on the system itself and its contribution to a sustainable use of Earth orbits.

1.2.1 Sustainability through applications

The constellation aims to monitor both natural disasters as well as the environment. The images generated by the system can be used to detect changes in atmospheric properties, soil properties, oil spills, forest fires and ice surfaces, among others. This data can be used to study the Earth's climate change and its effects. Furthermore,the monitoring of environmental disasters provides better insight into their behaviour and thus could reduce the impact of these disasters through planning. Additionally, the images can be used to make agriculture more effective; nitrogen concentrations can be detected with the near infrared camera such that fertilizers can be used more effectively. Furthermore, the images can provide a more precise overview of infected crops in order to reduce the amount of pesticides needed. All in all, the environmental impact on the world's food production can be reduced by using satellite data.

1.2.2 Designing for sustainability

The largest consideration for sustainable development in space is related to orbital debris mitigation. In order to have a sustainable mission, satellites must de-orbit as soon as they are out of service. International guidelines dictate a maximum de-orbit period of 25 years. The lowest segment automatically meets this target period because of its natural orbital decay of less than a year. The two higher segments have extra propellant mass so that they also de-orbit within a year. This is much quicker than the targeted period of 25 years. The satellite generates electricity using solar panels, therefore no radioactive material needs to be produced and distributed.

Chapter 2 | Cameras

An Earth observation mission is nothing without its cameras; a selection of cameras applicable for such missions in a CubeSat package must be carried out. The camera choices are however fixed, which leads to the use of three different cameras: the ARCTIC[31], the ANT-2 RCC (Ritchey-Chretien Cassegrain) and TMA (Three Mirror Anastigmat) cameras which are the product of previous DSE groups and later improved [30]. In table 2.1 the specifications of these cameras are shown.

Parameter	Unit	ANT-2 RCC	ANT-2 TMA	ARCTIC
Spectral band	-	VIS	VIS + NIR	TIR
Spectral response	*nm*	400 - 700	400 - 1000	9000 - 11000
Resolution	*pixels*	2048 x 2048	2048 x 2048	640 x 480
Image bit depth	*bpp*	10	10	12
Field of View	*deg*	1.76	5.86	5

Table 2.1: Camera specifications

2.1 ANT-2 RCC Camera

The ANT-2 RCC Camera is an improved version of the Advance Nano Telescope (ANT) designed by a DSE-group from the TU Delft in 2011. While the ANT-camera is optimized for the green waveband, the RCC is capable of taking images in the entire visible spectrum. This is achieved via the addition of two hyperbolic mirrors and two correcting lenses[30].

Although the RCC camera has a very good ground sampling distance, the swath width is very low. This results in good quality and high resolution images, but requires a large amount of images for large coverage. Therefore, this camera generates large amounts of data which requires a considerable downlink budget. Regardless, its ability to provide high resolution imagery makes it suitable for applications that require a ground resolution of less than 10 m.

2.2 ANT-2 TMA Camera

The ANT-2 TMA Camera is another variant of the RCC camera, which can monitor in the visual as well as in the near infrared spectral band. This is achieved by adding an elliptical mirror besides the two hyperbolic mirrors[30].

A second improvement over the RCC is the field of view angle, which results in a much larger swath width. However, this is achieved at the cost of ground sampling distance. The TMA camera and its ability to image in the near infrared and large swath width make it ideal for forestry as well as oceanography.

2.3 ARCTIC

The Advanced Remote-sensing CubeSat Thermal Infrared Camera (ARCTIC) images in the thermal infrared spectral band. Therefore the ARCTIC can be used best to measure differences in temperature, where it can resolve changes of 95 mK. As such, it is ideal to measure surface temperature as well as ice monitoring[31].

The downside of the ARCTIC is its ground sampling distance and the altitude limitation: 66 m at a 540 km orbit and a 300 km limit due to thermal cooling, respectively.

Chapter 3 | Market Survey

In this chapter the space industry is analysed, providing context for the design of an Earth observation constellation. After the global space economy is discussed in section 3.1, the focus narrows down to the Earth observation market segment where mission trends are discussed and the advantages and disadvantages for CubeSat missions are pointed out in section 3.2. In section 3.3 a thorough overview of all possible applications is given. As this spectrum of applications is very broad and not all applications can be served competetively, a selection is made of the most interesting applications for a CubeSat mission. Next, in section 3.4 a thorough overview of current competitors is listed, giving insight in their business case and performance. A short elaboration on the customer pool is presented in section 3.5. Finally all the findings of this chapter are used to form a vision which results in a market need statement in section 3.6.

3.1 Space economy

Over the past 5 years the space industry seemed resilient to economic uncertain periods[1]. According to the OECD report on Space economy[2] there are two possible reasons for this. Firstly, the space sector is a key strategic sector in terms of national imperatives (e.g. national security), institutional research and development funding. Secondly, applications developed with government funding are spilling over into the commercial mass markets, e.g. GPS and communication systems, resulting in a highly active commercial space economy.

Space programs are labour and capital intensive and have a long development time, making it a high risk investment. Governments often take the initiative of investing in such high risk programs of which commercial markets at a later stage take advantage[3]. Private investment alternatives, e.g. venture capitalist funding, demand high returns on investments up to 300%[3] to account for the risk incurred. Naturally these costs are passed on and influence the product pricing.

Recent fiscal austerity in Europe and the US aimed at reducing the yearly budget deficits and government debts is putting strain on the option of government funding[1]. A practical example is the recent proposal by president Obama to decrease the 2013 NASA budget[4] with respect to the 2012 budget. Developments like these may result in a substantial decrease in funding to the space industry in Western economies[1]. Developing economies and BRIC countries however are undergoing a vast expansion in space activity, with Russia having more launches than any other country since 2006 and China outdistancing Europe in terms of number of satellites inserted in orbit[1].

From a demand point of view a strong growth can be outlined for the near future. Topics like security, food and water scarcity, climate change and the global movement to an information society (e.g. news broadcasting, navigation devices, real time land monitoring) are ever increasing in demand and could provide a stable pull for technology innovation.

The commercial space mass market, like any capitalist market, has the inherent imperative of providing competitive products. Together with the decreased availability of government funding in Western economies this points in the direction of a need for lower cost solutions. This could mean a change in design approach in which development time, risk and operational cost are reduced.

Because of the expected increasing overall demand, and the inherent demand for low cost solutions in the commercial space market, it is expected that the space industry is continuing to grow in an above average tempo, with a tendency towards a lower cost design methodology.

3.1.1 Market sectors

The satellite market can be divided into three sectors, each having their own macro segments and subsequent market segments[5]. The break down is shown in table 3.1. In 2009, telecommunications was the largest segment with revenues of around 80 billion USD, followed by the navigation segment with a 15 billion USD revenue and finally the Earth observation sector, which obtained a revenue of 1.2 billion USD in 2009[1]. The Earth observation sector is the field of research of this report and is investigated in the next section.

3.1.2 Earth observation

According to the Earth Imaging Journal[6] the market for Earth observation satellites is expected to more than double between 2010 and 2019, adding another 123 satellites to the already existing 107 and increasing the number of participating countries from 26 to 41. The journal states that the revenue in the high optical segment, which accounts for 83 percent of the commercial data sales, was about 1.1 billion in 2009. This is approximately the same as the OECD statistics of 1.2 billion, discussed in the first section. These numbers are suggesting an enormous market expansion over the next ten years, which entails major opportunities for new Earth observation businesses.

Figure 3.1 shows the development in commercial remote sensing revenues obtained between 2004 and 2009 in USD. As stated above the increase that is clearly visible from 2007 to 2008 and 2009 is expected continue over the next ten years.

Sector	Macro Segments
Navigation	Governments
	Infrastructure
	Consumer
	Transport
Communication	Telecommunication
	Television
	Internet
Earth observation	Environmental monitoring
	Defense & Security
	Disaster monitoring
	Meteorology

Table 3.1: Space market segmentation

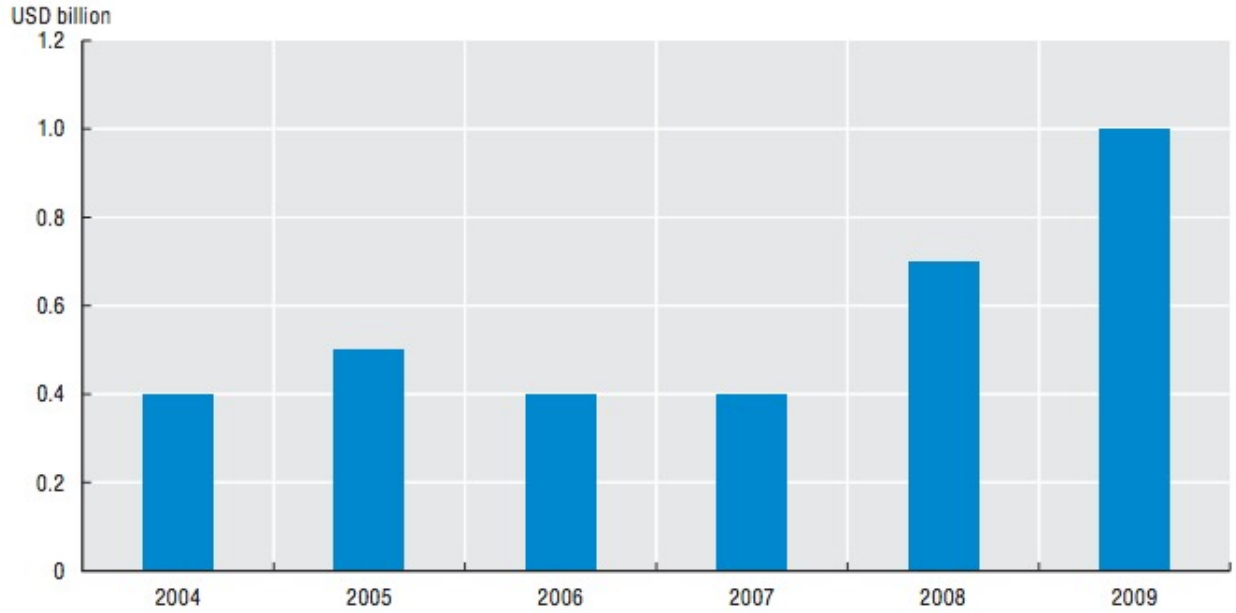

Figure 3.1: Development of commercial remote sensing revenues, 2004-2009 [2]

3.2 CubeSats

3.2.1 Design evolution

Under the influence of technological advances design choices of satellites have varied over time. Early satellite design in the 50's was based on small satellites. The spatial resolution however, depends on camera aperture and altitude[7]. A higher spatial resolution can be obtained by choosing a lower orbit, or by increasing the aperture[8], or both. The first option is restrained in the sense that a lower altitude has the disadvantage that a higher density is encountered, causing drag that needs to be overcome in order to maintain orbit. The second option requires a larger satellite which is more expensive to develop. It is clear that the trade-off between altitude and aperture size is not unambiguous and highly dependent on the available technology. Over the last years the prevailing conditions resulted in the design of large satellites orbiting at an altitude of 600 km, where atmospheric drag is negligible[7]. In section 3.4 about competitors more information is displayed about the manner in which Earth observation constellations were designed in the past, in terms of mass, altitude and cost.

Recent developments however, provide the ability to achieve higher imaging performance with a smaller camera. Previous DSE groups of the TU Delft's faculty of Aerospace Engineering designed two of these high performance, competitive cameras of 1.5 U size each, which are able to be positioned in a CubeSat.

CubeSats are miniaturized satellites consisting of one or several units of each 10 by 10 by 10 cm. The definition of nanosatellites often comes into play when discussing CubeSats and refers to the mass: satellites with a mass between 1 and 10 kg fall within the definition of nanosatellite. Development of these types of satellites is driven by the increasing availability of smaller, cheaper components and the fascination of launching a personal satellite into space[8]. These drivers have ensured that mainly the field of academics has spent its resources on these types of satellites. Some of the first were launched in 2003 and since then over 40 have followed[8], as can be seen in figure 3.2.

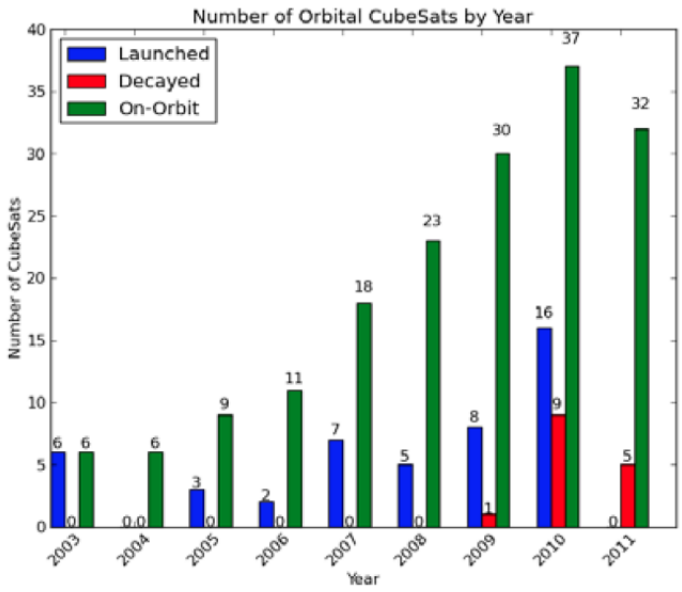

Figure 3.2: Amount of CubeSat launches per year [2]

In particular universities played a large role in these developments, with the DELFI and DELFI-N3XT nanosatellites, designed and produced by students of the TU Delft's Aerospace engineering faculty as a good example. The main goal of these projects was to demonstrate that it was technological possible to develop and launch these small satellites.

A couple of projects were aimed at designing a nanosatellite capable of producing images and downlinking them to the Earth. For example the Romania's *Goliat* which was capable of providing a 25 $m/pixel$ spatial resolution from a 600 km orbit. However, just as the other examples the goal was to show a proof of concept and not to deliver a serious competitor to already existing Earth observation systems.

The advantages of small low mass satellites over large, high mass satellites are evident and explained in section 3.2.2. The academically driven nanosatellite development embraces newest commercially available technologies, shifting technological paradigms and applying unorthodox development techniques. These developments are not without drawbacks however. The small package of a nanosatellite is cause for a few problems that yet remain to be solved. Regardless, many new mission possibilities arise that were hardly possible before.

3.2.2 Advantages

Several advantages for nanosatellite missions hold true due to improvements in the field of engineering. The miniaturization of commercial-of-the-shelf technology decreases component cost, while the increase in processing power gives satellite systems a plethora of new applications that can be performed on-board. Advances also become apparent in the field of systems engineering. Furthermore, the low-cost approach catalyses mission opportunities and variety, involving more industries than before.

Miniaturization

Miniaturization allows satellites to be built in a small size, saving weight and cost. Two possibilities embracing miniaturization to a great extent are the *SpaceChip*[9] and *PCBSat*[10] studies. These studies show that the current technological advance allows for low-cost and mass production of satellites.

Processing power

The ever-increasing performance of electronic components give rise to new applications usable for space missions. Seeing that processing power of individual components still increases today and shows no sign of stopping[11], it can be expected that nanosatellites will feature more powerful processing over time. As a result, a satellite now has the capability of efficiently performing many computation-heavy tasks by itself, thereby decreasing the up- and downlink required.

Furthermore, trends have shown a significant decrease in power consumption for electronic components as well[12], enabling more subsystem possibilities with the same power budget.

Faster development time

Many recent developments in the field of electronics, space hardware and system engineering approaches result in a decrease in development time. In fact, the size of a nanosatellite alone results in a shorter development time, since a nanosatellite is normally less complex.

As a consequence, this faster development time can actively fill in a shorter term demand of the market and end users. Furthermore, newer technology can be used in the designs, making it ideal as a test platform unlike long term missions, which by the time they are launched are already outdated.

Lower cost

The advantage of using nanosatellite technology for an imaging mission is that it can be achieved at low cost. The cost breakdown for an imaging mission consists of unit cost, launch cost and operation cost. For all these three components nanosatellite technology is beneficial.

Unit cost of a nanosatellite will be very low. This is in the first way achieved by the the small size of a nanosatellite, since cost generally scales with size and complexity[12]. It is also achieved by using commercial-off-the-shelf (*COTS*) components, which mitigates material cost of the design while only slightly decreasing the reliability of the satellite. The cost of electronic components that are hardened for the space environment are normally relatively high due to low production quantities. However, the low unit cost of a nanosatellite allows for the use of less redundant systems, since a single satellite no longer is a single-point-of-failure. COTS components have been proven to be reliable in the space environment, but they won't be as reliable as the expensive space hardened components[12].

The launch and operation cost for a nanosatellite mission are relatively low as well. Contrary to large satellites who need a large and dedicated launcher, nanosatellites have several cheaper abilities to get into orbit. A popular option is for example the piggy-back option, where nanosatellites are launched with a dedicated launcher containing a larger satellite. The low operational cost are caused by the (still ongoing) reduction in mission and management complexity of Earth observation missions[13].

The low cost of nanosatellite missions will fuel the increasing number of earth observation missions. The decrease in total mission cost enables countries to step into the Earth observation market, as was pointed out in section 3.1.2.

More mission opportunities

A reduction in cost and an increase in flexibility give users cheaper and more direct access to scientific and commercial data. While earlier space missions were rather expensive, the low-cost approach of nanosatellites allows for academic institutions, research groups, and commercial end users (mass markets) to set up their own space mission.

Increase in mission variety

An advantage of the low-cost and fast development time of nanosatellites is that satellite mission developers have a large flexibility in choosing an application. Therefore nanosatellites serve a great mission variety and will likely induce more creativity and innovation.

Design flexibility using COTS components

Using COTS components ensures a high design freedom compared with specially designed space hardened components. Normally the latter components are produced and designed by one single subcontractor that is selected by the mission designer. The use of COTS components greatly diversifies the component selection and thus also greatly diversifies the companies that are able to deliver the components that are required to perform the mission[13]. Therefore a trade-off can be made between the different subcontractors and the different components that they offer, to ensure that the low-cost and performance requirements are met in the most optimal way.

3.2.3 Disadvantages

Due to their small nature, nanosatellites are bound by a few limitations. These become apparent in the field of communication and launcher selection.

Antenna design

In a mission where multiple nanosatellites are active in a distributed network, inter-satellite communications might be required. The problem with setting up a communication link between two satellites is that a satellite initially has no knowledge of the location of the other satellite. This is required in order to set up a crosslink successfully[8].

A solution to this problem would be the use of omnidirectional antennas. This solution has two drawbacks: the power available on a nanosatellite is very limited and eavesdropping of the signal by unauthorized users is possible, which might be a drawback for systems where a certain level of network security is required.

Another solution for the antenna design would be the use of retrodirective antennas. Retrodirective antennas have the ability to sense the direction from which an incoming signal is coming. These antennas can then tune to the direction of that signal, essentially establishing a direct connection. This connection would then be secure and consume little power. The use of a retrodirective antenna would be very satisfying, however this technology is not extensively proven on satellite missions[14].

Launcher restrictions

Nanosatellite missions are restricted in launch possibilities because very little low-cost dedicated launchers are available[15] for individual nanosatellites. Instead, these missions are mostly restricted to piggy-back launches such as a an Ariane ASAP[12]. Other options include launches with converted inter-continental ballistic missile (ICBM) launchers, like the Dnepr[16]. These launch options incur that launch possibilities are restricted to the small number of launch dates. Especially with piggy-back options, nanosatellite missions have to wait until a launch with a large satellite is planned onto which they can participate.

For constellations of nanosatellites however, several launchers are available. Especially the Russian market offers a variety of launchers suited to launch multiple nanosatellites into orbit at once.

3.2.4 Resulting mission types

The advances in technology and decrease in cost for space mission components open up a new world of applications. Assuming the design limitation discussed in section 3.2.3 are overcome in the future, several mission types arise which were previously unfeasible or only feasible at high cost.

Fast deployable mission

Due to nanosatellite's low mass, launch costs are considerably lower. Assuming a small launcher is available, one has the possibility of launching a nanosatellite or even several nanosatellites into orbit within a weeks notice, providing customers with rapid access to imagery. Event-driven missions, such as disaster monitoring, are an example of this[17][8]. The customers are security groups, who quickly want to have access to imagery from any disaster. For these customers, a short delivery time of imagery is very important. In the case where no satellite is in the proper orbit for that, new satellites can be easily launched.

Missions providing high temporal resolution

Some applications will require frequent updates of imagery. This can be achieved by a network of satellites with a short revisit time over a specific area. While the revisit time of one specific satellite may not be short, the fact that a constellation consists of many satellites means that the revisit time of any location on Earth is short. In other words, the *temporal resolution* of any location on Earth is high. An example applications requiring frequent updates is disaster monitoring[17]. Other examples are the more generic surveillance missions or environmental monitoring missions.

The low-cost approach of nanosatellite missions offer a high temporal resolution without the high mission pricetag. Due to the fact that individual satellites can be cheap, missions requiring many satellites in orbit are possible while mitigating the mission cost.

Missions with platforms in very low Earth orbit (VLEO)

The small size of nanosatellites is beneficial when orbiting in a VLEO because aerodynamic drag is an important issue and it is directly influenced by the size of the satellite. By placing them in a lower orbit, they can achieve the same spatial resolution as larger sized satellites at a higher altitude at a lower cost. Larger sized Earth observation missions like the GeoEye[18], need a larger and more precise camera as the satellite is placed in higher LEO. The nanosatellite that can be placed in an orbit closer to the Earth and can achieve the same results with a more simple and cheaper camera.

The nanosatellites in VLEO also have the advantage of having a very short revisit time, as the orbital period is shorter at lower orbit height. This is an advantage for a mission that requires a high temporal resolution.

3.2.5 Outlook

The advent of CubeSats opens up a whole new opportunity within Earth observation. Traditionally this market has been served by highly expensive missions, whereas right now the possibility has presented itself, with the development of cheaper high performance cameras, to use a constellation of nanosatellites. This could potentially be a highly competitive alternative in terms of cost.

This raises the question as to what imaging data is actually interesting to cover. The next section will therefore go into more detail about possible applications for an imaging payload onboard a nanosatellite.

3.3 Applications

In this section an evaluation is made regarding the applications that can be covered, and the applications that are interesting to cover. This leads to a set of requirements per application, as the required imaging data differs for each. The requirements are based on spatial resolution, temporal resolution and spectral resolution. Furthermore, the locations at which an application is relevant are examined as this can influence the constellation design and types of orbit applied. Combined with the resolution requirements these are taken into account in the constellation design so that the most optimal orbit characteristics are chosen to meet them. All applications are assigned a spatial and temporal resolution, with which they can be compared. As exact metrics can't be provided for the required spatial or temporal resolution, the scale shown in figure 3.3 is used to indicate relative resolutions.

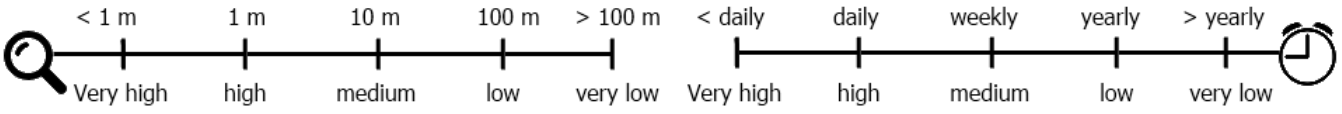

Figure 3.3: Relative scale of spatial resolutions (left) and temporal resolutions (right)

3.3.1 Applications of interest

Agriculture

The increasing global population requires an increase in agriculture production, in turn requiring better monitoring of agricultural resources. Numerous remote sensing approaches have been applied to identify the quality of vegetation and livestock. Crop growth and failure can be monitored closely by remote sensing applications, improving the quality and quantity of agricultural products produced.

The capability of remote sensing applications to monitor vegetation and land quality is ever increasing, but many issues remain unsolved. One of these examples is precision crop management, a method to optimise the production of agricultural land and mitigate the effects on the environment. The quantity of spatial and temporal resolution remains insufficient for this approach to provide adequate information to end users however [19]. Timely monitoring of agricultural activities is therefore required to offer agricultural end users with the data they need, enhancing the production and decreasing the effects on the environment.

Forestry

Forests are an important natural resource on which humanity depends for air quality, wood, and many other purposes. As forests are of vital importance to humanity and the ecosystem, monitoring their health is of equal importance. Forests are however subject to a range of disturbances like degradation, pollution, understory fires and logging.

Remote sensing tools help mapping forest health and composition, the health of the ecosystem and damage done to a forest by natural forces. Examples are floods, damaging winds, but the effects of soil erosion as well. Furthermore logging activities can be monitored; deforestation and reforestation can be clearly seen from space. Finally monitoring the wildlife habitat and recreation resources is of importance when assessing the health of a forest.

The changes in forest quantities influence the carbon stock, as forests are one of the main elements in the carbon ecosystem. This is why the Kyoto protocol from 1990 states that many nations are required to monitor the levels of deforestation, reforestation and afforestation in their country, effectively forcing nations to have access to remote sensing data relevant for forestry[20].

Polar ice

Polar ice sheets have a dominant effect on the global ecosystem and the climate of the planet. The effects of polar ice on oceanic and atmospheric circulation are tremendous as the large quantities of ice have a significant effect on heat dissipation[21].

Another significant feature of ice sheets is the vast storage of fresh water. In fact, 70% of the world's fresh water is estimated to be stored in ice sheets, of which Antarctica is the most significant contributor. The global sea level could raise by a staggering 70 m in case these ice sheets melt completely. As the melting of ice heavily influences the rise in sealevel and the impact this has on inhabited coastlines, monitoring the behaviour and growth of ice sheets is of ubiquitous importance[21].

Another effect is the high reflectivity of ice sheets, which results in a high albedo. This in turn has a significant effect on the release of greenhouse gases, as the reflectance of ice decreases the heating of the atmosphere due to the sun.

Instruments in a wide range of the electromagnetic spectrum can assist in monitoring ice sheets. For example, in the visual and infrared spectrum, behaviour and dissipative effects can be studied. Then there is microwave imagery, which provides insights in the composition of ice below the surface. Due to the importance of ice sheet monitoring, adequate remote sensing is required to guarantee sufficient insight.

Oceanography

Several types of sensors help in monitoring the ocean colour, temperature and surface. Firstly, the visible waveband sensors help mapping the chlorophyll or phytoplankton levels. Phytoplankton for example is a main contributor to the carbon ecosystem, which is why close monitoring is required. Secondly, the thermal infrared spectrum is perfectly capable of measuring the surface temperature, an important measure in its own right. Finally the microwave spectrum has the ability to measure the surface roughness of the ocean, unveiling metrics about the wind, waves and tidal conditions[22].

As the oceans make up roughly 70 % of the Earth surface it becomes evident that global monitoring on several wavelengths is required to give useful measures about their composition.

Glacier monitoring

Glaciers are a prime example of the effects of global warming on the climate. Their composition and health are therefore interesting metrics to monitor. The rate of decrease of a glacier is a fine example. Together with the glacier area, these effects can be adequately studied.

As the areas covered by glaciers are vast and hardly accessible, satellite remote sensing technology is often the only means of studying them. The visual and infrared spectra give excellent measures regarding glacier length and areas. Spectral characteristics of snow and ice can be mapped using these spectra as well, making them important tools in monitoring the state of glaciers.

Damage monitoring

The damage done by various natural disasters as Earthquakes or tsunamis causes significant loss of life and a vast impact on local economies and communities. Therefore monitoring and predicting these disasters is of vital importance as it decreases the loss of life and damage done to civilisation.

The consequences of damage on coastlines and regions influenced by a disaster are of vital importance for damage and recovery assessment. By monitoring the effects of a disaster in the visual spectrum, an overview of damage can be given to aid with restoring the land and coastal lines in their old state.

Forest fires

In order to monitor the consequences of forest fires as well as for forest management and protection, quantitive information is required on the distribution and movement of the fires. Forest fires have an effect on ecology, atmospheric chemistry, wildlife and land cover[23]. The ecological effects due to forest fires remain largely unknown. Due to the vast area of forestry, the fires release a significant amount of carbon stock every year, and are thus one of the most dominant contributors to the global carbon budget. In order to quantify the carbon stock released by the fires, monitoring of forested areas with frequent updates is required[23].

High-frequency monitoring of forested areas is required for hazard monitoring of forest fires. A high temporal resolution is required in order to ensure new fires can be located early. This guarantees the ability for emergency services to react adequately.

Volcanoes

Volcanoes have a major impact on the ecosystem and their surroundings in particular, giving rise to the need of monitoring them. Especially since active volcanoes affect the surrounding atmosphere.

Infrared monitoring is ideally suited for monitoring hydrothermal activities and changes in gas release at the volcano surface for example. Lava flows and thermal hot spots are often an indicator for eruptions and can be monitored in the infrared band as well. Cloud sensing is another field of study, which visualises eruption clouds by comparing thermal imagery.

Hurricanes

As hurricanes and cyclones are significant natural forces causing vast amounts of damage yearly, closely monitoring them is important. Windspeeds and temperature differences can be easily measured in the infrared spectrum. The temperature differences in different layers of hurricanes are a main indicator for wind speed and pressure.

Like with other natural disasters, the effects of a hurricane on a region can be come quickly apparent once visual imaging is taken. This is of great importance to emergency crews and damage assessment teams, effectively helping them in mitigating the damage caused.

Oil spills

According to Chuanmin Hu et al. [24], oil pollution, caused by transportation leakages and oil platform accidents, causes extensive damage to marine and terrestrial ecosystems each year. Detection of spills and tracking their movement is desirable for effective clean-up and reduced impact on the environment.

Monitoring from airplanes provides the highest spatial resolution and the fastest response, but is limited in frequency and coverage and is more expensive.

Currently, optical, microwave and SAR sensors are used for monitoring. SAR, which can monitor difference in surface roughness, is mostly used. Its images are cloud free which is a big advantage over images in the visual spectrum, however it has a high cost and low swath width, resulting in a temporal resolution of days to weeks. Radar is not an option for this CubeSat constellation, and as Chuanmin Hu et al. [24] suggest it is desirable to seek alternatives for SAR observations.

MODIS, MODerate resolution Imaging Spectroradiometer (NASA), is capable of providing images in the visual band with a 250-500 $m/pixel$ spatial resolution.

Defence & Security

Visual high-resolution imaging data provide valuable information to security agencies and governments. The assessment of this data aids in protecting invaluable properties, but also in saving lives and retrieving the hot spots of malevolent activities. Furthermore imaging data assists police and security forces in enhancing the law enforcement.

Recommended resolutions

The requirements of all applications described in this section lead to a set of recommendations for the constellation. An overview of these resolutions is given in table 3.2. As there is a wide range of possible resolutions, the subsequent sections will deal with achieving the most optimal resolutions while staying competitive.

	Spectral band	Spatial res.	Temporal res.
Environmental applications			
Agriculture	VIS & NIR	High	Medium high
Forestry	VIS & TIR	Medium	Medium
Polar ice	VIS & TIR	Low	Very low
Oceanography	VIS & TIR	Low	Medium
Glacier monitoring	NIR & TIR	Medium	Low
Disaster monitoring applications			
Forest Fires	NIR	Medium	High
Volcanoes	NIR & TIR	Medium	Medium
Hurricanes	VIS & TIR	Medium low	High
Damage monitoring	VIS	High	High
Oil spills	NIR	Medium	High
Other applications			
Defence & Security	VIS	Very high	Very high

Table 3.2: Environmental monitoring applications

3.3.2 Filtering viable applications

In the concept phase a bottom-up design process has been followed to determine the potentially competitive areas of a CubeSat constellation consisting of the three given cameras. The main conclusions are that a CubeSat constellation:

- Is unable to compete with constellations capable of delivering very high spatial resolutions (below 3.75 m) due to technical restriction of the camera
- Can compete with constellations providing medium to high spatial resolution images (above 3.75 m), by delivering the same performance for a much lower price
- Has the inherent advantage of providing a high temporal resolution because of the many satellites it consists of

In order to get the best design the constellation must be able to meet application requirements while being competitive. The key factor of being competitive is defined above as providing mid to high resolution images for a lower total cost than competitors. The total cost is greatly dependent on the amount of satellites in the constellation. In other words, the number of satellites is a direct cost driver.

A bottom up approach in constellation design is applied in the sense that for a given constellation, as many applications are covered as possible. By finding an optimum between the applications covered and the total constellation cost, the most optimal competitiveness of the constellation can be found. For this, the set of application requirements in terms of spatial, temporal and spectral resolution, are used from table 3.2.

Approach to constellation optimisation

The approach of optimising a constellation design follows two steps. First, a constellation is designed by taking into account the requirements of *all* relevant applications, which results in a constellations that is capable of covering all applications but which

however is not necessarily competitive. Then the competitiveness of this system is analysed and expressed as difference in total cost between the CubeSat constellation and the total cost of competitors delivering the same performance. At this stage it will become clear whether or not this typical combination of spatial/temporal resolution, number of satellites and total cost is competitive.

Taking this competitiveness analysis as guideline, decisions must be made to change the constellation in such a way that a more efficient balance between meeting application requirements and being competitive is obtained. For example, lowering the number of satellites makes the constellation less expensive but also lowers the temporal resolution. The significant reduction in cost can however, potentially, increase the competitiveness, causing a possible market push. Another outcome can be that it is impossible to serve a certain application need in any competitive way, meaning that this application is disregarded altogether. This new, probably smaller, set of requirements is backed by the competitiveness analysis and will result in a new constellation design. In practice this iteration is done multiple times; e.g. changing spatial requirements within the range in which they are expected to serve the needs and monitoring the impact on total cost and thus competitiveness. The goal is to end up with the best combination of meeting requirements while at the same time being competitive meeting these requirements.

Initial Constellation Design

The initial constellation design encompasses all applications mentioned in section 3.3. The resulting requirements are listed in table 3.3.

	Unit	ANT-2 RCC (VIS)	ANT-2 TMA (VIS&NIR)	ARCTIC (TIR)
Spatial resolution	$m/pixel$	1-4	15	58
Temporal resolution	-	Daily	Daily	Daily
Orbital height	km	250	300	461

Table 3.3: Requirements of initial constellation design

This design meets all requirements for each application in terms of spatial, temporal and spectral resolution and coverage as can been seen by comparing table 3.2 and 3.3. Now it is time to check if this constellation is competitive; e.g. delivering the same mid resolution performance as already existing satellites for a lower cost.

To meet the requirements in terms of spatial and temporal resolution the RCC must be positioned in a 250 km altitude orbit. However at this altitude it has a considerably low swath width of 7.5 km resulting in the need of 114 satellites for a temporal resolution of one day. Comparing to competitors like *RapidEye* it becomes clear that this design overshoots its goals: it is not delivering the same mid resolution performance for a lower cost, but for around the same cost, and thus is not competitive.

The combination of high spatial resolution of 3.75 m and temporal resolution of 1 day for all cameras is technically feasible but not competitive. This means that these requirements should either be discarded, eliminating certain applications, or the requirements must be relaxed.

An argument for relaxing the requirements could be finding a new, possibly competitive balance between spatial/temporal resolution and cost, essentially entailing a market push. In other words, delivering slightly less quality for a considerably lower cost could serve a new customer pool.

Improved constellation design

Following the results of the competitiveness analysis from the first constellation design, some requirements were relaxed and others were disregarded totally, resulting in a new set of requirements, stated in table 3.4. Herein, the spatial resolution has been mostly kept, while decreasing the temporal resolution of the RCC camera platform. As a result, significantly fewer satellites are needed, dramatically decreasing the total cost.

Parameter	Unit	ANT-2 RCC (VIS)	ANT-2 TMA (VIS&NIR)	ARCTIC (TIR)
Spatial resolution	$m/pixel$	4	25	56
Temporal resolution	-	Weekly	Daily	Daily
Orbital height	km	288	500	443

Table 3.4: Requirements of improved constellation design

Analysis of improved design

The result of the improved design is that it serves all the requirements for a subset of applications. A total of 88 satellites are used while the constellation meets the mid-resolution requirements which can be competitive compared to companies like *RapidEye*.

Several uncertainties and variations remain however, which need to be taken into account:

- Total cost is estimated as a multiplication of number of satellites and unit cost only
- Application requirements are uncertain. Market needs constantly change, knowing what customers exactly are willing to pay or find attractive is very difficult
- Impossible to predict the benefit of delivering a slightly less quality for much less money; a market push at this state is hard to predict

3.3.3 Coverage

The satellites do not need to take images from the Earth during the entire orbit. If it does so, the amount of data for downlink becomes too large, especially for the visual spectrum. Therefore, the satellites only image the parts of the Earth that are interesting for the application. In this section, this coverage area is determined per camera.

Required coverage

For further sizing of the spacecraft and ground segment, a measure called the *required coverage* will be calculated. The required coverage defines the percentage of the area which is of interest to a certain camera, with relation to the global area. The required coverage is therefore not only a requirement for an imaging mission wanting to image the applications mentioned in this analysis. It is also a measure for the percentage of the Earth area covered, and thus the quantity of imaging data that can be sold.

Area covered by the ANT-2 RCC camera platform

As shown in table 3.2 the images from the ANT-2 RCC camera serve applications for agriculture, oceanography and disaster monitoring. The camera can only image a subset of oceanography however, being coral monitoring. This is reflected in figure 3.4. An assumption is made where disasters are most likely to occur. Only disasters regarding earthquakes, floods and damage due to tsunamis are considered. In addition, the areas where the corals can be monitored and the areas where crops are grown, are included in figure 3.4.

By calculating the percentage of the area of interest shown in figure 3.4 the duty cycle can be determined. It thus appears that the duty cycle for the RCC camera is 17 %.

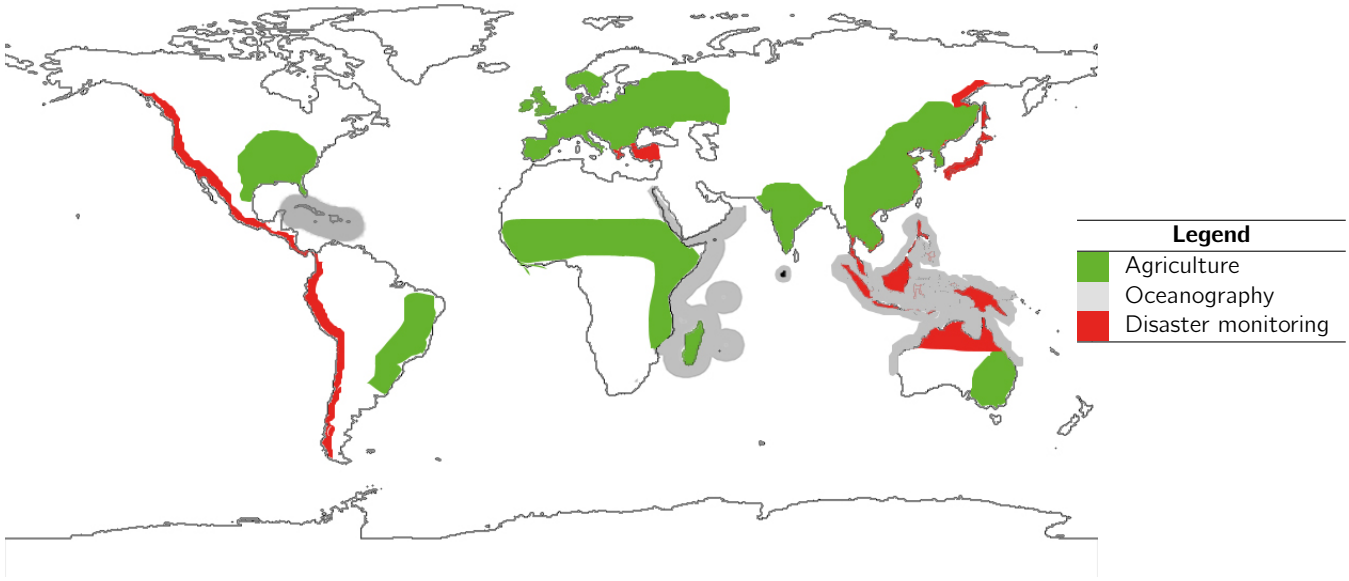

Figure 3.4: Area covered by the ANT-2 RCC camera platform

In figure 3.4 is shown that there is no need for a global coverage for the ANT-2 RCC camera. The part of the Earth that should be imaged is mainly between 60°N and 60°S.

Area covered by the ANT-2 TMA camera platform

The ANT-2 TMA camera is suitable for monitoring agriculture, forestry, polar ice and oceanography. The main driver for the coverage area of the TMA camera is the phytoplankton application. Phytoplankton exists especially in cold waters just above and below the polar cycles (between 60° and 80° latitude). Furthermore in the area of disaster monitoring applications, the TMA is very well suitable for forest fires, volcanos, floods, etc., as can be seen in table 3.2. In figure 3.5 the interesting areas for the TMA camera are shown.

For this camera, the coverage is 28 %.

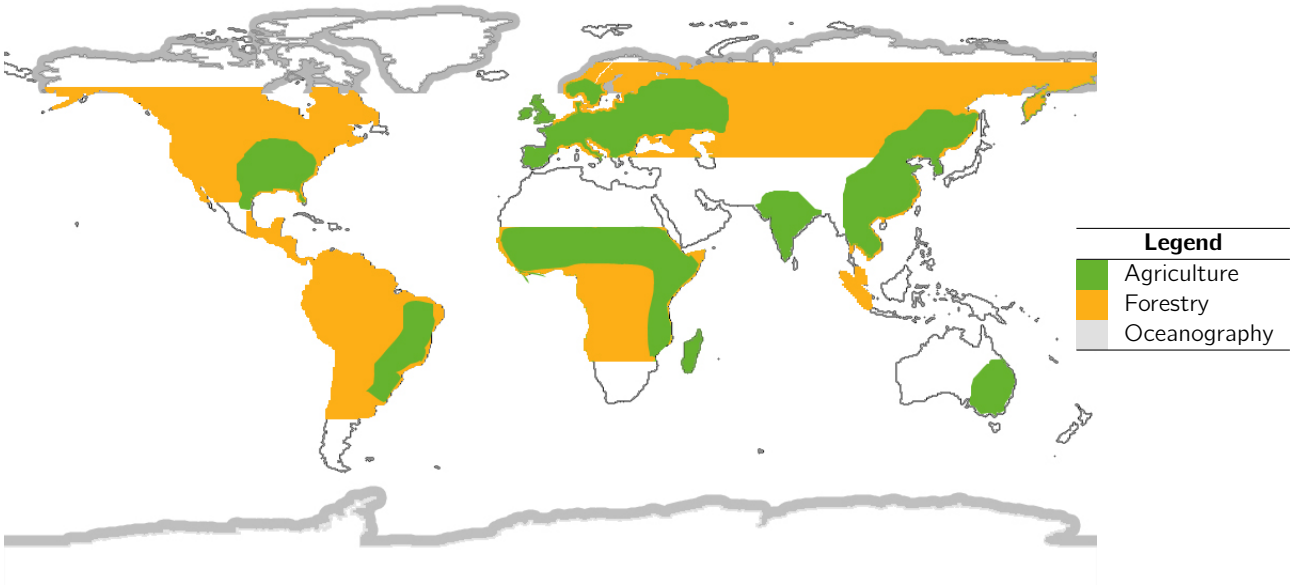

Figure 3.5: Area covered by the ANT-2 TMA camera platform

Area covered by the ARCTIC camera platform

As stated in table 3.2 the ARCTIC is used to monitor ice and surface temperatures. Ice monitoring applies to the polar areas and mountainous areas where glaciers are present. The applicable areas for these applications are given in figure 3.6.

For this camera, the coverage is 29 %. As can be seen in figure 3.6, the main driver for the large coverage is the coverage for ice monitoring, which takes up all space above 60°N and below 60°S.

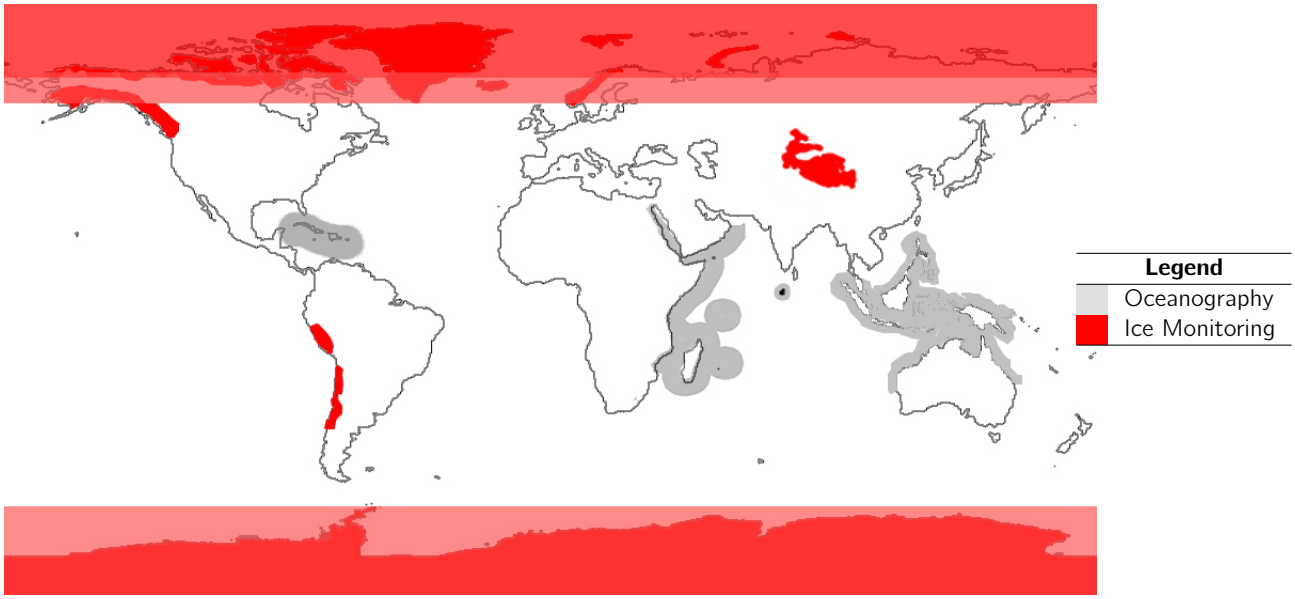

Figure 3.6: Area covered by the ARCTIC camera platform

To monitor the coral reefs a lower inclination orbit, with an inclination of about 30°, is sufficient. However, since the ARCTIC should also monitor the ice at the poles, full coverage of the Earth is needed. Therefore the only way to serve these application is to use a polar orbit.

Total required coverage

Table 3.5 lists the required coverage for all platforms. The ARCTIC and ANT-2 TMA camera cover approximately equal areas, albeit different areas, as can be seen in figures 3.6 and 3.5. These numbers show that a constellation containing all three of these cameras covers an average of **25 %** of the Earth surface.

Camera platform	Req. coverage
ANT-2 RCC	17 %
ANT-2 TMA	28 %
ARCTIC	29 %
Average	25 %

Table 3.5: Coverages

3.4 Competitors

The Earth observation sector is already being served by a number of constellations, giving rise to the question where an interesting market niche or area of improvement is present. An overview of the current competitors is found in table 3.6. The tendency towards heavy satellites has already been revealed in section 3.2.1, but is endorsed in this section with some examples.

3.4.1 Disaster Monitoring Constellation (DMC)

The *Disaster Monitoring Constellation* currently consists of five satellites, all designed by Surrey. Three of them are SSTL-100's and are owned by Nigeria, the UK and Spain. Then there is a SSTL-150 owned by China and a SSTL-300 owned by Nigeria [25]. Performance varies from 5 to 32 $m/pixel$ spatial resolution in the multispectral band and the constellation has a temporal resolution of one day. The unit cost of a SSTL-300 is USD 23.5 M and the unit cost for the SSTL-100 is assumed to be lower than the SSTL-150. Adding up these unit costs gives a total spacecraft cost around USD 80 M. Taking into account launch and operational cost however, the total cost will be much higher.

More importantly in terms of competition, recently Surrey received a 110 M pound contract to develop a new DMC constellation, the DMC3[26]. Consisting of three SSTL-300S1 satellites with an assumed unit cost higher than the SSTL-300 these satellites have a spatial resolution of 1 $m/pixel$ and a daily revisit time. The launch of these satellites is planned for 2014. Important to note is that the DMC website[25] states that it provides free imagery in the case of international disaster.

3.4.2 GeoEye

The *GeoEye* constellation currently consists of the GeoEye-1 and IKONOS satellites. In the near future the GeoEye-2 satellite will be added to the constellation. Panchromatic spatial resolution ranges from 0.34 (GeoEye-2) to 0.82 (IKONOS) $m/pixel$ and multispectral spatial resolution from 1.36- 3.2 $m/pixel$. The satellites have a mass higher than 700 kg and are positioned in a 681 km orbit around the Earth.

3.4.3 RapidEye

The *RapidEye*[27] constellation consists of 5 SSTL-150[28] satellites designed by Surrey. These satellites have a mass of around 150 kg, have a daily revisit time and provide a spatial resolution between 2.5 and 5 $m/pixel$ from their orbit altitude of 630 km. The unit price of each satellite is USD 16.5 M adding to a minimum of USD 80 M constellation material cost. This is of course only the spacecraft cost; by including launch and operating cost the total cost is much higher.

As *RapidEye* is a commercial competitor offering imaging data at a fixed price per square kilometer to a wide range of customers, this company appears to be the most direct competitor to the C^{3}EO constellation. As *RapidEye* sells imaging data at 0.95 EUR/km^2, a straightforward goal becomes apparent: in order to become competitive in this market segment, the C^{3}EO constellation must offer the same performance for a lower price [27].

Characteristics	Units	DMC	DMC3	RapidEye	GeoEye (2013)
In operation since	-	2005	2014(planned)	2008	1999
Number of Sats	-	5	3	5	2 (3)
Type of sat	-		SSTL-300S1	SSTL-150	GeoEye-1/2/Ikonos
Sat Cost	M USD	10 - 23.5		16.5 m	?
Sat Mass	kg	100-350	350	153	726-2150
Orbit height	km	> 600	500	630	681
GSD M/S	m	5-32	3	5	1.36 - 3.2
Spectral bands	-	RGB,NIR	RGB,NIR	RGB, NIR	RGB, NIR
Mission lifetime	y		7	7	>10
Revisit time	$days$	1	1	2	3
Swath width	km		23	20	11.3 - 15.2
Development time	$months$			24	

Table 3.6: Constellation comparison

3.4.4 Conclusion

It is clear from these examples that current Earth observation constellations consist of a small number of satellites, each having a high mass and high unit cost, with a roughly estimated total mission cost in the order of several hundreds of millions of euros when cost like operational and launch cost are taken into account. These constellations typically have a high performance in terms of spatial resolution, varying between 5 $m/pixel$ up to the sub-meter level, together with a daily revisit time. A direct competitor in the field of a nanosatellite constellation for Earth observation is currently non-existent. However, it has become apparent, that *RapidEye* is a direct competitor, albeit using conventional satellites. Therefore, this competitor will be compared with in the cost analysis in chapter 18, to validate the competitiveness of C^3EO.

At the moment a nanosatellite constellation can not compete with the very high resolution these expensive constellation deliver, in the order of 0.5 - 1 m, due to technological restriction in the camera. A spatial resolution that is slightly less, e.g. 4 $m/pixel$ is feasible however, and could potentially be highly competitive with already existing systems. It is important to note that further technological improvement in the area of CubeSat sized camera performance has the potential to compete even with the highest performance, expensive Earth observation constellations.

3.5 Customers

Governments will continue to take up a large part of the consumers pool. This is expected to be a result of security reasons and research. Furthermore, governments are expected to continue their contribution to disaster monitoring constellations, like for example the Disaster Monitoring Constellation [25] because of their clear importance in times of disaster.

Besides governments, organizations form a possible customer pool. The fields of research and humanitarian affairs could request image data for their resource allocation. Examples are independent organizations occupied with tackling the food and water scarcity problem, wildlife funds monitoring deforestations and animal population.

Delivering imagery to mass markets is another market strategy aimed at increasing the number of customers. By making use of the internet as an interface and by forming a market need by delivering a product for such a low price that individuals become customers would radically increase the customer pool; this principal follows the push-pull technology.

3.6 Vision & Market need statement

In this section a vision is formed using the results from the market survey. This vision is translated into a market need statement; which is a single sentence containing market requirements and drives the conceptual design.

The advantages of small satellites over large satellites in terms of reduced development time and cost are pointed out in section 3.2. However, a reduced satellite size results in a limited camera aperture. If a high spatial resolution is required the orbiting altitude has to be lowered, increasing the temporal resolution of a single satellite. The significantly low unit cost of a single satellite however provides the option to use more satellites in a constellation, which compensates the loss in temporal resolution, while still having a lower total cost. Thus a constellation of low-cost satellites potentially is a highly competitive alternative for missions requiring high spatial resolution together with high temporal resolution. The design of such a competitive constellation is the vision of this project. The two cameras, ANT-2 and ARCTIC, designed specifically for these nanosatellites by two previous DSE groups, with the ANT-2 being an improved version of the ANT, are used in the design process and implicitly need to be inserted in a VLEO to achieve the competitive spatial resolutions. Satellites in VLEO require a ΔV budget to account for the drag that is encountered at this lower altitude.

The vision results in the following market need statement:

> *"Produce images for environmental and disaster monitoring using a low-cost solution equipped with ARCTIC and/or ANT-2 cameras at a low altitude to achieve high spatial resolution."*

Chapter 4 | System definition

Before starting the design of a constellation and the corresponding satellite, it is important to know which requirements need to be fulfilled and what the relation between the single parts of the system are. In this chapter the requirements, which were determined in earlier phases of the project, are presented. In section 15.7, the design is checked with these requirements and possible alterations are explained. Furthermore the system definition and the used cameras are presented. The interrelation between subsystems as well as functions that must be performed are presented in the system definition section. Finally, an overview on the three camera cornerstones is provided in section 2

In section 4.2 the interrelation between the subsystems and the functions which need to be performed is shown. The section about cameras gives a short overview of the cameras used in this project.

4.1 Requirement analysis

A solid list of requirements is important in the design process of the systems being developed during the detailed design phase. These requirements determine which specifications the subsystem needs to fulfil. The requirements are based on research performed during earlier phases of the project and requirements given in the project guide [29]. The requirements are presented in a list and a discovery tree. In the table the requirements are split up in market and system requirements.

4.1.1 Requirement discovery tree

The requirement discovery tree is a tool to compile and organize all identified requirements. It is used to visualize to the list of requirements and show their relation to each other. These are distributed on an AND-Tree which has two main branches, the market requirements and the system requirements, as shown in figure 4.1.

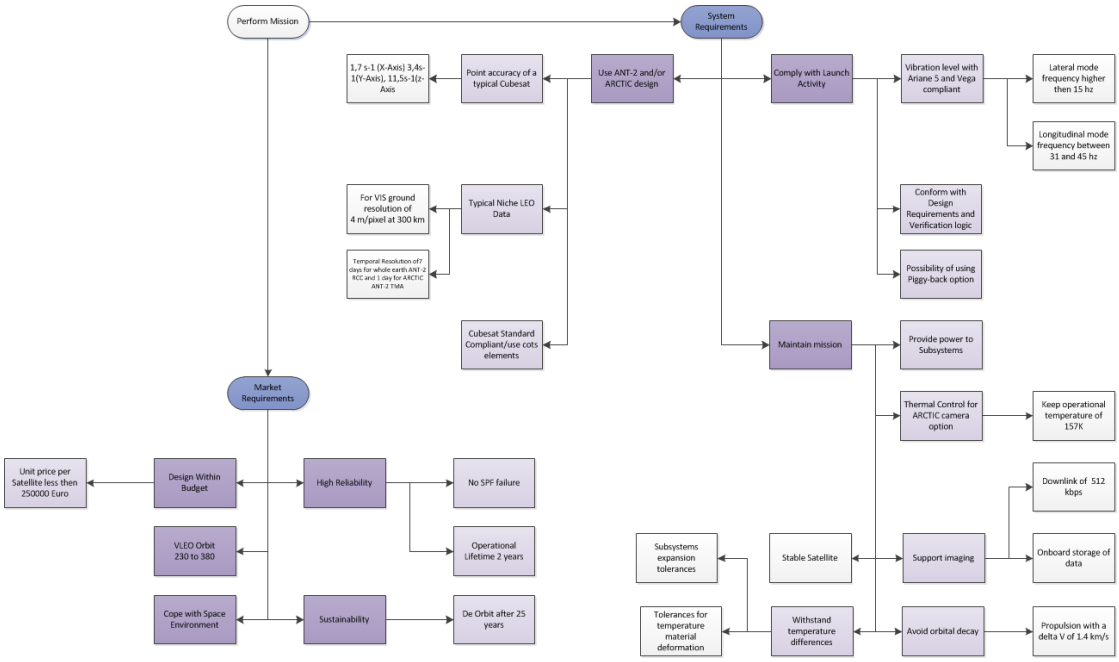

Figure 4.1: Requirement Tree

Market requirements

The market analysis formulates the need for a niche application in a very low orbit. To fulfil this need, additional requirements such as drag compensation are added to the list. Furthermore, the market requirements dictate the cost budget which defines the competitiveness of the system.

System requirements

The system requirements are determined using the project guide[29], the ARCTIC and ANT-2 Reports [30][31], the user manuals of the launchers [32][33] and research done in earlier phases of the project. It defines which specific requirements should be fulfilled by the system, such as payload requirements and mission maintenance.

List of Requirement

A list of requirements based on the requirement discovery tree is provided in table 4.1. A unique identifier is assigned to each requirement as well as a source. Requirements related to outside sources are referenced in the last column. The Top-level requirements are mostly based on the the project guide [29], which are the source from which most of the other requirements are determined. The major requirement is to use an ANT-2 or ARCTIC design camera, all other sub requirements relating to the camera design are taken from the project guide [29]. The driving requirements have a large impact on the design of the constellation. These are the unit price, the cameras used and the range of possible orbits heights.

ID Lvl. 1	ID Lvl. 2	ID Lvl. 3	ID Lvl. 4	Description	Type of Requirement	Source
1.0				Market requirements		
	1.1			Design within budget		[29]
		1.1.1		Unit price per satellite less than 250000 EUR	Driving requirement	[29]
	1.2			High reliability		[29]
		1.2.1		No SPF failure	Top Requirement	[29]
		1.2.2		Operational Lifetime of 2 years	Top requirement	[29]
	1.3			VLEO orbit	Driving requirement	
		1.3.1		230 to 380 km		
	1.4			Cope with space environment		[29]
	1.5			Sustainability		[29]
				De-Orbit after maximum of 25 years		[29]
2.0				System requirement		
	2.1			Use ANT-2 and/or ARCTIC design	Driving requirement	[29]
		2.1.1		Pointing accuracy of typical CubeSat		[29]
			2.1.1.1	1.7 s^{-1} (X-Axis), 3.4 s^{-1}(Y-Axis), 11.5 s^{-1}(Z-Axis)		[29]
		2.1.3		Provide typical LEO Earth observation data		[29]
			2.1.3.1	VIS ground resolution of 4 m/pixel		[29]
			2.1.3.2	Temporal Resolution of 24 hours for whole Earth and 30 min for 5%		[29]
	2.2			Comply with launch activity	Top requirement	[29]
		2.2.1		Withstand vibration level of Ariane 5 and Vega		[29]
			2.2.1.1	Lateral mode frequency higher than 15 Hz		[33] [32]
			2.2.1.2	Longitudinal mode frequency between 31 and 45 Hz		[33] [32]
		2.2.2		Possibility of using piggy-back option		
	2.3			Maintain mission	Top requirement	[29]
		2.3.1		Provide power to camera		TB
		2.3.2		Thermal control for ARCTIC camera option		[31]
			2.3.2.1	Keep operational temperature at 157K		[31]
		2.3.3		Support imaging		[29]
			2.3.3.1	Downlink capabilities of 512 kbps		[31]
		2.3.4		Avoid orbital decay	Driving requirement	
			2.3.4.1	Propulsion capabilities to compensate drag over two years lifetime		Astro
		2.3.5		Withstand differences		
			2.3.5.1	Keep subsystem expansion tolerances		
			2.3.5.2	Keep tolerances for temperature material deformation		
		2.3.6		Stable satellite	Top requirement	

Table 4.1: List of Requirements

4.2 System breakdown

Before the subsystems are developed in detail it is important to define what the system consists of and what the interrelations of the parts are. This is possible with systems engineering tools, such as the functional flow diagram and the N^2 chart. These tools are used to identify all important design parameters such as interfaces and functions. Visualizing these provides a clear overview and acts as guideline during the design process.

4.2.1 N2-Chart

The N2 chart is a systems engineering tool to identify and visualise the various interdependencies and relations between the different subsystems of the constellation. Main functions of the system are arranged on the diagonal of a square matrix and their relations on the other field. For the space segment subsystem such as structure, power and thermal control are not shown as these need to perform during the total mission duration. The space space segment describes the functions of a satellite and the ground segment describes the terrestrial operations. A description of each relation can be found in table 4.2.

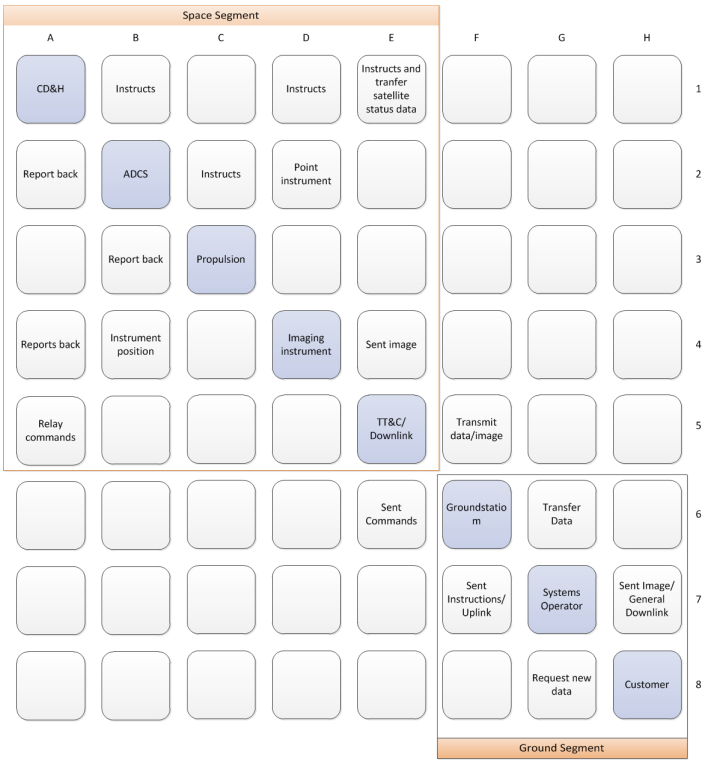

Figure 4.2: N2 Diagram

A different visualization of the system is shown in figure 4.5. In the diagram the interrelations are shown between single part of the systems. It includes systems which are omitted in the N^2, to show the influence of system such as structure, power, orbit mechanics and thermal control. Its main focus is in the subsystems of a single satellite.

4.2.2 Functional flow diagram

The diagram shows the order of the functions the system needs to perform. A general concept of an Earth observation mission is created in a Functional flow diagram in figure 4.3. It shows the required system functions from launch to de-orbit of the system. The diagram can be divided into three different phases: the build-up, the operation and the end of life. The build-up phase consists of all activities which are performed before the satellite can enter normal operating condition. This phase includes the launch and all initial orbit operations. The normal operation phase follows, in which the constellation performs the Earth observation mission. It continues until the satellite reaches the end of their life time after two years. At the end of life phase the satellites de-orbit. It is important to note that this diagram does not include time-independent variables such as thermal control or attitude control which are active throughout the whole mission. The diagram is used to identify the functions that the system performs and their sequence. A more detailed diagram for the functional flow of a single satellite of the constellation is shown in figure 4.3.

4.2.3 Functional breakdown structure

The Functional Breakdown Diagram splits every function the system has to perform in an ordered way. Unlike the Functional flow diagram, it also contains all time-independent functions and presents a different view on the system. It splits the mission into two functions which need to be performed, one is the operation of the system of satellites and the other is the ground operation. A breakdown into lower level function can be seen in the diagram figure 4.4.

Location	Description
B1	The CD & H instructs the ADCS for possible orbit manoeuvres.
D1	The CD & H commands the Imaging Instrument to take images.
E1	The CD & H instructs the TT & C/Downlink when to downlink the data.
A2	The ADCS informs the CD & H with the completion of its assignment.
B2	The ADCS instructs the propulsion unit to activate if needed for manoeuvre.
D2	The ADCS is pointing the imaging instrument to its designated target area.
B3	The Propulsion unit reports back to the ADCS if its finished with its assigned tasks.
A4	The Imaging Instrument reports back to the CD & H if it is finished with its assigned tasks.
B4	The Imaging Instrument reports its current position to the ADCS.
E4	The Imaging Instrument sends the captured image to the TT & C/downlink.
A5	The TT & C/Downlink relays the received commands from the g/s to the CD & H.
F5	The TT & C/Downlink transfer the images and other data to the g/s.
E6	The g/s transmit commands to the TT & C.
G6	The g/s transfer the data to the systems operator.
F7	The System Operator sends new commands to be transferred to the g/s
H7	The System Operator transmits the edited images to the customer
G8	The customer requests new images from the System operator

Table 4.2: N2 Chart

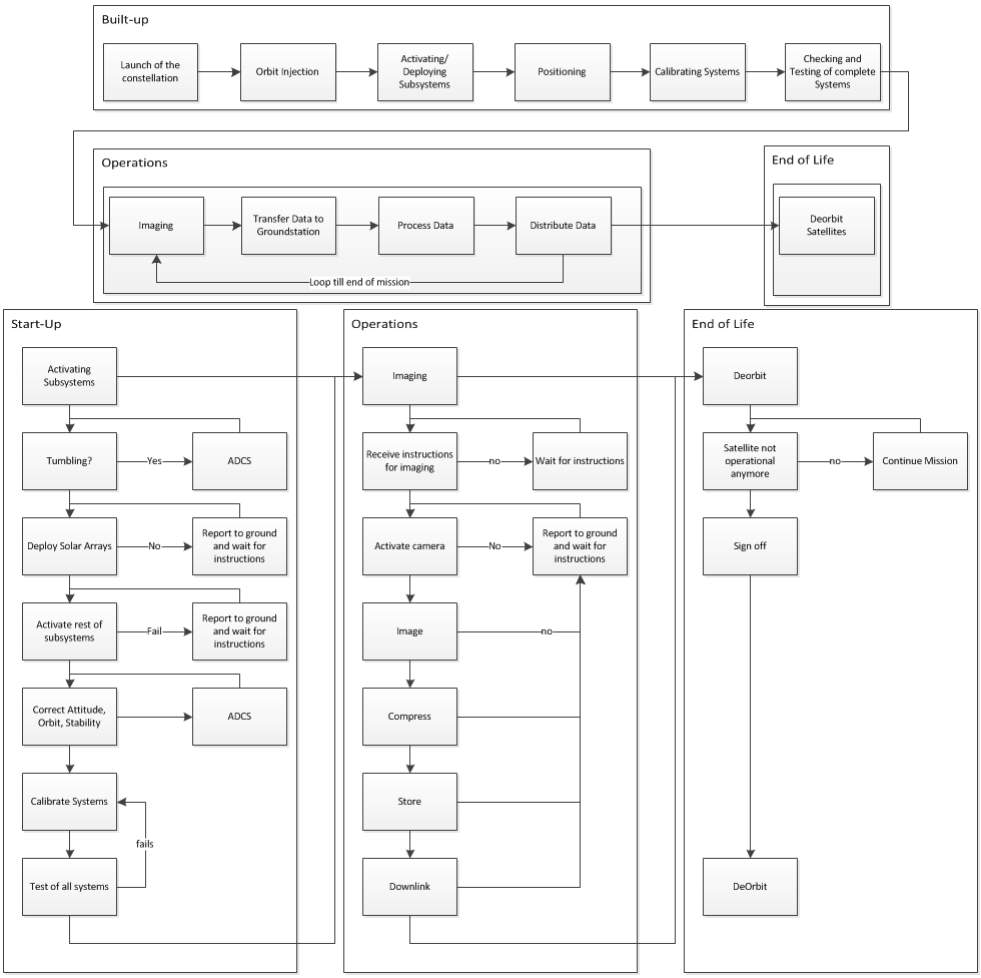

Figure 4.3: Functional flow diagram for a Satellite

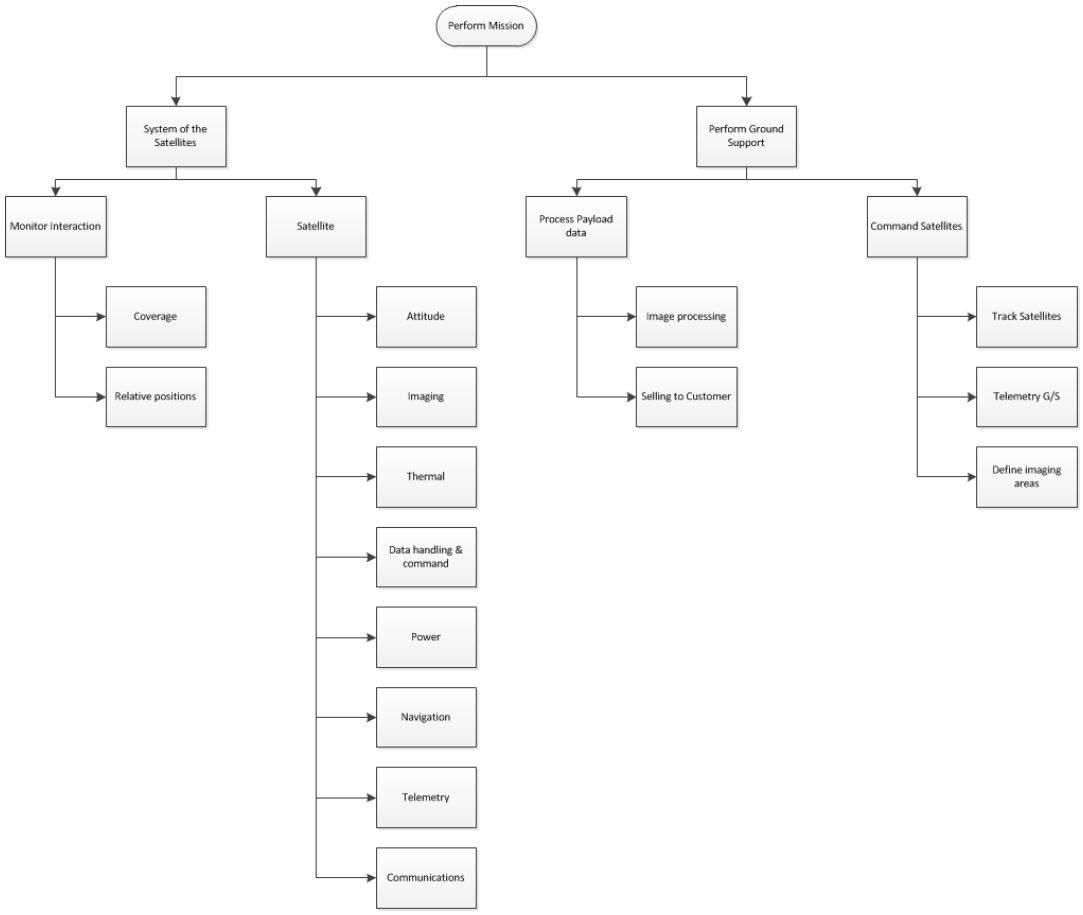

Figure 4.4: Functional breakdown structure

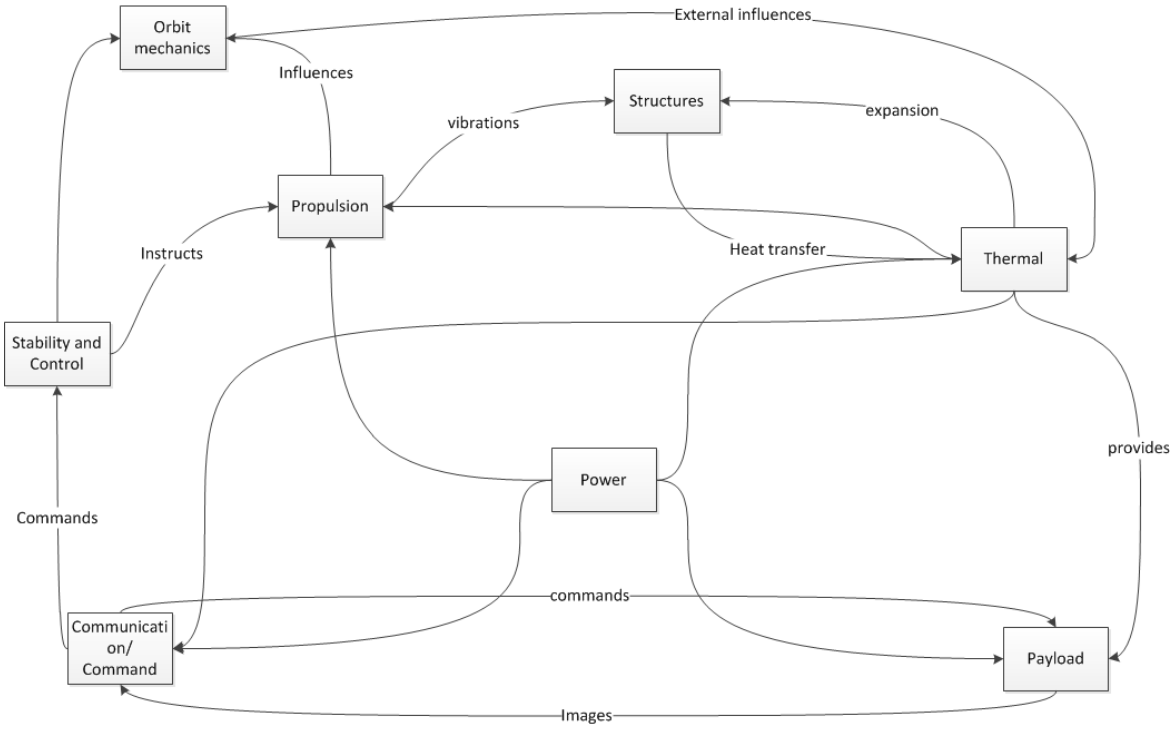

Figure 4.5: Overview of the System Interrelations

PART II

CONSTELLATION SEGMENT

Chapter 5 | Constellation

In this chapter the design process of the constellation is described. Each satellite type used has a set of requirements for the spatial resolution and revisit time. These requirements are given in section 5.1 and drive the orbit design for single satellites. This is provided in section 5.2. In this section the calculation of the minimum number of satellites is also described. The first problem in the selection of orbit heights is caused by repeating orbits. This is covered in section 5.3 as well as the final selection of the orbit heights for the different satellites. With these variables set, it is determined whether a solution with the minimum number of satellites actually exists, which is done in section 5.4. In section 5.5 the problem caused by the difference in ascending and descending ground tracks is dealt with. The final step of positioning all satellites within the constellation is worked out in section 5.6.

5.1 Orbit specifications

The constellation is built up of three parts. Each part is a collection of satellites using a single type of camera. For each part there are different requirements for spatial resolution and revisit time. The spatial resolution has a linear relation with the orbit height, so the required resolution results in a maximum orbit height. The maximum orbit height (H_{orbit}) is calculated using the orbit height (H_{org}) and spatial resolution (res_{org}). These are given for each of the cameras. The target resolution (res_{target}) is determined by the market analysis in chapter 3. The maximum orbit height is calculated using equation 5.1:

$$H_{orbit} = res_{target} \cdot \frac{H_{org}}{res_{org}} \tag{5.1}$$

Lowering the orbit only increases the spatial resolution and is therefore possible. However this decreases the amount of ground covered by the satellite within a time interval. Therefore the number of satellites to meet the required revisit time increases. To prevent this the maximum orbit height dictated by the spatial resolution is used when possible. The choice of camera and application also requires the use of specific orbits. For both the visual cameras daylight is required to function, while even constant lighting is preferable. Therefore for the two parts of the constellations equipped with visual cameras the sun-synchronous dawn-dusk orbit is selected. In the third part of the constellation no lighting is needed for the infrared ARCTIC camera to function, however for the selected applications coverage of the poles is needed. To provide this coverage, a polar orbit is selected for these satellites. In table 5.1 an overview of these values is provided.

Camera	Spatial resolution [m/pixel]	Maximum orbit height [km]	Revisit time [days]	Inclination [deg]
ANT-2 RCC	4	288	7	96.6
ANT-2 TMA	25	500	1	97.4
ARCTIC	56	443	1	90

Table 5.1: Requirements for each part of the constellation

5.2 Ground coverage of a single satellite

In order to calculate what part of the Earth is imaged by a single satellite, a number of variables have to be known. The first is the orbit height of the satellite. This height has been determined in the previous section. The second variable is the field-of-view angle of the camera used on board the satellite. These two values determine the area that the satellite can image at a single point in time. The satellite covers the earth in a straight track, therefore the important factor is the width of this track. This swath width is determined in equation 5.2. For this calculation the part of the Earth that is imaged is assumed to be flat. The curvature of the Earth is negligible for the small area that is covered.

$$w_{swath} = 2 \cdot \tan(\frac{\theta_{FoV}}{2} \cdot H_{orbit}) \tag{5.2}$$

Multiplying the swath width by the circumference of the Earth leads to the total area covered by a single satellite in one revolution. Dividing the total surface area of the Earth by the coverage of a single satellite over a specific time period leads to a minimal number of satellites for full coverage in that time period. However there is no way to devise all orbits in such a way that these areas are covered without any overlap.

A second approach is mainly focussed on the equator. Every orbit crosses the equator at some point. After a certain number of passes by satellites, the entire equator has been viewed. Assuming the same inclination for all satellites, full coverage of the equator leads to maximum coverage of the Earth. The maximum attainable coverage is only limited by the inclination chosen. This maximum coverage is considered the full coverage for the selected inclination. The ground paths of the satellites only move closer together when further away from the equator, so no gaps can form between the paths. For now it is assumed that the different ground paths of the satellites fit perfectly together. In section 5.5 this is dealt with in more detail.

The downside of this method is that at higher latitudes the amount of overlap of the ground tracks increases greatly. However, assuming only a single inclination for all satellites, this yields the minimum number of satellites to achieve maximum coverage.

The part of the equator imaged on a single pass also depends on the inclination (i) used. With lower inclinations a single pass will cover a larger part than the swath width. For polar orbits the part covered is exactly the swath width. The calculation for the number of passes required for maximum coverage becomes:

$$n_{pass} = \frac{L_{eq} \cdot \sin(i)}{w_{swath}} \tag{5.3}$$

With each revolution the satellite passes the equator twice, once ascending and once descending. The time between two consecutive passes is half the orbital period of the satellite:

$$\frac{T_{orbit}}{2} = \pi\sqrt{\frac{a^3}{\mu}} \tag{5.4}$$

The total time needed to provide the full coverage is the number of passes times half the orbital period. The last step is dividing this total time by the necessary revisit time. This results in the minimum number of satellites to provide the full coverage of the Earth in the time allotted.

$$t_{total} = \frac{T_{orbit}}{2} \cdot n_{pass} = \frac{\pi \cdot L_{eq} \cdot \sin(i)}{w_{swath}}\sqrt{\frac{a^3}{\mu}} \tag{5.5}$$

$$n_{sats} = \frac{t_{total}}{t_{revisit}} \tag{5.6}$$

5.3 Avoiding repeat orbits

Performing the calculation for the number of satellites in section 5.2 results in the minimum number of satellites for which full coverage may be possible. Using fewer satellites is not possible since the sum of the coverage of all the satellites is insufficient. However, designing a constellation with this minimum number of satellites is still impossible for certain orbit heights.

In order to determine exactly which part of the equator is covered by a satellite a simulation is made. The total length of the equator is divided into a number of sections. Each section has a counter that indicates the number of times it has been imaged by a satellite. The orbital characteristics of the satellites are used to determine the locations at which it crosses the equator. According to the height and swath width a number of sections close to the satellite's position are imaged. The counter of these sections is therefore increased by 1. This process is repeated until the total time the satellite has been orbiting passes the chosen maximum revisit time. The percentage of the equator that has been covered by the single satellite this way determines the minimum number of satellites required.

This first part of the simulation gives an indication of a number of impractical orbit heights. These orbits are mostly repeat orbits. All circular orbits are in essence repeat orbits, but the problem arises when the satellite repeat time is smaller than the required revisit time. At this point additional satellites are needed to provide full coverage. The exact height at which the satellite enters repeat orbits depends on the inclination used. A second problem that arises is caused by descending tracks crossing a part of the equator already imaged on an ascending track. These give smaller spikes in the number of satellites, but orbits with this effect should be avoided. When an inclination and maximum orbit height are selected for a constellation the previously described calculations are used for the final selection of the orbit height.

5.3.1 Constellation layer ANT-2 RCC camera

The first part of the constellation uses the ANT-2 RCC camera. In order to get the required resolution of 4 m/pixel the satellites need to be at an orbit height of 288 km. The satellites are in a sun-synchronous orbit and the required revisit time is 7 days. The number of satellites necessary to meet these requirements for different orbit height are given in figure 5.1. The selected orbit height is close to the large peak between 291 km and 295 km. This peak contains the one day repeat orbit, which causes the large increase in satellites needed. The orbit height of 288 km is not in any local peak and is therefore a practical orbit height to use. This orbit height results in a total number of satellites carrying the ANT-2 RCC of 22.

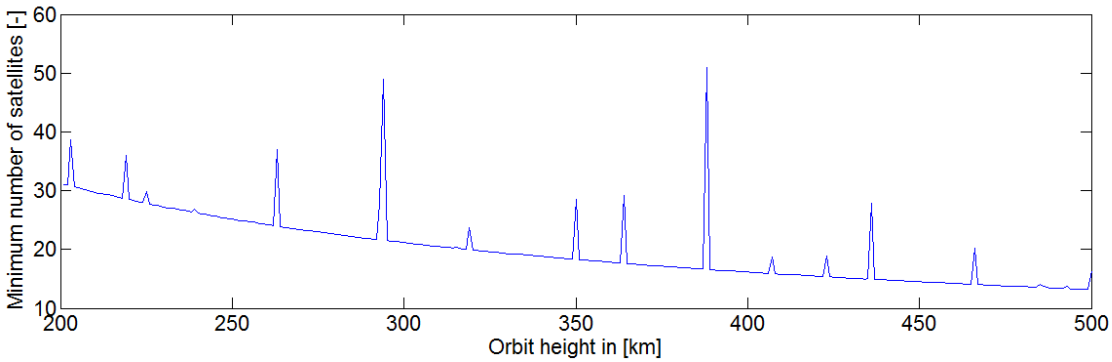

Figure 5.1: Satellites per orbit for ANT-2 RCC

5.3.2 Constellation layer ANT-2 TMA camera

For the second part of the constellation the ANT-2 TMA camera is used. To achieve the resolution of 25 m/pixel the satellite has to be positioned at an orbit height of 500 km. The orbit is sun-synchronous for this visual camera and the revisit time is to be a single day. From figure 5.2 it is determined that there is a slight bump in the number of satellites around the 500 km mark. The bump cannot be caused by repeat orbits because the simulation is only done for a single day. The only other cause is that the descending tracks of the satellites cross the equator at the same point where some ascending tracks pass. The bump causes a small increase in the number of satellites. However the number of satellites indicated in the figure always have to be rounded up. Both before and after the small bump the number of satellites, when rounded up, is 26. Therefore there is no need to change the orbit height.

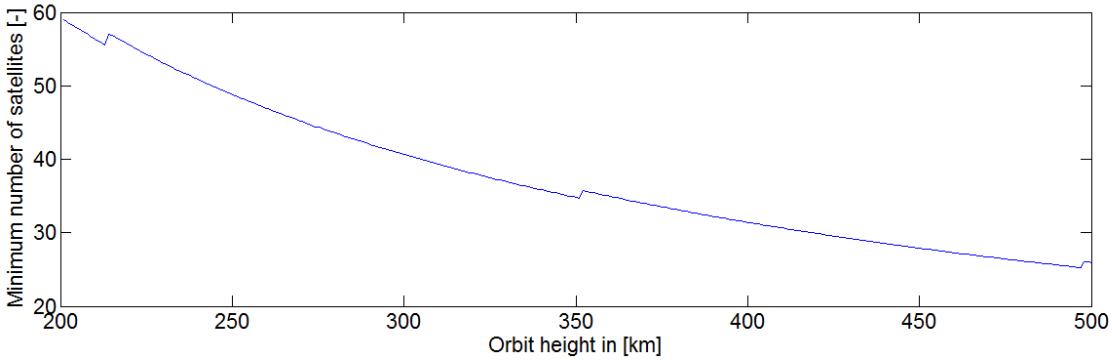

Figure 5.2: Satellites per orbit for ANT-2 TMA

5.3.3 Constellation layer ARCTIC camera

For the third and final part of the constellation the ARCTIC camera is used. The required resolution for the camera is set at 56 m/pixel. This results in a maximum orbit height of 443 km. The inclination for these satellites differs from the previous part, since it uses an inclination of 90 degrees. As in the previous part of the constellation the graphs have no major spikes, as can be seen in figure 5.3. The smaller bumps are around 350 and 500 km. These bumps have no influence anywhere near the required orbit height. Therefore 443 km can be used for the part of the constellation. This results in a minimum number of satellites of 36.

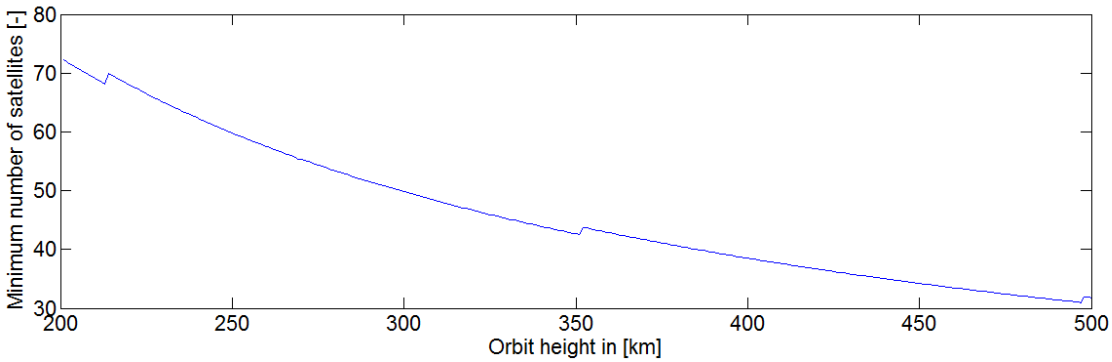

Figure 5.3: Satellites per orbit for ARCTIC

5.4 Solution with minimum number of satellites

At this point the orbit height and inclination for each part of the constellation is determined. The heights are selected in such a way that the coverage of a single satellite does not repeat within the necessary revisit time. The part of the equator covered by the satellite in this time leads to the minimum number of satellites that could possibly provide full coverage. A simplified pattern of the coverage of the equator is provided in table 5.2. In this table the A represents the coverage by the ascending path of the satellite. The D represents the coverage of the descending path.

A	0	0	D	0	0

Table 5.2: Simplified coverage of the equator for one satellite

A simple solution as given in table 5.2 would result in a minimum number of satellites of three. Adding two more satellites and shifting the coverage of each satellite to the right by one step leads to:

A	A	A	D	D	D

Table 5.3: Simplified coverage of the equator for three satellites

This simplified example indicates that for a given configuration the optimal solution might be possible. Providing proof that this holds for any satellite configuration is harder. An example for which the optimal solution is not possible can be easily provided:

The example in table 5.4 shows that for an arbitrary coverage array it is not always possible to get full coverage with an optimal number of satellites. A single satellite fills up a third of the array, but after adding a second satellite there is no longer a way to fit a third satellite without overlap. This example does, on second inspection, have a flaw. The patterns generated by a satellite always result in a repeating pattern. The distance between the first ascending path and the first descending path is equal to the distance between the descending path and the next ascending path. For a period of one day the coverage pattern is a simple repeating pattern. By adding a couple of these patterns the result is full coverage. The simple example is given in tables 5.2 and 5.3, but the same technique works for larger patterns.

For patterns of satellite coverage over a period of several days combining them becomes more complex. The first assumption to be made is that only efficient orbits are used. This means that for a single satellite, for a given number of days, the ascending and descending tracks will never cover the same part of the equator twice. The orbits to be avoided are determined in section 5.3. As in the case for a single day, for multiple day coverage, the distance between the ascending and descending path remains equal. The distance between the first ascending path on day one and the first on day two is also constant.

Table 5.5 shows three examples for two day coverage of a single satellite. In all three examples the pattern can be filled by correctly adding a single satellite. In the case of examples two and three extending the coverage to four days would fill the pattern with only one satellite. This is not possible for the first example because the ground track of A_3 would cover the same part as D_1. When the distance between the tracks in increased, more satellites are required to fill the pattern. But the repeating nature of the tracks stays the same. Therefore even with pattern for the coverage of several days, a full coverage pattern can always be created with the minimum number of satellites.

Satellite 1	A	0	D	0	0	0
Satellite 2	0	A	0	D	0	0
Total	A	A	D	D	0	0

Table 5.4: Simplified coverage and summation for two satellites

Example 1	A_1	0	A_2	0	D_1	0	D_2	0
Example 2	A_1	A_2	0	0	D_1	D_2	0	0
Example 3	A_1	0	0	A_2	D_1	0	0	D_2

Table 5.5: Simplified coverages for one satellite over multiple days

5.5 Discrepancy between ascending and descending paths

The first assumption made for this approach is that the full coverage of the equator provides complete coverage of the Earth. One part of this assumption is that all ground tracks have the same direction. If the ground track of a ascending path goes straight up, the track of the descending path goes straight down. However this is a unique case for a special inclination. The inclination is in this case such that it exactly compensates for the rotation of the Earth underneath the orbit, therefore resulting in a ground track perpendicular to the equator. When any other inclination is used there will be an angle between the ground track and the perpendicular path. Ground tracks that are under an angle still fit together, but the angle is in the opposite direction for the ascending and descending paths.

When the track of an ascending path is next to a descending path on the equator, there is a gap in the coverage on one side of the equator. The location on the opposite side of the equator has double coverage at the same time. At any location on the Earth the ground tracks form a pattern as shown in figure 5.4.

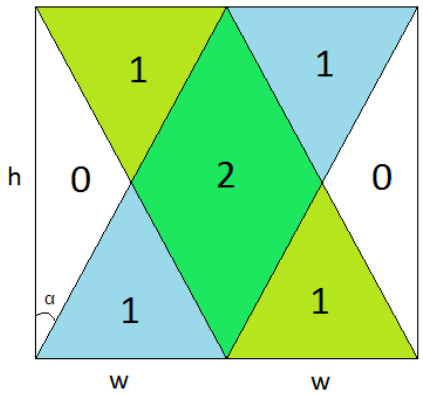

Figure 5.4: Repeating pattern of ground tracks

The figure shows two ground tracks with opposite angles with respect to the equator. The center of the figure shows the overlap of the paths with double coverage. To the right and left are the gaps in the coverage. The tracks shown in this figure can consist of any number of tracks. Any number of ascending tracks next to each other are followed by the same number of descending tracks. Therefore this pattern repeats all over the Earth. The height in the figure depends on the angle between the tracks and the equator. When the angle α becomes smaller the whole figure is elongated, but still the resulting pattern will repeat. The part of each repeating pattern that is not covered can be calculated:

$$\frac{2\frac{\frac{1}{2}wh}{2}}{2wh} = \frac{\frac{1}{2}wh}{2wh} = \frac{1}{4} \tag{5.7}$$

From equation 5.7 it can be determined that the area not covered is independent from either h or w. Therefore the angle between the equator does not change the coverage gap. An exceptional case is the perpendicular one, where the gap remains zero.

Additional satellites are required to avoid these gaps. Every added satellite increases the overlap at the equator, but also adds extra ascending and descending paths to the system. The gaps in the coverage decrease in size with each added satellite. The gaps disappear once the number of satellites is doubled. In this case the descending paths can be ignored completely. There are enough satellites to fill the coverage pattern with only ascending paths. This option is however not very efficient because each part of the Earth is now covered at least twice within the revisit time.

For the requirement that each location should be covered within the revisit time at any point during the mission, there is no other option than to double the number of satellites. However looking at an average over the whole mission, the calculated minimum number of satellites is sufficient. Though a specific location is not imaged during one revisit period, it is recorded in one of the next periods. This loss of information is compensated in a later period, when the area is covered twice. additionally, the further the location is from the equator the more times it is covered per period, because the ground tracks start to converge closer to the poles.

Taking into account that covering the last 25% of the Earth requires doubling the number of satellites, and that the requirements are already met on average, increasing the number of satellites is very costly for little gain. Therefore it is assumed that the minimum number of satellites per constellation part calculated in section 5.4 is sufficient for the complete constellation.

5.6 Division of satellites in orbit planes

The next step in designing the constellation is to position every satellite in an orbit in such a way that the maximum coverage is attained. From section 5.4 it follows that such a solution exists. Simulation of a single satellite results in a pattern similar to the simplified patterns from section 5.4. The only difference being the size of the pattern, since it now represents the entire equator with steps of 100 m. The first satellite will start of at 0 degrees longitude at the equator, on an ascending path. The second satellite is positioned on a slightly higher longitude in such a way that the ground tracks exactly fit together. This process is repeated until a newly added satellite would cross a part of the equator that is already covered. The first conflicting path discovered in this way is either a descending path, or an ascending path from a later day of the satellites ground coverage (only in the case of multiple day revisit time). It is possible that at this point the full equator has been imaged, but this would require a very specific coverage pattern. In most cases the coverage is again zero after the conflicting path. The next satellite is positioned so that its ground track fits at the end of the conflicting track. At this point the previous steps are repeated until the total number of satellites equals the minimum number calculated previously. At that point the constellation provides full coverage of the equator.

Each satellite is now positioned in a different orbit plane. This is impractical for two reasons. First, for the visual cameras light is required. When arbitrary orbits are used some satellites are unable to image due to darkness for large parts of the orbits. At the same time the lighting conditions are not the same for any two satellites. The second problem with different orbit planes is the deployment. The amount of δV required for changing planes is very high. If each satellites has to perform a great amount of plane change, the required propulsion increases drastically. The best way to solve these problems is to put all satellites into one orbit plane and phase them out in the same plane. For the visual satellites the optimal orbit is the sun-synchronous dawn-dusk orbit. For the infra red satellites no specific orbit plane is determined, but the satellites are grouped to reduce the deployment cost.

It is possible to shift a satellite from one orbit plane to another while keeping the ground coverage the same. Apart from the change in orbit plane a change in orbit phase is applied for a satellite. The result is that the satellite provides coverage of the same part of the Earth, only at a different local and universal time. The change in local time is the part that was required, since now the lighting conditions are equal for all satellites. The change in when the part is covered (universal time) is of no influence because the coverage is provided over the course of a full day (or multiple days).

Now the steps described in this section are applied to each of the parts of the constellation.

5.6.1 Placement of ANT-2 RCC satellites

The ANT-2 RCC camera used in the first part of the constellation has the smallest field of view angle of the three cameras. It is also at a low altitude which makes the swath width very small. The result is that the initial positioning of the satellites along the equator requires the satellites to be grouped closely together. The longitudinal offset between two successive satellites at the equator is 0.073 deg. The first group of six satellites starts with the first positioned at 0 deg longitude. A seventh satellite cannot be placed next to the first six because its ground track overlaps a previous one. The second group starts at 3.2 deg longitude and consists of six satellites. The third group is positioned at the same interval at 6.4 deg. A smaller group of four satellites is used to fill the last gaps in the coverage. This last group is positioned at 9.6 deg longitude.

The orbital period for a satellite at 288 km is 5409 s. This results in a total number of orbits per day of 15.98. The completion of one orbit changes the longitude of the satellite by 22.5 deg. If all satellites are shifted to a single orbital plane the offset between two successive satellites in the orbital plane becomes:

$$360 \cdot \frac{0.073}{22.5} = 1.168\,\text{deg} \tag{5.8}$$

The same calculation results in a 51.1 deg for the offset between the satellite groups. The resulting constellation is depicted in figure 5.5

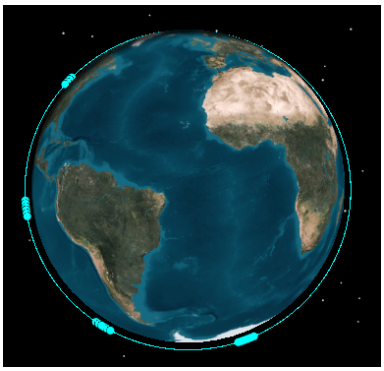

Figure 5.5: ANT-2 RCC satellites in the constellation

5.6.2 Placement of ANT-2 TMA satellites

The second part of the constellation consists out of satellites carrying the ANT-2 TMA. This camera has the largest field of view angle of the three cameras used and is also at the highest altitude (500 km). This results in the satellites being placed further apart, however more are needed since this part of the constellation has a revisit time of one day. The offset between two successive satellites is set at 0.46 deg. This offset assures that two successive ground tracks exactly fit together.

The satellites are put together in three groups of 8 and a single group of 4. The offset between the groups is set at 6.85 deg. Every completed orbit changes the location of the ascending path by 23.6 deg. When the satellites are shifted to a single orbit plane the offset between two successive satellites becomes: 7.0 deg. The offset between the groups of satellites is: 104.4 deg. The resulting constellation is depicted in figure 5.6

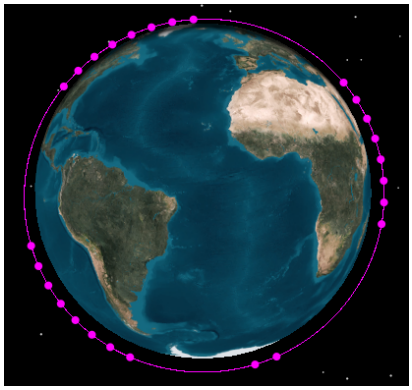

Figure 5.6: ANT-2 TMA satellites in the constellation

5.6.3 Placement of ARCTIC satellites

The final part of the constellation consist of the satellites with the ARCTIC camera. These satellites are in a polar orbit with the inclination of 90 deg. The orbit height is set at 443 km. To fit the ground tracks the individual satellites should be split by 0.326 deg at the equator. The satellites are grouped together in two groups of 18 satellites. The offset between the two groups at the equator is 180 deg. These distances on the equator result in a division on the same orbit plane of 5.03 deg per satellite and 258 deg between the two groups. The resulting part of the constellation is depicted in figure 5.7.

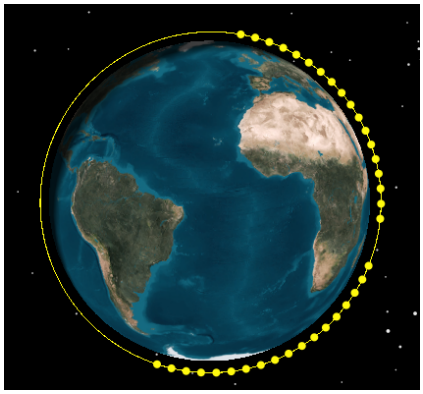

Figure 5.7: ARCTIC satellites in the constellation

Chapter 6 | Launcher

In this chapter the selection and consideration of the launch segment is presented. Since no big missions are planned to the required altitudes and inclinations, piggy back options are not considered. Therefore a dedicated launch vehicle is selected. Focus in the selection process lies on cost effectiveness. First, some general considerations on the possible launch vehicles are presented, followed by a trade-off. Concluding the most important parameters and implications of the selected launch vehicle are presented.

6.1 Launcher considerations

The constellation consists of three different platform configurations orbiting on three different inclinations. To avoid plane change manoeuvres, which require high ΔV and are very complex, the three elements will be launched on three different launchers. Since each element is modest in mass as depicted in 6.1 the launch vehicle should be modest in capacity as well. By using a small launch vehicle, the launcher can be filled effectively resulting in a low price per launched payload. In the total constellation mass there is a 10% contingency included.

Parameter	Unit	RCC constellation	TMA constellation	ARCTIC constellation
Launch mass of constellation material only	kg	130	150	210
Orbit height to which payload must be send	km	288	500	443
Inclination which payload must be send	deg	96.6	97.4	90

Table 6.1: Mission parameters

The three launch segments consist of 24 ANT-2 RCC satellites, 27 ANT-2 TMA satellites and 37 ARCTIC satellites. It should be noted that the launcher payload mass does not include only the satellite masses but also the mass of a deployment system and payload fairing. An ejection pod that can be considered is the one used for the QB-50 mission. It is assumed that ejection pod and fairing will be 20% of the total satellite mass.

Four launch vehicles are considered; the Shtil 2.1, Rockot, Dnepr and Vega. The main parameters of each launch vehicle are presented in table 6.2. It should be noted that the presented payload capability decreases with the orbital height that the payload should be delivered to as well as the inclination. Launching to a higher inclination lowers the payload capacity. The four presented launch vehicles are all designed to launch small payloads in a cost effective way.

Parameter	Unit	VEGA	Dnepr	Shtil 2.1	Rockot
Launch cost	$MEUR$	32	10-13	1-3	11
Payload Capacity max	kg	2000	4.500	230	1.950
Reference inclination	deg	69.5	98	25	70

Table 6.2: Launch vehicle parameters

All selected launchers are capable of reaching a sun synchronous inclination.

6.2 Trade-off

As seen in table 6.2 ,it becomes clear that the Shtil 2.1 is the most efficient option from a cost and mass perspective. Therefore the launch segment will consist of three Shtil 2.1 launch vehicles launching the three constellation segments into orbit.

The total mass of the payload that has to be launched is 20 % above the launch mass of the constellation, shown in table 6.1. It is assumed that this fits the 230 kg payload capacity of the Shtill 2.1. The Shtill 3.0 can be used if this is not the case. The latter is a final proposed version with 430 kg payload capacity instead.

6.3 Shtil 2.1

The Shtil 2.1 is used three times for the three batches of platforms. It is launched from the Barents sea on a submarine. The launch is relatively cheap since it is a converted intercontinental ballistic missiles and has already been produced in great quantities and is funded by the Russian government. It is built and operated by the Makayev Design Bureau. In 2015 the Shtil 2.1 will be used for the first time. That is to launch the QB50 mission, 50 NanoSats into LEO. The Shtil is a three stage liquid fuelled rocket and is one of the smallest launch vehicles available.

Figure 6.1: Types of Shtil Rockets

Table 6.3: Shtil 2.1 parameters

Parameter	Units	Value
Static Loads	g	3 with peaks to 7
Altitude accuracy	km	5 - 10
Inclination accuracy	deg	0.05 - 0.1
Max orbital height	km	400

Table 6.3 gives an overview of the most important parameters of the Shtil 2.1 launch vehicle. The Shtil 2.1 has some inaccuracies in its orbit injection. These quantities are taken into account in the design of the propulsion subsystem as seen in chapter 11. If the inaccuracies are unacceptable for the mission, the propulsion system compensates for them. It should be noted that the angular inaccuracies are one order of magnitude smaller that the accuracies of COTS CubeSat sensors. The launch loads are assumed to be manageable by the COTS components as the Shtil is used to launch the QB 50 mission which uses standard CubeSat structures.

A launch price of 3 million EUR is assumed per launch vehicle, but a margin of thirty percent is taken into account. This margin should account for adapter cost as well as possible need for a kick stage if the upper stage of the Shtil 2.1 proves to be incapable of the required plane change manoeuvre. It also accounts for the increase in cost if the Shtil 3 is required. With this margin, the total launch cost is projected to be 13 million EUR.

Launch vehicle Parameter	Unit	Shtil-1	Shtil-2.1	Shtil-2R	Shtil-3
Launch vehicles		Shtil-1	Shtil-2.1	Shtil-2R	Shtil-3
Number of stages		3	3	3	3 + booster
Missile length	m	14.8	16	18.3	19
Missile diameter	m	1.9	1.9	1.9	1.9
Launching weight	$tons$	39.3	39.7	40	44
Volume of payload	m^3	0.195	0.25	1.17	3.6
Characteristics circ. orb 79°:					
Orbit altitude	km	200/ 400/ 600	200/ 400/ 600	600/ 800/ 1000	200/ 400/ 800
Payload weight	kg	280/ 80/ 80	200/ 140/ 50	220/ 200/ 170	430/ 360/ 240

Table 6.4: Shtil family characterstics

6.4 Conclusion

The launch vehicle selection is mainly based on cost. Since the three launch batches are of low mass, a small launch vehicle in needed. Currently the Shtil 2.1 is the most cost effective solution available to launch the entire constellation. The launch segment consists of three Shtill 2.1 launchers which will each inject a platform of satellites into their target orbit. Doing so the satellite needs to be designed to account for phase change manoeuvres, but complex plane change manoeuvres are not necessary. Injection inaccuracies are small but need to be accounted for by the propulsion system design. The total projected launch cost is estimated to be 13 million EUR.

PART III

SPACECRAFT SEGMENT

Chapter 7 | CubeSat Structure

The structural integrity of the platforms is of utmost importance if it is to withstand launch operations and the space environment. Furthermore, attention should be given to the component positioning and satellite cross-section area for drag reduction in a low Earth orbit. In this section a walk-through of the structural requirements is given, followed by the available options and final design choice. A mass budget is also provided at the end of this section.

7.1 Structural requirements

The requirements are mainly driven by launch loads as well as payload fairings and drag issues. The worst case launch loads are taken in order to choose a structure, which can be seen in table 7.1. Furthermore, the qualified design loads for CubeSat standard skeletons available off-the-shelf are also shown for comparison.

Load type	Unit	Highest Load	Launcher	CubeSat Design Loads
Static longitudinal Load	g	+8.1	ROCKOT	21.6
Lateral Static Load	g	+2.5	PSLV	21.6
Sine Vibration	g, Hz	3.85, 5-100	PSLV	4, 5-100
Random Vibration	$grms$	6.7	PSLV	14.1

Table 7.1: Launch loads and associated Launcher compared to design loads

From table 7.1 it can be seen that the launch loads are met by standard CubeSat structures. Secondly, since the platforms are using these standard structures, the payload fairing requirements are automatically met. The remaining requirement is then related to drag reduction, i.e, get the maximum possible reduction in cross-section area perpendicular to the satellite's movement. This is achieved by selecting the positioning and orientation of the camera.

7.2 Camera positioning

In order to reduce drag in a very low Earth orbit, three approaches are considered:

1. Conventional design with 4 CubeSat units placed in a row with a camera in the bottom 2 units and pointed nadir, as shown in figure 7.1
2. place the camera horizontally in a 5U CubeSat structure with a mirror to redirect the image into the camera. A sketch of this option can be seen in figure 7.2.
3. place the camera vertically in a 2 by 2 CubeSat structure, as seen in figure 7.3.

The first option is a conventional CubeSat structure with the 4 units positioned in a row other and the camera in the bottom, as shown in figure 7.1, directly pointing to the Earth. Such a design has a frontal area of 0.04 m^2. This option yields the highest cross-section area perpendicular to the movement and poses a challenge in terms of antenna positioning; a patch antenna pointing nadir can only be achievable by developing a deployment system that releases it from the side of the CubeSat, increasing overall complexity.

The 5U arrangement shown in figure 7.2 provides the smallest cross-section with $10 \times 10cm$, reducing it by a factor of 4 when compared to the conventional design. Furthermore, the horizontal placement of the units provides a practical placement for the transceiver and telemetry antennas facing nadir. The implication is however that the camera is now pointing into space instead of onto the Earth. To overcome this problem an extra Cube needs to be added to accommodate a mirror. Taking the CubeSat mass values from the CubeSat shop [34] a single cube has a mass of 200 grams for primary and secondary structure.

The mirror should have a low thermal expansion coefficient to be able to maintain its shape in space. Taking Zerodur [35] as reference with a 2.53 g/cm^3 density and using it for a mirror of 10 by 10 cm and 1 cm thickness this adds up to a mirror mass

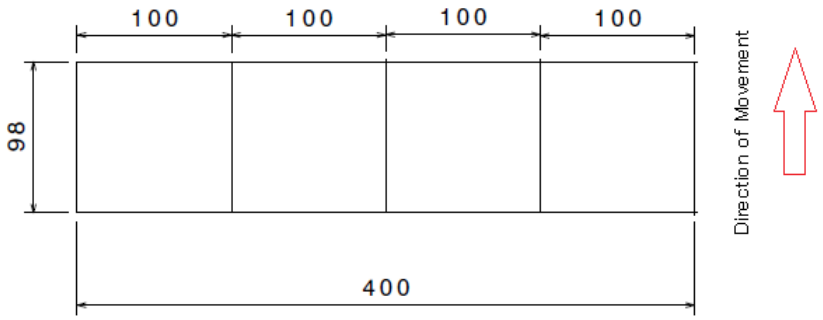

Figure 7.1: Draft of a 4 Unit design; dimensions in mm

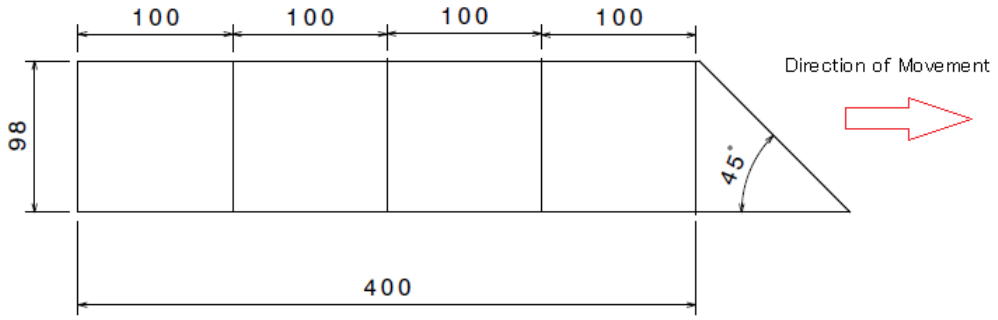

Figure 7.2: Draft of a mirror design; dimensions in mm

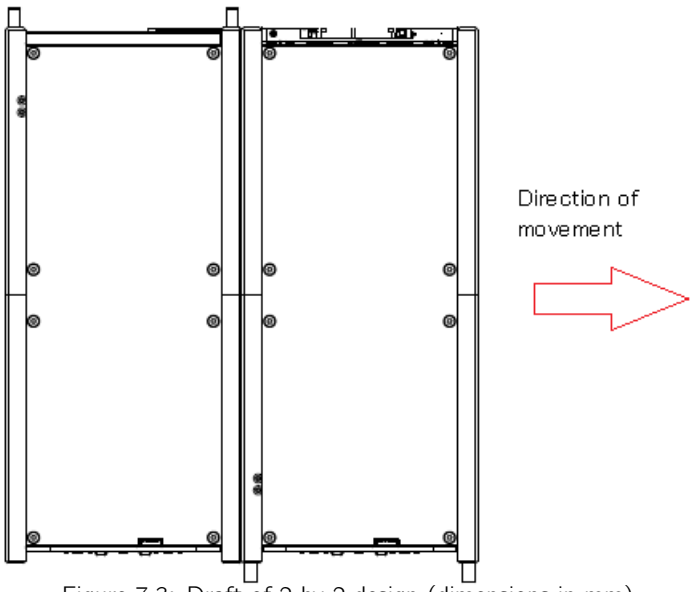

Figure 7.3: Draft of 2-by-2 design (dimensions in mm)

of around 250 grams. Assuming 50 grams of mounting materials to mount the mirror in the Cube this adds to a total added weight of 500 grams.

The 2-by-2U option shown in figure 7.3 has a cross section which is twice larger than the mirror arrangement,at 0.02 m^2, but requires no structural modification for a mirror, resulting in a 4U instead of a 5U structure. It also provides a position for a telemetry antenna and patch antenna at the bottom for nadir pointing.

Of these options the 2-by-2U is deemed to be the most interesting. Even though it has twice the cross-section area and thus increased drag, the extra propellant mass needed to compensate for the drag is still smaller and the mass of an extra cube unit with a mirror attached to it; 100 g extra propellant versus 500 g of a cube with a mirror attached, as further explained in chapter 11. Furthermore, this design choice is as simple as the conventional configuration, since the only modification is attaching two 2U CubeSat structures, whereas the mirror option is more complex and would have to be re-qualified for launch loads.

It is important to note that all three camera platforms follow the same structural arrangement for conformity and consistency's sake. However, the solar panel placement and thermal structure differ for the ARCTIC platform as its requirements are different thermal- and orbit-wise.

7.3 Subsystem arrangement

Given the 2-by-2U CubeSat layout, an arrangement of the several subsystems is required. The internal layout of the RCC and TMA cameras can be seen in figure 7.5. The ARCTIC platform's layout is fundamentally different as the camera alone takes up 2 units of space, versus the 1.5 units taken up by the RCC and TMA. This is not an issue, because the ADCS of the higher orbiting platforms are likely to weigh less than the lower orbiting platforms as disturbance torques will be smaller for the higher orbiting platforms.

The solar panel placement is mainly dependent on the solar cell area required as well as the type of orbit.

For the RCC and TMA platforms, the solar panels have to be placed on the CubeSat's side. The platforms are in sun-synchronous dawn dusk orbit, which mean their relative attitude to the sun is constant and the incidence angle between sun and solar panels can be minimized. This arrangement can be seen in figure 7.6. During launch the solar panels are folded over each other and deployed by a simple spring design once in orbit.

The ARCTIC platform is placed in a polar orbit, such that the solar panels must be placed on the top face of the CubeSat for minimum incidence angle. The remaining views and dimensions of the RCC and TMA assembly can be found in appendix F.

7.4 Mass budget

Since most of the components of the CubeSats are off-the-shelf the mass budget is relatively accurate, with exception to the ADCS, propulsion and thermal systems; these still require a high contingency due to their low technology readiness and level of detail used in its mass estimation. The contribution of all the subsystems and contingencies of the platforms can be seen in table 7.2. A more detailed sheet with all the components and individual masses can be found in appendix E.

Subsystem	Mass [g] ANT / ARCTIC	% of total mass	Contigency %	Allocated mass [g]
ADCS	515	12	30	670
C & DH	497	9 / 8	0	497
EPS	640 / 940	13 / 18	8 / 7	707 / 1060
Mechanical system	100 / 150	2	15 / 20	115 / 180
Payload	1650 /1664	36 / 29	20 / 0	1980 / 1664
CubeSat Structure	780	15	5	819
Thermal Control	40 / 250	1 / 5	50 / 35	60 / 312
Connections	90	2	15	104
Propulsion system	200	10 / 9	29 / 27	258 / 254
Dry mass	4512 / 5086	100	16 / 10 (average)	5210 / 5560

Table 7.2: Allocated mass of each subsystem for all platforms

As expected, the largest contribution is from the payload which comprises of the cameras. The mass budget of the ARCTIC platform is heavier than the other two platforms due to its necessity to have a thermal shield and different solar panels.

The contingencies shown in table 7.2 are mostly related to technology readiness as well as the satellites total mass which varies considerably through the research and development phase. For example, the high contingency of the propulsion system is associated to how it is still a technology in an experimental phase. Those with low or non-existent contingencies are COTS components where precise mass values are known. The end masses are well within acceptable ranges, especially taking into account the limiting factor imposed by the structure, which can carry a maximum of 8 kg. Surprisingly, the final mass is also not very different from the initial estimate obtained during the conceptual design phase. A record of the masses throughout the detailed design phase was kept such that the evolution in platform mass can be assessed; these values are shown in a scatter plot according to the date in which they were generated in figure 7.4.

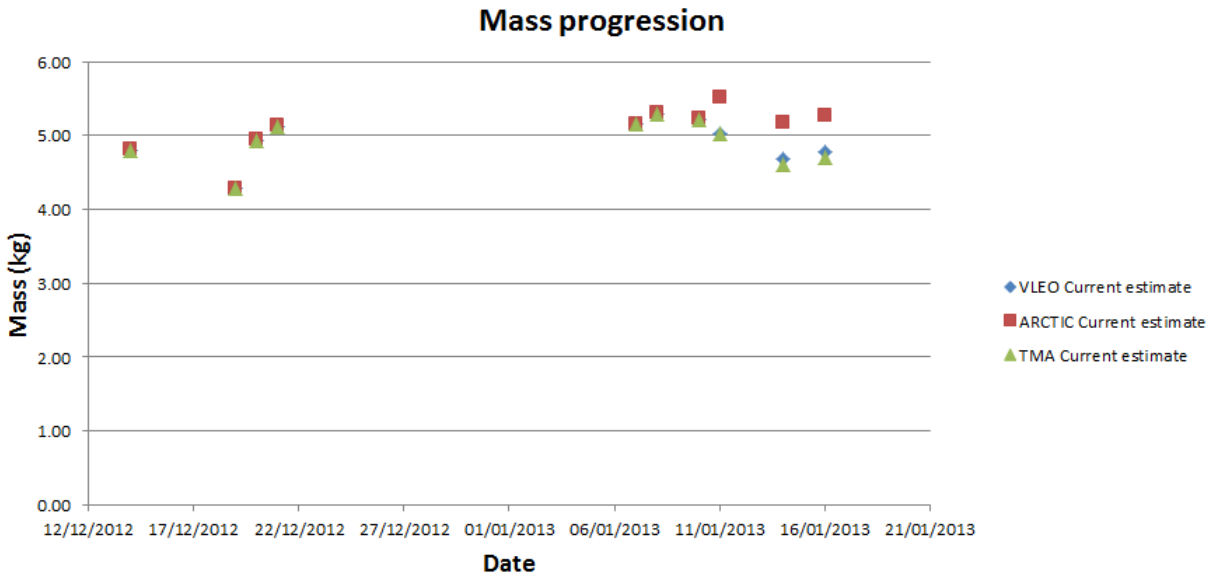

Figure 7.4: Platform mass budget changes through the detailed phase

7.5 Constellation mass

The total constellation mass can be computed once the number of satellites is known as well as the unit mass. The breakdown of the mass per platform can be seen in table 7.3.

Platform	Unit mass [kg]	# of satellites [-]	Total dry mass [kg]
ARCTIC	5.1	37	189
RCC	4.5	24	108
TMA	4.5	27	122
Total	-	88	419

Table 7.3: Total constellation mass

When selecting a launcher, it is important to pay attention to the fact that each platform must be placed in a different orbit, hence that they will have to be launched separately. Furthermore, it is important to account for the added weight of the payload fairings required to launch and deploy the satellites. These can add as much as 3 kg per satellite to the total launch mass [36].

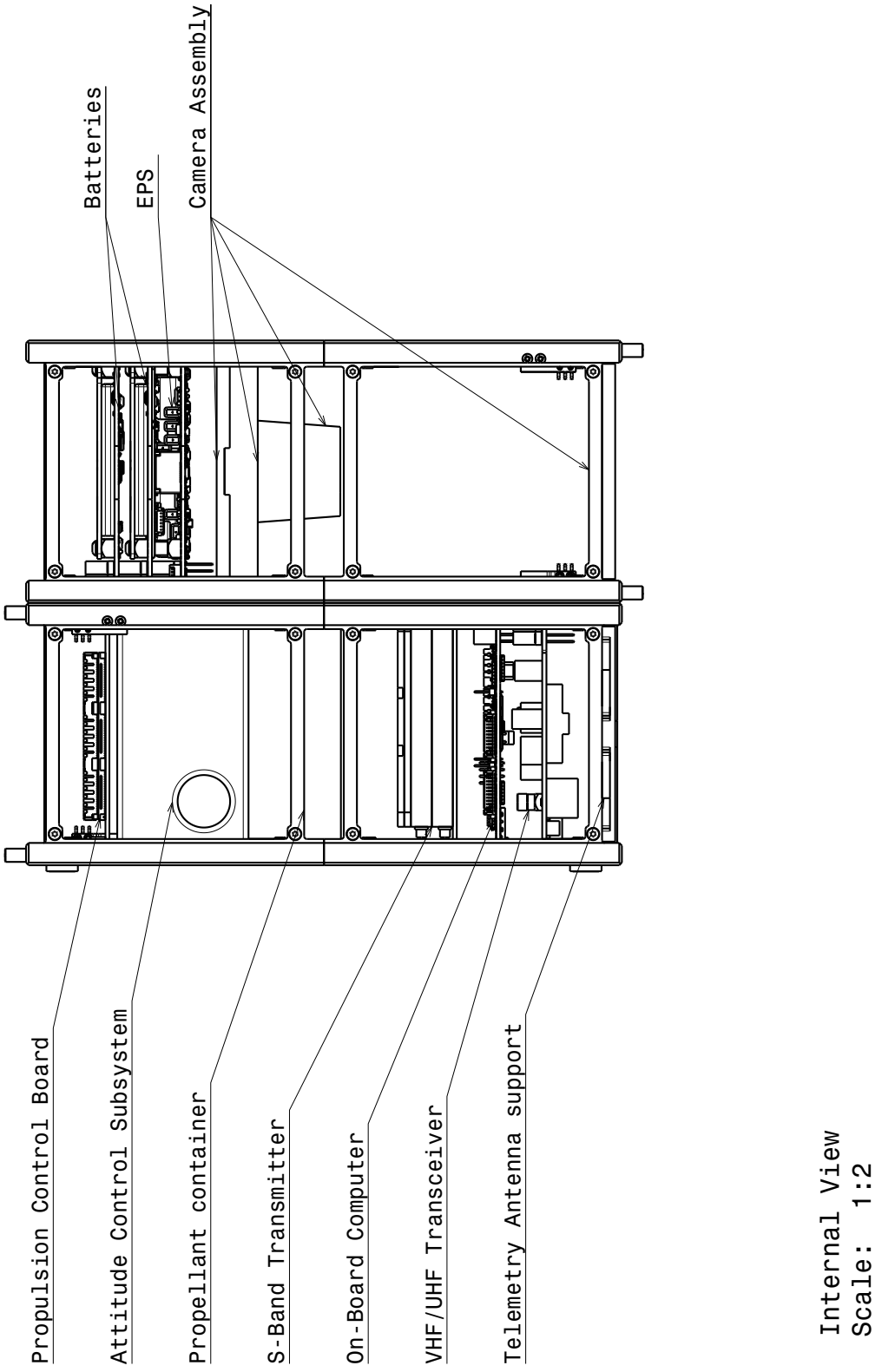

Figure 7.5: Internal view of the RCC and TMA platforms

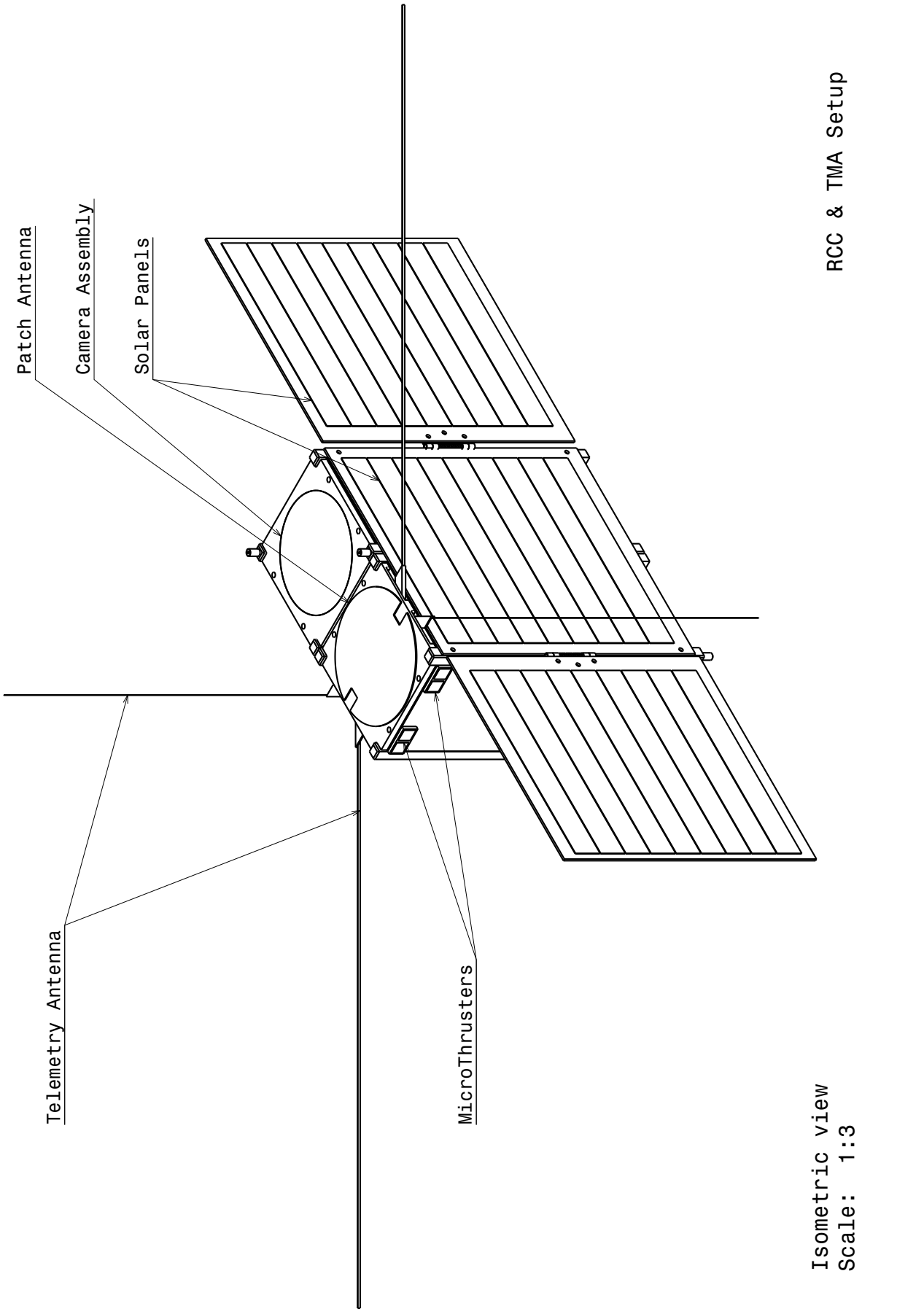

Figure 7.6: Isometric view of the design, fully deployed

Chapter 8 | Power Management

The power management of a satellite is one of the most important aspects of the design of a satellite, as without power none of the the other systems work. The power system consists of three main components: the power source, the storage and the control system. There are several different kinds of power sources available for satellites, such as solar arrays, solar thermal dynamic systems, radioisotopes, nuclear reactors and fuel cells[12]. However, for nanosatellite applications, solar cells are the only viable option, as all other possible power sources are too large to be installed on nanosatellites. Storage for the energy produced is provided by chemical batteries. The electronic control system (EPS) is a dedicated panel in the satellite that distributes the power to the subsystems.

In this chapter the different EPS options, solar cells and batteries are discussed and traded off. The size of the power management systems in terms of battery and solar array size is calculated for the low orbiting satellite platform with the ANT-2 RCC camera. At the end of the chapter the results for the ANT-2 TMA and ARCTIC are presented.

8.1 Power budget

The power budget, presented in table 8.1, is the summation of all power requirements from each subsystem. Thus it influences the size of the power system directly. Regarding the ANT-2 RCC, its satellites are orbiting the Earth in a sun-synchronous orbit in dawn-dusk configuration, this means that the solar arrays have constant lighting conditions and can produce energy constantly. This is noted in the table as P_{system}. Furthermore, the communication system is active if the satellite is in range of a ground station, which is true for 24% of the orbit (see chapter 12). In the table the average power needed for the communication system is denoted as P_{com} and the total as P_{total}.

Subsystem	Part	Nominal Power [mW]	Duty	Average Power [mW]
Payload	ANT-2 RCC	1590	1	1590
Communication	S-Band	9500	0.24	2280
	Transceiver	1500	1	1500
ADCS	Mechanics	2400	1	2400
Propulsion	Electrothruster	3200	1	3200
System Bus		1012	1	1012
			P_{system}	9702
			P_{com}	2280
			P_{total}	11982

Table 8.1: Power budget of the ANT-2 RCC

8.2 EPS System

The electrical power system (EPS) is part of the system bus of the satellite; it regulates the incoming power from the solar arrays, controls the charge and discharge of the batteries and provides power to the loads. There are different versions of EPS, the main difference being the use of Peak Power Tracking (PPT) or Direct Energy Transfer (DET) and the difference between regulated and unregulated buses. DET uses shunt regulators to dissipate excess energy and to keep the bus voltage constant. PPT employs DC/DC converter which can track and change the operating point of the solar arrays on the I-V curve. With DC/DC converters no shunt regulation is needed, but as a consequence it uses 4-7% of the total power and thus larger solar arrays are needed.[37] For the discussed satellite the PPT method is chosen as it removes the need of shunt regulators. These introduce extra sources of heat. The PPT method also has the advantage of providing maximum power to the loads even at the end of the lifetime.

The type of regulation determines how much the system bus influences the voltage delivered to the battery and to the loads. Possible regulations are: unregulated, quasi-regulated and fully regulated. Unregulated and quasi-regulated deliver the voltage of the batteries to the loads. Quasi-regulated means only controlling the charging process of the batteries, thus converters are needed at loads which need different voltages than the battery voltage. The regulated systems controls both the charging and discharging voltage of the batteries. [37]

For nanosatellites it is beneficial to use the fully regulated option, as it removes complexity from the system since only one central voltage conversion is needed. The exceptions are the communication and propulsion units which require a higher voltage. This conversion introduces losses of power that increases the total power requirement. The loss for the communication system

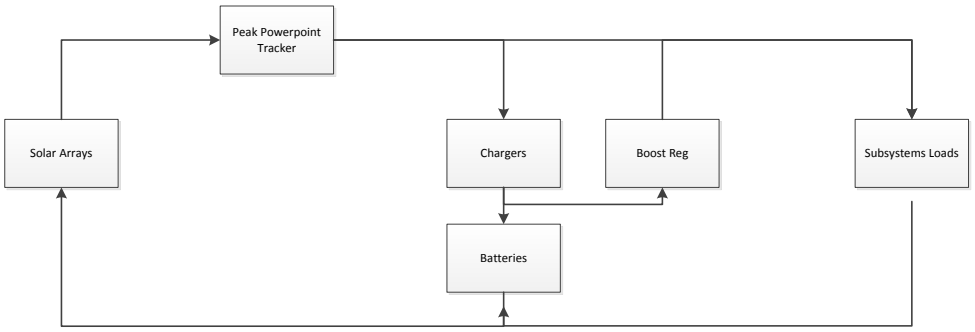

Figure 8.1: Electrical Block Diagram

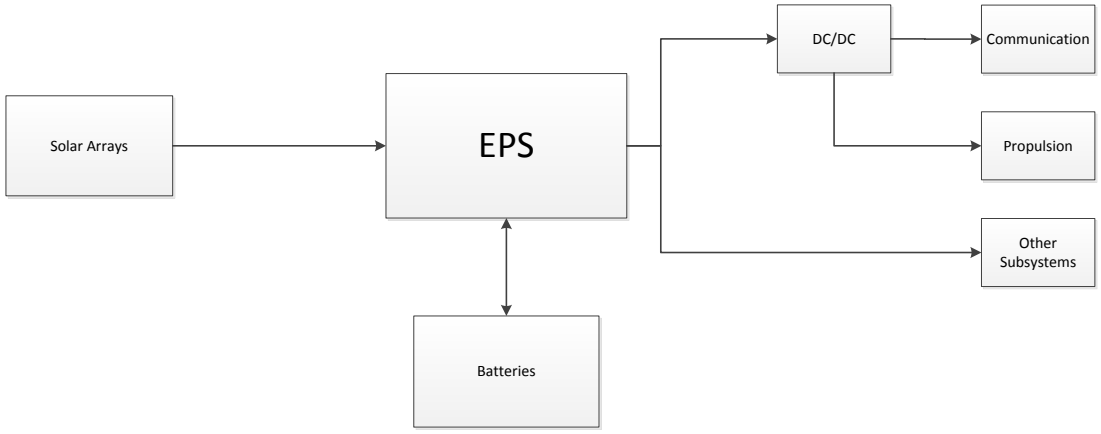

Figure 8.2: EPS Overview

is 8 W. For the propulsion system it is 0.2 W. A schematic representation of the whole power system can be seen in figures 8.1 and 8.2.

To reduce development cost it is beneficial to use COTS components such as the "fleXiblE" system from Clydespace which can be seen in figure 8.3.

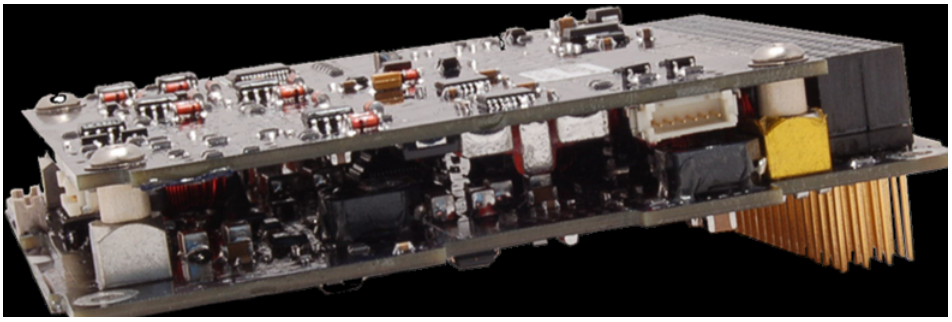

Figure 8.3: fleXible EPS from Clydespace[38]

8.3 Solar arrays

Solar arrays are used to provide the required power loads. There are many different versions of solar cells, mainly differing in the material used to produce them. These cells have different properties in terms of efficiency, mass and cost. As a consequence

the amount of solar cells of a certain type influences the cost and mass of the satellite.

The working principle of solar cells is to transform light into electric energy. When light, which consists of photons, hits the surface of a cell with enough energy, it can free a electron from the top layer which moves to the back layer and hence creating a electric circuit. This process can be improved by using several junctions as it allows to capture more than the visible spectrum of the sun. [39]

As previously mentioned there are different types of solar cells. Hence, a cell trade-off for the satellite is performed. There are three basic types of cell possibilities for space applications: simple crystalline silicon cells, CIGSSe (Copper indium gallium (di)selenide) thin film and multi-junction Gallium Arsenide cells. While Silicon and Gallium Arsenide are traditionally used in the space industry, thin film cells were developed to maturity during the last decade. The main characteristic of thin film is the low mass and cost which is traded for a lower efficiency. The price of thin film solar cells for ground application is below 10 $\frac{EUR}{W}$ [40]. However, as cells which can withstand space conditions with high efficiency are needed, the price is assumed to be two thirds of the silicon cells. Silicon cells are a well proven technology and have average values in term of mass, efficiency and cost. Multi-junction Gallium-Arsenide Cells are high performing cells with the highest efficiency for a high price. These cells are mostly used for space applications, as they reduce the required mass and area significantly.

The specific characteristics of each type can be seen in table 8.2. To determine the efficiency of the cells used it is assumed that it is 75% of the best achieved laboratory value. This reasoning is validated as the average of values given in [12] and [37] also indicate a factor of 75%.

Parameter	**Unit**	**Gallium Arsenide**	**Silicon**	**Thin film**
Type	-	Triple Junction	Crystalline	CIGSSe
Efficiency	-	28.1 [41]	18.75[41]	14.7[41]
Operating Temperature	$°C$	25	25	25
Power Density	W/m^2	385	257	202
Mass Density	kg/m^2	2.06 [42]	2.3 [12]	1.1 [37]
Price	EUR/W	460 [12]	280 [12]	190

Table 8.2: Solar cell characteristics

To perform the trade-off between the three different types of solar cells, the area, mass and price need to be calculated. In order to calculate these, variables given in table 8.3 are used.

The communication time is the amount of seconds the communication subsystem is active. Furthermore, 'path-loss direct' and 'path-loss battery' are indicators of how much energy is lost due to inefficiency in the system. Another important variable is the angle of incidence of the solar panels to the Sun, in case of a sun-synchronous orbit it depends on the inclination of the orbit and is constant at 7°. Lastly, the lifetime of the satellites has an impact on the degradation over time of the solar cells.

Variables	**Units**	**Values**
Orbital Period	s	5400
Communication Time	s	810
Path-loss Direct, X_s	-	0.8 [12]
Path-loss Battery, X_b	-	0.6 [12]
Inherent Degradation	-	0.85 [12]
Minimum Angle of Incidence	deg	7
Mission Time	$years$	2
Degradation GaSe/CIGSSe	-	0.0275 [37]
Degradation Silicon	-	0.0375 [37]

Table 8.3: List of variables for ANT-2 RCC

The first step in calculating the values for mass, area and cost is to determine the power the solar array has to provide. This consists of the energy used by the general systems and an extra term for the energy which is used to charge the battery to provide power to the communication systems. Combined this results into equation 8.1.

$$P_{sa} = \frac{P_{system}}{X_s} + \frac{P_{S-Band}}{X_b} \tag{8.1}$$

P_{system} is the energy used by all systems except the S-band communication system (P_{S-Band}). This means that the system loads are at all times powered by the solar arrays and the batteries are solely used for providing power to the S-Band communication system. More information of the exact properties of the communication system can be found in the dedicated chapter (12). The next step is to determine the power per square meter at the beginning of the mission. This value is calculated using equation 8.2.

$$P_{BOL} = P_0 I_d \cos\theta \tag{8.2}$$

P_0 is the power per square meter the cells can provide at the beginning of life, I_d is the inherent degradation and θ is the angle of incidence to the sun. During the mission the cells degrade due to external influences, such as cosmic radiation. For the solar cell size estimation it is important to calculate this degradation. It differs for the different kinds of cells: GaAs-TJ and CIGSSe degrade by about 2.75% and Silicon cells by about 3.75 %[12]. The total degradation can be estimated by equation 8.3.

$$L_d = (1 - \frac{degradation}{yr})^{satellitelife} \tag{8.3}$$

The next step is to equate the power at beginning of life with the degradation which results in the power at the end of the mission. Which is calculated in equation 8.4.

$$P_{EOL} = P_{BOL} L_d \tag{8.4}$$

Finally the size of the arrays can be determined with equation 8.5.

$$A_{sa} = \frac{P_{sa}}{P_{EOL}} \tag{8.5}$$

The results from the calculations for each type of solar cell are shown in table 8.4.

Variables	**Units**	**GaAs-TJ**	**Silicon**	**CIGSSe**
Total Power	W	15.92	15.92	15.92
P_{BOL}	Wm^2	324.4	216.24	169.53
Lifetime Degradation	-	0.94	0.92	0.94
P_{EOL}	W/m^2	306.7	200.3	160.3
$A_{solarcells}$	m^2	0.05	0.08	0.1
Mass	kg	0.11	0.18	0.11
Price	EUR	6300	3800	2600

Table 8.4: Sizing of solar panels for ANT-2 RCC

From the table can be seen that the GaAS-TJ cells are best suited to to provide the required power with the smallest area. On the other hand the CIGSSe cells require about double the area but are equal in terms of mass and a third cheaper than the GaAs-TJ cells. The silicon cells are, while requiring slightly less area than the CIGSSe, not competitive in terms of price or mass. However, it is important to quantify the effects that the area difference in the solar panels causes. By using a satellite CAD assembly it is possible to accurately estimate these values for the different panels configurations, where the only points of interest are the extremes: GaAs-TJ and CIGSSe cells. With the same configuration of side-mounted panels for a sun-synchronous orbit, the moments of inertia vary considerably as shown in table 8.5.

Moment of Inertia [$kg \cdot m^2$]	**CIGSSe**	**GaAs-TJ**	**Change [%]**
I_{xx}	0.024	0.024	0
I_{yy}	0.047	0.038	24
I_{zz}	0.033	0.024	38

Table 8.5: Moment of inertia comparison

A 24 and 38 % is quite considerable and poses a challenge with respect to the stability and attitude control of the satellites. The ADCS simulation in chapter 10 is used to measure the changes in its mass and it is concluded that the changes are so small, in the order of a gram, that the increase in solar panel area of the CIGSSe cells is not a significant disadvantage.

As result of the trade-off the thin film CIGSSe solar cells are chosen to be utilized for the satellite carrying the ANT-2 RCC camera. The mass given in the table is for the actual cells, but since the cells make up one third of the solar array system[43], the total mass is approximately 0.3 kg. It is important to note that the price is only an indication, more accurate prices need to be determined when the concept moves out of the initial design phase.

8.4 Batteries

As the power for the communication system is provided solely by the batteries, it is important to determine the their size. Another possibility is be the use of superconductors, which are still in development at the moment and are not further considered due to their lacking technological readiness. Batteries are divided into two different kinds: primary and secondary. The main

difference is that primary batteries are not rechargeable and secondary batteries are[37]. Thus for the satellite a secondary battery is required. There are different materials available, the most common for space application are: nickel cadmium (NiCd), nickel hydrogen (NiH^2) and lithium ion (Li-Ion). A trade-off is performed between the different types of batteries. The most relevant property to compare different batteries is the required capacity, a higher needed capacity is detrimental as it increases the mass of the batteries. It is calculated with equation 8.6.

$$C_r = \frac{P_{com} T_{com}}{(DOD) N n} \tag{8.6}$$

DOD is the depth of discharge. It is a measure of how much the battery is discharged every cycle. As such it is dependent on the total number of cycles. The more cycles a battery experiences in its lifetime the lower the DOD becomes. Furthermore the amount of cycles is high in LEO orbits as a satellite experiences several dozen discharges each day, resulting into more than 15000 cycles per mission year. N is the number of batteries, most satellites use more than one to ensure redundancy in case a battery fails. Finally n is the charge/discharge efficiency. A comparison for all three materials can be seen in table 8.6.

Parameter	Unit	NiCd	NiH^2	Li-Ion
Number of Cycles	-	30000+	30000+	30000+
DoD	-	0.25	0.5	0.8
Capacity	$W \cdot hr$	9.8	4.6	2.7
Energy Density	$W \cdot hr/kg$	25	40	155
Mass	kg	0.39	0.11	0.017
Number of Batteries	-	2	2	62
Charge/Discharge Efficiency	-	0.7	0.75	0.8

Table 8.6: Comparison batteries ANT-2 RCC

From the trade-off it becomes apparent that the Li-ion batteries are optimal for all parameters. The reason for this decision is that the required capacity for batteries is the lowest for Li-ion and thus reduces the mass of the satellite, As the calculations give theoretical values only, suitable COTS components need to be found. One such a component is the CS-SBAT2-10 battery from Clydespace, which is shown in figure 8.4. It has a capacity of 10 Whr, a mass of 100 g per battery and has a cost of about 1200 EUR per unit [38].

Figure 8.4: Battery from Clydespace[38]

8.5 ANT-2 TMA / ARCTIC

As the constellation consists of satellites with different cameras in different orbit types, it is important to investigate if the satellites with ANT-2 TMA and ARCTIC can use the same solar arrays as the satellites with RCC, or that different solar array configurations are needed to meet the required power loads.

8.5.1 ANT-2 TMA

The satellites carrying the ANT-2 TMA camera are in sun-synchronous dawn dusk orbits, similar to the ANT-2 RCC satellites. As the camera uses only slightly less energy, the difference to the ANT-2 RCC is relatively low at about 1 W. The changes in power budget and and solar arrays are shown in table 8.7 and 8.8. Furthermore the battery size stays the same as for the ANT-2 RCC, since the power required by the S-band antenna remains the same, and all other loads are directly powered by the solar arrays.

Subsystem	Part	Nominal Power [mW]	Duty	Average Power [mW]
Payload	ANT-2 TMA	600	1	600
Communication	S-Band	9500	0.24	2280
	Transceiver	1500	1	1500
ADCS	Controller	2400	1	2400
Propulsion	Electrothruster	3200	1	3200
System Bus		1012	1	1012
			P_{system}	8712
			P_{com}	2280
			P_{total}	10992

Table 8.7: Power budget ANT-2 TMA

Variables	Units	GaAs-TJ	Silicon	CIGSSe
Total Power	W	14.69	14.69	14.69
P_{BOL}	W/m^2	324.4	216.24	169.53
Lifetime Degradation	-	0.94	0.92	0.94
P_{EOL}	W/m^2	306.7	200.3	160.3
$A_{solarcells}$	m^2	0.05	0.07	0.09
Mass	kg	0.1	0.17	0.1
Price	EUR	5700	3500	2300

Table 8.8: Sizing of solar panels for ANT-2 TMA

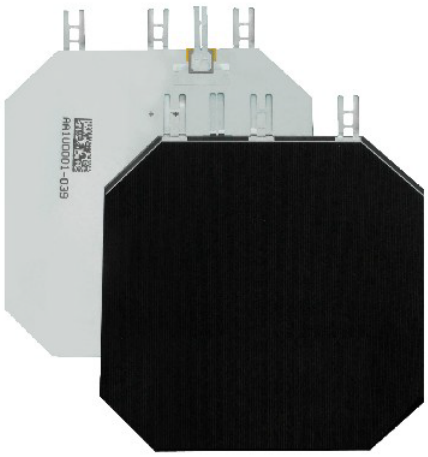

Figure 8.5: GaAs-TJ Solar Cell[42]

8.5.2 ARCTIC

In contrast to the satellites carrying the ANT-2 variant, the ARCTIC is in a polar orbit. As a consequence the satellite moves into eclipse for parts of the orbit. This increases the necessary power which needs to be generated by the solar arrays by about 100%. The reason for the increase is due to fact that the solar arrays have a third less time to charge the batteries for use of the communication system. Additionally the rest of system needs to powered during the eclipse by the batteries as well. The results for power budget, variables, solar arrays and batteries are shown in tables 8.9, 8.10, 8.11 and 8.12.

As the ARCTIC is orbiting the Earth in a polar orbit it experiences eclipses in every orbit. In addition the angle of incidence changes to 23.5 ° for the worst case lighting condition.[12] The changed variables are given in table 8.10. This increases the power which needs to be provided by the solar arrays and equation 8.1 is adapted to equation 8.7 to accommodate the changes.

$$P_{sa} = \frac{P_{system}}{X_s} + \frac{P_{S-Band}}{X_b}\frac{T_{orbit} \cdot DutyCycle}{T_{sun}} + \frac{P_{system}}{X_b} \cdot \frac{T_{ecl}}{T_{sun}} \tag{8.7}$$

Subsystem	Part	Nominal power [mW]	Duty	Average power [mW]
Payload	ARCTIC	1590	1	1590
Communication	S-Band	9500	0.24	2280
	Transceiver	1500	1	1500
ADCS	Mechanics	2400	1	2400
Propulsion	Electro thruster	3200	1	3200
System Bus		1012	1	1012
			P_{system}	9702
			P_{com}	2280
			P_{total}	11982

Table 8.9: Power budget ARCTIC

Variables	Units	Values
Sun Time	s	3600
Eclipse Time	s	1800
Minimum Angle of Incidence	deg	23.5

Table 8.10: Changed variables for ARCTIC

The sizing of the solar panels shown in table 8.11 shows that for the ARCTIC carrying satellite it is not possible to use CIGSSe based solar cells as the required area is too large. As a result the choice for solar cell material differs from the ANT-2 carrying satellites by using GaAs-TJ cells instead of CIGSSe. A GaAs-TJ cell can be seen in figure 8.5. This increases the price for the solar arrays significantly, but as the area available for solar cells is limited GaAs-TJ cells are the only option. In terms of batteries, the same model as for the ANT-2 can be used.

Variables	Units	GaAs-TJ	Silicon	CIGSSe
Total Power	W	29.7	29.7	29.7
P_{BOL}	W/m^2	303	211	165
Lifetime Degradation	-	0.94	0.92	0.94
P_{EOL}	W/m^2	286.6	195.8	156.7
$A_{solarcells}$	m^2	0.1	0.15	0.19
Mass	kg	0.1	0.17	0.1
Price	EUR	11000	6800	11000

Table 8.11: Sizing of solar panels for ARCTIC

Parameter	Unit	NiCd	NiH^2	Li-Ion
Number of Cycles	-	27375	27475	27375
DOD	-	0.25	0.5	0.8
Capacity	$W \cdot hr$	23.6	11	5.9
Energy Density	$W \cdot hr/kg$	25	40	155
Mass	kg	0.94	0.27	0.038
Number of Batteries	-	2	2	62
Charge/Discharge Efficiency	-	0.7	0.75	0.8

Table 8.12: Comparison batteries ARCTIC

Chapter 9 | Thermal Control

The thermal control of a satellite is important to consider during the design process of a satellite. In this chapter it is investigated if the platform discussed in this report can achieve a feasible equilibrium temperature in a very low Earth orbit. To determine this temperature, the outer surfaces of the satellite and their thermal properties need to be defined. This forms the basis for future thermal investigation of this satellite concept. Possible modifications to the concept to support the ARCTIC camera are discussed at the end of this chapter.

9.1 Thermal Equilibrium

The thermal equilibrium temperature of a body can be found with formula 9.1 [37], which yields the average temperature of the satellite. Although single parts and areas can have higher or lower temperatures, it is a reasonable first indication.

$$T = \sqrt[4]{\frac{Q_{in}}{\epsilon \sigma A_r}} \tag{9.1}$$

To solve this equation all heat inputs and their corresponding areas with their thermal properties need to be determined. There are four external sources: solar radiation, albedo reflection, infrared (IR) radiation from Earth and heat generated by free molecular heating. Additionally, heat is dissipated by the electric components inside of the satellite. ϵ is emissivity of the satellite and A_r is area of the satellite which radiates into free space.

9.1.1 Solar radiation

The solar radiation Φ is approximately 1367 $\frac{W}{m^2}$ at a distance of 1 AU, which is the main source of heat for the satellite. The amount of received heat from solar radiation can be calculated with equation 9.2. An important parameter in this equation is the incidence angle. As the satellite is in sun-synchronous orbit with 97° inclination in dawn-dusk configuration, its sun-facing areas are offset to the sun (incidence angle θ) by 7°. The heat is absorbed by the A_{solar}.

$$Q_{Solar} = \Phi \cdot \cos\theta \cdot A_{solar} \tag{9.2}$$

9.1.2 Albedo

Solar radiation is reflected back into space by the Earth, which is another source of heat for the satellite. The albedo reflection is highly dependent on atmospheric properties and whether the satellite is above ground or above water. A global average of 40% is used for this initial calculation. Q_{albedo} is thus a 40% of the solar radiation calculated in equation 9.2.

9.1.3 Planet IR

In addition to the albedo the Earth emits IR radiation. This radiation is relativity constant and only dependent on the height of the satellite. The received Earth IR radiation can be calculated by equation 9.3

$$Q_{PlanetIR} = F \cdot PlanetIR \cdot A_{PlanetIR} \tag{9.3}$$

Where F is the viewfactor which is a measure how much the radiation decreases due to distance between the two bodies. Thus high orbiting satellites will experience little or no IR radiation. In the case for the low orbiting satellites (280 km) F has a value of 0.98 and the average IR radiation $PlanetIR$ is 234 $\frac{W}{m^2}$.[44]. The absorbing area is $A_{PlanetIR}$

9.1.4 Internal heat

The electrical equipment inside the satellite dissipates heat, with the main contribution coming from the patch antenna, dissipating around 8 Watts of energy into the interior of the satellite. However, as the antenna is only active during small parts of the orbit, it it will only increase the temperature of the satellite for a relatively short duration.

9.1.5 Free molecular heating

For spacecraft flying in a relatively low orbit, heating due to collision with air particles has an impact on the temperature of the satellite. It is possible to determine this type of heating with equation 9.4. [44]

$$Q_{fmh} = \frac{1}{2}\rho V^3 A_{fmh} \tag{9.4}$$

Surface Area	Input
A_{solar}	5,7,8
$A_{PlanetIR}$	1, 3, 4, 6, 9, 10
A_{albedo}	1, 3, 4, 6, 9, 10
A_r	1 - 10
T_{normal}	25 $^{\circ}C$
T_{com}	32$^{\circ}C$

Table 9.1: Results for thermal calculations

Calculating the heat with standard atmospheric values [12] on a height of 275 km is resulting into an added heat of about 0.2 W which is negligible in comparison with the other heating values.

9.1.6 Equilibrium temperature

For calculating the temperature of the satellite it is necessary to define the radiating and emitting outside surfaces of the satellite. The surfaces experiencing solar input are: 5, 7, 8. The surfaces under the influence of albedo and the IR are: 1, 3, 4, 6, 9, 10. A graphic representation of the surfaces can be seen in figure 9.1. Each of the faces can be applied with different materials, coating and paintings to achieve a favourable thermal balance. After an iterative process of manipulating the thermal properties of the areas, the temperature of the satellite is 32$^{\circ}C$ with an activated antenna and 25 $^{\circ}C$ for nominal operations. An overview of the thermal properties of the surfaces can be seen in table 9.2. An overview of all values is shown in table 9.1

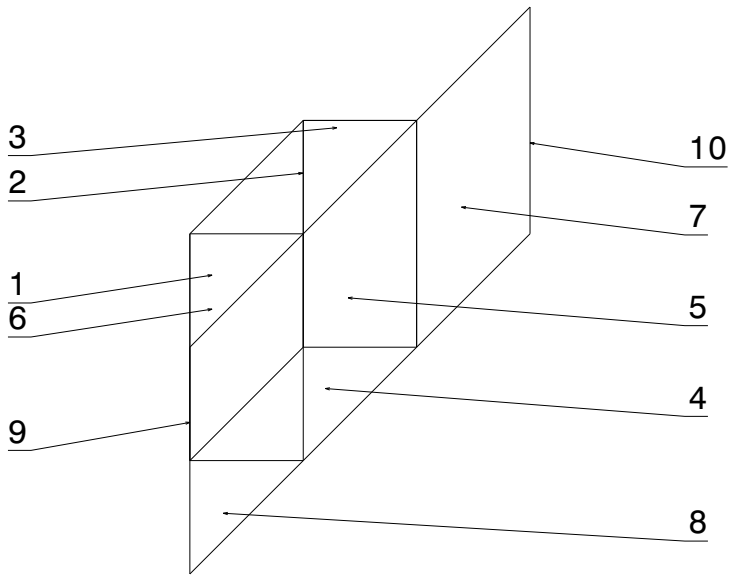

Figure 9.1: Radiating/emitting areas of the satellite

Area	Size [cm^2]	Absorptivity	Emissivity	Material
1	200	0.05	0.8	8mil Quartz Mirrors[12]
2	200	0.05	0.8	8mil Quartz Mirrors
3	200	0.05	0.8	8mil Quartz Mirrors
4	200	0.05	0.8	8mil Quartz Mirrors
5	400	0.9	0.9	Solar Panel
6	400	0.05	0.8	8mil Quartz Mirrors
7	400	0.9	0.9	Solar Panels
8	400	0.9	0.9	Solar Panels
9	400	0.4	0.6	8mil Quartz Mirrors
10	400	0.4	0.6	8mil Quartz Mirrors

Table 9.2: Overview of thermal properties

9.2 Satellites in higher orbits

The ANT-2 TMA and ARCTIC are in higher orbits than the ANT-2 RCC. In case of the ANT-2 the planet IR will decrease as the viewfactor reduces to 0.94 [44], resulting into an about 10 W decreased heat input from the IR radiation of the Earth. This is however not significantly different from the ANT-2 RCC as the temperature difference between the two is approximately 1 K.

On the other hand the satellite carrying the ARCTIC camera is in a different orbit (polar) which includes eclipse phases and has a sensor in the camera which needs to operate at a very low temperature of 160 K. For the ARCTIC [31] the area additional radiating surfaces were calculated, but as the design of the platform discussed in this report differs, the results are not valid any more.

There are several problems with the current design. One is that the communication subsystem is directly placed next to the camera, which dissipates 8 Watts of heat into the satellite. Another problem is the attachment and placement of the required extra radiating surfaces on the satellite. As a consequence for the further development of this concept a new thermal node analysis has to be performed to determine the new size of the required radiators. A possible design configuration is shown in figure 9.2.

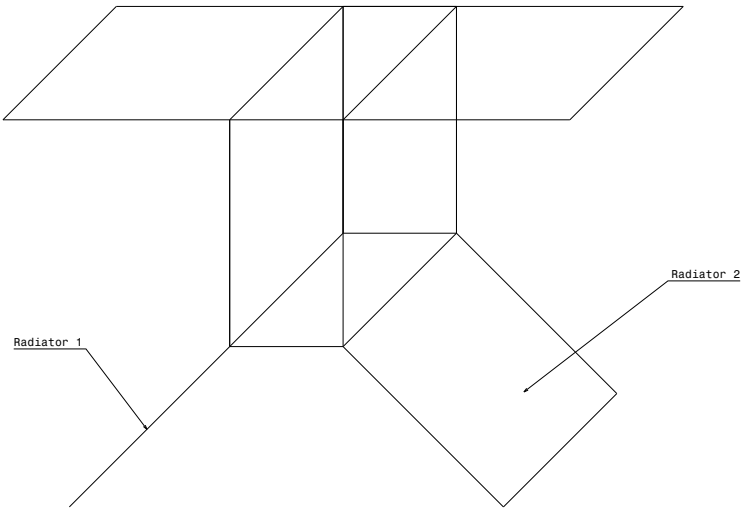

Figure 9.2: Radiating & Emitting Areas of the Satellite

As this discussion is at an initial stage, there are many topics still to be investigated during future development of the satellite and constellation. First, a detailed thermal node analysis for the VLEO design needs to be performed to assure that all parts of the satellite are operating in their allowed temperature range. This is possible by using dedicated software which can also include the time dependency of the temperature and the change of incidence angles for the satellite. As already discussed the thermal model for the ARCTIC camera needs to recalculated to assure that the sensor operates at 160 K.

Chapter 10 | Attitude control

"The attitude determination and control subsystem (ADCS) stabilizes the vehicle and orients it in desired directions during the mission, despite the external disturbance torques acting on it"[12],p 354. As the C^{3}EO is an imaging mission, the ADCS design is highly driven by the requirements of the cameras that the satellites carry. To make stable pictures, the rotational movement of the satellites is restricted.

In the following chapter the design procedure of the ADCS and the design of the ADCS itself is described. In section 10.1 the requirements are set, after which in section 10.2 it is explained how disturbance torques acting on the satellite are estimated. After this section follows the sizing of the control actuators in section 10.3. The ADCS design also incorporates several different sensors, which is elaborated upon in section 10.4. A short summary of all the components in the ADCS is given in the last section of this chapter, section 10.6. In this section an evaluation of the requirements is also present.

10.1 Control modes and requirements on ADCS

The design of the ADCS starts with distinguishing the control modes. In different control modes the ADCS has different functions, for which different requirements are set. The control modes and the corresponding requirements are shown in table 10.1 and table 10.2 for both camera types.

Control mode	Function of ADCS	Requirements
Orbit insertion	No attitude control	
Acquisition	Support initial determination of attitude and stabilize the S/C	Detumble from angular velocities of 100 $^\circ/s$
On-station	Provide stability to support communication and imaging	Maximum angular velocities (x,y,z): 0.1, 0.2, 0.05 $^\circ/s$. Nadir pointing better than 0.25 $^\circ$, three axis.
Safe	Support communication and thermal control	Maximum angular velocity 3 $^\circ/s$ three axis. Nadir pointing better than 3 $^\circ$, three axis

Table 10.1: Control Modes for ANT-2 RCC and TMA carrying satellites

Control mode	Function of ADCS	Requirements
Orbit insertion	No attitude control	
Acquisition	Support initial determination of attitude and stabilization of the S/C	Detumble from angular velocities 100 $^\circ/s$
On-station	Provide stability to support communication and imaging	Max angular velocity (x,y,z): 1.55, 3.09, 11.54 $^\circ/s$. Nadir pointing better than 0.25 $^\circ$, three axis
Safe	Support communication and thermal control	Max angular velocity 15 $^\circ/s$ three axis. Nadir pointing better than 3 $^\circ$ three axis

Table 10.2: Control Modes for a ARCTIC carrying satellites

It needs to be noted that none of the C^{3}EO satellites has an eclipse mode. It is clear that the ARCTIC, which images in the thermal infrared spectrum, continues imaging the Earth when it is in an eclipse. The ANT-2 carrying satellites are in a sun-synchronous dawn-dusk orbit, which means they only experience an eclipse twice a year. It is therefore unnecessary to specify an eclipse mode.

10.1.1 Acquisition mode requirements

After launch, the deployment system pushes the satellites out of the launcher into target orbit. By doing so, the satellite suffers an initial rotational velocity which depends on the type of ejection pod that is used.

It is very important that the system is designed for the maximum rotational velocity it can get, otherwise it is not possible to detumble the satellite. For DELFI-N3XT an initial rotational velocity of 10 $^\circ/s$ is expected, however the satellite is designed to be able to detumble from initial velocities of 60 $^\circ/s$. The mission designers of SNAP-1 satellite expected the rotational velocity to be 5 $^\circ/s$, but the satellite was not able to detumble because velocities were actually 30 $^\circ/s$. Similarly, the SwissCube mission failed because it experienced a rotational velocity of 200 $^\circ/s$, whereas the controller was only designed for 50 $^\circ/s$[45].

The rotational velocity from which the satellites within the C^{3}EO constellation have to detumble is determined to be 100 $^\circ/s$. This is based on the assumption the ejection pod that will be used will be similar to the one used for releasing the QB50

satellites [46], which will cause maximum rotational velocities of 100 $^{\circ}/s$. Compared to the DELFI-N3XT, SwissCube and SNAP-1 missions this seems a good initial estimate.

10.1.2 On-station mode requirements

A rotated satellite causes an offset in the field of view. A rotation around the body's x-axis causes the required imaged swath to be shifted in longitude. A shift around the body's y-axis causes the satellite's field of view to shift within its path and a rotation around the z-axis causes the field of view to be rotated. The maximum allowed shift in longitude, hence around body x-axis, must be less than half the angular field of view of the camera. In this case, no matter the direction of the offset the center part of the swath width is always covered. However, this requirement can not be derived from other design characteristics and therefore it is just chosen to be less than 0.25 $^{\circ}$. This means that for the ANT-2 TMA camera with an angular field of view of approximately 5°, it can be guaranteed that the groundtrack that has an angular view of 4.5°.

"For a perfectly sharp image, the satellite has to have zero rotational velocity"[31] p 63. However, as torque control is unlikely to be perfect, this is never the case. Therefore, ARCTIC design recommendations are given for the maximum rotational velocity that the satellite is allowed to have [31], p 66. The calculations made are based on the aperture diameter of the camera, integration time, wavelength of the imaged light and the maximum allowed shift of the image.

The calculations for the required maximum angular velocity are redone for the ARCTIC carrying satellites. The results are very close to the results that the engineers that designed the ARCTIC camera came up with. The only parameter that differs is the wavelength, whereas the ARCTIC is optimized for the average wavelength of the light it captures. For the stability calculations the minimum wavelength is taken.

The stability analysis for the ANT camera has not been carried out by the previous DSE group. Therefore the same calculations as for the ARCTIC camera are done for the ANT-2 RCC and TMA carrying satellites. Of course for the RCC and TMA cameras the integration time, aperture diameter, wavelength of the imaged light differ from the ARCTIC design.

The results of the calculations are in the same order of magnitude as for the initial ARCTIC design. The results are given in table 10.2 and 10.1, the detailed calculations are found in appendix A.

10.1.3 Safe mode Requirements

When a vital function of the satellite fails, the main board computer turns the satellite into safe mode. In the safe mode it is important that the still-working vital functions of the satellite have enough power. This means that the payload shuts down and the satellites stop imaging. Often, vital functions also have a safe mode, in which they consume less power than during operational mode.

The ADCS also has a safe mode, during which the rotational velocities are allowed to be larger than the velocities required for on-station mode. However it is required that the satellite does not tumble, so a limit has to be set for the angular velocity. Tumbling is dangerous for a satellite; in the first place it can cause the temperature to rise or fall very fast, which can cause damage to the satellite. In second place, a tumbling satellite cannot guarantee ground communication any more, as it is not able to point to a ground station.

Furthermore, as the satellite needs to avoid tumbling during operational mode, the safe mode requirements for the ADCS do not differ greatly. However, it must be said that it is satisfactory that the ADCS consumes as little power as possible. Therefore the pointing accuracy and the allowed angular velocity are not that strict as during operation. It is assumed that a pointing accuracy of better than 3° is accurate enough to provide enough power to the solar panels. With respect to the operational mode, the safe mode allows a slightly higher angular velocity.

10.2 Disturbance torques

When the satellite is in orbit, torques disturb its attitude. The ADCS needs to be able to counteract these disturbance torques and needs to store the angular momentum that is caused by counteracting the disturbance torques. It also needs to be able to counteract the worst case disturbance torques that can occur in one of the modes specified in table 10.1 and 10.2. This subsection explains how the worst case disturbance torques and required angular momentum storage are estimated for the satellites.

As the disturbance torques the highest for the ANT-2 RCC carrying satellite at an orbit height of 288 km, they are used for the ADCS actuator sizing. A summary of the maximum disturbance torque and the required angular momentum storage is given by table 10.3. The results are checked with the calculations that were made for the DELFI-N3XT. The results of this validation activity can be found in appendix B.

In this section the torques around the three different body axis of the satellite are estimated. For clarity, figure 10.1 shows how a right handed body axis system is set on the satellite.

10.2.1 Solar radiation pressure

A force on the satellites' surface is caused by solar radiation incidence. This force causes a moment around the center of gravity. The ANT-2 carrying satellites are placed in a sun-synchronous dawn-dusk orbit, which means the solar panels, mounted on the

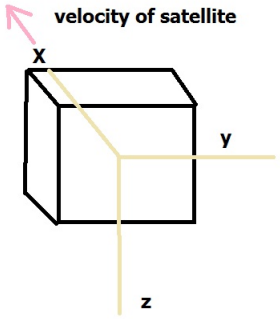

Figure 10.1: coordination of the right hand coordinated axis system with respect to the satellite

Disturbance type	Disturbance torque [Nm]	Angular momentum storage	Storage type	Axis
Aerodynamic	$1.16 \cdot 10^{-5}$	0.063	secular	x,y,z
Solar	$4.02 \cdot 10^{-9}$	$2.18 \cdot 10^{-5}$	secular	z
Solar	$7.45 \cdot 10^{-9}$	$4.04 \cdot 10^{-5}$	secular	y
Magnetic	$2.68 \cdot 10^{-7}$	$3.73 \cdot 10^{-5}$	cyclic	x,y,z
Gravity	$1.82 \cdot 10^{-8}$	$34.92 \cdot 10^{-5}$	cyclic	y
Total	$1.19 \cdot 10^{-5}$	0.0632		y

Table 10.3: Disturbance torques and required angular momentum storage for the ANT-2 RCC carrying satellite

side of the satellite (see figure 7.6) are always facing the sun under the same incidence angle. The worst case disturbance torque can now be calculated using equation 10.1.

$$T_s = \frac{\Phi}{c} A_s (1+q)(c_{p_s} - c_m) cos\theta_{sun} \tag{10.1}$$

where T_s is the solar radiation pressure torque, Φ is the solar flux (Φ = 1367 $\frac{W}{m^2}$ at 1 AU), c is the speed of light, A_s is the sunlit surface area in m^2, q is the unitless reflectance factor, θ_{sun} is the worst case angle of incidence of the Sun, and c_{p_s} and c_m are the centers of solar radiation pressure and mass in kg.

The solar pressure is most likely to act in the geometric center of the surface that faces the sun. However, as the determination of the center of pressure is not part of this conceptual study, a conservative offset of 10 mm (x,y and z directions) is taken with respect to the geometrical center [47].

The worst case disturbance torque is assumed to be the same for the ARCTIC and ANT-2 carrying satellites. The solar radiation force is acting in the y-direction of the satellite, hence it causes a torque around z and x axis. In table 10.4 one can find the inputs and outputs for the estimation of the worst case solar radiation torque. Of course this constant disturbance torque causes a reaction wheel to become saturated. If the maximum disturbance torque is integrated over one period, the required maximum angular momentum storage per orbit can be calculated.

Inputs			Outputs		
Parameter	**Unit**	**Value**	**Parameter**	**Unit**	**Value**
Φ	W/m^2	1367	T_{s_y}	Nm	$7.45 \cdot 10^{-9}$
A_s	m^2	0.12	T_{s_z}	Nm	$4.021 \cdot 10^{-9}$
q	$-$	0.1	H_{s_y}	Nms	$4.04 \cdot 10^{-5}$
$C_{p_{x,y}}$	m	[0.01 -0.01]	H_{s_z}	Nms	$2.18 \cdot 10^{-5}$
$C_{og_{x,y}}$	m	[-0.0026 0.0037]			
ϕ	rad	0			

Table 10.4: inputs and outputs for the calculation of the worst case solar radiation torque

10.2.2 Atmospheric drag

Atmospheric drag is caused by atmospheric particles hitting the satellite. For satellites at low altitudes (below 300 km), the atmospheric drag causes the satellite to de-orbit if it does not have a propulsion system. The atmospheric torque can be calculated using eq. 10.2.

$$T_a = \frac{1}{2} \rho C_d A_r V^2 (c_{p_a} - c_m) \tag{10.2}$$

T_a is the atmospheric drag torque, ρ is the atmospheric density in kg/m^3, C_d is the drag coefficient, A_r is the ram (frontal) area in m^2, V is the spacecraft's orbital velocity in m/s, and c_{p_a} and c_m are the locations of the centres of aerodynamic pressure and mass in m.

In the worst case scenario the satellite is turned on its side, when the solar panels are turned directly into the flow. Now the worst case ram area equals the solar panel area, 0.12 m^2 The atmospheric density as well as the orbital velocity differs for every type of satellite of the C^{3}EO, so the atmospheric torques are calculated for every satellite type. The results are shown in table 10.5. It can be seen that the difference between aerodynamic center and center of mass is taken 0.05 m. This is a very conservative value, as it is expected that the center of pressure is likely to be very close to the geometrical center. As the center of gravity also lies close to the geometrical center (the distance is in the order of mm), the worst case offset can be considered as very conservative. It is assumed that this offset accounts for the three axis, so the worst case disturbance torques are equal around all three axis. The worst case required angular momentum storage is calculated for one orbit.

Inputs			Outputs		
Parameter	**Unit**	**Value**	**Parameter**	**Unit**	**Value**
ρ_{288km}	kg/m^3	$3.34 \cdot 10^{-11}$	$T_{RCC_{xyz}}$	Nm	$1.16 \cdot 10^{-5}$
ρ_{443km}	kg/m^3	$3.02 \cdot 10^{-13}$	$T_{ARCTIC_{xyz}}$	Nm	$1.029 \cdot 10^{-7}$
ρ_{500km}	kg/m^3	$7.73 \cdot 10^{-14}$	$T_{TMA_{xyz}}$	Nm	$2.61 \cdot 10^{-8}$
C_d	$-$	2.3	$H_{RCC_{xyz}}$	Nms	0.0630
A_r	m^2	0.12	$H_{ARCTIC_{xyz}}$	Nms	$4.76 \cdot 10^{-4}$
V_{288km}	km/s	7.73	$H_{TMA_{xyz}}$	Nms	$1.48 \cdot 10^{-4}$
V_{443km}	km/s	7.64			
V_{500km}	km/s	7.61			
$C_{p_a} - C_m$	m	0.05			

Table 10.5: inputs and outputs for the calculation of the worst case torque due to atmospheric drag

10.2.3 Magnetic field torque

The magnetic field of the Earth causes a torque on the satellite. This torque depends on the residual dipole moment of the satellite, which is assumed to be 0.05 Am^2. Now the magnetic torque on the satellite can be estimated using equation 10.3 [47].

$$T_m = D \times B = D \frac{M}{R_{orbit}^3} \sqrt{1 + 3sin^2(\lambda)} cos(\theta_{magn}) \tag{10.3}$$

In equation 10.3 $D \times B$ is a cross product, which means that if the magnetic fields of the satellite and Earth are aligned, no residual moment exists. T_m is the magnetic torque, D is the spacecraft's residual dipole moment in Am^2 and B is the magnetic field strength in Tesla. B can be estimated making use of the magnetic constant M ($M = 7.8 \cdot 10^{15}$ Tesla·m^3), the orbital radius R_{orbit} and the latitude λ of the satellites position in orbit. θ_{magn} is the alignment of the satellites and Earth's magnetic field in radians.

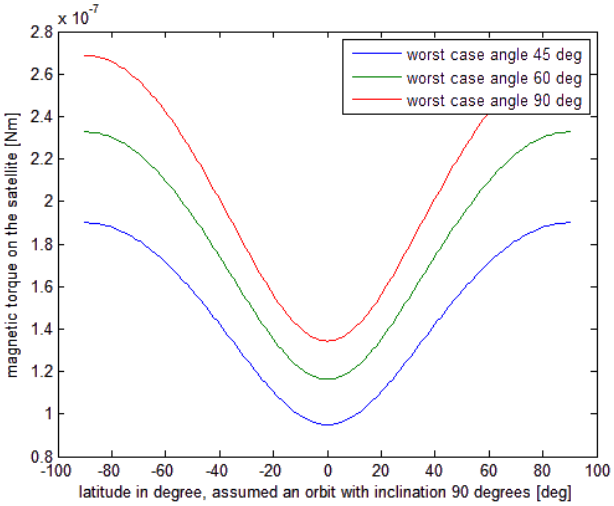

Figure 10.2: Magnetic disturbance torques for the ANT-2 RCC carrying satellite

In table 10.6 the input values that are used for the estimation can be found. Since the disturbance torque depends on the latitude, a function is created from which the results can be seen in figure 10.2. Naturally the disturbance torques are the highest

when θ is 90 °. The maximum disturbance torque for the three satellite types and the required angular momentum storage (integration over half a period) are given in table 10.6.

At every point in space (specific orbit height, latitude and longitude), the magnetic field of the Earth has a defined strength in three directions. This can cause the satellite to rotate around its x and y body axis. As the interference of two magnetic fields doesn't result in a torque around the field lines itself, the Earths magnetic field doesn't cause the satellite to rotate around its z-axis (under the assumption the satellites magnetic field lines are parallel to the body z-axis). It is assumed that the torque given by equation 10.3 is the maximum disturbance torque around x or y-axis. For further studies it is recommended to model the Earths magnetic field and satellite in 3D, such that a better estimate can be given of the actual disturbance torques acting around x and y-axis.

Inputs			Outputs		
Parameter	**Unit**	**Value**	**Parameter**	**Unit**	**Value**
D	Am^2	0.05	$T_{RCC_{magn}}$	Nm	$2.68{\cdot}10^{-7}$
M	$Tesla \cdot m^3$	$7.8{\cdot}\ 10^{15}$	$T_{ARCTIC_{magn}}$	Nm	$2.51{\cdot}10^{-7}$
R_{288km}	km	6666	$T_{TMA_{magn}}$	Nm	$2.45{\cdot}10^{-7}$
R_{443km}	km	6821	$H_{RCC_{magn}}$	Nms	$3.73{\cdot}10^{-5}$
R_{500km}	km	6878	$H_{ARCTIC_{magn}}$	Nms	$3.48{\cdot}10^{-5}$
			$H_{TMA_{magn}}$	Nms	$3.40{\cdot}10^{-5}$

Table 10.6: inputs and outputs for the calculation of the worst case torque due to the Earth's magnetic field

10.2.4 Gravity gradient

As the satellite is non-symmetric, it experiences a torque around its center of gravity due to the Earth's gravitational force varying over the object. The gravity gradient disturbance torque can be calculated using equation 10.4.

$$T_g = \frac{3\mu}{2R}|I_{zz} - I_{xx}|sin(2\theta_{grav}) \tag{10.4}$$

T_g is the gravity gradient torque around the body x-axis, μ is the Earth's gravitational constant (μ = $3.986 \cdot 10^{14}\ m^3/s^2$), I_z and I_{xy} are the moments of inertia in kg·m^2 around the body z and the x/y-axis, respectively. θ_{grav} is the angle between the local vertical and the body z-axis.

The maximum gravity gradient torque is either around the x or the y-body axis, depending on which of the moments of inertia is the smallest. In the case of the C^{3}EO satellites the moment of inertia around the x-axis is the smallest, and hence the maximum disturbance torque on the satellite acts around the body's y-axis.

The torque has a cyclic and a secular (constant) part. The estimation of the secular part is not part of this study, the gravity gradient torque is assumed to be fully cyclic [47]. As the secular part of the magnetic disturbance torque is important for momentum build up, it is recommended that this is investigated in further studies. It can be seen from figure 10.4 that the maximum torque occurs when θ is 45 °.

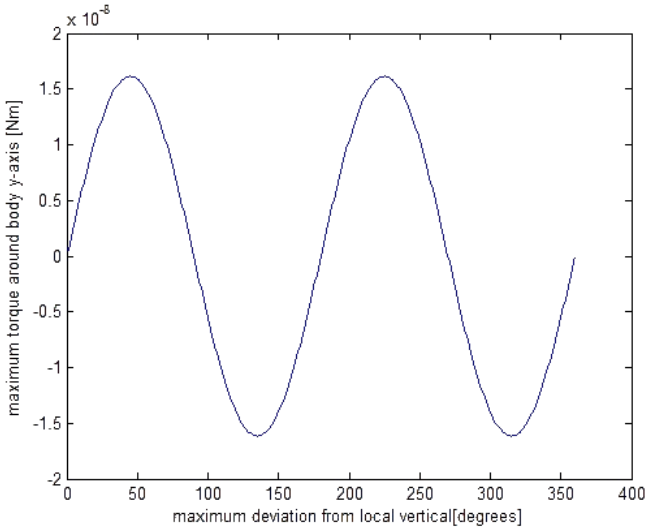

Figure 10.3: Maximum gravity gradient torque for ANT-2 RCC carrying satellite

The maximum torque and the required angular momentum storage (over half a period) can be found in table 10.7. In this table only the torque and angular momentum storage for the ANT-2 RCC carrying satellite is given, as can be seen in equation 10.4 this satellite experiences the highest torque as it has the lowest orbital radius.

Inputs			Outputs		
Parameter	**Unit**	**Value**	**Parameter**	**Unit**	**Value**
μ	km^3/s^2	$3.98{\cdot}10^9$	$T_{RCC_{y,grav}}$	Nm	$1.82{\cdot}10^{-8}$
R_{288km}	km	6666	$H_{RCC_{y,grav}}$	Nms	$4.92{\cdot}10^{-5}$
I_z	kg/m^2	0.033			
I_x	kg/m^2	0.024			

Table 10.7: inputs and outputs for the calculation of the worst torque due to the gravity gradient

10.3 Control actuator sizing

Using the estimation of the worst case disturbance torques the controller actuators can be sized. Several control actuator types exist, but not all meet the mission requirements. In the concept phase of the ADCS a feasibility study is done on all these actuator types. An overview of the study is provided in appendix C, table C.1. It concludes that only a zero momentum system with either reaction wheels or thrusters can be used for the mission.

For the ACS design (attitude control subsystem) the option of having a reaction wheel system in combination with a thruster system that counteracts drag is analysed. However, if a very mass efficient thruster system is developed for the C^{3}EO mission, it is possible to replace the ADCS's functions.

In this section the design and selection of the controller actuators is discussed, which is comprised of the micromotor, reaction wheels and magnetotorquers.

10.3.1 Motor

The flywheels of the reaction wheel systems are attached to a small micromotor. The characteristics of this micromotor together with the flywheel mass moment of inertia determine the performance of the reaction wheel system.

There are several suppliers for microengines which have over a hundred engine types. Therefore, the motor of the DELFI-N3XT is taken for the C^{3}EO satellites, the Faulhaber 1202 004BH see figure 10.4, as this engine has already proved its performance. The characteristics of this engine are given in table 10.8.

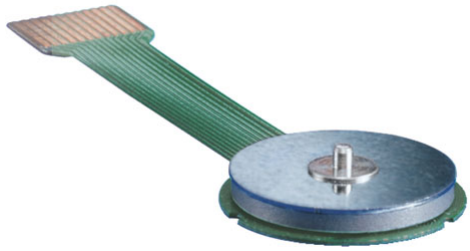

Figure 10.4: Faulhaber brushless DC-micromotor 1202 004 BH, [48]

Characteristic	**Unit**	**value**
Mass	g	1.1
Maximum torque	mNm	0.16
Power supply max angular velocity	W	1.3
Maximum angular velocity	rad/s	4200
Maximum angular acceleration	rad/s^2	1800
Assumed design angular velocity	rad/s	3100
Assumed design angular acceleration	rad/s^2	1500

Table 10.8: Characteristics of Faulhaber 1202 004 BH flat brushless DC-micromotor[48]

10.3.2 Reaction wheel sizing

For the sizing of the reaction wheels, the worst case disturbance torques and the highest required angular momentum storage are taken. It can be seen in table 10.3 that the required angular momentum storage is the highest for the reaction wheel that counteracts torques around the y-axis. Using these torques and angular momentums for the wheels for the other axis as well means that there is a chance that they are over-designed.

The ACS needs to be able to counteract the maximum disturbance torque, but also needs to be able to store the angular momentum. The maximum torque and the stored angular momentum of the flywheel can be calculated by equation 10.5 and 10.6.

$$T_{max_{wheel}} = I_{wheel} \cdot \alpha_{max_{wheel}} \tag{10.5}$$

In this equation, $T_{max_{wheel}}$ is the maximum torque delivered by the reaction wheel Nm, I_{wheel} is the mass moment of inertia of the wheel $kg \cdot m^2$,$\alpha_{max_{wheel}}$ the maximum angular acceleration of the wheel rad/s^2.

$$H_{max_{wheel}} = I_{wheel} \cdot \omega_{max_{wheel}} \tag{10.6}$$

In this equation, $H_{max_{wheel}}$ is the maximum angular momentum to be stored in the reaction wheel Nms, I_{wheel} is the mass moment of inertia of the wheel $kg \cdot m^2$ and $\omega_{max_{wheel}}$ the maximum angular velocity of the wheel $[rad/s]$.

It is concluded right away that with the use of the Faulhaber 1202 engine the maximum disturbance torque can be accounted for, as it can deliver 0.16 mNm, and the maximum required torque is only $1.19 \cdot 10^{-5}$ Nm (see table 10.3). This means that the required angular momentum storage determines the mass moment of inertia of the flywheel, hence its mass. Applying a safety factor of 1.3 and using the maximum required angular momentum storage of 0.063 Nms, the calculation results in a required design mass moment of inertia of $2.61 \cdot 10^{-5} kg \cdot m^2$. The resulting mass and dimensions of the flywheel system are found in table 10.9

Characteristic	Unit	Value
Mass one flywheel	g	43
Material density (bronze)	kg/m^3	8900
Wheel diameter	mm	70
Wheel height	mm	1.4
Number of wheels	-	4
Mass reaction wheels (incl engine)	g	175

Table 10.9: Characteristics of disk flywheel system

The height of the flywheel is small in comparison with its diameter. For a further study it is recommended to give another shape to the reaction wheel. The shape is now disk-like, but a configuration can be used that is thicker at its outer radius, such that the flywheel becomes more compact. It also has to be noted that it is not convenient to have a flywheel with just 1.4 mm thickness, as manufacturing and assembly deviations can cause the system to vibrate and increase power consumption.

As stated in table 10.9, the reaction wheel system has four flywheels. Three of them are placed perpendicular to each other, the fourth redundant one is placed slightly off the three orthogonal planes. In this way the redundant reaction wheel is able to produce a torque around all three axis. This is visualized in figure 10.5, in whicn also the magnetotorquers and supporting structure are shown.

10.3.3 Magnetotorquer sizing

Secular torques cause momentum build up in the reaction wheels, but the reaction wheels have a maximum angular velocity and acceleration. Therefore the reaction wheels have to be offloaded once in a while, which can be done with a magnetotorquer.

A magnetotorquer is an electromagnet, through which a current is applied. An electric field is created, causing the satellite to rotate in such a way that the field of the electromagnet and the Earth's magnetic field become aligned. If it is known how the magnetic field of the Earth is aligned with the magnetotorquer (measured by the magnetometer), a torque can be applied.

The magnetometer is sized with the help of an existing magnetotorquer rod provided by cubesatshop which weighs 30 grams and has a magnetic moment of $0.2A \cdot m^2$. The required magnetic moment of the magnetotorquer can be calculated using equation 10.7

$$D_{torquer} = \frac{T_{design}}{B_{Earth}} \tag{10.7}$$

$D_{torquer}$ is the magnetic moment of the magnetotorquer and T_{design} is the maximum disturbance torque the ACS is designed for. B_{Earth} is the magnetic field of the earth at orbit height, which can be taken $5.37 \cdot 10^{-5}$ Tesla at 288 km altitude. With the maximum disturbance torque given in table 10.3 (taking the safety factor into account), this results in a required dipole moment of 0.29 $[A \cdot m^2]$.

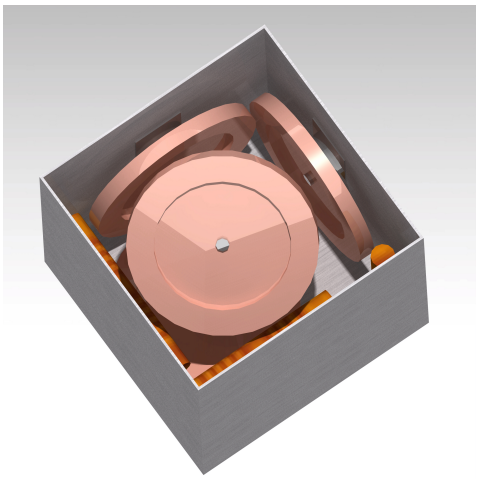

Figure 10.5: Scematic representation of the reaction wheel assembly, including flywheel and micromotor, which shows the position of the three normal operating flywheels and the redundant flywheel.

The magnetic moment of a magnetotorquer linearly depends on the number of coils, the applied current and the cross-sectional area. This means that the weight of the magnetotorquer linearly depends on the magnetotorquer mass. The mass of one magnetotorquer is calculated to be 43 g, which results in a total mass of 130 g for the magnetotorquer system consisting out or three magnetotorquers.

10.4 Sensors of the ADCS

Pointing the satellite goes in two phases: first the attitude of the satellite is determined, after which it is controlled. To provide the satellite with a high pointing accuracy the satellite needs a high determination accuracy and control accuracy. To determine the attitude of the satellite a sensor will be used. Several more sensors are needed to support the actuator system.

10.4.1 Attitude determination

Nadir pointing has to be better than 0.25 ° for all the satellites in the C^{3}EO constellation, meaning that the sensors have to determine the satellites' attitude to 0.25 ° accuracy.

To determine the satellites' attitude with respect to the local vertical, horizon and nadir, a combination of sensors can be used, such as sun sensors and magnetometers. However, a fine sun sensor is, at best, able to determine the attitude of the S/C with a precision of 1 °. A better option is to use a star tracker, which are currently under development for nanosatellites. An example is the STELLA star tracker, being developed by the University of Würzburg . The star tracker has a power consumption of 200 mW, weighs 120 g and is able to determine its attitude in the order of 0.01° around pitch and yaw axis and 0.04° around its roll axis.

If a star tracker with a very high accuracy is used for this mission, the structure on which it is mounted has to be very temperature stable. As the temperature of the ARCTIC carrying satellite varies in a range of ± -80°- ± 25°, errors in the attitude determination can arise. It is recommended to further study the influence of the structure on this error and the possibilities to decrease it.

Using a star tracker requires a sensor that provides the star tracker with information of in-orbit position. Combining the information of the star tracker and this sensor leads to the attitude offset of the required nadir pointing position. This subsystem could be a GPS receiver, which can be bought on the CubeSat shop for 12.000 EUR.

10.4.2 Measuring angular velocities

The control system makes use of a PID or PD control. This means that the controller torque is proportional to the attitude, the angular velocity of the S/C and the angular acceleration. A gyroscope is needed to determine the angular velocity, from which the angular acceleration can be determined as well. An example is the 3-axis gyroscope L3G3200D, which weighs ± 10 grams and for which the bandwidth of the measured velocities can be adapted by the user.

10.4.3 Measuring linear acceleration

The sensors of the ADCS also include a 3-axis linear accelerometer. This sensor is needed to determine the acceleration in the direction of the velocity vector, such that the thruster system can apply a force to counteract the drag. An example of a sensor

that can be used is the 3-axis linear accelerometer LIS331HH. It is space graded and weighs only 24 g.

10.5 Attitude control simulation

The attitude control of the satellite can be simulated with MATLAB. A simple simulation using PD control and simplified S/C dynamics is made for the ADCS. The MATLAB program, which does not take sensor inaccuracies into account, can be used to determine whether the satellite can be stabilized. This is an interesting part of the ADCS design, where by running the simulation several times for different inputs, the impact of the satellites' design parameters on the ADCS design can be seen. An explanation on the algorithm of the simulation can be found in appendix D.

10.5.1 Detumbling phase of the satellite

As can be found in tables 10.1 and 10.2 that the satellite must be able to detumble from initial rotational velocities of $100°/s$. It can be seen in figure 10.6 that the reaction wheels are not be able to detumble the satellite, meaning that the satellite cannot stabilize.

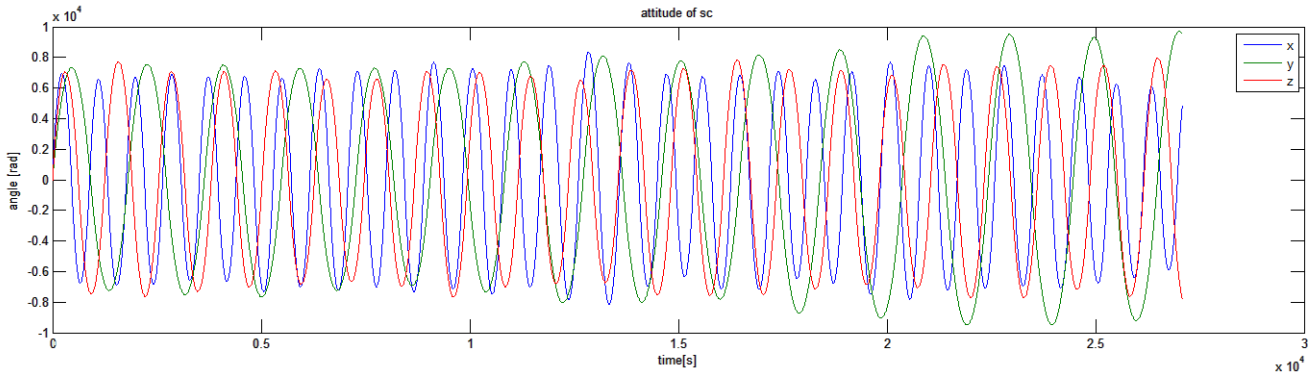

Figure 10.6: Attitude of the RCC carrying satellite for an initial rotational velocity of 100 $°/s$ around all axis, simulated for five orbital periods

It can be concluded that to detumble the satellite, the magnetotorquers, the thrusters and the reaction wheels need to cooperate. The main devices that detumble the satellite during acquisition mode are the magnetorquers and the thrusters.

10.5.2 Effect of solar panels on attitude control

In an initial stage of the design, the solar panels were designed to be placed on top of the satellite. In a later stage of the project the solar panels moved to one of the the sides of the satellite. The influence this has on the reaction wheels can be clearly seen in figure 10.7 and 10.8.

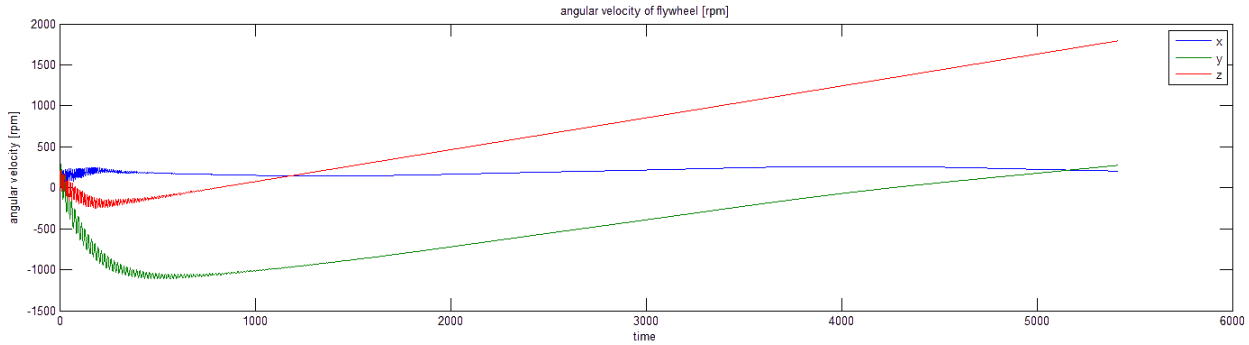

Figure 10.7: Simulated angular velocity of the flywheel for one orbital period, for an initial rotational velocity and attitude of the satellite of 0.01 rad/s and rad around all axis, simulated for one orbital period. Solar panels are mounted on the top

By comparing the two graphs it can be seen that the change of location of the solar panels does not greatly influence the reaction wheel that compensates torques around the x-axis. However it can be seen that the wheel that counteracts for torques around the y-axis has to rotate much faster when the solar panels are mounted on the sides. The angular velocity of the reaction

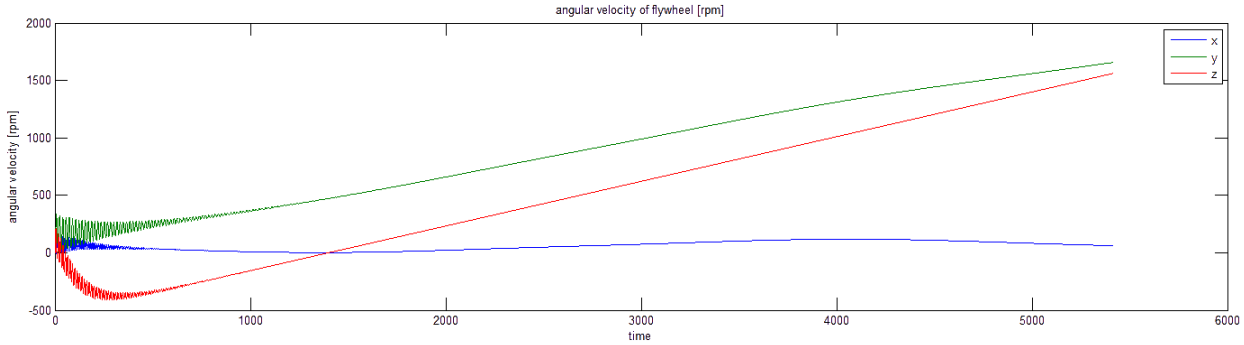

Figure 10.8: Simulated angular velocity of the flywheel for one orbital period, for an initial rotational velocity and attitude of the satellite of 0.01 rad/s and rad around all axis, simulated for one orbital period. Solar panels are mounted on the side

wheel around the z-axis is lower for the satellite which has its solar panels mounted on the side, however in the graph it can be seen that there might be a point after t=5000 where the angular velocities around y and z-axis equal each other. This means that the z-axis is the most hard to control.

Changing the location of the solar panels from the top to the side does not change the stability of the satellite. The satellite is still stable around body x, y and z-axis, as can be seen in figure 10.9.

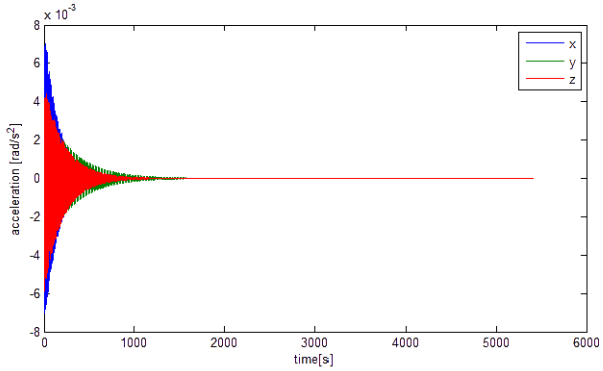

(a) Angular acceleration of spacecraft

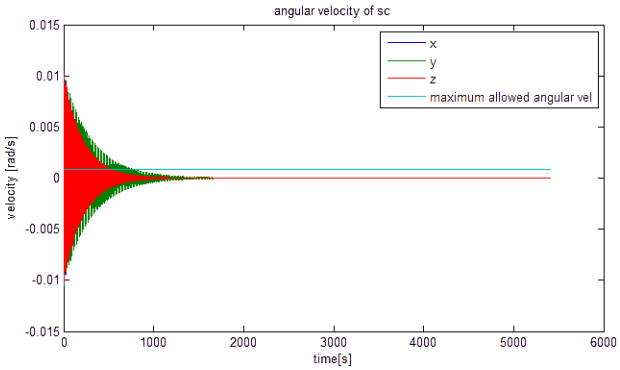

(b) Angular velocity of spacecraft

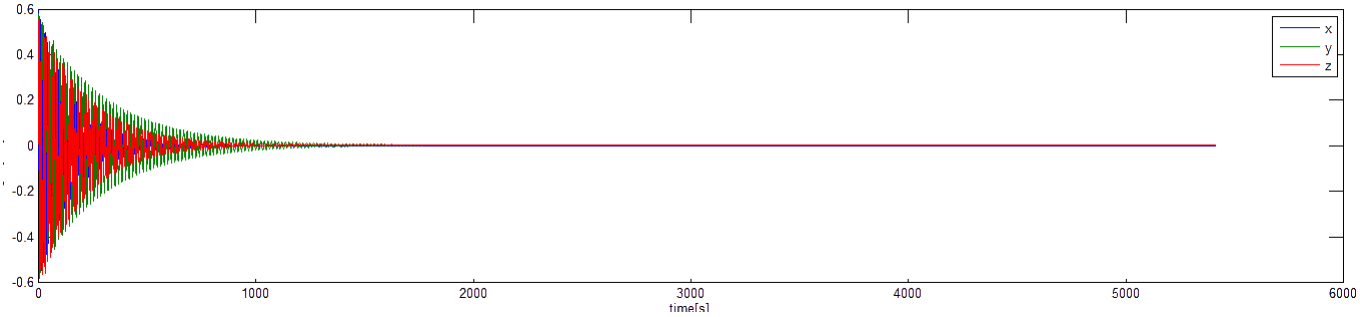

(c) Attitude of spacecraft

Figure 10.9: Angular velocity of spacecraft [rpm]

10.5.3 Control accuracy of the satellite

The pointing accuracy of the satellite depends on two values: the control accuracy and the determination accuracy of the ADCS. With the help of the simulation the control accuracy can be estimated. The simulation does not take time delays of the actuators into account, so a margin has to be taken into account when interpreting the results.

In figure 10.10 it can be seen that the satellite stabilizes itself during the imaging mission. The control accuracy is in the order of 10^{-3} rad It may be assumed that even when taking a margin for actuator delay into account, the control accuracy stays below $10^{-}2$ rad.

In figure 10.11 the flywheel characteristics can be found. It can be seen that after one period the flywheel reaches a rotational velocity in the order of 10^{2} rad/s As the engine can spin up the flywheel up to 3100 rad/s it is concluded that the flywheel does not need to be desaturated for another 10 orbits.

However a recommendation can be made for another more compact low-weight flywheel design. This recommendation

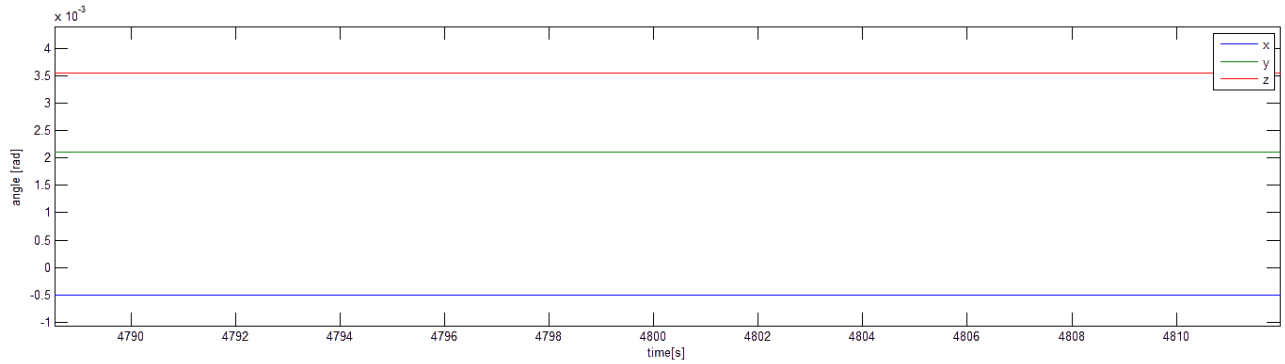

Figure 10.10: Detail of figure 10.9 showing the angles around x y and z-axis around which the satellite stabilizes

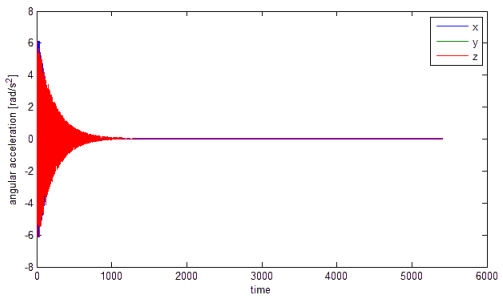

(a) Angular acceleration of flywheel

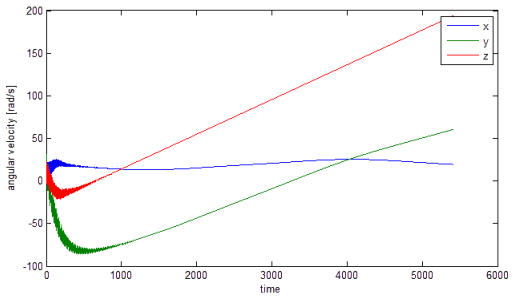

(b) Angular velocity of flywheel

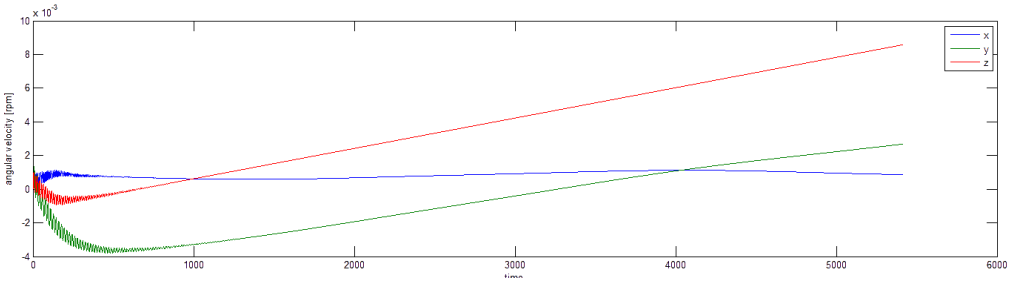

(c) Angular velocity of flywheel [rpm]

Figure 10.11: Control wheel angular motions for an initial rotational velocity and attitude of the satellite of 0.01 rad/s and rad around all axis, simulated for one orbital period

consists of decreasing the weight of the flywheel and increasing the use of the magnetotorquer. Namely, if the magnetotorquer is used more constantly throughout the mission, the flywheel momentum build up will be lower. The magnetotorquer can even be designed to counteract all the secular disturbance torques in such a way that the reaction wheel only has to account for the cyclic torques. In a further study a simulation of this situation should prove that while using this control strategy throughout the whole mission, the flywheel never saturates.

Figure 10.12 shows the total disturbance torque and the control torque of the flywheel. It shows that the disturbance torque on the satellite is one order magnitude lower than the control torque. The reaction wheels were designed to desaturate once per orbit when it delivers a torque equal to the maximum disturbance torque it experiences. However as the torque the flywheel delivers is higher than the disturbance torque, this means that in a worst case scenario it has to deliver a torque which is *higher* than the maximum disturbance torque. Although the flywheel itself is not designed for this, the micromotor is able to deliver the required torque. However, momentum build up will be larger than H_{design} and the the flywheel becomes saturated faster than it is designed for. It is possible to change the actuator controller torque by lowering the proportional and derivative controller gains.

As shown in table 8.5 choosing for the thin film solar panels instead of the triple junction cells means that the satellite has a larger mass moment of inertia. Using the simulation a similar graph as shown in figure 10.8 can be made for the case when the satellite would have the triple junction cells. However the the difference with graph representing the current design is so small it cannot be seen from simple comparison. Precise estimations done by MATLAB point out the velocities are 1.5% lower for the case of the triple junction cells compared with the thin film solar cells. Hence it can be concluded that the type of solar cells doesn't have significant influence on the design and performance of the ADCS.

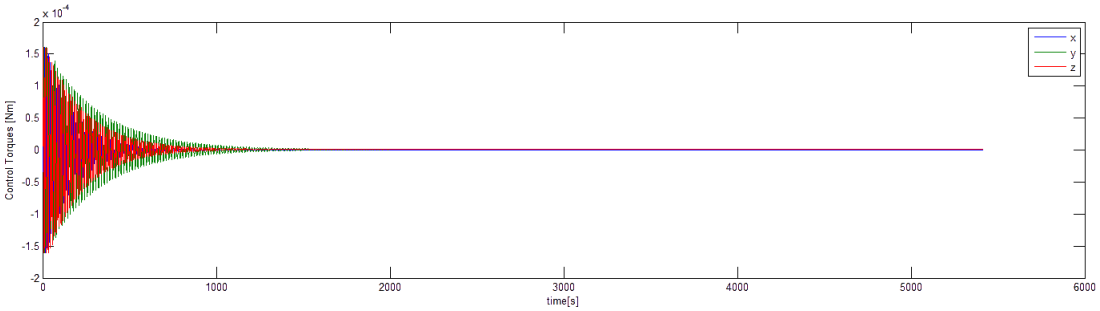

(a) Control torques of flywheel

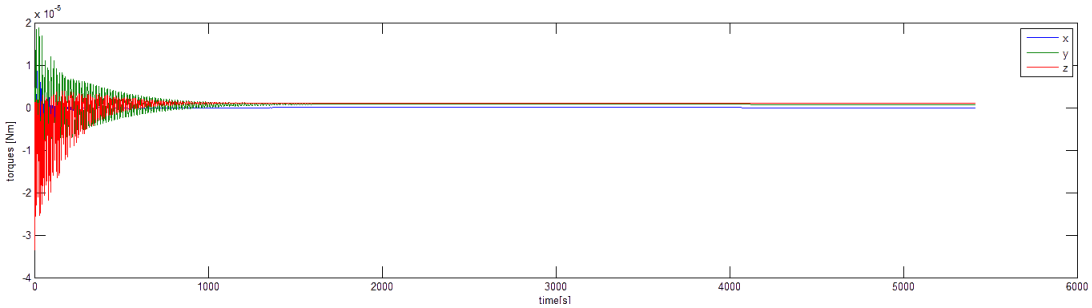

(b) Disturbance torques acting on the satellite

Figure 10.12: Control and disturbance torque for an initial rotational velocity and attitude of the satellite of 0.01 rad/s and rad around all axis, simulated for one orbital period

10.5.4 Stability of the satellite

The required maximum angular velocities of the satellite are restricted. It is therefore important to check if the velocities do not exceed the limits. The most strict allowed angular velocity on the satellite that is carrying an ANT-2 camera, being 0.05 °, is plotted in the figure 10.9b. It can be seen that the angular velocities are around zero when the satellite is stabilized and are lower than the maximum allowed angular velocity. However as in this simulation sensor inaccuracies are not taken into account nothing can be said about the actual angular velocities that will be experienced during operation, as they depend on the inaccuracy of the attitude determination and gyros.

10.5.5 Validation of the results

Without validation of the results from the simulation no conclusions can be drawn from the algorithm that has been written. Therefore, a comparison has been made between the results for the C^{3}EO and the DELFI-N3XT missions. Control accuracy of the DELFI-N3XT satellite highly depends on the mode of the satellite. DELFI-N3XT makes use of sun-sensors, which are not able to determine the satellites attitude during eclipse. Therefore, during eclipse the controller only uses information about angular velocity and acceleration of the satellite, which causes the satellite to start tumbling. When the satellite is out of the eclipse the satellite first has to detumble again before it can reach its pointing accuracy of 3 °.

For the C^{3}EO mission, an expert on the DELFI design, J. Bouwmeester, has recommended the use a small star tracker to determine its attitude, such that the satellite is able to ensure pointing continuously. Of course, making a comparison between DELFI-N3XT and C^{3}EO missions is difficult without taking sensor and actuator inaccuracies into account, but a comparison has shown that the results are within an acceptable range.

10.6 Summary of the ADCS characteristics

In this section the results of this chapter are summarised. The results from the ADCS design are also compared to the requirements.

10.6.1 Summary of actuators and sensors

In table 10.10 a summary can be found of the most important design characteristics of the ADCS. A cost estimate is made as well, for which the cost budget of DELFI-N3XT was taken as a reference. The cost of the star tracker and the linear accelerometer are roughly estimated, and their contingency factor is assumed to be relatively high.

Element	Mass[g]	Average power supply [mW]	Estimated cost [EUR]	Contingency on cost [%]
Reaction wheels	175	1500		
Magnetotorquer	130	150		
Magnetometer	15	10		
Gyroscope	10	100	3,000 (sum of above)	20
Star tracker	120	200	10,000	200(based on expert estimate)
Linear accelerometer	24	250	800	50
electronics and support	150	150	2,000	20
GPS reveiver	100	30	12,000	0

Table 10.10: Design characteristics of the ADCS

10.6.2 Evaluation of the requirements

Requirements were set for detumbling, pointing accuracy and maximum angular velocity.

The program used to simulate the control of the spacecraft points out that the flywheel is not able to detumble the satellite from initial velocities of 100 $^{\circ}/s$ by itself. It is recommended to let the magnetotorquer and the thrusters detumble the satellite in its acquisition phase.

The simulation also shows that the control accuracy, without taking controller inaccuracies into account, is in the order of magnitude of $10^{-3} rad$. Together with the very high pointing accuracy of the star tracker, which which is around 0.04 $^{\circ}$, it is likely that the satellite is able to have a high pointing accuracy. However, nothing can be concluded yet about the order of magnitude of the accuracy, as the created simulation does not take sensor inaccuracies into account.

The simulated results for the angular velocities of the satellite are within the limits that have been set. However, nothing can be concluded without taking control and actuator inaccuracies into account.

For further studies it is recommended to use a randomizer to simulate the control inaccuracies. This randomizer has to produce values with a normal distribution, as this approximates the real behaviour of the sensors most accurately. It is also recommended to check how fast data is measured by the star tracker and gyroscope, as this induces a delay in the control system. Furthermore, extra attention should be paid to simulation of the engine, as the model does not take into account the time that the motor needs to accelerate or decelerate to a certain angular velocity. When the ADCS is modeled more precisely, the average angular velocities of the flywheel can also be estimated better, from which it can be derived how much power they consume. This will result in better power requirements and solar panel design.

Chapter 11 | Propulsion subsystem

In this chapter an elaboration on the propulsion subsystem design is given. First a summary of propulsion performance requirements is presented in section 11.1. The atmospheric drag effects on different satellite configurations, in terms of propellant mass, are analysed in section 11.2. In section 11.3 a propulsion system is chosen that can meet the requirements in the most efficient way. Finally, the propulsion subsystem is sized and an overview of characteristics is displayed in section 11.4.

11.1 Performance requirements

The propulsion system should be able to provide the required velocity change for the two year mission duration in the most efficient way, meeting the challenging design constraints for a CubeSat sized satellite in terms of volume, mass and power. Aspects of influence for the ΔV budget are: orbit insertion, orbit phasing, orbit maintenance, controlled de-orbit and attitude control. The theory and equations to calculate these velocity changes are explained over the next sections. In the final section all the calculation results are displayed in a single table.

11.1.1 Orbit insertion

The three groups of different satellites must be launched to their correct orbit altitude and inclination. Each group, consisting of the same satellites, is launched together in a single Shtil[49] launcher, adding up to a total of three launchers. Although a launcher should deliver the satellites to the exact correct orbit, injection errors are a common occurrence. As a result, the satellites themselves should be able to adjust these errors by performing small plane changes and orbit raising manoeuvres. The Shtil launch manual[50] provides an indication of the order of magnitude of the injection errors; an overview is listed in table 11.1. For the calculations the most conservative values are used: 10 km for altitude inaccuracy and 0.2 deg for the inclination inaccuracy.

Orbit insertion error	Units	Shtil
Altitude error	km	4-10
Inclination error	deg	0.08-0.2

Table 11.1: Orbit insertion error

For now, the orbit adjustments are assumed to be performed separately. This means that the inclination is changed according to a so-called *simple plane change*[12] manoeuvre, in which the orbit size remains the same. The orbit raising is performed using a so called *spiral transfer*[12] in which the orbit altitude is changed by using a constant low-thrust burn. The velocity changes required for reaching the correct orbit altitude, ΔV_h, and plane change, ΔV_ω, can be calculated using equations 11.1 and 11.2, respectively;

$$\Delta V_h = \sqrt{\frac{\mu}{R_b}} - \sqrt{\frac{\mu}{R_a}} \tag{11.1}$$

$$\Delta V_\omega = 2 \cdot V \cdot sin\frac{\Delta\omega}{2} \tag{11.2}$$

where V are the orbital velocity, $\Delta\omega$ the required plane change angle, μ the standard gravitational parameter and R_a and R_b is the orbit radius of the initial and final orbit respectively.

11.1.2 Phasing

When the satellites, that are destined to be in the same orbit but in different orbit phases are launched together, they need to phase out after launch. A maximum phasing distance of half an orbit, π, is assumed to determine the required velocity change. The equation for the required ΔV for phase change is:

$$\Delta V_\theta = 4 \cdot \frac{r \cdot \theta}{t} \tag{11.3}$$

where r is the orbit radius, θ the required phase change which is π in this example and t which is the required time for orbit phasing. A phasing time of 10 days is regarded as acceptable with respect to a 2 year mission duration.

11.1.3 Orbit maintenance

The presence of particles in the low Earth orbit causes atmospheric drag. The density of these particles strongly depends on altitude and solar activity, as can been seen in figures 11.1 and 11.2. Above 600 km the drag is so weak that its influence can easily be neglected or easily accounted for, however, at lower orbits atmospheric drag does play a very important role.

In the Earth's thermosphere, between 120 and 600 km, ultraviolet radiation is absorbed which has as a result that the temperature increases and approaches the limiting exospheric temperature at an altitude around 225 km[12]. Furthermore, the thermosphere may also be heated from geomagnetic activity. This increase in temperature results in an expansion of the thermosphere, causing the molecules to shift to higher orbits, thereby increasing the local density.

As can be seen in figure 11.1[51] the solar activity seems to vary on an 11 year basis, with large differences up to a factor of four between solar maximum and a solar minimum on a single altitude. When looking at the altitude range between 250 and 500 km the variation can even build op to one order of magnitude.

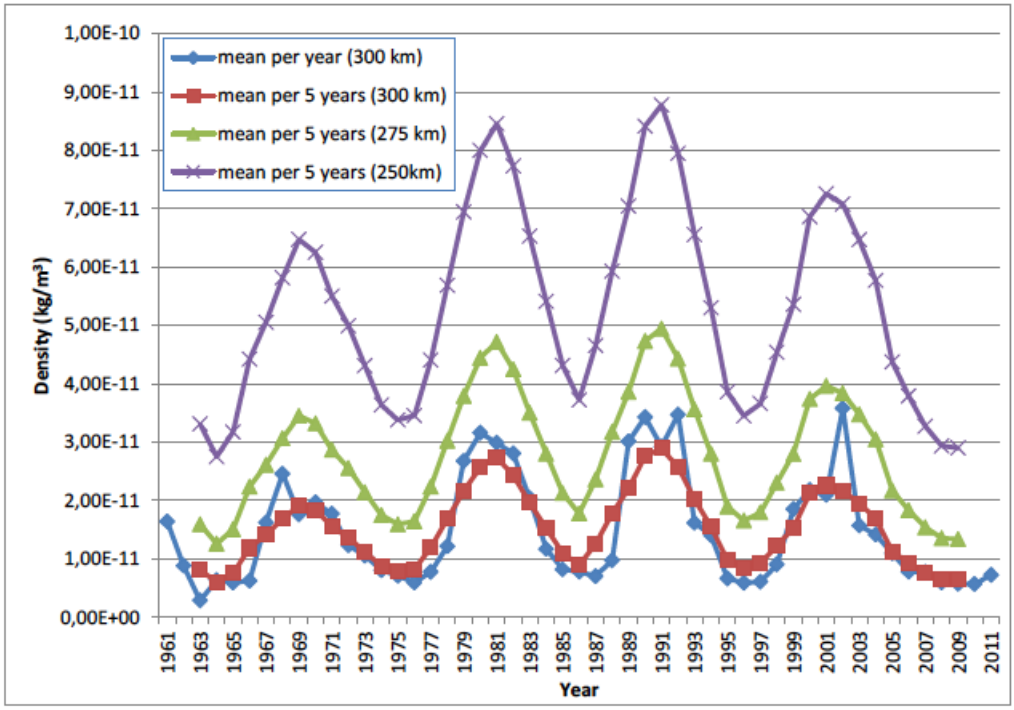

[51]

Figure 11.1: Solar activity variation

Next to this, the day to day activity can also change significantly, making density prediction very difficult. The $F10.7$ index indicates mean daily solar radio flux and can be used to calculate average solar activity over longer periods. Next to the $F10.7$, the Ap index is a measure of geomagnetic activity, which also influences the density. Both indices are used to calculate a 20 year average from 1992 until 2012. For solar activity, $F10.7$, an average of 108.7 10^{-22} $Wm^{-2}Hz^{-1}$ is determined and for the geomagnetic activity, Ap, an average of 12.4 nT. Because of their effect on density, the solar and geomagnetic activity have a great impact on the decay rate of satellites: they decay faster in periods of high activity and vice versa. The density variation as a function of altitude for the average values of $F10.7$ and Ap is demonstrated in figure 11.2 .

The ballistic coefficient is an indicator of the sensitivity of certain satellite shapes to orbital decay. Satellites with a high ballistic coefficient decay slower than satellites with a low coefficient. The equation is given by:

$$\beta = \frac{m}{C_d \cdot A} \tag{11.4}$$

Atmospheric drag removes energy from the orbit thereby reducing the orbit height. At a lower orbit height a higher density is encountered which further increases the drag. If this drag is not counteracted by some form of propulsion, the satellite quickly re-enters the Earth's atmosphere. The drag force and the corresponding velocity change to overcome the drag are given by:

$$F_d = 0.5 \cdot \rho \cdot V^2 \cdot C_d \cdot A \tag{11.5}$$

$$\Delta v_D = 0.5 \cdot \rho \cdot (\frac{C_D \cdot A}{m}) \cdot V^2 \cdot \Delta t \tag{11.6}$$

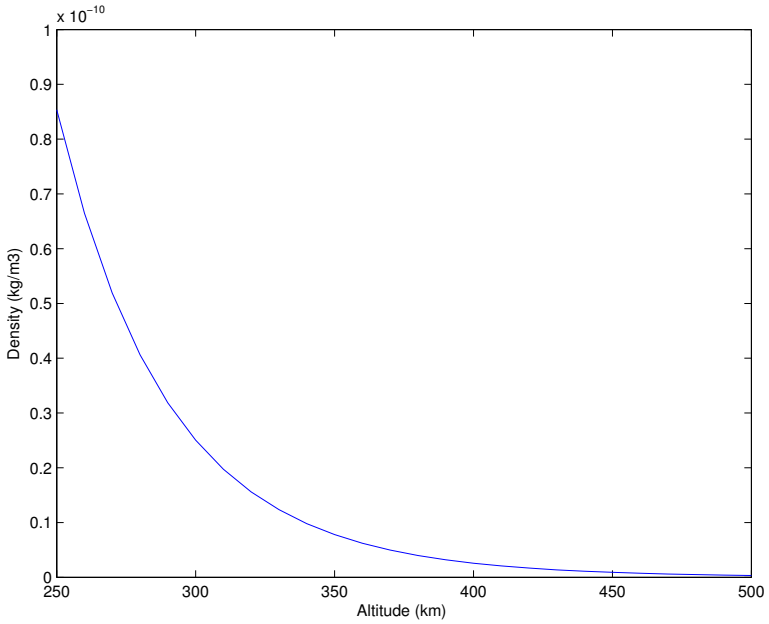

Figure 11.2: Density as function of altitude for mean values of F10.7 (108.7) and Ap (12.4)

Where ρ is the density, C_d the drag coefficient, A the cross sectional area, m the satellite mass, V the orbital velocity and Δt the mission duration.

The drag coefficient depends on the satellite shape and the way in which the molecules impact on it. For all satellites a drag coefficient of 2.3 is assumed. However, the drag coefficient is not easily determined, and real life drag coefficients can differ substantially from predictions. Some sources[51][52] assume that a drag coefficient of 2.2 or 2.3 is reasonable. At the same time, standard flat plate theory suggests a C_d of 1.28[53]. The Oscar-1 satellite is an appropriate satellite for reference; it is a 5 kg, box shaped satellite and has an estimated minimum C_d of 2 and maximum C_d of 4[12], which is factor 2 difference.

As can be seen from equation 11.5 the drag coefficient directly determines the required ΔV for drag compensation, and thus has a great impact on the propellant mass, which is given by equation 11.7.

Next to the drag coefficient, the specific impulse(I_{sp}) is also of great importance to the propellant mass. It is measure of how efficient the propellant is used to generate a velocity change and its value varies a lot between the different propulsion systems. Its influence on the propellant mass can also be seen in equation11.7[51];

$$m_p = m_0[1 - e^{\frac{-\Delta V}{(I_{sp} \cdot g_0)}}] \tag{11.7}$$

Acknowledging the fact that these parameters, C_d and I_{sp}, are very important for the propellant mass budget and at the same time highly uncertain, a risk map is created to get an overview of the possible set of outcomes in terms of propellant mass. For this plot a satellite mass of 5.94 kg, a cross sectional area of 0.023 m^2 and an altitude of 288 km are used. The propellant mass values in the plot are for drag compensation only. Figure 11.3 shows the propellant mass as function of specific impulse, for three different values of drag coefficient; 1.28, 2.3 and 4.0.

It can be seen from this graph that the uncertainty related to both the drag coefficient and the achievable specific impulse causes a great distribution in outcomes for the required propellant mass. The best case scenario, having the lowest drag coefficient of 1.28 and the high specific impulse of 6000 s, requires less than 30 $grams$ of propellant while the worst case scenario, with a drag coefficient of 4.0 and specific impulse of 500 s requires over 1000 $grams$. For the calculations in the remainder of the chapter the expected values of 2.3 for the drag coefficient and 2500 s for the specific impulse are used. The possible spread in the outcome should be kept in mind however.

11.1.4 De-orbit

At the end of life the thrusters are turned off and thus the drag force is no longer counteracted, which results in the natural de-orbit of the satellite. The orbit altitude gradually decreases and eventually the satellite burns up in atmosphere. The decay time to burn up can be calculated as follows. The changes in semi major axis, orbital period and velocity for each revolution are given by [12]:

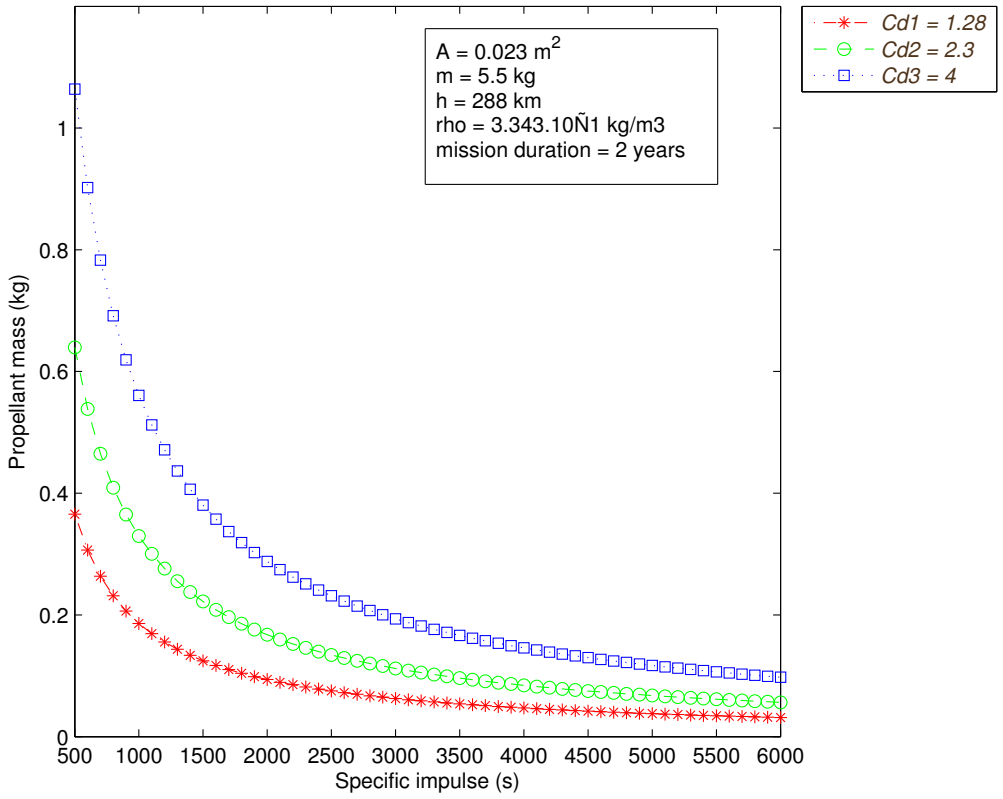

Figure 11.3: Uncertainty map of varying specific impulse ISP and drag coefficient C_d

$$\Delta a_{rev} = -2\pi(C_D A/m)\rho a^2 \tag{11.8}$$

$$\Delta T_{rev} = -6\pi^2(C_D A/m)\rho a^2/V \tag{11.9}$$

$$\Delta V_{rev} = \pi(C_D A/m)\rho a V \tag{11.10}$$

Where C_D, m and A are constants and the initial semi major axis a, the initial orbital period T_{orbit} and the initial orbital velocity V are given by:

$$a = R_{earth} + H_{orbit} \tag{11.11}$$

$$T_{orbit} = 2\pi\sqrt{\frac{a^3}{\mu}} \tag{11.12}$$

$$V = 2\pi\frac{a}{T_{orbit}} \tag{11.13}$$

The only variable that is needed to calculate the change in semi major axis is the density, which depends on altitude and solar activity level. Using Matlab these equations can be calculated repeatedly from a specific starting height. This cycle ends when the newly determined height is beneath 180 km. At this point the satellite is assumed to have burned up in the atmosphere. With each run of these calculations, the new orbital period is added to a total time variable. Once done, this gives the total time for the satellite to decay from a specific height.

Using these equations the orbital decay time is calculated for all satellites. The RCC platforms at an altitude of 288 km have an orbital decay time of 82 days which is far below the 25 years internationally agreed upon as acceptable[54]. The TMA and ARCTIC platforms at an altitude of 500 km and 443 km have a decay time of 58.6 and 16.7 years respectively, however. Instead of leaving these non-operational satellites orbiting for years, a more sustainable approach is to actively de-orbit in a spiral transfer with a constant thrust. The available thrust to de-orbit is set equal to the required thrust to overcome the drag at a 288 km orbit, when the same thruster setting is used. This reduces the decay time for the TMA and ARCTIC to 212 and 189 days, respectively.

11.1.5 Attitude control

All the disturbance torques, including the aerodynamic moment, are covered by the attitude determination and control system in the current design. It is noted however as recommendation, that the propulsion system could take over the role of 3 axis attitude control by appropriately placing the thrusters. This would make the usage of reaction wheels and magneto torquer no longer necessary.

11.1.6 Summary of ΔV requirements

All requirements for the the different satellites at different orbit heights are listed in table 11.3. For the specific impulse I_{sp} and the drag coefficient C_d the most likely values of 2500 s and 2.3 have been used. The reason for a 0.023 m^2 cross sectional area is explained in the next section, where a configuration trade-off is made. As can be seen from the table the ΔV required for drag compensation is quite significant, as expected from satellites in a very low Earth orbit.

Parameter	Units	RCC Platform	TMA Platform	ARCTIC Platform
Orbit height	km	288	500	443
Satellite mass	kg	5.5	5.3	5.7
Satellite cross section	m^2	0.023	0.023	0.023
Density	kg/m^3	$3.343 \cdot 10^{-11}$	$3.35 \cdot 10^{-13}$	$1.04 \cdot 10^{-12}$

Table 11.2: Satellite characteristics

Parameter	Units	RCC Platform	TMA Platform	ARCTIC Platform
Drag force	μN	52.9	0.5	1.6
Orbital decay without thrust	$years$	0.2	58.6	16.7
Orbital decay with thrust	$days$	76.2	212.4	188.9
$\Delta V_{de-orbit}$	m/s	0	183.5	151.8
ΔV_h (orbit raising)	m/s	5.8	5.5	5.6
ΔV_ω (orbit plane change)	m/s	27.0	26.6	26.7
ΔV_D (drag compensation)	m/s	606.4	6.1	17.8
ΔV_θ (orbit phase change)	m/s	97	100	99.2
ΔV_{tot}	m/s	736.2	321.8	301.1

Table 11.3: Propulsion subsystem requirements

As can be seen from this table, the ΔV budget for drag compensation takes up the most part of the total ΔV budget of the RCC platform.

11.2 Configuration effects on propellant mass

With the clear importance of atmospheric drag demonstrated, its effect must be reduced in the most efficient way. Three different CubeSat configurations which were covered in chapter 7 are analysed in this section in terms of their propellant mass; only the atmospheric drag and the required ΔV for drag compensation of each configuration is studied. It is important to state the other variables that are used in these calculations; they are listed in table 11.4. The RCC platform, the lowest flying satellite, is chosen as the example as it is the worst case scenario in terms of drag.

Parameter	Units	Value
Specific Impulse	s	2500
Drag coefficient	-	2.3
Mass	kg	5.5
Orbit height	km	288
Density	kg/m^3	$3.34 \cdot 10^{-11}$
Mission duration	$months$	24

Table 11.4: Variables

11.2.1 'Conventional' design

The first option is a conventional CubeSat structure with the 4 units positioned on top of each other and the camera in the bottom, directly pointing to the Earth. Taking into account a 15% contingency factor for the sticking out of antennas and solar panels the frontal area adds up to 0.046 m^2. For this design the amount of propellant mass required is 265 $gram$.

11.2.2 Rotated design

Another option is to tilt the CubeSats towards the direction of flight, thereby decreasing the frontal area by a factor 4. As can be found in chapter 7, the added mass to accommodate a mirror is 500 $gram$. For a satellite mass of 6 kg and a cross sectional section of 10 by 10 cm with a contingency factor of 15% this results in a required propellant mass of 68 $grams$. This propellant mass is significantly less than the propellant mass required for the conventional design. However, the total satellite mass has increased by around 300 $grams$ with respect to the conventional design due to the extra mass needed to place the mirror.

11.2.3 2 by 2 units

A third design option is to position the cubes in a 2 by 2 configuration. This means that no extra mirror is needed to point the camera, so no extra mass is added, while at the same time the cross sectional area is halved with respect to the conventional design, but still twice the size of the rotated design. This design results in a required propellant mass of 134 $grams$ which is clearly the best result in terms of mass as can be seen in table 11.5.

Parameter	Units	Conventional	Rotated	2 by 2
Cross sec. area	m^2	0.046	0.0115	0.023
Propellant mass	g	265	68	134
Added mass	g	0	500	0
Prop + added mass	g	265	568	134

Table 11.5: Propellant mass for different designs

When evaluating the propellant mass together with the extra required mass that belongs to a different satellite configuration it is clear that the 2 by 2 configuration, with 134 $grams$ is the solution with the lowest mass with respect to the conventional design (265 $gram$) and the rotated design(568 $gram$).

11.3 Propulsion system selection

The significant ΔV budget together with the strict volume and mass constraints that accompany the CubeSat standard requires a propulsion system with a high specific impulse, which can be delivered by electric propulsion.

11.3.1 Propulsion system trade-off

The list of considered electric propulsion systems is presented in table 11.6. It is important to note that all these propulsion systems are somewhat experimental and are undergoing continuous development. The decision is made on power required, specific impulse delivered, simplicity of the technology and technology readiness level.

Propulsion systems	I_{sp}[s]	Power [W/N]
Electrospray Thruster [55]	800	$1.3 \cdot 10^4$
Arcjet [56]	1000	$10.4 \cdot 10^4$
FEEP [51]	8000	$6 \cdot 10^4$
Colloid Thruster [51]	1150-7500	$3.7 \cdot 10^4 - 4.4 \cdot 10^4$
3 cm RF Ion Thruster [55]	2800	$5 \cdot 10^4$
Miniature Ion Electrospray Thrusters [57]	2500	$1.75 \cdot 10^4$

Table 11.6: Propulsion system characteristics

From table 11.6 it is clear that the miniature electrospray thruster is the most favourable in terms of both specific impulse and power consumption. Regarding the FEEP option, the power required is too large and the colloid's high specific impulses are only achieved in lab-scale thrusters where as flight ready models have a specific impulse of around 1000 s[55]. According to SMAD[37] the main technical barrier to a widespread application of the electrospray thruster is due to the difficulty in scaling from microscopic single emitters to large parallelized ion extraction arrays. This is now changed, as MIT claims that they are equipped for rapid production of the micro machined emitter arrays[57]. In addition, the design suggested by MIT is a flexible, modular and compact design. Due to the modular nature of this thruster, the thrusters can be distributed over the surface of

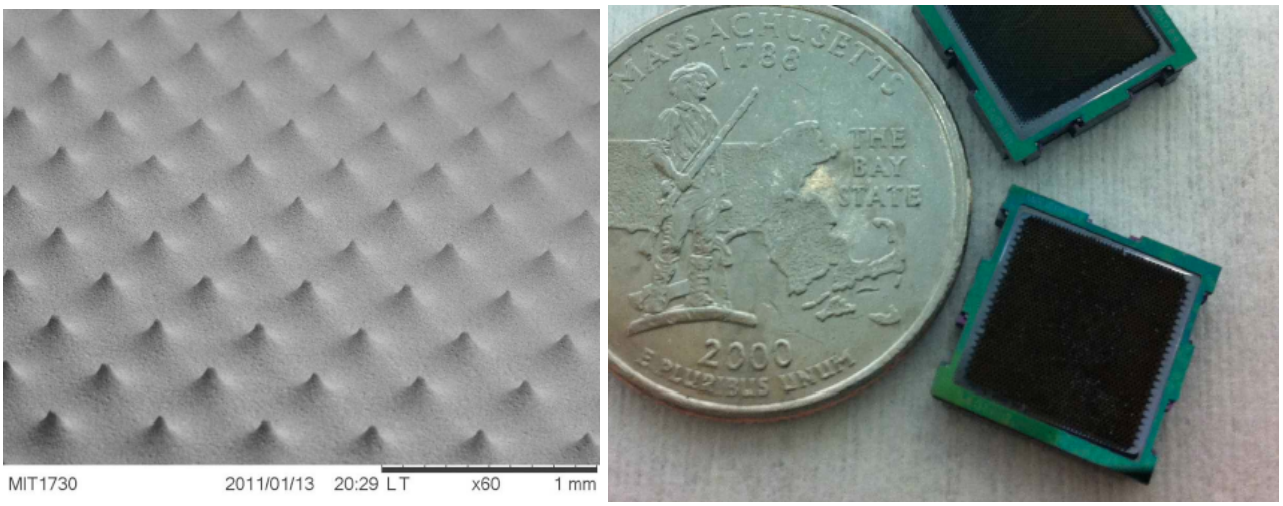

Figure 11.4: Thruster size indication

the satellite hence they can also be used for 2 or 3-axis control. Hence the Miniature Ion Electrospray Thruster is chosen to propel the spacecraft.

11.3.2 Miniature ion electrospray thruster

Miniature ion electrospray thrusters are specifically designed for CubeSats by the Massachusetts Institute of Technology[57] and offer a highly promising propulsion system in terms of efficiency and compactness. The system has no moving parts, no valves, unpressurised tanks and makes use of a zero-vapour pressure liquid. The volume size is within 1/3 of a CubeSat unit and it is potentially capable of providing three-axis attitude control and precision thrusting with an Isp of over 2500 s and potentially up to 5000 s.

Electrospray propulsion is based on the electrostatic extraction and acceleration of ions from ionic liquids. Ionic liquids have a very low vapour pressure, a high thermal stability and relatively high electrical conductivity. By electrically stressing it, the ionic fluid forms a thin layered Taylor cone over the micro-machined emitter cones. When a potential difference of between 1 and 2 kV is applied the ions are extracted and accelerated.

Advancements in electrochemical micro-fabrication made it possible to micro machine emitter cones out of porous materials. This allows them to transport the liquid via capillary forces which eliminates the need for an active propellant feeding system between the propellant tank and the emitters.

Each Taylor cone is capable of providing a thrust of 0.1 μN and by putting them into an array with an emitter to emitter distance of 450 μm a thrust density of around 0.5 N/m^2 is achieved. Each thruster module is 12 by 12 mm, has a thickness of 2.5 mm and can be positioned at any desired location on the satellites.

The thruster modules can produce either positive or negative ions. To avoid spacecraft charging the levels of both should be the same. The thruster modules come in pairs where one module emits positively charged ions and the other negative yielding a neutral exhaust plume. At the same time the voltage is alternated at a frequency of 1 Hz to maintain electrochemical neutrality so that corrosion is avoided. All this is regulated by the Power Processing Unit (PPU).

The system is, by design, very flexible and built up in three different parts: the HV electronic board provides the required voltage change from the voltage delivered by the Electrical Power System (EPS) to the required high voltage for the potential difference with a power conversion efficiency of 70%. The SW electronic board controls the voltage alternation and the ET board houses the thruster modules.

The MIT laboratory has set up their equipment for rapid production of the thruster micro-fabricated emitter arrays, assuring technological readiness and availability upon completion of the experimental phase.

11.4 Sizing

The propulsion system is sized so that the requirements are met using the capabilities of the miniature ion electrospray thrusters. For each platform, the same propulsion system is used; the only difference is in the amount of propellant mass that is taken aboard. In this way the modular approach to the usage of CubeSats is maintained.

A third of a CubeSat unit (U) is required to house all the propulsion system components. The required power is calculated using the jet power equation (equation 11.14) where the thrust is set equal to the drag force. MIT claims[58] that a 70% power conversion efficiency is achieved to which an 50% contingency is added, to account for additional losses that could occur due to the great voltage difference, of two orders of magnitude, between the EPS and the required voltage for the thrusters .

$$P_{input} = \frac{P_{jet}}{\eta_{power}} = \frac{0.5 \cdot F_{thrust} \cdot I_{sp} \cdot g_0}{\eta_{power}} \tag{11.14}$$

The drag force for the RCC, TMA and ARCTIC is 52.9 μN, 0.51μN and 1.61 μN respectively. Using the Isp of 2500 s, this results in a required power for drag compensation of 1.86 W, 0.018 W and 0.0048 W. While the RCC platforms do not need a de-orbiting manoeuvre, the TMA and ARCTIC do. The available power for this manoeuvre is set equal to the required power for drag compensation for the RCC platform of 1.86 W. The advantage of this, is that the power subsystem requirements for all the satellites are the same, which is easier for mass production.

The thruster modules are 12 by 12 mm in cross section and have a thickness of 2.5 mm. To avoid spacecraft charging they come in pairs. With a thrust density of 0.5 N/m^2 each module delivers a thrust of 72 μN which is theoretically enough to overcome the drag force. However the counteract the moment, that is created when the drag force is not working at the center of mass, the thruster elements are positioned in the corners of the satellites, as can be seen in appendix F, so that a moment arm with respect to the center of mass can be provided. Therefore, 4 thruster elements in total are used (8 modules); one thruster element in each corner.

The propellant mass is calculated using equation 11.15 for the different ΔV budgets of each satellite.

$$m_p = m_0[1 - e^{\frac{-\Delta V}{(I_{sp} \cdot g_0)}}] \tag{11.15}$$

For the RCC, TMA and ARCTIC platform a propellant mass of 163, 69 and 70 g is required to deliver the required ΔV budget. The propellant mass is dependent on the total mass, which is again dependent on the propellant mass. Therefore the propellant mass is determined by an iterative process in which some iterative loop calculations are performed. As a result the total satellite mass values from table 11.2 are calculated with a propellant mass as stated above. Included in the total mass however is a propellant mass contingency of 50% to account for the variation in density, drag coefficient and specific impulse, as is explained earlier. This means that the RCC, TMA and ARCTIC platforms are designed to actually bring along a propellant mass of: 245, 104 and 105 g respectively. Whereas the conservative value of 2500 s is used for the specific impulse, MIT suggest that an I_{sp} of 5000 s can be achieved, reducing the required propellant mass even further.

The requirements for the propulsion system are summarised in table 11.3 and the parameters of the resulting design are presented in table 11.7.

Parameter	Units	RCC Platform	TMA Platform	ARCTIC Platform
Specific impulse	s	2500	2500	2500
ΔV_{tot}	m/s	736.2	321.8	301.1
Propellant mass	g	245	104	105
System Mass	g	445	304	305
Power	W	1.86	1.86	1.86
Volume	U	1/3	1/3	1/3

Table 11.7: Propulsion system sizing

Chapter 12 | Communications & Data Handling

The communications & data handling subsystem establishes a connection to a ground station for both downlink of imagery and telemetry, and uplink of commands and firmware. As the same subsystem is responsible for several operational tasks, the subsystems *communications* and *command & data handling* have been grouped into one subsystem. This subsystem needs to be sized in order to ensure a proper connection between the constellation and ground stations. The sizing depends on the requirements of the data that needs to be imaged. Several limitations are imposed on the subsystem design as well.

In this section the requirements leading to a properly sized communication bus are described. Firstly, the subsystem responsible for uplink of commands, firmware and downlink of telemetry data is described in section 12.1. Secondly, the trade-off to select an on-board main computer of the satellites is covered in section 12.2. Next the process of acquiring imaging data is described in section 12.3. The requirements and limitations leading to the sizing of the data communication bus are also dealt here. Finally, the sizing of the data communication bus is described in section 12.4.

12.1 Telemetry

To ensure that status information of the satellite is known and commands can be given to the main bus or individual subsystems, a communication bus is required. This bus is responsible for the downlink of telemetry data, the uplink of commands and new firmware to the satellite.

12.1.1 Transceiver

The selection of a transceiver mainly depends on the ability to establish a connection with a ground station with as less transmit power as possible. Furthermore, the selected transceiver should be readily available on the commercial market. As the frequency bands to be used are relatively fixed for satellite communication, the main driver in a trade-off of available transceivers will be the power required. An overview of available transceivers is given in table 12.1.

Transceiver	Frequency [MHz]	Baudrate [bps]	Mass [g]	Power [W]	Cost [EUR]
CMCi CubeSat UVTRX	130 - 150 (down) 420 - 450 (up)	9600 (down) 1200 (up)	90	4.0 (down) 0.3 (up)	6500
ISIS Full duplex transceiver	**130 - 160 (down)** **400 - 450 (up)**	**1200 - 9600 (down)** **300 - 1200 (up)**	**85**	**1.7 (down)** **0.2 (up)**	**6750**
GomSpace U482C	? (down) 435 - 437 (up)	1200 - 9600 (down) 1200 - 4800 (up)	75	5.0 (down) 0.2 (up)	8000

Table 12.1: Telemetry transceivers

As becomes apparent from the product specifications shown in table 12.1, the frequency ranges offered do not differ much, although the *GomSpace* transceiver has a tight range. Clearly, the *ISIS* transceiver offers a slightly wider range but this is regarded insignificant as all allow for down- and uplink in allocated frequency bands.

The masses of the individual transceivers differ only slightly as well, with the *CMCi* transceiver having a 6 % higher mass than the one from *ISIS*, and a 20% higher mass than the *GomSpace* transceiver.

Most interesting is the power requirement, which is highest for the *CMCi* transceiver in uplink mode. In downlink mode however, the difference becomes even more severe as the *CMCi* consumes 135 % more power and the *GomSpace* even 200 % in this mode. As power is of ubiquitous importance, it becomes apparent that both the *CMCi* and *GomSpace* transceivers would be unwise choices and are therefore discarded.

12.1.2 Antenna

The selection of a proper antenna for the telemetry not so much depends on the performance, but rather on geometric and volumetric requirements set by other subsystems. Multiple COTS antennas are available with various RF configurations to offer both downlink and uplink by various companies. Any of these could be selected by merely looking at the price. A few constraints in the structural design become apparent however:

1. As the imaging transmitter needs to be mounted nadir-facing, the only mounting option is underneath the antenna. This requires the antenna to have space available to pass through connection interfaces.
2. The spacecraft will consist of a 2x2x1 cubesat configuration, limiting the deployment of turnstyle antennas, as one side of the antenna will be blocked

Following these constraints, a dipole deployable antenna system from *ISIS* is chosen, as it offers a 30*mm* center hole for pass through of other interfaces and is confirmed to be modifiable in order to cope with the geometric constraint.

12.1.3 Link budget

The link budget as set up for the telemetry up- and downlink is shown in table 12.2. As an equal type of VHF/UHF groundstation will be used for telemetry up- ad downlink, it can safely be assumed that the same losses occur for the transmitter and receiver as is apparent for the *Delfi-N3XT* telemetry. These losses consist of transmitter and receiver losses, which are broken down into:

Transmitter
- Connector loss: -0.1 dB (up), -0.2 dB (down)
- Line loss: -1.9 dB (up), -0.05 dB (down)
- Circuit & internal losses: -0.2 dB (up), -2.7 dB (down)

Receiver
- Connector loss: -0.2 dB (up), -0.1 dB (down)
- Line loss: 0 dB (up), -0.4 dB (down)
- Circuit & internal losses: -4.15 dB (up), -0.4 dB (down)

Here, *circuit & internal losses* consist of circuit losses, but also surge protector and phasing losses for example. All these losses are reflected in the link budget shown in table 12.2. Furthermore it is assumed that the system noise temperature is 500 k. The contributions to this noise are purely due to galactic and man-made noise [12].

			Uplink		Downlink	
	Link parameters	**Units**	**Value**	**Totals**	**Value**	**Totals**
General	Transmission frequency	MHz	434		140	
	Transmitter power	W			1.00	
	Orbital altitude	km	500.00		500.00	
	Contact distance (max.)	km	2564.8		2564.8	
	Data rate (max.)	$bits^{-1}$	1200		9600	
	Bit error rate (BER)		10^{-5}		10^{-5}	
	Modulation scheme		*AFSK*		*BPSK*	
Transmitter	Power amplifier output	dBW	24.00		−8.00	
	Connector loss	dB	−0.10		−0.20	
	Line loss	dB	−1.90		−0.05	
	Circuit & internal losses	dB	−0.20		−2.70	
	Antenna gain	dB	16.00		2.00	
	Transmitted EIRP	dB		**37.89**		**-8.95**
Channel	Path loss	dB	−153.37		−153.37	
	Pointing loss	dB	−1.00		−1.00	
	Atmoshperic loss	dB	−1.50		−1.50	
	Total channel loss	dB		**-155.87**		**-155.87**
Receiver	Antenna gain	dB	−10.00		24.00	
	Connector loss	dB	−0.20		−0.10	
	Line loss	dB	0.00		−0.40	
	Circuit & internal losses	dB	−4.15		−0.40	
	Received EIRP	dB		**-14.35**		**23.10**
	Data rate	dB	−30.79		−39.82	
	Total Eb	dB		**-163.12**		**-181.54**
	Receiver noise temperature	K	500.00		500.00	
	Total N0	dB		**201.60**		**201.60**
	Received Eb/N0	dB	38.48		20.26	
	Required Eb/N0 for BER	dB	−10.30		−10.30	
	Minimum link margin	dB	−3.00		−3.00	
	Resulting link margin	dB		**25.18**		**6.76**

Table 12.2: TT & C link budget

12.2 On-board computer

In order to provide an automated CubeSat constellation an on-board computer is required. This component provides the links and commands required by the data handling and telemetry subsystems, as well as storage for software applications necessary to operate them.

The choice of on-board computer mainly lies in its ability to provide the necessary interfaces to link with the subsystems. As an example, the SPI interface is necessary to transfer payload data to the communication system and being compliant with the CubeSat Space Protocol (CSP) provides further interface possibilities such as the RS-232, which the ARCTIC platform uses. Furthermore, its mass, cost, power consumption and additional functions should be taken into account for a proper trade-off. The focus is placed in three COTS options, as seen in table 12.3.

It is important to note that the cameras are a standalone platform with their own processing unit, such that data processing is not a main driver for performance of the on-board computer.

OBC	Interface	Mass [g]	Power [mW]	Cost [EUR]	Notes
NanoMind A712C	**I^2C, SPI, CAN, USART**	**55**	**312**	**4,750.00**	**CSP compliant**
CubeComputer	I^2C, SPI, UART	66	435	4,500.00	CSP compliant
SA-MIC-EM	I^2C, SPI, USART	62	1250	7,560.00	2 CPUs, Radiation tested

Table 12.3: CubeSat on-board computers

The NanoMind A712C is an interesting option which can deal with four interfaces as well as being CSP compliant. Furthermore, it provides part of the attitude control platform by allowing interface connections to sun sensors, gyroscopes and direct control to three magnetorquers. Its mass and power consumption are the lowest of the three, with its cost being 4,750.00 EUR and the PCB is produced with space grade material [59].

The CubeComputer is the cheapest of the three, albeit by a small difference. It is also CSP compliant like the NanoMind and provides support for three interfaces. Furthermore, it can provide attitude commands and bus data (on-board temperature and current monitoring). Its mass is 11 g higher than the previous model and its power consumption is 40 % higher [60].

Thirdly, the Mission Interface Computer developed by steepest ascent provides three interfaces, but no information has been provided with respect to CSP support. Of the three, it is likely to be the most reliable option as it is radiation tested up to 15 krads and has two processing units, improving redundancy. Its mass is similar to the other options, but its power consumption is 3 to 4 times higher and its cost is 60 % higher [61]. All three options have the ability to provide extra data storage with 2GB SD cards.

Taking into account their properties, the NanoMind A712C is chosen as the on-board computer of the constellation platforms. This decision is backed by its lower mass and power consumption, as well as its attitude control capabilities and partly space graded equipment. Furthermore, it is compliant with the most interfaces and its cost is on par with the lowest option.

12.3 Imagery data

It is not possible to continuously transmit payload data to a ground station, causing the need for precautions to ensure no data is lost in transmission. The opportunities at which data can be transferred to a ground station, i.e. downlink opportunities, are limited by the moments at which an ground station is in range of the spacecraft. However, the imaging data generated by the on-board camera constantly grows. The approach taken to optimise the data volume and its transmission to the ground segment is described in this section.

12.3.1 Data flow

Due to the fact that data can only be downlinked in a fraction of the time, methods must be applied to store the data on the spacecraft until a downlink window arises. A *store-and-forward* paradigm solves this problem. Herein, a spacecraft stores all payload data locally on storage devices. The data is subsequently transmitted to a ground station once it is in range of the spacecraft.

As soon as a downlink opportunity appears, *data bursting* is applied. This method uses a transmission that combines a short transmission time with a high data rate. The imaging data is stored locally until this opportunity arises, as defined by the store-and-forward paradigm. This process is illustrated in figure 12.1.

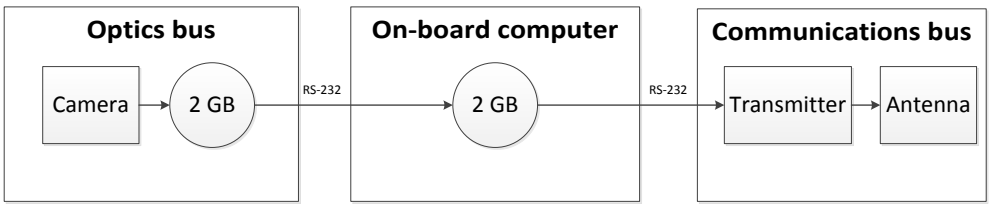

Figure 12.1: Flow of imaging data through the spacecraft

The storage in figure 12.1 consists of two buffers. Not only does the computer offer 2GB (see section 12.2), an additional 2GB is provided by the storage on the camera [30],[31], yielding a total of 4GB available for imaging storage.

12.3.2 Data volume

The amount of data generated by the constellation is heavily dependent on the cameras used; the ANT-2 platforms have an image file size of $2048 \cdot 2048 \cdot 10 = 42Mbit$ at 10 bpp, while the ARCTIC's file size is $640 \cdot 480 \cdot 12 = 3.7Mbit$ at 12 bpp, a considerable difference. Secondly, orbiting height, swath width, data compression and camera duty cycle have a large impact on the amount of data generated per orbit.

The total data volume produced per orbit defines the required capability of the downlink. It is a function of the image resolution, bit depth, imaging frequency and compression rate where the imaging frequency is defined as the number of images taken per second. The imaging frequency again is dependent on the speed at which the satellite crosses the area that is photographed by one shot. This frequency can be defined as follows:

$$f_{imaging} = \frac{2 \cdot \pi \cdot R_{Earth}}{T_{orbit} \cdot S_l} \tag{12.1}$$

Where S_l is the swath length, R_{Earth} the equatorial radius and T_{orbit} the orbital period. Applying equation 12.1, the data rate for each camera can be found:

$$DR = \cdot f_{imaging} \cdot \frac{I_{size} \cdot I_{bitdepth}}{comp} \tag{12.2}$$

Where I_{size} is the size of the raw image in pixels, $I_{bitdepth}$ the bit depth and $comp$ the compression rate. Equation 12.2 gives the data rate for a given camera, yielding the maximum which can be achieved at a given compression and image size. An overview of the maximum data rates per camera is given in table 12.4.

Parameter	Unit	RCC	TMA	ARCTIC
Resolution	$pixels$	2048x2048	2048x2048	640x480
Bit depth	bpp	10	10	12
Compression factor	-	10	10	5
Imaging frequency	s^{-1}	0.84	0.14	0.20
Datarate	$kbits^{-1}$	3520	587	147

Table 12.4: Datarates for individual cameras

Clearly, the results in table 12.4 show that the RCC camera produces the highest data rate. This number is firstly important for the sizing of the communication between subsystems as the transfer of the data from the optics to the transmitter imposes some requirements on the wiring and protocols used. Secondly, the data rate is an important factor in closing the link budget of the communication bus.

Nevertheless, the data rate can be reduced as well by using proper compression techniques, although a loss in quality might occur while doing so. Such compression possibilities are described in the next section.

12.3.3 Data compression

Data compression is usually necessary when dealing with a high data rate, providing the means to reduce it. Compression can be lossless, where no information is lost, and lossy, which incurs irreversible loss of information. State-of-the-art lossless compression can reduce data size by a factor of 2 to 5x, depending on what is being imaged. If more reduction is required, lossy compression can provide up to 10x image size reduction [62]. However, it is important to note that compression carries a set of issues:

1. Compression algorithms require considerable computing power, increasing power consumption and heat dissipation issues;
2. SNR is decreased in most lossy algorithms, with the exception of pixel binning, which increases the SNR at the cost of spatial resolution;
3. Lossy compression reduces the quality output of the cameras
4. Errors can be induced during compression, making images prone to artefacts.

Both cameras are independent of the main bus to capture and compress imagery as a microprocessing unit is included in their design [31] [30]. The ARCTIC uses the Miniz software to carry out compression with an efficiency of 80%, a 5:1 ratio. As a result, each image is 737 kbit large. On the other hand, the ANT design uses the JPEG2000 algorithm to provide an image compression ratio up to 10:1, reducing the image size to 4.2 Mbit.

12.3.4 Downlink sizing

The downlink time required per camera is affected by its duty cycle and limited by the data storage available in the spacecraft bus. The duty cycle is a result of the frequency in which the camera will image the globe per orbit. The duty cycle is thus a function of the ground track covered and the area photographed:

$$dc = \frac{A_{covered}}{A_{groundtrack}} \tag{12.3}$$

This duty cycle relates to the required coverage described in section 3.3.3 in such that the required coverage equals the minimum duty cycle that must be achieved as to avoid missing imagery data of interesting applications. In other words, the cameras in a constellation should be turned on for at least such a fraction of the total time that the required coverage is achieved.

The output of data is directly proportional to the duty cycle; a 50% duty cycle reduces the data volume by a factor of 2 compared to a full duty cycle. This imposes a requirement on the downlink time as an increase in duty cycle increases the data volume that needs to be sent down to a ground station. Assuming the maximum data rate is limited, the downlink time required is then a result from the data volume and the number of ground stations available. An increase in ground stations will decrease the downlink time per ground station, as the total data volume can be more evenly spread out over several downlink opportunities.

The possibility of decreasing the number of ground stations moves the limitation to the data storage provided on board. As a ground station comes into view every so often, the data storage on board the spacecraft is only required to buffer the imaging data in between two consecutive downlink opportunities. However, the capacity of this data buffer is fixed by the storage provided by the camera and on-board computer. As was described in section 12.3.1, the maximum capacity is 4GB over the entire system.

The rate at which the capacity of the data buffer saturates depends solely on the rate of data generated by the camera.

Maximising the duty cycle

It is desirable to maximise the achievable duty cycle, which provides more freedom in imaging. The maximum achievable duty cycle is a measure for the imaging capacity, as a higher duty cycle means a higher quantity of imaging data. To find the maximum duty cycle, a simulation is used which calculates the data flow from the spacecraft to any ground station over a few consecutive orbits. By evaluating the data flow for individual steps in time, the total data flow over time can be shown. This measure will then be used to determine whether the buffer in the spacecraft saturates.

As the duty cycle of the space segment is increased, more data moves in and out of the buffer. At some point the buffer is saturated, at which no more imaging data can be stored. Such a situation should be avoided at all costs, as this results in loss of viable data.

A simple solution to the saturation of the data storage would be to increase the size of the datastorage. If the downlink datarate does not match or exceed the imaging datarate however, increasing the datastorage will not avoid the saturation of the datastorage but only postpone it. An approach is therefore applied which seeks for methods to increase the downlink datarate for a given size of the datastorage.

By simulating the effect of the duty cycle over time using the simulation described above, the saturation of the buffer can be calculated. The maximal achievable duty cycle is then the duty cycle for which the buffer remains just below full saturation at all times. To visualise this, a simulation is run using the following input variables:

- Two ground stations: Svalbard at $78^\circ N$ $15^\circ E$ and Trollsat at $-72^\circ N$ $2^\circ E$
- Transmit power: $2W$
- Maximum achievable data rate: $10 Mbits^{-1}$
- Transmitter antenna gain: $2dBi$
- Receiver antenna gain: $30dBi$
- $BER = 10^{-5}$. no coding gain

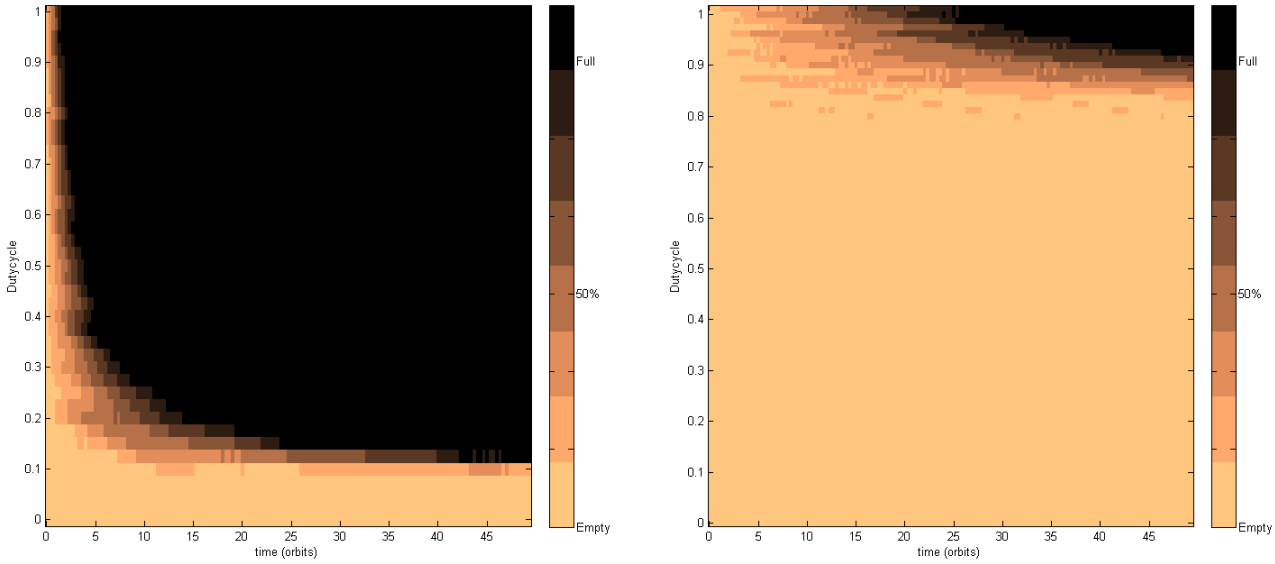

(a) Saturation over time for the RCC (b) Saturation over time for the TMA

Figure 12.2: Saturation of local data storage. Darker colours indicate a higher saturation.

The results become apparent in figure 12.2 which shows the saturation levels of the buffer for both the RCC and TMA camera. It can be seen that the buffer is saturated quicker for the RCC camera, as a maximum duty cycle of 10% can be achieved. For the TMA camera, this is 90%.

This very approach can be used to select the transmitter needed and size the ground segment. By evaluating the achievable duty cycle for different combinations of transmit power, antenna gain, transmitter limitations and number of ground stations, an optimum can be found.

12.3.5 Ground station placement

The mission architecture relies heavily on the downlinking of imaging data to ground stations and thus a proper approach to its placement needs to be incorporated. Two design paradigms are interesting with respect to downlinking data:

- Provide the spacecraft bus with adequate power and data storage to ensure all imaging data can be downlinked to few ground stations
- Provide an abundance of ground stations in order to offer many downlink opportunities and hence focus the communications load on the ground segment

The former approach relies heavily on the available power and volume in the spacecraft. As power is at a premium in nanosatellites, this approach can be quickly disregarded. Furthermore, the total equipment and operating cost of ground stations are expected to be low which gives more freedom to the use of several ground stations [63]. The cost figure of the ground segment is further elaborated in section 13.4.

The approach described in section 12.3.4 can be used to correctly size the number of ground stations. For several combinations of transmit power and number of ground stations, the duty cycle can be determined. The selection of ground stations is dealt with in the next chapter, while the required transmit power will be determined in the following section. A trade-off can then be made between duty cycle and the number of ground stations needed. This method of iteratively sizing the ground segment and communication bus ensures the most optimal design for imaging downlink can be found.

12.4 Communication bus sizing

12.4.1 Band selection

The selection of the proper frequency band is of significant importance as only a limited number of frequencies can be used and the selection of a frequency effects the design of both the communication bus and the ground segment. Figures 12.3, 12.4 and 12.5 display the frequency band allocations. As the mission is of a commercial type, only non-governmental exclusive and bands shared between government and non-government instances can be used.

S-band

The S-band is the band in the electromagnetic spectrum which ranges from 2 to 4 GHz according to the IEEE frequency band allocation. This band is used by a wide variety of applications, both governmental and non-governmental, as can be seen in figure 12.3. The UHF part of the S-band is most interesting for this mission, as this part of the S-band is commonly used for Earth observation. The governmental band allocations within the S-band can't be used due to the commercial nature of the mission.

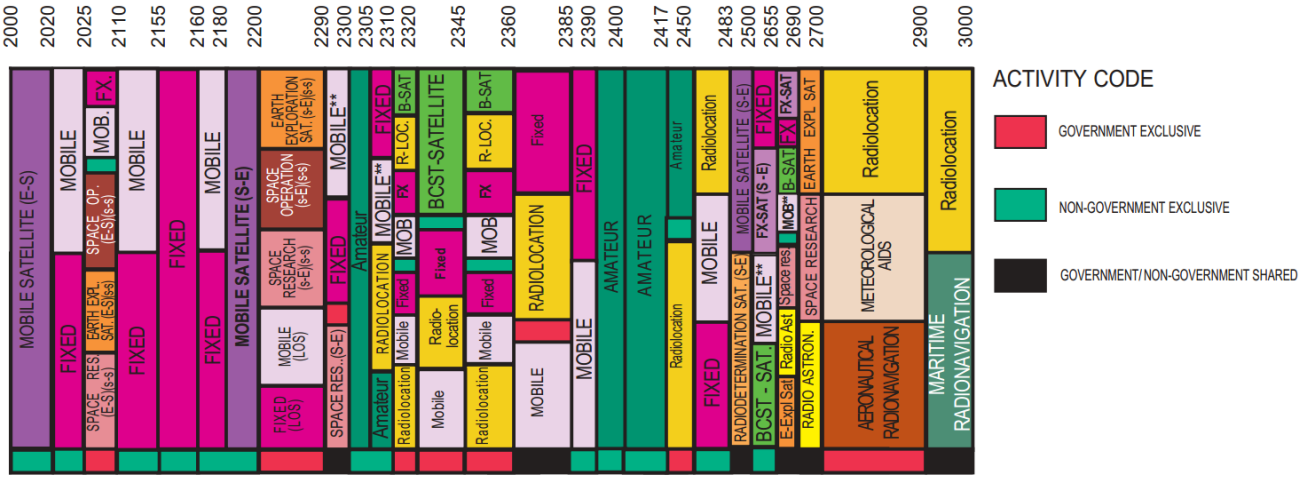

Figure 12.3: S-band allocations [64]

C-band

The C-band is designated to the frequency range of 4 - 8 GHz according to the IEEE specifications. Within the satellite market, this band is mainly used for telecommunications and radar applications.

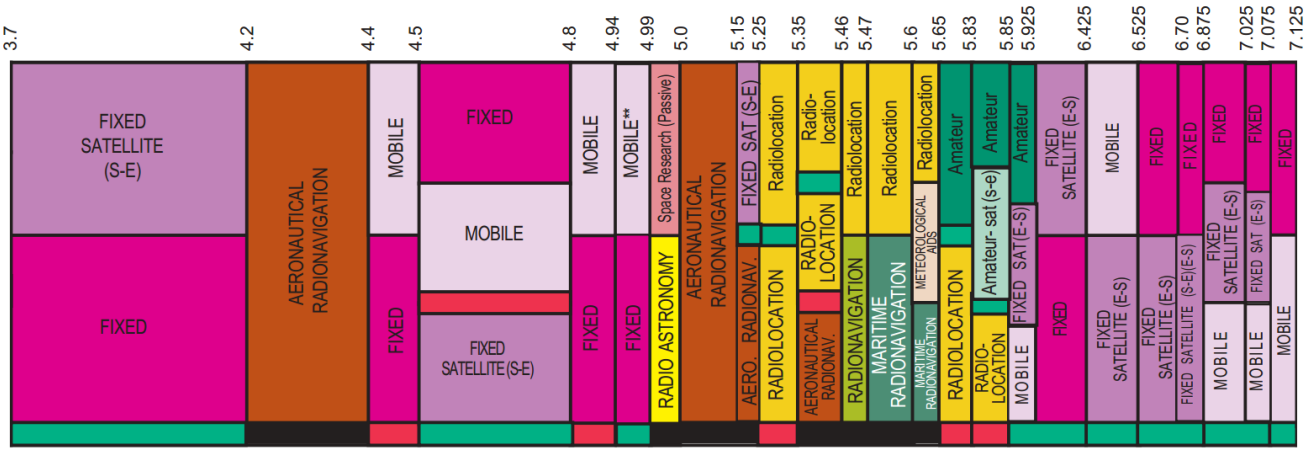

Figure 12.4: C-band allocations [64]

X-band

The X-band is specified by the IEEE as the range of 7 - 12 GHz. This band is mainly used for (deep space) communications and scientific applications and is dominated by government exclusive designation, as can be seen in figure 12.5. This makes the X-band less interesting for commercial applications. The viable frequency bands are limited, as can be seen in table 12.5.

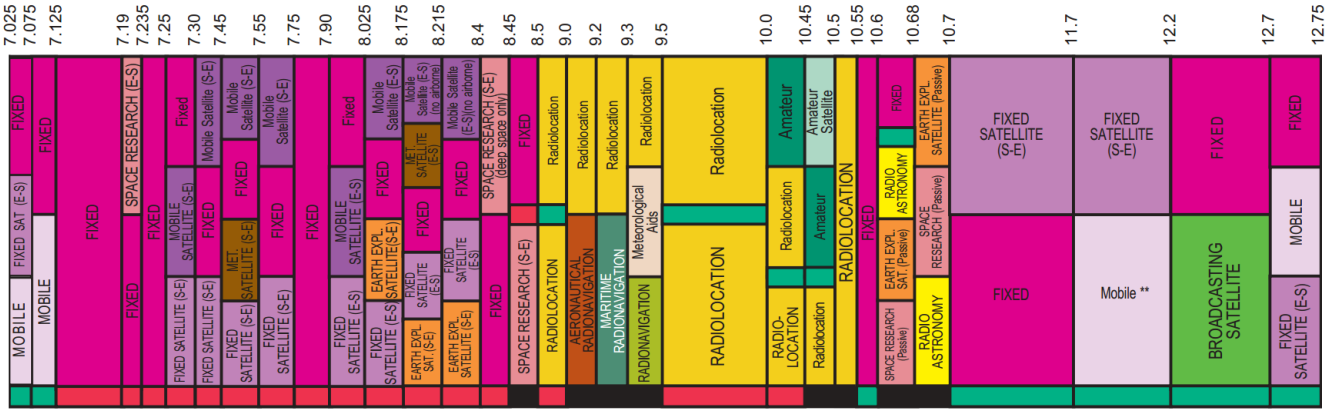

Figure 12.5: X-band allocations [64]

12.4.2 Possible frequency bands

The frequency bands described in this section leave open a set of frequencies to use. These frequencies are listed in table 12.5. The selected frequency depends on the frequencies that the transmitters can provide.

In the end, the frequency used mainly depends on the frequency that authorities allow to use. This process is considered irrelevant for the moment, and at this point it can thus be assumed that all frequencies listed in table 12.5 can be used.

12.4.3 Transmitter

Several commercial transmitters are currently available on the market which are suitable for downlink of imaging data on a nanosatellite platform. From the list of transmitters the most suitable option for the mission has to be selected.

Requirements & Limitations

Mission requirements and characteristics of other subsystems impose requirements and limitations upon the imaging transmitter.

S-band	C-band	X-band
2.000 - 2.025 GHz	3.700 - 4.400 GHz	7.025 - 7.125 GHz
2.110 - 2.200 GHz	4.500 - 4.800 GHz	8.450 - 8.500 GHz
2.290 - 2.310 GHz	4.940 - 5.250 GHz	9.000 - 9.500 GHz
2.385 - 2.417 GHz	5.350 - 5.650 GHz	10.45 - 12.75 GHz
2.450 - 2.700 GHz	5.925 - 7.125 GHz	
2.900 - 3.000 GHz		

Table 12.5: Possible bands

The chosen approach to downlinking relies on using several ground stations in order to lower the burden of downlink performance on the space segment. Therefore, it is not necessary to increase the transmit power to close a link budget by the highest possible margin. In fact, the allocated power budget for the communication bus is 11W during transmission time 8.1. This budget has been determined by iteratively sizing the power subsystem to support all the transmitters selected for trade-off. During this process limitations become apparent in the power subsystem beyond which no additional power can be provided, yielding the figure of 11W. Once a transmitter is selected, the power subsystem is either down- or up-sized to exactly fit the needs of that transmitter.

The distance between the ground station and the satellite significantly influences the maximum data rates that can be achieved. As the data rate is dependent on having a closed link budget, it can only be increased by either increasing antenna gain or transmit power, or decreasing the distance between the ground station and satellite. In order to maximise the data rate and thus the possible throughput, methods need to be found to achieve its optimum.

As the antenna gain and transmission frequency are set, the data rate merely remains a function of distance. During every ground station pass the distance varies significantly, and thus an assessment of what the real affects are of distance on the data rate is done. These effects can be shown by simulating the movement of a satellite over a ground station. During the time at which the satellite and ground station are in contact data offloading occurs. Here, the following assumptions are made:

- The satellite passes directly over the ground station
- The orbital altitude is 288 km. Values differ for different altitudes

The results can be seen in figure 12.6.

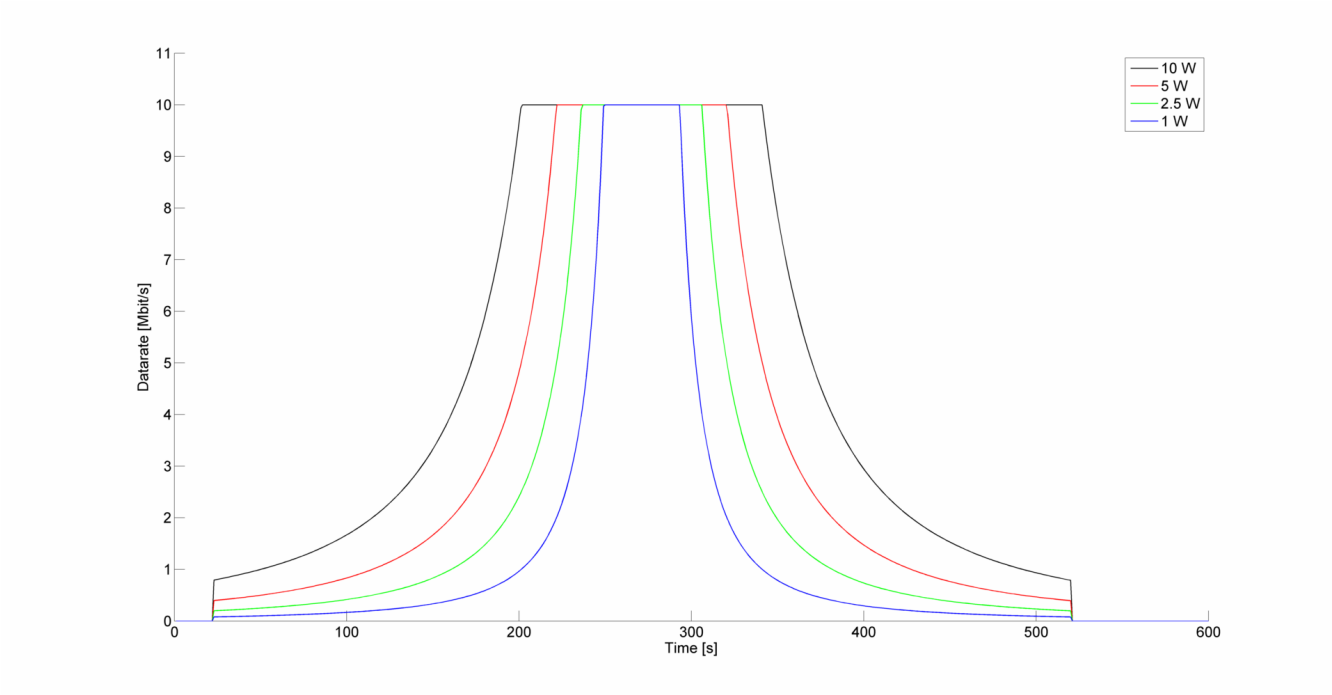

Figure 12.6: Datarate during a ground station pass

As power is at a premium on nanosatellites, it is important to be conservative with increasing the transmit power.

Figure 12.6 demonstrates that increasing the transmit power for a given frequency and antenna gain does not necessarily increase the total throughput by the same rate. While the jump from 1 W to 2.5 W of transmit power is still relatively significant, furthermore doubling the transmit power causes a lesser increase in throughput. Thus, a transmit power of 2.5 W is an optimum.

Available transmitters

Several commercial transmitters are currently available on the market whose limitations and performance however differ significantly.

Five COTS transmitters are selected for the trade off. An overview is given in table 12.6. Three of these are depicted in figure 12.7 to give a general impression of their size.

Parameter	Unit	ClydeSpace	ST5000-S	ST5000-C	CubeSat X-band	TX-2400
Band		S	S	C	X	S
Frequency	GHz	2.2 - 2.483	2.2 - 2.4	4.4 - 4.95	8.025 - 8.4	2.0 - 2.4
Transmit power	W	1	10	10	1	2.5
Datarate	$Mbits^{-1}$	2	40	40	50	10
Power consumption	W	6	17 - 47	17 - 47	10	10
Mass	g	90	225	225	300	200
Size	mm^3	95 x 90 x 12	76 x 51 x 25	76 x 51 x 25	100 x 100 x 40	68 x 35 x 15
Modulation		QPSK, OQPSK	SOQPSK	SOQPSK	?	QPSK
Price	EUR	6.700	?	?	?	19.000

Table 12.6: Transmitters

As becomes apparent in the research of transmission bands, the *CubeSat X-band transmitter* can be quickly disregarded due to the non-commercial nature of the X-band. Nevertheless, this transmitter is a very interesting alternative for non-commercial cubesat applications as it provides a datarate unpreceded in the cubesat market, and is therefore worth mentioning.

In the field of power, the ClydeSpace transmitter gives a decent figure for input power consumption, although this comes with a lower datarate and transmit power. Unlike the ClydeSpace transmitter, the *ST5000* and *TX-2400* from *L3 Telemetry* and *SpaceQuest* respectively offer a far higher datarate and transmit power, albeit at a significantly higher power requirement. Nevertheless, these transmitters all offer the possibility of selecting the transmit power, which positively influences the input power that they need.

Costwise the *ClydeSpace S-band transmitter* offers the cheapest solution, followed by the *TX-2400*. Unfortunately, the transmitters from *L3 Telemetry West* don't offer a cost figure, as these are currently only sold to military users in the U.S, and can therefore be disregarded. This is most unfortunate as their capabilities are outstanding performance wise.

The transmitter of *ClydeSpace* offers a significantly lower datarate than the transmitter offered by *SpaceQuest*. Nevertheless, it has been confirmed that the *ClydeSpace* transmitter can be modified to improve transmit power and datarate[65].

As the *TX-2400* does not need any modifications to offer the desired performance, this transmitter is the most suitable and is therefore selected to be used for the transmission of imaging data.

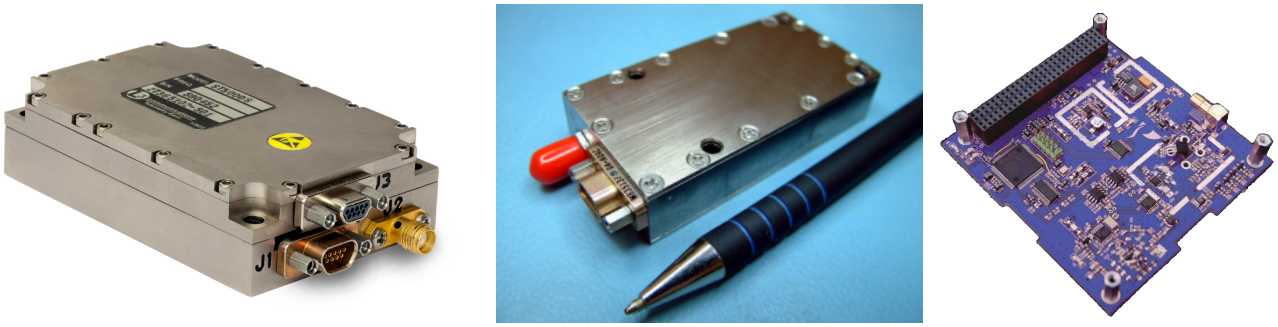

Figure 12.7: From left to right: The L3 Telemetry ST5000-S, the SpaceQuest TX-2400 and the ClydeSpace S-band transmitter.

12.4.4 Antenna selection

Now the transmit power is determined and the transmitter selected, a suitable antenna can for the downlink of the imaging data can be selected. This antenna is required to support high datarates while still being able to fit in a CubeSat package. The limitations in this regard are based on size and weight. The antenna aperture is very limited by the CubeSat format, as it generally needs to fit on a 10 x 10 cm plane. The low weight design approach of nanosatellites is a reason to keep the antenna weight as low as possible. This factors out any complicated antenna designs which contain multiple reflectors or are even steerable.

This leaves the selection of antenna types to very simple designs, like a standard parabolic antenna or a patch antenna. Parabolic antennas generally offer higher antenna gains than patch antennas at the cost of beamwidth. This would result in a more complex antenna design, as a low beamwidth results in a low contact time. This in turn raises the need for the possibility

to steer the antenna to keep it pointed at a groundstation. The design approach used for subsystem design states however that the spacecraft must be kept as simple as possible while relying heavily on groundstations. It is therefore wise to avoid complex antenna designs and to make use of a patch antenna, which provides a high beamwidth combined with sufficient antenna gain.

As a result, the selection of antennas is limited to COTS patch antennas currently available. These antennas must be able to support the radiation of at least 2.5 W transmit power at a decent beamwidth. *ClydeSpace* provides such antennas for the S-band at a price of 4,000 EUR.

Because the design for a patch antenna is relatively straightforward it is recommended to design a custom patch antenna which is scaled for this mission. For reference however, the *ClydeSpace* patch antenna is selected as it provides the required performance for a decent price.

12.4.5 Link analysis

Modulation

The transmission of digital data through an analog communication system requires the selection of a proper encoding scheme, which ensures that digital data is encoded onto an analog carrier signal. The process of encoding as well as decoding is hereby referred to as *modulation* and *demodulation* respectively. Several modulation schemes are typically used, being frequency modulation (FM), amplitude modulation (AM) and phase-shift keying (PSK). The choice of the modulation relies heavily on the supported modulation types by the chosen transmitter, albeit phase-shift keying has distinct advantages over frequency and amplitude modulation in space communications [12].

The modulation as given by the chosen transmitter in section 12.4.3 limits the use to *QPSK*. QPSK stands for *Quadruature Phase Shift Keying*, which basically means that four phases are used to encode a symbol such that two bits can be encoded per signal. This is in contrast to for example *BPSK*, which enodes one bit per signal.

As the bandwidths for a selected frequency band are limited, QPSK has a distinct advantage over BPSK as it offers double the datarate for the same bandwidth.

Channel capacity

The theoretical maximum data rate that can be achieved for a given bandwidth is calculated by the *Shannon limit* which states the following:

$$C = B \cdot log_2 \left(1 + \frac{S}{N}\right) \tag{12.4}$$

where C is the Shannon limit, in $bits^{-}1$, B the bandwidth frequency in Hz, and S/N the signal-to-noise ratio. This limit can be used to find the required signal-to-noise ratio, while using the bandwidth given by the selected transmitter and antenna.

An interesting measure is the signal-to-noise ratio required for the given design parameters, as to verify the validity of the link budget. Rewriting equation 12.4 for the signal-to-noise ratio yields:

$$S/N = 10 \cdot log_{10} \left(2^{\frac{C}{B}}\right) \tag{12.5}$$

According to equation 12.5, the required signal-to-noise ratio should be at least $60.21dB$.

Error control

In order to avoid data corruption at reception at the ground segment, a margin is taken into account to account for the errors occurring during transmission. This margin can be quantified by the *Bit Error Rate* (BER). For a data link, a high BER is required to sustain the vast quantity of bits transmitted. An advisable BER value for data applications is $BER = 10^{-11}$ [12]. This figure gives a probability of 10^{-11} that a bit is lost in transmission, although the numbers of errors occurring can be decreased by other measures.

As it is desirable to make use of *Coding gain* to decrease the probability of a bit being corrupted, it can safely be assumed that the uncoded BER is 10^{-5}. Further improvements are made to decrease the corruption of bits, so that the margin required in the link budget for the BER can be mitigated.

An effect of applying coding gain to reduce the BER is that a lower uncoded BER can be used, thus saving on energy needed in the link budget.

The quality of the transmitted signal can be improved by using redundancy in the digitally encoded data as a means of error control. A powerful error control algorithm which is increasingly popular is the *Forward Error Control*, (FEC). This algorithm is used to encode the imaging data transmitted, effectively decreasing the error margin required. FEC basically uses a number of redundancy bits r for every n number of bits sent, effectively decreasing the number of errors occurring in a data set.The downside of this approach is however an increase in data rate, as a certain number of redundancy bits need to be transmitted as well.

The effects of redundant bits on the data rate are significant figures to account for while calculating the maximum achievable data rate. The code rate of the used FEC-method is defined as $\rho = n/n(+r)$, where ρ is the factor in a data set which is made up of actual imaging data, while the remaining data consists of redundancy bits.

Link budget

To verify that the link design is adequate enough to downlink imaging data, the relationship between transmit power, antenna gains, data rate, path loss and other losses is constructed. This relationship is shown in the link bugdet in table 12.7, which gives an overview of the concluding link design.

			RCC		TMA		ARCTIC	
	Link parameters	**Units**	**Value**	**Totals**	**Value**	**Totals**	**Value**	**Totals**
General	Transmission frequency	GHz	2.30		2.30		2.30	
	Transmitter power	W	2.50		2.50		2.50	
	Orbital altitude	km	288.00		500.00		443.00	
	Contact distance (max.)	km	1928.54		2564.82		2408.42	
	Data rate (minimum)	$Mbits^{-1}$	3.31		1.87		2.12	
	Data rate (maximum)	$Mbits^{-1}$	10.00		10.00		10.00	
	Modulation scheme		$QPSK$		$QPSK$		$QPSK$	
	Bit error rate (BER)		10^{-5}		10^{-5}		10^{-5}	
	Error correction		FEC		FEC		FEC	
Transmitter	Power amplifier output	dBW	3.98		3.98		3.98	
	Losses	dB	−3.00		−3.00		−3.00	
	Antenna gain	dB	2.00		2.00		2.00	
	Transmitted EIRP	dB		**2.98**		**2.98**		**2.98**
Channel	Path loss	dB	−165.38		−167.86		−167.31	
	Pointing loss	dB	−0.50		−0.50		−0.50	
	Atmoshperic loss	dB	−1.80		−1.80		−1.80	
	Total channel loss	dB		**-167.68**		**-170.16**		**-169.61**
Receiver	Antenna gain	dB	30.00		30.00		30.00	
	Losses	dB	−1.00		−1.00		−1.00	
	Received EIRP	dB		**29.00**		**29.00**		**29.00**
	Data rate	dB	−65.20		−62.72		−63.27	
	Total Eb	dB		**-200.90**		**-200.90**		**-200.90**
	Receiver noise temperature	K	135.00		135.00		135.00	
	Total N0	dB		**207.30**		**207.30**		**207.30**
	Received Eb/N0	dB	6.40		6.40		6.40	
	Required Eb/N0 for BER	dB	−9.60		−9.60		−9.60	
	Coding gain	dB	6.20		6.20		6.20	
	Minimum link margin	dB	3.00		3.00		3.00	
	Resulting link margin	dB		**0.00**		**0.00**		**0.00**

Table 12.7: Downlink budget

As the datarate is scaled to account for the maximum achievable data rate for a given transmission distance, the datarate is related to the path loss only. The results from this can be seen at the value for *Eb*, the received energy-per-bit, which is indeed equal for all camera platforms used. The method of transmission dictates that the datarate from the transmitter should be increased when the contact distance decreases, ensuring that the maximum datarate can be achieved at all times. The link budget states the data rate for the minimum elevation angle, and thus the maximum contact distance. For other combinations of distance and elevation angle, the value of *Eb* thus stays the same.

It is assumed that the losses are equal to those applicable in the telemetry, described in section 12.1.3.The internal losses under the scope of the transmitter thus consist of the following:

- Coupler loss
- Connector loss
- Line loss
- Circuit loss

Together, these losses are assumed to be $3.0dB$, as is reflected in the link budget.

Same applies for the internal losses of the receiver, albeit the total of losses is constructed subtly different:

- Connector loss
- Line loss
- Surge protector loss
- Pre-amplifier loss

The sum of these losses is assumed to be $1.0dB$.

The figure of receiver noise temperature is related to the transmission frequency selected. This frequency is $2.3GHz$, and the resulting noise temperature thus is $135K$ [12].

The link budget closes while assuming a minimum of $3dB$, to account for contingency.

12.5 Cost figure

Now that all components are chosen, a cost figure can be given to show the total cost of the communications and data handling subsystem. Table 12.8 provides this overview, where it can be seen that the total material cost of the subsystem is 39,000 EUR.

Component	Unit cost [EUR]	Qty	Total cost [EUR]
Command			**4,750**
NanoMind A712C	4,750	1	
TT & C			**11,250**
ISIS Full duplex transceiver	6,750	1	
ISIS dipole deployable antenna	4,500	1	
Imaging transmission			**23,000**
ClydeSpace S-band patch antenna	4,000	1	
SpaceQuest TX-2400 2.5W S-band transmitter	19,000	1	
Total subsystem cost			**39,000**

Table 12.8: Cost figure

12.6 Recommendations

In this chapter the communication & data handling subsystem design is adequately sized to ensure a connection can be successfully established for both the imaging data and telemetry and control. However, this design does not necessarily need to be the most optimal design. Therefore in this section recommendations stated are meant to further improve the subsystem.

Band selection

By using the C-band instead of the S-band for transmission of imaging data, a higher frequency can be used and thus a higher data rate can be achieved. This does however enforce the design of a new competitive C-band transmitter, as it has been shown that these are currently not on the market.

Transmitter optimisation

As was shown in section 12.4.3, current COTS transmitters are severely limited in performance. Therefore, a custom transmitter design is recommended. By doing so, an adequate data rate can be obtained. Also, as the transmit power is set, the transmitter can be designed for that specific value, optimising the power consumption. Lastly, a custom transmitter design allows vastly more freedom in frequency selection, like C-band frequencies.

Antenna design

The current design relies on a simple patch antenna for downlink of imaging data. This is however not necessarily the most optimal antenna design. By selecting a different antenna type, like a parabolic antenna, the antenna gain can be increased. Also, a spacecraft side mounted antenna can be designed to be able to rotate. This way, the antenna can point efficiently to a ground station, effectively increasing both gain and directivity.

Error correction

While currently use is being made of FEC to decrease the uncoded BER, more elaborate error correction methods can be applied to ensure an even higher decrease in bit error rate. This can be achieved by using *Turbo codes*, a set of high performance FEC codes which are known to almost approach the Shannon limit. In other words, the use of turbo codes would allow to push the data rate almost to its theoretical limit.

PART IV

OPERATIONAL SEGMENT

Chapter 13 | Ground Segment

In this section the ground segment for the constellation is described. The ground segment consists of several ground stations all across the Earth, to which the satellites send their data. The requirements for the sizing of a ground segment are stated in section 13.1. In section 13.2 the sizing of the ground stations for the constellation is described for commercial and own ground stations. The data handling in the ground segment is stated in section 13.3. In section 13.4 an estimate on the ground segment costs is given and in section 13.5 the conclusion is drawn and recommendations for further research are described.

13.1 Driving requirements for designing the ground segment

The requirements for the location of a ground station are mainly based on the type of orbit. For example, when dealing with a low Earth orbit with an high inclination it is convenient to place ground stations at the poles. This is because these satellites pass the poles every orbit, so there is a downlink opportunity twice an orbit. Since the constellation consists of orbits with an inclination between 90° and 100°, ground stations at the poles are used.

To determine the number of ground stations, the limiting factor is the amount of data that needs to be transmitted and the data rate, see section 12.3.4). Since the ANT-2 RCC camera generates a large amount of data there is need for more ground stations. It is convenient to place these additional ground stations at locations with a high duty cycle, such that the image data can be transferred to Earth immediately. These areas of interest can be derived from the figures in section 3.3.3 (figures 3.4, 3.5 and 3.6).

13.2 Ground station network

In this section the ground station network is described as well as the iteration process of the optimization of the locations. The constellation uses two commercial ground stations, as described in section 13.2.1, to downlink the data. Since these two ground stations are not nearly enough to downlink all the relevant data, additional ground stations are placed in interesting areas, which is described in section 13.2.2.

13.2.1 Commercial ground stations

In order to reduce hardware costs, the constellation uses commercial ground stations. This ground station network is called *Kongsberg Satellite Service* (KSat). KSat provides several ground stations for commercial use all over the globe, with numerous L/X/S-band antennas up to 13 m diameter. [66]

As stated before, it is convenient to use ground stations located near the poles, when dealing with an high inclination, low Earth orbit. KSat provides two ground stations near the poles. The first ground station is called SvalSat and is located in Svalbard, 78°N, 15°E, 1200 km south of the north pole. The second ground station is called TrollSat and is located at 72°S 2°E in Antarctica.

13.2.2 Sizing additional ground stations

The amount of data that needs to be downlinked is far too much for two commercial ground stations alone. For the RCC camera, the average duty cycle using only two ground stations is around 10%, which is shown in section 12.3.4. Therefore it is necessary to place additional ground stations around the planet. From figures 3.4, 3.5 and 3.6 in section 3.3.3, it can be seen that there is a lot of imaging in North and South America and along the east coast of Asia. Hence, 10 additional ground stations are added and located especially in these regions. Among with the commercial ground stations, these locations are given in table 13.1.

To optimize the ground station network, these locations need to be chosen carefully. There should not be any overlap between ground stations nor should they be placed in sequence in areas with a low duty cycle.

Location	Abbreviation	Latitude	Longitude
Buenos Aires	BUE	-34°35'	-58°23'
Cayenne	CAY	4°55'	-52°19'
Chengdu	CHE	30°39'	104°4'
Dubai	DUB	25°15'	55°17'
Jakarta	JAK	-6°55'	107°36'
Orlando	ORL	28°32'	-81°22'
Port Augusta	POR	-32°29'	137°46'
Pretoria	PRE	-25°43'	28°14'
Sapporo	SAP	43°3'	141°21'
Svalbard (kSat)	SVA	78°	15°
TrollSat (kSat)	TRO	-72°	2°
Vancouver	VAN	49°15'	-123°7'

Table 13.1: Options for Ground Station Locations

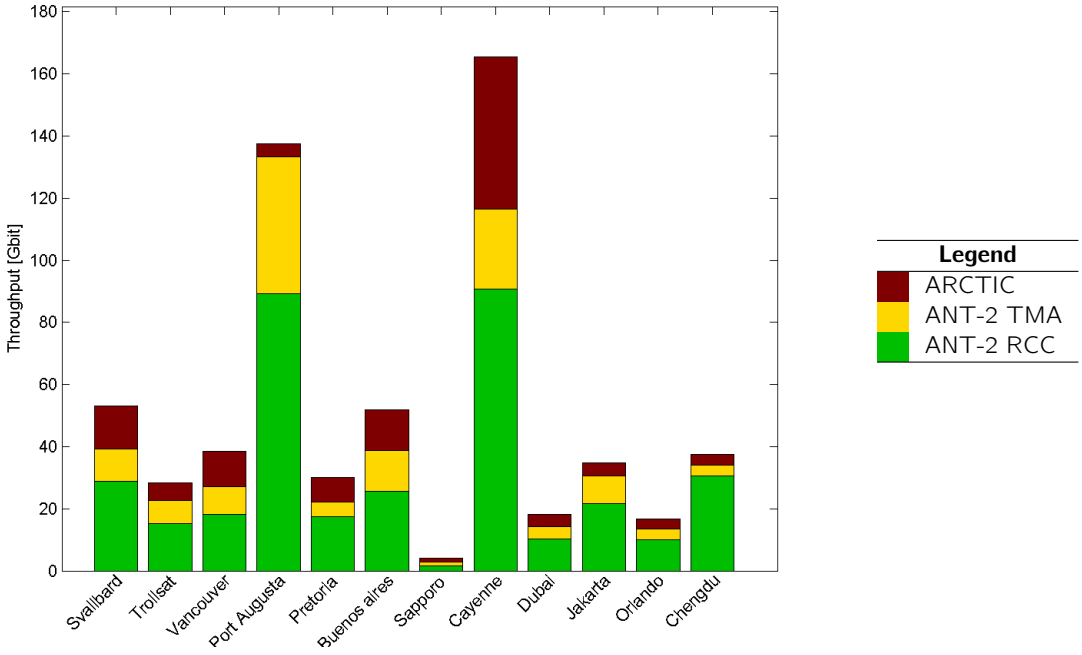

Figure 13.1: Data throughputs per ground station per camera

Therefore, it is convenient to know how much data is sent down per ground station. If it turns out that one of the ground stations does not collect a sufficient amount of data, there is no use in operating it. The ground stations are then removed or moved to a more suitable location. A 160-orbit simulation is used to compute the data throughput per ground station for all three cameras. The results are shown in figure 13.1.

From figure 13.1 it can be seen that the ground station in Sapporo receives much less data than the other ground stations. In fact, the satellite passes either the ground station in Svalbard first or gets there from the pacific ocean, so there is less data available for downlink when it passes Sapporo. Therefore, the ground station in Sapporo is removed as the other two stations can downlink the imagery data.

The same applies to the Orlando station. The satellite flies over Cayenne where it sends its data to Earth and then passes Orlando where in between it does not produce images. Therefore, the solution is to replace these two ground stations by one half way, such as in Curacao (CUR, 12°11' N, 68°59' W).

Iteration Process

This iteration process is done several times, resulting in a new number of ground stations on different locations. After this process the ground station in Pretoria is scrapped and the ground stations in Chengdu and Jakarta are replaced by a single ground station in Singapore (SIN, 1°17' N, 103°50' E).

The iteration process is broadly illustrated in table 13.2. In this table the average duty cycle, the throughputs and data

Nr.	Ground Segment Locations	Average Duty cycle RCC	TMA	ARCTIC	Throughputs	Max. Data Storage [Gbit] RCC	TMA	ARCTIC
2	SVA, TRO	10%	78%	100%	equally distributed	full	7.71	6.88
12	BUE, CAY, CHE, DUB, JAK, ORL, POR, PRE, SAP, SVA, TRO, VAN	50%	100%	100%	too few in ORL & SAP	4.42	1.14	1.26
10	BUE, CHE, CUR, DUB, JAK, POP, PRE, SVA, TRO, VAN	45%	100%	100%	Not much in JAK & PRE compared to other g/s	5.96	1.19	1.46
8	BUE, CUR, DUB, POR, SIN, SVA, TRO, VAN	40%	100%	100.%	Not much in BUE compared to other g/s	9.31	2.37	1.25
7	CUR, DUB, POR, SIN, SVA, TRO, VAN	37%	97%	100%	data throughputs more or less equally distributed	12.43	2.92	1.56

Table 13.2: Iteration process for the Ground Segment

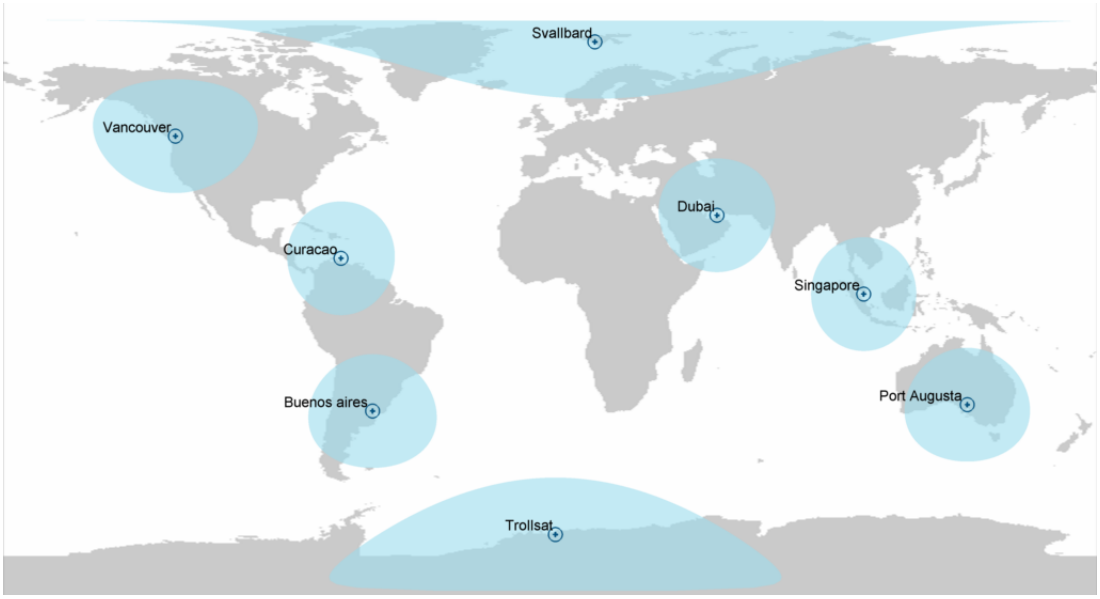

Figure 13.2: Locations of ground stations

storage are computed for a number of iteration steps. Each iteration step consists of a combination of a number of ground stations and their locations. The average duty cycle is computed for each camera platform as being the maximum achievable duty cycle (see section 12.3.4).

For every iteration step the throughputs per ground station are computed as shown in figure 13.1. From here conclusions are drawn in terms of which ground stations are operating effectively and a new combination of ground station locations can be derived from that.

In the last columns the maximum data storage is shown. This is the maximum amount of data on the SD-cards in the satellite, computed in $Gbit$ and determined for each camera platform. This value should not exceed the maximum capacity of the onboard storage, which equals 32 $Gbit$. For these last two parameters the actual duty cycle, which is used for the applications, is used.

Eight ground stations are used in total, although a network consisting of only seven ground stations is also sufficient; the ground station in Buenos Aires is left in the network for some redundancy. One of the applications this constellation serves is damage monitoring due to natural disasters. Therefore, most of the ground stations are located in areas where the possibility of such a disaster is larger than in other areas. This means some redundancy is required, since the ground stations can suffer damage in such disasters.

In figure 13.2 the final locations of all the ground stations are shown. In addition, the range of each ground station for an altitude of 288 km, which is the altitude for the RCC platform is shown in this figure. Hereby a minimum elevation angle of 5° in any direction is assumed. This elevation angle is assumed to be enough for a solid contact between the ground station and the satellite.

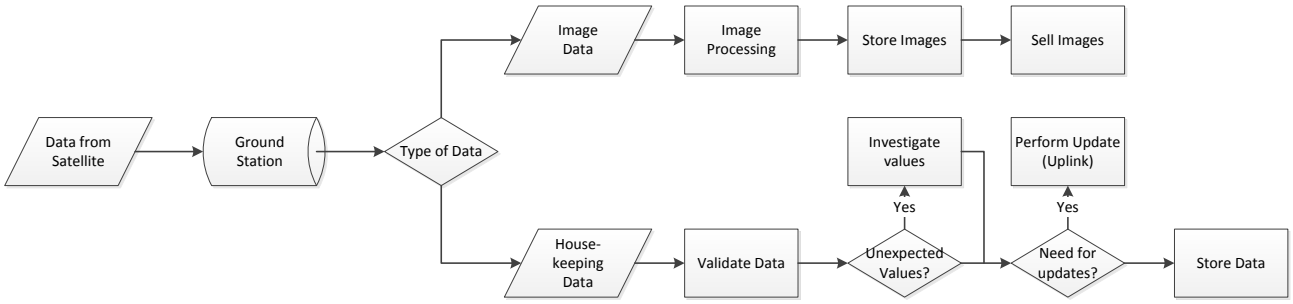

Figure 13.3: Data Stream within the ground segment

13.3 Data processing in the ground segment

In this section the data processing within the ground segment is described. When the data is received from a satellite the difference between image data and housekeeping data is made. Imagery data which is to be sold must first be processed, as described in chapter 14, to improve the quality of the image and bring out the relevant features. After that, the images can be provided to the customer. An illustration of the data stream is given in figure 13.3.

Housekeeping is an important operation to maintain the performance of the system. The software has to check whether or not the data contains unexpected values. These values contain orbital characteristics, attitude characteristics, etc.. The values need to be validated with designed values to see if there is a deviation in these values. If this is the case, one must investigate what caused the unexpected values. After that, an update for the on board computer software, containing data how to adjust the satellite, should be ready for uplink. Then the system itself will be able to perform this update to improve its performance.

13.4 Costs of the ground segment

In order to provide an estimate for the costs for the ground segment, the data from the Delfi - N3XT ground station is used as a reference. It states that the costs for a small ground station equals 150 k EUR. A more detailed breakdown is shown in table 13.3. Here the costs for image storage and a contingency factor are taken into account.

Components	**Cost [k EUR]**	**Quantity**	**Total Costs [k EUR]**
Hardware Costs	50	6	300
Operational Costs	100	8	800
Image Storage	600	1	600
Total			1700
Contingency factor			0.50
Total			2550

Table 13.3: Cost Breakdown for the Ground Segment

Since the constellation uses the commercial ground stations at the poles from ksat, the hardware costs for these two stations are not taken into account in the breakdown. This reduces the cost by 100 k EUR. The total cost for the entire ground segment is around 1.7 million EUR.

It is important to consider the risk of failure of a ground station. Since most ground stations are located in areas where there is a possibility for natural disasters, such as Earthquakes, this risk increases slightly. Therefore a large contingency factor of 50% is taken into account in the cost estimation to cover extra maintenance. In this case the total costs are around 2.55 million EUR. The locations rental costs are not taken into account in this break down, because further research is required to determine them.

13.5 Conclusions and recommendations

It can be concluded that the use of 8 ground stations, including the commercial ground stations at the poles, is sufficient to transfer all the relevant imagery data of the constellation. Furthermore, after a sufficient number of iterations the locations are optimized. For eight ground stations, the throughputs per ground station and the on board data volume per camera are computed in figure 13.4 over a period of 160 orbits.

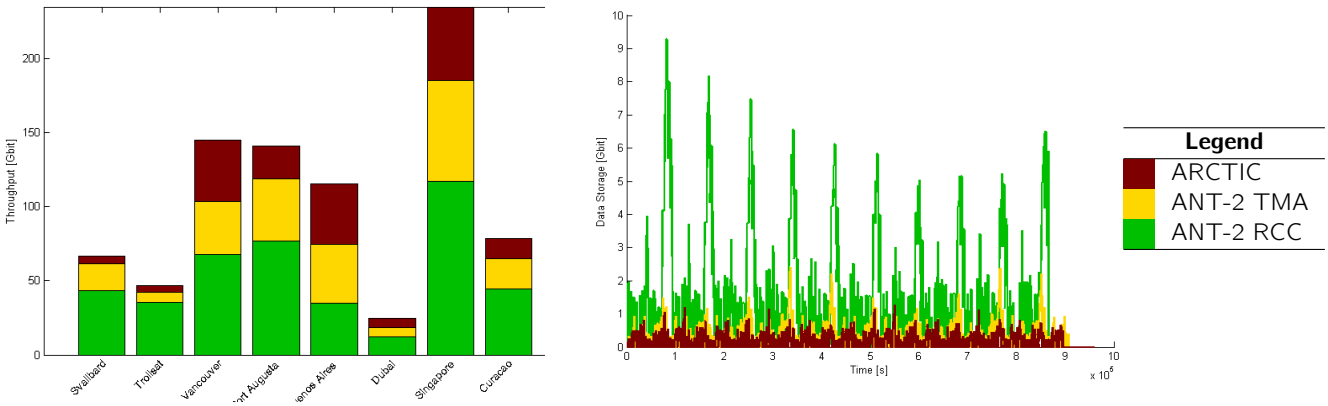

Figure 13.4: Throughputs per g/s and Onboard Data Volume per Camera during 160 orbits

Using eight ground stations the maximum achievable average duty cycle for the TMA and the ARCTIC platforms are equal to 1. For the RCC platform the data storage occupancy is computed and shown in figure 13.5. From here the maximum achievable average duty cycle can be determined, which equals 0.40.

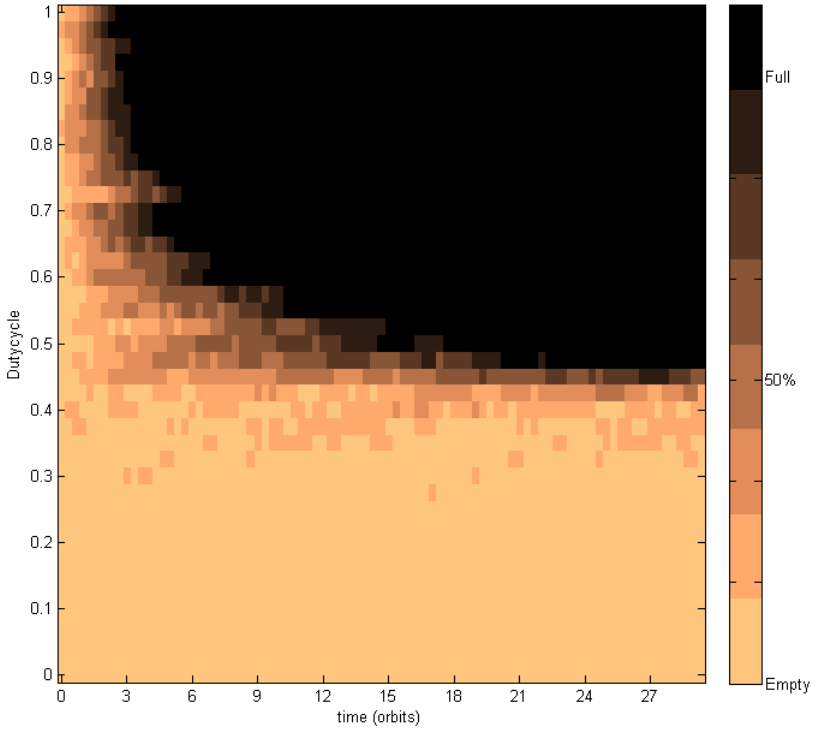

Figure 13.5: Duty cycle Simulation for RCC Camera using 8 Ground Stations

Recommendations

However, further research on these locations is required. A recommendation for further research is to find out whether or not local authorities allow to operate a ground station at that specific location.

Another recommendation for further research is to determine the elevation mask for all the ground stations. The locations are chosen for their coordinates on the globe and if this location turns out to be next to a mountain chain, the time in view will decrease significantly.

The last recommendation for further research is to investigate the climate in the chosen areas. Temperature, for example, can have significant influence on the performance of the receiving antenna.

Chapter 14 | Image Processing

In this chapter the processing of images is dealt with. It is intended to give a system level overview of the steps that need to be taken in order to perform useful analysis on the data acquired by the satellites. First the process of image calibration is described followed by the need to ortho-rectify the image. Then the possibilities for image co-registration, stitching and feature detection are discussed followed by a suggested mathematical routine. Finally the software related themes of image formats and available image processing toolboxes are discussed.

14.1 Calibration

Before useful analysis can be performed on the images, the instruments need to be calibrated both radio-metrically and geographically.

For radiometric calibration, the sensor must be pointed at a target with a known colour for the ANT-2 instruments or with a known temperature for the ARCTIC instrument. For the ANT-2 instruments, images of objects with distinct and known colours like icebergs, grasslands and deserts can provide reference signals for determining the colour scale of the images produced by the instruments. Since the ARCTIC looks at temperature differences, an object with a known temperature needs to be imaged in order to provide calibration data. The ARCTIC report suggests pointing the instrument to deep space [31].

For the geographic calibration, the instruments need to image objects with a known location on the globe to calibrate the position of the spacecraft in order to make proper geo-referenced images. Known and distinct landmarks like large bridges or buildings can be used. For the ARCTIC however, the pixel size is too large to use man made landmarks as reference points. It does however see temperature differences; hence small lakes can be used as reference points. Since bodies of water generally have a different temperature than the surrounding land, they will be easily recognised in the images. Note that many other landmarks are usable for both radiometric and geographic calibration. Also due to constant deterioration of the sensor due to radiation, calibration should be performed as much as possible.

14.2 Slant to ground range conversion

In order to measure true distances on the images and to detect differences between two images of the same area, the images need to be rectified. Ortho-rectification is the process of converting images into a form suitable for maps by removing satellite motion and projection effects from the raw imagery. Basically it is converting the distances in the image from slant range to ground range. This becomes more important as the field of view increases.

14.3 Co-registration and image stitching

Since the different cameras in the constellation are used together for a multitude of applications, a co-registration method is required. Co-registration is the process of transforming multiple datasets into one coordinate system. In the case of the constellation, multiple images of the same area are transformed to one image in order to get more information out of the datasets. The base image, meaning the template of the result is called the master image whereas the image delivering the added information is called the slave image. Different methods for co-registration are available, in the following section different algorithm classifications are described and selected. For each option one of the algorithms is selected.

14.3.1 Intensity based versus feature based methods

Intensity based co-registration methods define control points within an image based on the intensity variation of the image. Feature based methods look for distinct features in the image to define the control points. Since the satellites orbit on different altitudes and their lighting conditions may vary, feature based methods are preferred over intensity-based methods.

14.3.2 Spatial domain versus frequency domain methods

Spatial methods operate in the image domain matching patterns of features in images, whereas frequency methods work in the Fourier domain to find complex correlation between images. Since the images are non-coherent, (only the intensity is used and not the phase of the signal) spatial domain methods are used.

14.3.3 Use of co-registration in constellation

It should be noted that image registration will have little added value for the constellation as the resolutions of the different instruments greatly differ. For example, Using an ANT-2 RCC image as a master and an ARCTIC image as a slave will only

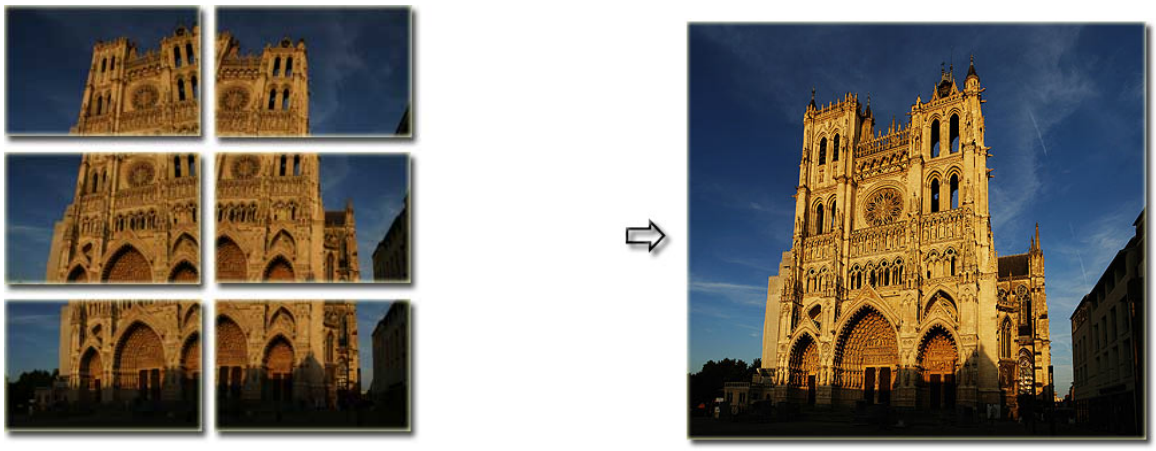

(a) six images before stitching

(b) Resulting image after stitching

Figure 14.1: Stitching of six individual images

provide the master image with rough averages of temperature data since the pixel size of the ARCTIC image are a factor ten larger. Hence there is no added value in this operation w.r.t. using the two images independently. External data could however be used. For example data of the future Sentinel satellites can be used for image registration. Sentinel 1will be launched in 2013 and provides high resolution SAR data and Sentinal 2, launched in 2014, shall provide multi spectral imaging data.

14.3.4 Image stitching

Image stitching is the process of merging multiple images to form an image with a larger area. Images from the same instrument, but from different satellites, can be stitched together to form a large map. For this process images need be converted to ground range. Also distinct features must be detected in the images to find the right stitching points between the images. In this way the overlapping area between two images can be determined to ensure a good fit. Many methods exist to correct for the edges of the different images. An example of image stitching is presented in figure 14.1 obtained from[67].

14.3.5 Feature detection

Feature detection is the process of recognising distinct features in images. Using automated routines, features like roads, buildings and crop fields can be detected by a computer. These features can be used as reference point for further operations like stitching and form the basis for useful analysis of the image.

14.3.6 Scale invariant feature transform

Due to different resolutions, a scale invariant method is required. The SIFT algorithm defines control points in the images based on their features. The features are recognised independent of the scale of the image. Using this method, the high-resolution images can be stitched together with the low-resolution images to get a more detailed picture. Several key stages can be identified:

- scale invariant feature detection
- feature matching and indexing
- cluster identification
- model verification by least squares
- outlier detection and removal

An algorithm like SIFT can be used for image co-registration, image stitching and feature recognition.

14.4 Image format

In order to process and analyse the images, it is preferred to have the GeoTIFF format. The GeoTIFF format is an adaptation of the TIFF (Tagged Image File Format) format with additional data on map projection, coordinate system and date. GeoTIFF is widely spread across the earth observation community due to fact that geographical information is stored in the image files.

Since the images are compressed in the satellite using the JPEG compression scheme, the down linked images will be in JPEG format, only having a timestamp. The additional data for GeoTIFF can be added on the ground. From the timestamp, the date and exact position of the imager can be deduced. Since the satellites all point nadir, the slant range is known as well as the map projection. With this data the JPEG image can be converted to GeoTIFF.

14.5 Earth observation image processing software

Different free toolboxes exist. For example the Basic Envisat Sar Toolbox (BEST) and Next Esa Sar Toolbox (NEST). These Toolboxes are paid for by ESA and are made available for free. The toolboxes are designed for Synthetic Aperture Radar images but can also handle non-coherent, hence real valued images. NEST features an extensive graphical user interface whereas BEST is a lighter application designed to be called from the terminal or from .ini files. Hence BEST is well suited for an automated approach. It is advised to generate batch files that command BEST to process large quantities of images.

Apart from these ESA applications, many more solutions exist. The French space agency (CNES) developed the ORFEO Tool Box (OTB). The ORFEO Tool Box is a C++ library for remote sensing image processing. It is originally designed for the French Pleiades satellites but can handle products from a wide variety of sensors. It has built in routines for feature detection (using SIFT and SURF), ortho-rectification, map projections, image conversion and change detection. Note that the open source toolboxes mentioned are only a few from the large number available.

Processing software can be designed for the constellation from scratch. However due to the wide variety of image processing software available (for free) it is advised to make use of existing toolboxes. It might be necessary to develop scripts to make the data generated by the constellation compatible with existing software. For example a script needs to written to convert the received data to GeoTIFF format. Since the preference for a specific toolbox is highly dependable on the costumer's applications and wishes, the presented description of available software is only an example.

Chapter 15 | Design Assessment

With the design of the constellation and the individual satellites complete, the results have to be assessed. The first section is used to describe the reliability of the individual satellites and the number of additional satellites required to mitigate the damage done on the constellation by failure of a single satellite. In the second section the risks for the entire constellation are described. While the failure of a single satellite does not affect the constellation at this point, other risks exist that compromise the constellation in different ways. The last section deals with factors that change the functionality of the constellation, but not directly compromise its functions. This sensitivity analysis displays the effects of changes in several variables on the entire constellation. finally the requirement compliance matrix shows which initial requirements were actually met during the design.

15.1 Reliability

Reliability is defined as "The probability that a device will function without failure over a specified time period or amount of usage" ([12], p 765). In this definition "without failure" is interpreted as "without failure of any kind" when referring to *basic reliability*. For *mission reliability* this can be interpreted as "without failure that impairs the mission".

For the C^{3}EO mission to be successful, a high platform reliability is required. As such, the following section covers the analysis of the constellation and platforms as a whole to determine its reliability requirements.

15.1.1 Reliability determination of a single satellite

Determining the reliability of each satellite and the complete constellation is simply not possible at this stage. Failure rates of most subsystems are not available and other subsystems are still in the experimental phase, such as the microthrusters. All the while, most COTS components are not even designed to function in space's adverse environment. Accordingly, it is not possible to calculate how many satellites fail during the mission's lifetime. Instead, a bottom-up approach is used; the reliability required per satellite such that at the end of the mission its performance is still acceptable is determined and from that the initial number of satellites is selected.

In order to determine the required reliability it is first necessary to define mission success. The strength of the C^{3}EO mission is its ability to provide imagery to a wide range of applications with a high temporal resolution. As such, the mission success is defined as the constellation's ability to maintain a high temporal resolution throughout its lifetime; a requirement of 90% of the initial temporal resolution at the end of the mission is set and the case study that follows is based on this figure.

The second step is to determine the minimum number of satellites required per platform such that the temporal resolution requirement lies in a 95% confidence region. This computation is done with MATLAB by making use of a binomial cumulative density function. This function calculates the probability that there are X successes in N attempts with probability P as shown in equation 15.1.

$$y = F(x|n,p) = \sum_{i=0}^{x} \binom{n}{i} p^i (1-p)^{n-i} I_{0,\ldots,n)(i)} \tag{15.1}$$

Where y is the probability of having up to x successes, i.e, surviving satellites in n independent trials, i.e, total number of satellites at the start of the mission. The probability p is the chance a satellite survives for the duration of its mission.

Two year Reliability	# ARCTIC	# RCC	# TMA
0.5	81	54	61
0.6	66	44	49
0.7	55	37	41
0.8	47	31	35
0.85	44	29	32
0.9	40	26	30
0.95	**37**	**24**	**27**
0.97	36	23	26
0.98	36	23	26
0.99	36	22	26
1	36	22	26

Table 15.1: Number of satellites required per platform for Yx > 0.95

However, the interest is in knowing how many satellites are need to have at least x successes and not "up to x" successes. This is achieved by simply modifying equation 15.1 to $Y = 1 - y$. Furthermore, in order to obtain the minimum number of

satellites, Y is predefined in the range of $Y > 0.95$ such that all results are in the 95% confidence region. The number of surviving satellites x is set as a constant defined by the number of satellites required such that only a 10% loss in temporal resolution is allowed to occur during the mission. The remaining variables n, the total number of satellites and p, the probability of success are allowed to vary. The results of this computation can be seen in table 15.1.

As can be seen in the table above, the number of satellites necessary at the start of the mission for successful completion increases as the unit reliability decreases. The most interesting point lies in the 95% reliability region, as it is the lowest reliability where all platforms suffer an increase of the number of satellites by one in the ARCTIC and TMA parts of the constellation, and by two in the RCC part; this ensures that each part has at least one extra satellite for contingency. The 90% temporal resolution requirement is directly proportional to the number of satellites required, i.e, 90% of the satellites necessary for 100% temporal resolution should still be functional at the end of the mission. From this it is possible to determine how many satellites are allowed to fail per constellation part with equation 15.2.

$$Failures = (\#satellites\ Yx > 0.95) - (\#satellites\ for\ 100\%temporal\ resolution\ \cdot 0.9) \tag{15.2}$$

With the number of satellites allowed to fail known it is then possible to calculate the failure rate λ and the Mean Time Between Failure (MTBF) using equations 15.3 and 15.4.

$$\lambda = \frac{Failures}{Lifetime(h)} \tag{15.3}$$

$$MTBF = \frac{1}{\lambda} \tag{15.4}$$

Here, λ is the failure rate per hour of each CubeSat and $Lifetime(h)$ is the mission duration in hours. $MTBF$ is the mean time between failure of each platform which can be seen in table 15.2.

Platform	MTBF(h)
RCC	4320
TMA	4320
ARCTIC	3456

Table 15.2: MTBF for each platform with a two year reliability of 95%

And so, a RCC and TMA satellite fails every 180 days, while the ARCTIC satellites suffer a failure every 144 days on average for the first two years. Furthermore, if each satellite is built with a 95% reliability figure, the total number of satellites in the constellation is then 24 RCC satellites, 27 TMA satellites and 37 ARCTIC satellites.

15.1.2 Redundancy

Individual CubeSat platforms are not flexible in terms of redundancy due to the limited space. However, this fact changes when a whole constellation is considered. The main advantage of such constellations is that a single satellite within the constellation is not a single point of failure. Even if the two year reliability of the satellite is below the desired 95%, it is possible to mitigate the constellation's performance degradation by increasing the amount of satellites in orbit. The only part of the mission which cannot be mitigated is the launch sequence. If a launcher has a reliability of 98%, no matter how many satellites are added to the constellation, launch failure will not be mitigated. The only way to ensure that a large portion of the constellation is not lost upon launch is to use multiple launches, which comes at a cost in terms of logistics and constellation start-up.

15.2 Availability

The availability of the constellation is determined by how much of an orbit's ground track is imaged per revolution. This is directly related to the duty cycle of the cameras covered in chapter 3. Basically, the power available and the downlink budget determine the availability of the constellation. Regardless, no matter how many ground stations are used to increase the downlink time, an uptime of 100% is difficult to achieve due to the power required by the communications subsystem, such that the solar panel area is too large to adapt to a 2-by-2U CubeSat. As it stands, the constellation has an uptime of 25%.

15.3 Maintainability

Maintaining a satellite is rarely an option due to accessibility issues; instead satellites are built to provide very high reliability and account for as many risky scenarios as possible. With a CubeSat constellation the accessibility remains an issue, but designing for extremely high reliability is not part of the CubeSat's design philosophy as the use of COTS components is encouraged. However, the fact that COTS components are used allow for a relatively simple assembly process; if enough satellites fail to impair the constellation's performance, new satellites can be deployed in order to "repair" the constellation.

15.4 Safety

Safety is related to the mitigation of dangers imposed on other entities by the CubeSat constellation. As such, safety is achieved through the avoidance of collision with other satellites to avoid creating extra debris and impair other missions. Special care should also be paid to collision avoidance between the constellation and the ISS, which is currently orbiting at 430 km. Furthermore, it is important that the satellites de-orbit in 25 years time. This is not an issue for the RCC platforms; due to their high density at their low altitude they de-orbit within 3 months when the propulsion system is turned off. The TMA and ARCTIC platforms are outfitted with some propellant mass for a de-orbit maneuver so that they also de-orbit within one year. Ground safety is not an issue either as the satellites disintegrate completely upon re-entry.

15.5 Risk management

In order to minimize the constellation's risk of failure, it is important to carry out a comprehensive study of possible malfunctions throughout its mission. Since a satellite is not a single point of failure, the risk analysis does not focus on sub-system failures and its effects, but on operational characteristics that affect the constellation as a whole. In the following sections a fault-tree diagram as well as technical risk map are used to properly document and prioritize constellation malfunctions.

15.5.1 Fault tree diagram

The fault tree diagram is an excellent tool to map top level faults of the constellation and its lower level causes as can be seen in figure 15.1. With such a diagram, it is then possible to determine which aspects of the constellation are prone to causing the most damage.

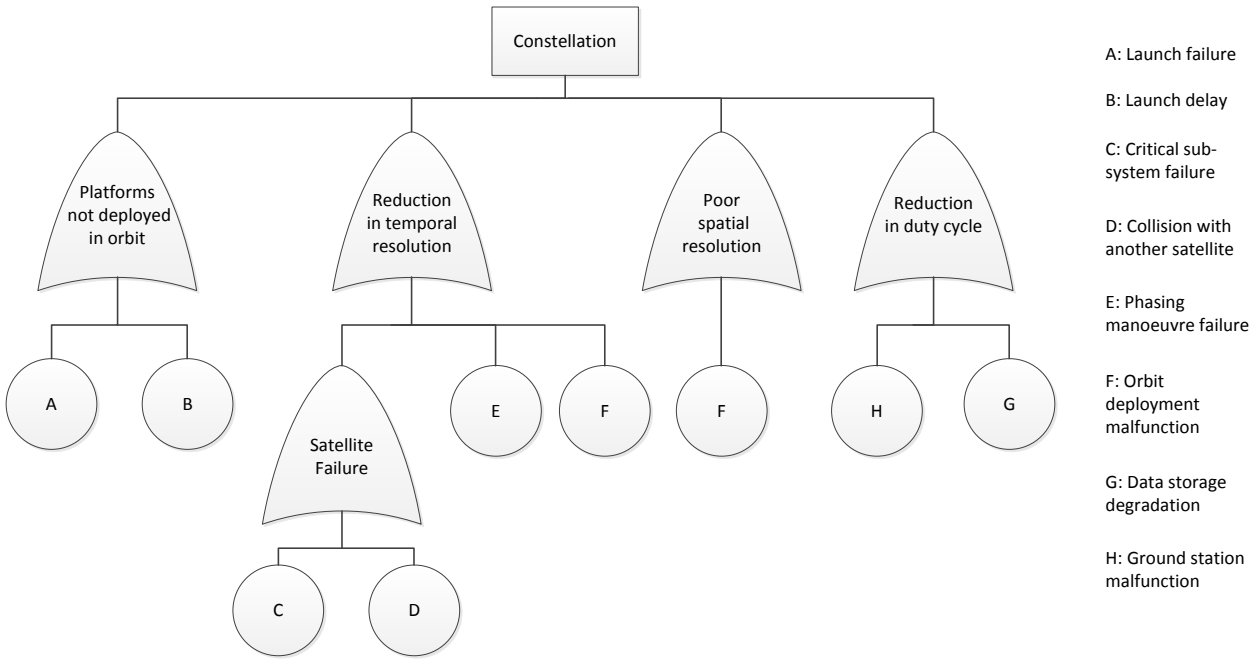

Figure 15.1: C^{3}EO constellation fault tree map

From the fault tree diagram it is clear that the most critical fault is related to the launch of the platforms, as a launch failure with a payload several CubeSats severely affects the constellation. Secondly, most of the remaining issues are also related to orbit maintenance such as phasing and deployment. However, a single satellite failure does not compromise the mission, but it does reduce its performance.

15.5.2 Technical risk map

With the constellation faults mapped and the critical aspects identified, a technical risk map can be created accordingly such that the risks are quantified in terms of likelihood and impact on the constellation. Firstly, an overview of the considered faults is shown in table 15.3.

	Fault	Likelihood	Impact
A	Launch failure	Low	Very high
B	Launch delay	Medium	High
C	Critical subsystem failure	Very High	Very low
D	Satellite collision	Very low	Very low
E	Phasing manoeuvre failure	Low	Low
F	Orbit deployment malfunction	Low	High
G	Data storage degradation	High	High
H	Ground station malfunction	Low	Very Low

Table 15.3: Likelihood and Impact of Risks

In order to provide a practical visualisation of the faults provided in table 15.3 a plot is provided such that a clear association between likelihood and impact is available. The vertical axis defines how large the impact is, while the horizontal axis provides an indication of its probability. Each cell is then coloured according to the severity of the fault, with light colouring (green) being associated with a small risk and dark coloured (red) associated to a high risk which should be mitigated. For a high chance of mission success, all faults should be located in the light coloured (green) region shown in table 15.4.

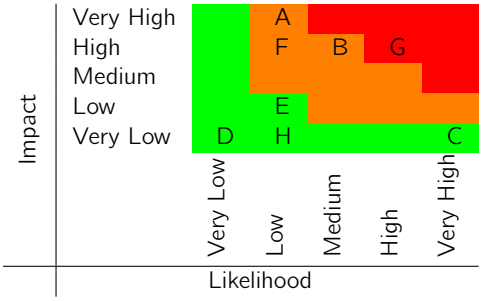

Table 15.4: Constellation Risk Map

A. Launch failure

A launch failure has the highest impact on the constellation as the satellites are sent in bulk. However, the probability of this event is low. Mitigation can only be done by choosing the most reliable launchers available or by spreading the constellation over multiple launches.

B. Launch delay

Launch delay can hamper the process of setting up a constellation, especially since each platform is sent in a different launch. If a platform launch is delayed, the constellation is incomplete and is not able to cover all the applications chosen in the previous chapters. The likelihood of this event is medium as the availability of the Shtil rocket is highly dependent on the political environment concerning the phasing out of ballistic missiles. The only means of mitigation is by using a different launcher at considerably higher cost.

C. Critical subsystem failure

A critical subsystem failure implies that a satellite becomes non-operational. The likelihood of this event is very high due to the sheer amount of satellites used with COTS components. However, its impact on the constellation is very low as the only consequence is a slight reduction in temporal resolution. Mitigation is already taken into account by adding extra satellites for contingency measures, which is further described in section 15.1.

D. Satellite collision

Satellite collision renders a single CubeSat non-operational. This event has a very low impact in the constellation and its likelihood is very low; no mitigation is considered regarding this fault.

E. Phasing manoeuvre failure

This event is mainly related to the reliability of the microthrusters used in the CubeSats. If the manoeuvre is not done properly, the constellation's temporal resolution will be slightly affected but its impact is low and its likelihood is also low.

F. Orbit deployment malfunction

Also related to launcher reliability, this event can have a high impact in the constellation. If the final orbit height is higher than planned, spatial resolution is decreased. If the orbit height is lower, the RCC platform's mission lifetime is reduced due to the increased ΔV budget. Mitigation can be done by increasing propellant mass contingencies.

G. Data storage degradation

This event poses the biggest risk on the constellation's performance. It is almost guaranteed to happen due to the SD card's inability to withstand radiation. This is a gradual process that severely limits the constellation's mission duration and duty cycle.

H. Ground station malfunction

A failure in the ground segment results in a reduction of downlink capability and thus the duty cycle of the constellation. The impact of this event is considered very low as the constellation depends on a total of eight ground stations. Furthermore, these stations are easily accessible and can be repaired, meaning that the downtime is only temporary.

15.6 Sensitivity analysis

During the design process many assumptions and simplifications are made. These assumptions have a great influence on the outcome of the assignment. In order to see the effects of changes in these assumptions a sensitivity analysis is presented in this chapter.

15.6.1 Propulsion

All satellites in the constellation are outfitted with micro electrospray thrusters based on the MIT design. This is still an experimental technique so there are some uncertainties involved. MIT claims that the micro thrusters have a specific impulse between 2500 and 5000 s. This is a large range and its exact value has a significant effect on the required propellant mass. Another factor that determines the required propellant mass is the drag force that the propulsion needs to counteract. The drag force is proportional to the drag coefficient. The drag coefficient for a cube is 1.15. This is however for continuous aerodynamics. In LEO the satellites will experience molecular flow which changes the experienced effects. The exact drag coefficient for satellites is as of yet unknown. Conventionally a value of 2.3 is assumed for compact satellites in the design process. This assumption however is hardly validated so the exact value is highly uncertain. In the design of reference satellite, Oscar-1 [12], with similar characteristics in terms size a drag coefficient of between 2 and 4 was estimated. Figure 15.2 gives an overview of the changes in propellant mass for different values of the specific impulse and experienced drag coefficient. It can be seen that the difference between the best case scenario and the worst case scenario is significant (more than 200 grams). It is also clear that in the worst case scenario 0.24 kg of propellant is needed, which is still possible given the modest satellite mass of around 6 kg. This figure is for the RCC segment that orbits at 288 km. For the higher orbiting segments the relative effects are the same but the magnitudes are smaller

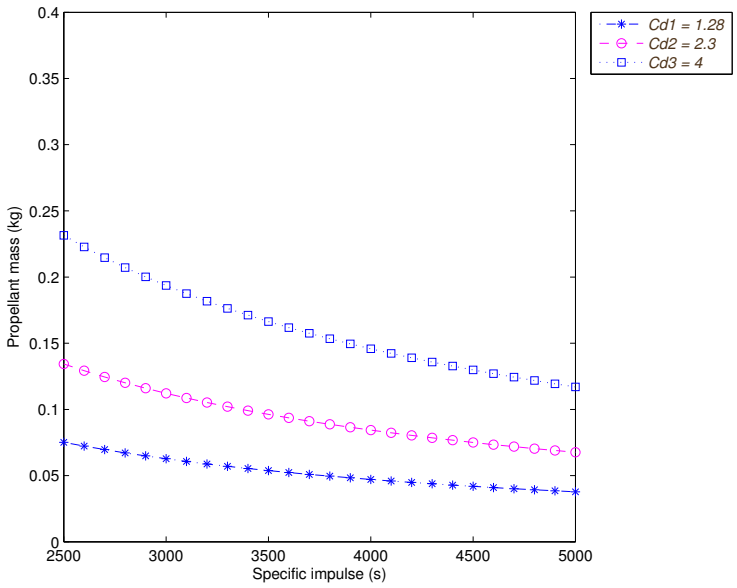

Figure 15.2: Sensitivity in Propellant Mass

15.6.2 Duty cycle

The amount of data generated is restricted by the duty cycle, currently 25 percent on average of the imaging satellites. This in turn is limited by the downlink capability of the satellites. The downlink capability is restricted due the power available and the maximum achievable data rate of the transmitters. These parameters are quite restricted due to the limited amount of power available in a CubeSat and the limitations of COTS transmitters. Therefore the most straight forward way to increase the satellites' duty cycle is to increase the total number of ground stations.

When the number of ground stations is increased, it would be wise to put the ground stations as far from the equator as possible since this would increase the coverage per ground station. This effect is shown in figure 15.3. However, the ground station's field of view should not overlap. The amount of duty cycle increase per ground station is heavily dependent on the exact location of the extra ground station.

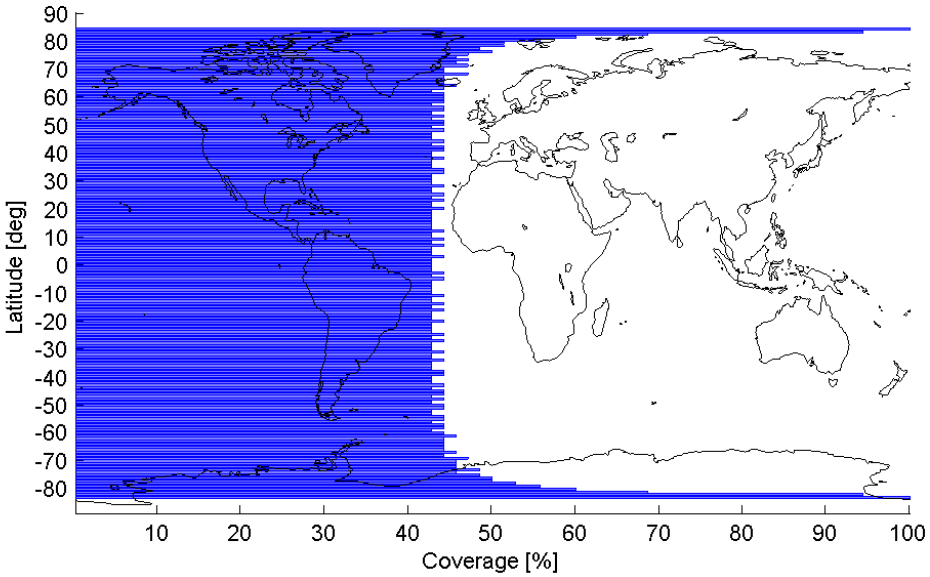

Figure 15.3: Coverage Frequency for different latitudes

15.6.3 Resolution

Since the camera features are set, the spatial resolution only depends on orbit altitude whereas the temporal resolution depends on the number of satellites in orbit. Both temporal and spatial resolution vary linearly. To increase the spatial resolution, the satellites need to be lowered. This will however reduce the field of view and increase the propellant mass. Since the air density increases exponentially with decreasing altitude, the drag and aerodynamic torque will increase to an unacceptable amount when the altitude drops significantly below 250 km. Therefore the spatial resolution is limited.

The temporal resolution is linearly proportional to the amount of satellites. Doubling the temporal resolution requires in doubling the number of satellites in orbit. Since the number of applications that require sub-day resolutions is limited and the additional investments are significant, there is little sense in increasing the temporal resolution.

15.6.4 Lifetime

The operational life time of the constellation affects the amount of data produced, hence the amount of revenue. In general increasing the lifetime will increase the return on investments (ROI) of the constellation and lowers the cost per image. It should however be noted that the operational lifetime is likely to be limited by the radiation tolerance of the COTS components. The exact effects of the space environment on these components are uncertain. The use of space grade components increases the lifetime of the constellation but is also likely to increase the hardware cost by one order of magnitude. Figure 15.4 shows the sensitivity of cost and revenues with lifetime. The effect of space grade components is hard to estimate and is not taken into account in this figure.

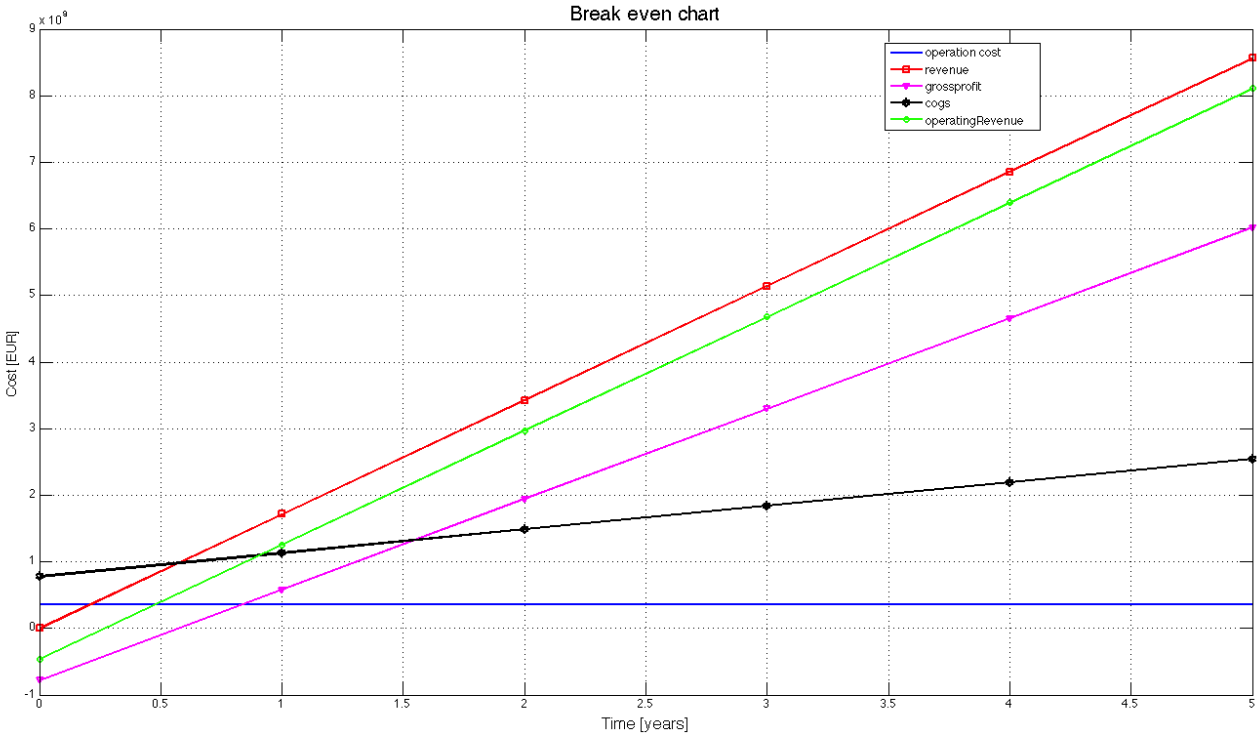

Figure 15.4: Revenues and cost versus operational lifetime

15.7 Requirement compliance matrix

15.7.1 Market requirements

The constellation is designed within budget since the unit price per satellite is less than 250k *EUR*. The constellation possesses no single point of failure, however a number of failure points are present in the single satellites. Redundancy is achieved by the amount of satellites and distributed ground stations. The operational lifetime of two years is met by the assumption that the COTS parts will survive that long, although this assumption contains some uncertainty. Only one out of three segment of the constellation orbits in the Very Low Earth orbit. Sustainability is achieved by de-orbiting within 1 year.

15.7.2 System requirements

Both versions of the ANT-2 as well as the ARCTIC cameras are part of the constellation. Due to the stringent pointing requirements of the cameras, the ADCS is designed to deliver a pointing accuracy exceeding typical Cubesat missions. The ground resolution of 4 meters per pixel is met with a weekly revisit time. The daily revisit time is only met on average with a resolution of 25 *m* in the visual spectrum and 56 *m* in the Infrared. To have a daily revisit time constantly over the whole earth results in doubling the amount of satellites which is not worth the effort. Also, since only high spatial resolution visual images are required, only the ANT-2 RCC segment orbits in the VLEO orbit.

15.7.3 Launch requirements

The constellation can handle all the launch loads of the Ariane V and Vega launch vehicles. Therefore there is a possibility of piggy back launches. However since the number of satellites is high and their orbits are unlikely to be used by large satellite, this option is not used in the final design. The satellites are designed to cope with the loads of the Shtil 2.1 launch vehicle, which are more severe than that of the Vega and Ariane.

15.7.4 Mission requirements

Power is provided for all of the payloads. The ARCTIC sensor is cooled. However a change in the thermal design was needed which is not analysed sufficient yet. Images are supported by a maximum downlink capacity of 10 *Mbps* which greatly exceeds the initial requirements. This is needed to get sufficient coverage. The micro machined electro spray thrusters provide enough impulse to compensate for the drag, perform phase out and to de-orbit after the operational phase.

15.7.5 Conclusion

At the end of the design phase it is concluded that most of the initial requirements are met. Some design requirements, like resolution and launch loads, changed overtime due to change of perspective on the applications and possibilities of the nanosatellite cameras. Since the design meets most of the requirements it is concluded that the constellation is a promising and feasible design.

ID Lvl. 1	ID Lvl. 2	ID Lvl. 3	ID Lvl. 4	Description	Type of Requirement	Compliance
1.0				Market requirements		
	1.1			Design Within Budget		✓
		1.1.1		Unit price per Satellite less than 250000 EUR	Driving requirement	✓
	1.2			High Reliability		✓
		1.2.1		No SPF failure	Top Requirement	✓ (for constellation)
		1.2.2		Operational Lifetime of 2 years	Top requirement	✓
	1.3			VLEO Orbit	Driving Requirement	
		1.3.1		230 to 380 km		✓ (only for RCC)
	1.4			Cope with Space Environment		✓
	1.5			Sustainability		✓
				De-Orbit after maximum of 25 years		✓
2.0				System Requirement		
	2.1			Use ANT-2 and/or ARCTIC design	Driving requirement	✓
		2.1.1		Pointing Accuracy of typical Cubesat		✓ (more precise than typical Cubesat)
			2.1.1.1	1.7 s^{-1} (X-Axis), 3.4 s^{-1}(Y-Axis), 11.5 s^{-1}(Z-Axis)		✓
		2.1.3		Provide typical LEO Earth observation data		✓
			2.1.3.1	VIR ground resolution of 4 m/pixel		✓
			2.1.3.2	Temporal Resolution of 24 hours for whole Earth and 30 min for 5%		✗ (only part of constellation)
	2.2			Comply with launch activity	Top requirement	✓
		2.2.1		Withstand Vibration level of Ariane 5 and Vega		✓
			2.2.1.1	Lateral mode frequency higher than 15 Hz		[33] ✓
			2.2.1.2	Longitudinal mode frequency between 31 and 45 Hz		✓
		2.2.2		Possibility of using Piggy-back option		✓ (although not used)
	2.3			Maintain Mission	Top Requirement	✓
		2.3.1		Provide power to Camera		✓
		2.3.2		Thermal Control for ARTIC camera option		✓
			2.3.2.1	Keep operational temperature at 157K		✓
		2.3.3		Support Imaging		✓
			2.3.3.1	Downlink capabilities of 512 kbps		✓ (exceeds it)
		2.3.4		Avoid Orbital decay	Driving Requirement	
			2.3.4.1	Propulsion capabilities to compensate drag over two years lifetime		✓
		2.3.5		Withstand temperature differences		✓
			2.3.5.1	Keep subsystem expansion tolerances		✓
			2.3.5.2	Keep tolerances for temperature material deformation		✓
		2.3.6		Stable Satellite	Top Requirement	✓

Table 15.5: Requirement compliance matrix

Chapter 16 | System specifications

This chapter gives an overview of the system specifications that follow from the design process. The specifications are broken down into the three design segments, i.e. the constellation, spacecraft and operational segment. Table 16.1 provides a clear overview of the most relevant specifications.

	Parameter	Unit	RCC	TMA	ARCTIC
Constellation segment	Orbit height	km	288	500	443
	Type of orbit		Sun-synchronous	Sun-synchronous	Polar
	Inclination	deg	96.6°	97.4°	90°
	Revisit time	$days$	7	1	1
	Number of satellites		24	27	37
	Field of view	deg	1.8°	5.8°	5.0°
	Swadth width	m	8847	51200	35818
	Spatial resolution	m	4	25	56
	Spectral band		VIS	NIR+VIS	TIR
Spacecraft segment	Dry mass	g	4512	4512	4998
	Delta-v	m/s	736.2	321.8	301.1
	Datarate	$kbits^{-1}$	3590	625	812
	Average power	mW	11982	10992	11982
	Solar panels		CIGSSe	CIGSSe	GaAs-TJ
	Unit price	k EUR	204.8	204.7	213.2
Operational segment	Required coverage	%	28	17	25
	Average required coverage	%	25		
	Ground stations		8		
	Ground segment cost	EUR	2.55 M		
	Launcher		Shtil 2.1		
	Launch cost	EUR	13.0 M		
	Payload mass	kg	112	124	187
	MTBF	h	4320	4320	3456

Table 16.1

Chapter 17 | Further Planning

If the C^{3}EO project would developed further after this DSE it is important to indicate the post-DSE activities. A model to used to plan the development of a project is the *waterfall* model, which is shown in figure 17.1. It describes the process of development from the initialisation of the project to the maintenance and operating of the system. The DSE covers the first two segments, the project initialisation and analysis. A planning for the next steps according the waterfall model is shown in figure 17.1.

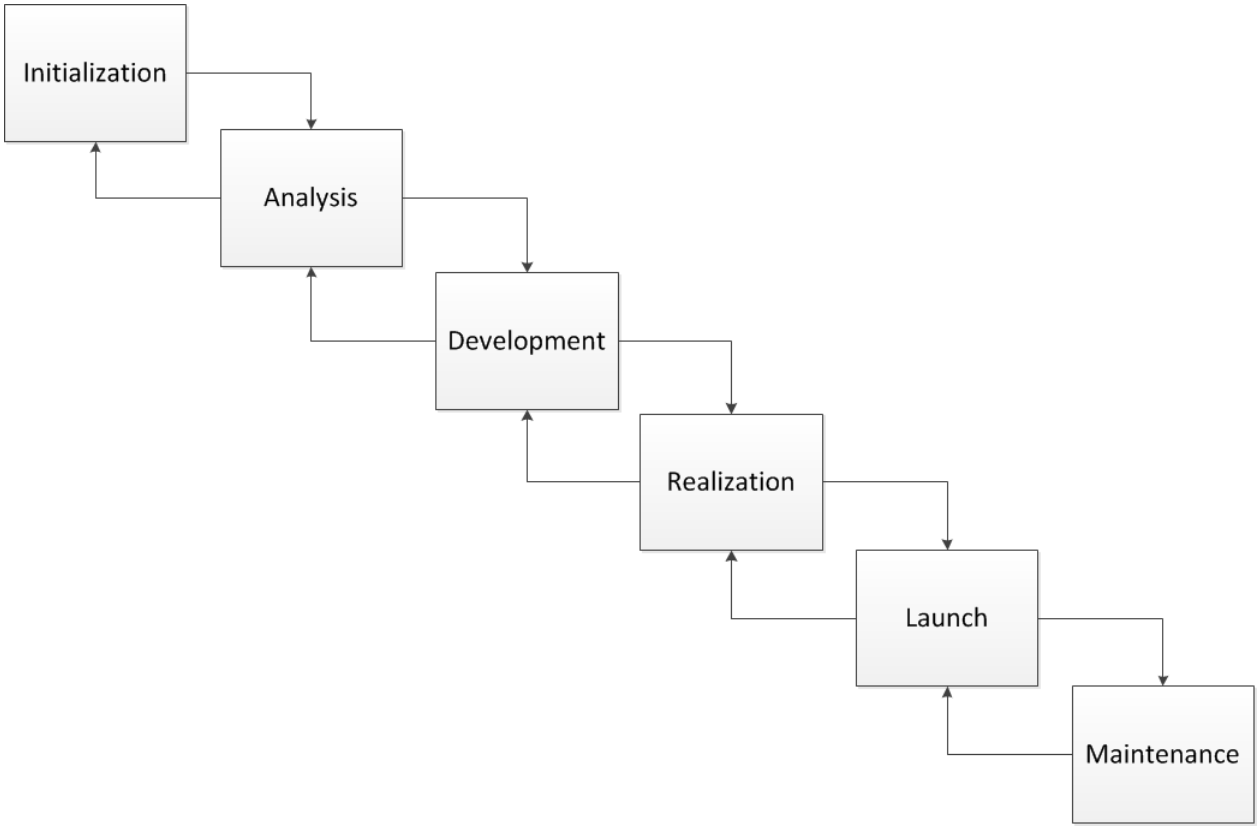

Figure 17.1: Waterfall model

The first step after the DSE is the development of the satellites, while during the DSE an initial definition of all components of the constellation is made, the development phase will result in a detailed design. This includes the detailed design of all components of the satellite, the design of the ground segment and other support functions. At the end of this phase the design is ready for the production.

The next step is the realisation phase. In this phase the actual product is produced and hardware is bought. This phase is very interesting as mass production satellite, is rarely done. Only few examples currently exist, being GPS, Galileo or the Iridium communication network. A further explanation is given in section 17.1. At the end of the realisation phase, the production of the system is complete and the system is entering the launch phase.

The launch phase includes all activities related to putting satellites into orbit, such as the testing, launcher integration and the actual launch of the satellite. The testing of the satellites is an important step to avoid problems later during the project. For the launch of over 30 satellites with the Shtil 2.1 launch vehicle new deployments methods need to be found. These need to be developed as well being part of the development phase. The satellites need to be installed into these deployment mechanisms. After the satellite are launched into orbit they are calibrated and tested. This is an important step as without calibration and testing the imaging data could be compromised. The launch phase also includes the start of pushing the product to the market such that customers get interested in it. When this phase is complete the system enters the maintenance phase.

The last phase is the actual operating and maintenance of the constellation. This means that the satellites are instructed what to image and possible errors on board are corrected with software updates. On the ground the data captured by the constellation are distributed amongst customers. The next step, which not shown in the waterfall diagram is when the mission lifetime is

reached. In case of a mission success a replacement constellation could be launched. The development of the replacement should be already be done during earlier phases of the project.

17.1 Production Consideration

As already mentioned the production of 100 satellites is a challenge in itself. The main problem is that there is no precedence and methods have to be found to complete the production. This includes several sub problems. One of these is the lack of skilled worker, as such a production would require a higher work force as a single satellite, which would increase costs. All components needed for the satellite would need to be available in a short time to allow a short system integration. A possible solution would be to adapt methods used for example in the automotive industry which deals with larger scale productions. The size is not comparable but certain methods could be adapted, such as *just-in-time* or *lean* methods and the use of a production line. A delay in one part of the production however would halt production or limit the capability and hence the business appeal of the whole constellation. Furthermore several components which are planned to be used for the satellite are in concept phase only, making a production risky. Additionally there are normal failures that can occur in any satellite mission.

Taskname	Start	End	Duration	2013	2014	2015	2016	2017
Initialisation	12/11/2012	19/11/2012	6d					
Analysis	20/11/2012	07/01/2013	53d					
Development	08/01/2013	01/09/2013	279d					
Production	02/09/2013	30/06/2014	261d					
Launch	01/07/2014	01/02/2015	154d					
Maintenance	02/02/2015	02/02/2017	524d					

Table 17.1: Post-DSE Gantt chart

Chapter 18 | Cost Analysis

In this chapter the cost analysis for the C^{3}EO satellite constellation is presented. All cost elements are identified and the feasibility of the design is analyzed in terms of profit. The analysis concludes that the C^{3}EO is a profitable business earning 300 M EUR gross profit over 2 years.

Overall, the C^{3}EO satellite constellation is reducing non-recurring development costs by making use of existing hardware and off-the-shelf components. In an attempt to credibly estimate costs of such programs, existing missions like the direct competitor RapidEye are analysed and the cost breakdown tree of the mission as well as the different costs per subsystem of one spacecraft are investigated. Additionally a reference for the subsystem cost estimation is given by the DELFI-N3XT cost breakdown.

In the cumulative return of investment, which is very high valued at 130% after 2 years, the reduction in non- recurring cost is seen. It should be noted that throughout the chapter a mission lifetime of 2 years is assumed due to the design life of the camera sensors used. The image price is determined to be an average price of **0.1 EUR**/km^2 as opposed to its direct competitor RapidEye with a price of 0.95 EUR/km^2.

It should be noted that all prices are preliminary estimates and due to many unknown factors like exchange rates and inflation they will differ from the actual numbers.

18.1 C^{3}EO detailed cost breakdown

The detailed cost breakdown specifies costs for all subsystems of one nanosatellite as well as costs for the total mission including non- recurring and recurring costs.

18.1.1 Cost breakdown tree

The cost breakdown tree as shown in figure 18.1 shows all the different costs contributing to the whole business expenses. All costs are grouped in either recurring or non recurring costs. The total mission cost for 2 years is valued at around 90 M EUR.

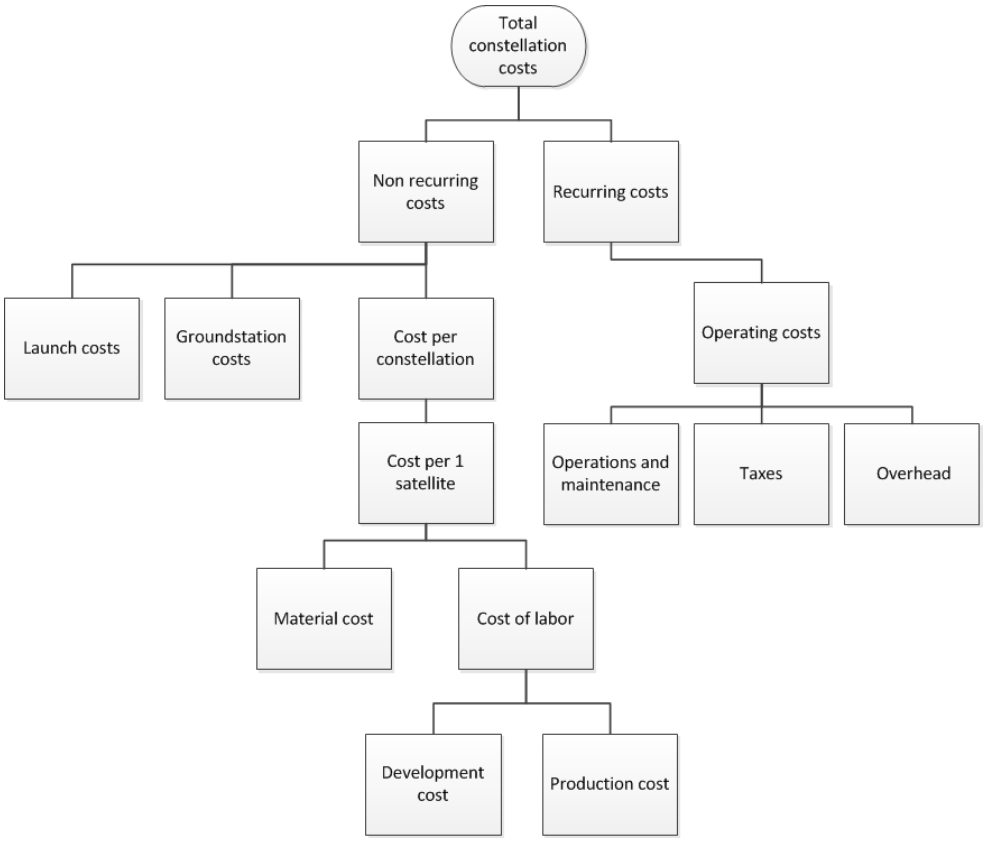

Figure 18.1: C^{3}EO mission total cost breakdown

As is seen from table 18.1 the non recurrent total costs are a summation of the constellation, ground station, and launch costs. In figure 18.2 a percentage breakdown of the total mission costs is presented.

It should be noted that throughout the chapter the sum of the non recurrent total cost is used with the contingency factor of 2. Note that the constellation material cost has been calculated with the average spacecraft cost of 208.3 k EUR as mentioned in table 18.2.

Type of Cost		**Value [M EUR]**
Non recurrent Total costs		
	Constellation material cost	18.3
	Launch cost	13.0
	Ground segment cost	2.6
SUM with contingency factor 2		67.8
	Labour cost	13.6
SUM including labour cost		**81.4**
Recurrent Total costs		
	Operation cost	**6.5**
Total Mission cost 2 years		**87.9**

Table 18.1: Cost breakdown for entire mission

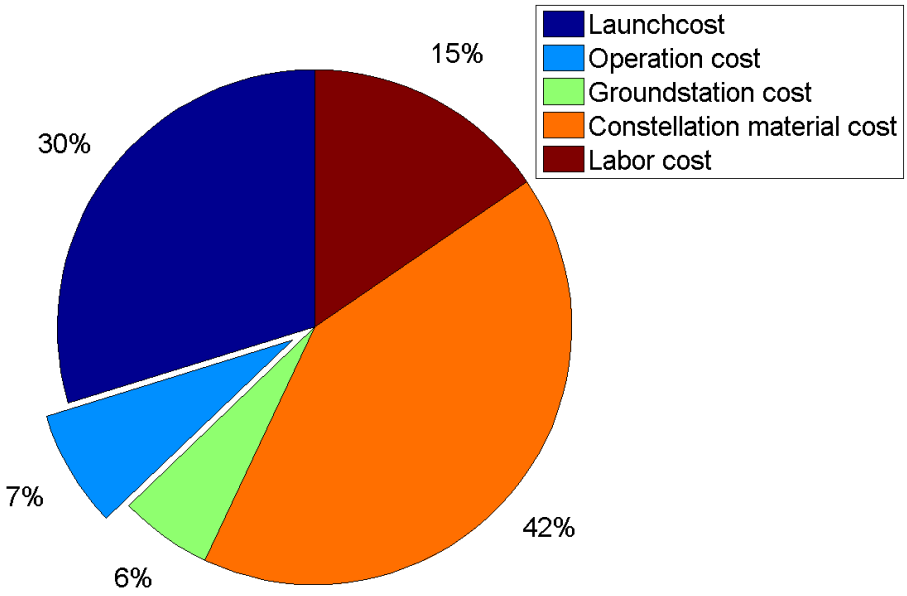

Figure 18.2: Cost breakdown of total mission cost of around 90 M EUR

The constellation material cost percentage is the highest with 18.3 M EUR (36.6 M EUR with contingency factor as seen in table 18.1), but nonetheless cheaper than any conventional small satellite mission.

The recurring operating costs fall under three basic classifications: operations and maintenance, taxes and overhead. Overhead costs refer to all ongoing business expenses not including or related to direct labour [68]. Examples of the operational costs are due to customer service, maintenance, image processing, insurance and marketing. The cost of labour includes development cost and production cost. The labour cost is assumed to be 20% of the non-recurrent total costs and is valued at 13.7 M EUR.

Computation of mission costs

To clarify the different costs the steps of computation are shown here. The non-recurrent total cost without labour ($C_{nonrec_{nl}}$) is the summation of the constellation material cost (M),launch cost (L)and ground station cost (GS), with the contingency

factor 2.

$$C_{nonrec_{nl}} = (M + L + GS) * 2 \tag{18.1}$$

The labour cost is 20% of the non recurrent total cost without labour $C_{nonrec_{nl}}$

$$C_{labour} = C_{nonrec_{nl}} \cdot 0.2 \tag{18.2}$$

The non recurrent total cost with labour $C_{nonrec_{wl}}$ is

$$C_{nonrec_{wl}} = C_{nonrec_{nl}} + C_{labour} \tag{18.3}$$

The operation costs C_{oper} are computed according to figure 18.4

$$C_{oper} = C_{nonrec_{wl}} \cdot 0.08 \tag{18.4}$$

18.1.2 Unit cost and constellation cost

The unit cost of one nanosatellite is **208 k EUR** on average for the three (ANT2-RCC, TMA and ARCTIC) satellite camera configurations. There is no contingency factor included in the subsystem cost since a factor 2 is accounted for in the total non recurrent cost. Hence also the constellation material cost is assumed to be twice as high as the beginning cost for several unexpected changes that might occur. An overview of the possibilities of the increase in cost is given in figure 18.3[69]. All the values are taken from the websites of CubeSatshop or Clydespace.

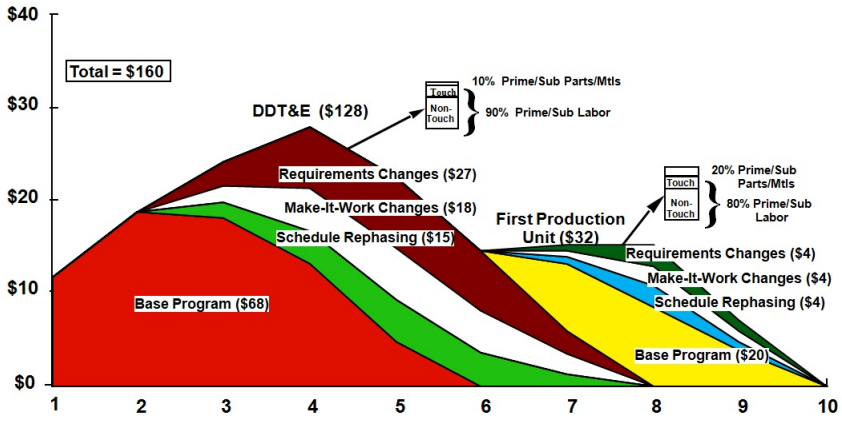

Figure 18.3: The significance of good estimation

As is seen from table 18.2 the total material cost of the constellation is around 19 M EUR. This rounded value is from this point on used. The unit cost is around 208 k EUR and this value is used henceforth. The most expensive subsystem is the C&DH with 33% of the total cost 18.6b directly followed by the Propulsion Subsystem with 30% of the cost.

18.1.3 Launch cost

The launch cost per SHTIL 2.1 as discussed in chapter 6 is assumed around 0.5-3 M EUR[70].The highest costs of 3 M EUR is taken and with a margin of 45% results in a total launch cost of 13 M EUR. The margin of 45% accounts for changes that needs to be made to the rocket, to make sure it fits the C^3EO mission. This will include for example changes to the rocket to encounter a higher target hight of the rocket, which is 400 km for the Shtil 2.1. The low cost is because there is heavy governmental funding from the Russian government and there are many SHTIL launchers available from the cold war since their nuclear payloads are disarmed.

18.1.4 Operation cost

The operation cost is usually given as percentage of capital investment. Hence, the cost of operation is 6.6 M EUR, given as 8% of the non recurring total costs, according to a statistical estimation of NASA for an average small satellites mission, see figure 18.4 [71].

Cost breakdown per subsystem	Unit cost[EUR]	Quantity	Cost[EUR]
ADCS			**27,800.00**
ADCS (see table 10.10)	27,800.00	1	27,800.00
Command and Data Handling			**39,000.00**
On-board computer	4,750.00	1	4,750.00
Antenna	4,000.00	1	4,000.00
Telemetry Antenna	4,500.00	1	4,500.00
Transceiver	6,750.00	1	6,750.00
Transmitter	19,000.00	1	19,000.00
Payload			**100,000.00**
ANT-2 TMA/ RCC /ARCTIC	100,000.00	1	100,000.00
Structural subsystem			**6,200.00**
2U CubeSat structure	3,100.00	2	6,200.00
Propulsion subsystem			**30,000.00**
ES Microthrusters	30,000.00	1	30,000.00
EPS			**(avg) 18,500.00**
Solar panels			(avg) 6,100.00
...TMA	2,500.00	1	
...RCC	2,600.00	1	
...ARCTIC	11,000.00	1	
Battery	1,200.00	2	2,400.00
Maximum power point tracking	10,000.00	1	10,000.00
Total cost per spacecraft			
...with TMA camera	217,900.00	27	5,883,300.00
... with RCC camera	218,000.00	24	45,232,000.00
... with ARCTIC camera	226,400.00	37	8,376,800.00
Unit Cost			**221,500.00 (avg)**
Total			**19,492,100.00**

Table 18.2: C^{3}EO cost breakdown

Operation cost normally vary daily. However for the C^{3}EO mission they are assumed to be constant over time. Using the total operation cost for two year of 6.6 M EUR, the daily operation cost are calculated to be 9035 EUR.

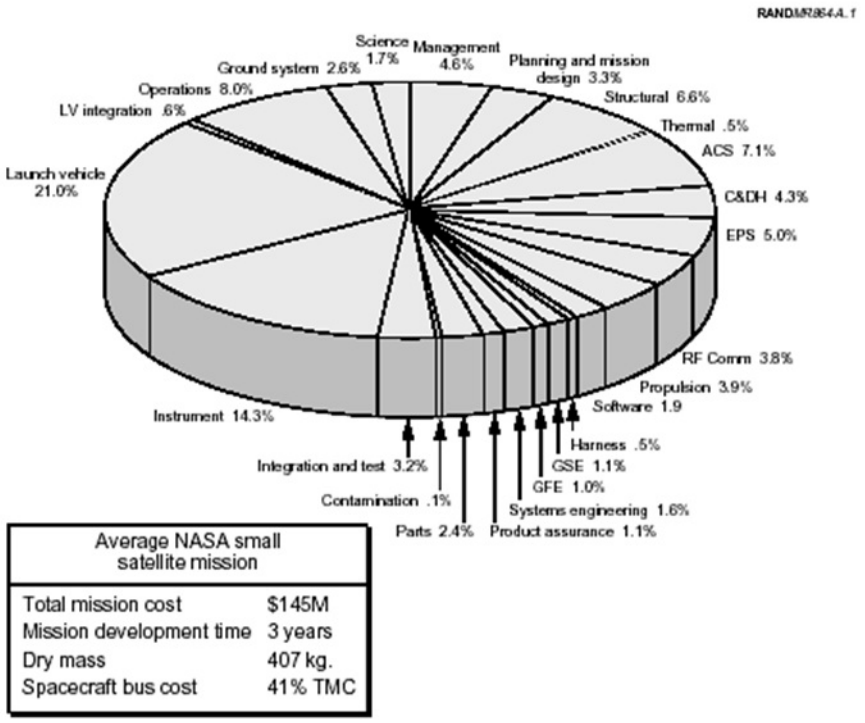

Figure 18.4: Cost Estimation from NASA

18.2 Comparison between C^{3}EO and DELFI-N3XT

In this section a cost-wise comparison between DELFI-N3XT and C^{3}EO missions is made. It must be noted that DELFI-N3XT is a science mission and the C^{3}EO mission is a commercial one, hence the cost and cost-breakdown will differ because of different mission needs and requirements. However the DELFI-N3XT gives a good percentage-wise cost breakdown of the satellite itself, which is used to verify the percentage-wise cost breakdown of the C^{3}EO satellites.

18.2.1 DELFI-N3XT detailed cost breakdown

First the subsystem cost breakdown of the DELFI-N3XT and the C^{3}EO mission are be compared. DELFI-N3XT carries a micropropulsion system and a transceiver as main payload. The cost of these subsystems are considerably lower than for the C^{3}EO main payload, namely being the ANT-2 and ARCTIC cameras. In figure 18.5 it is seen that the payload has a major contribution of about 50% to total system costs and is hence the most expensive part. The cost estimate given in table 18.3 is an expert estimate.

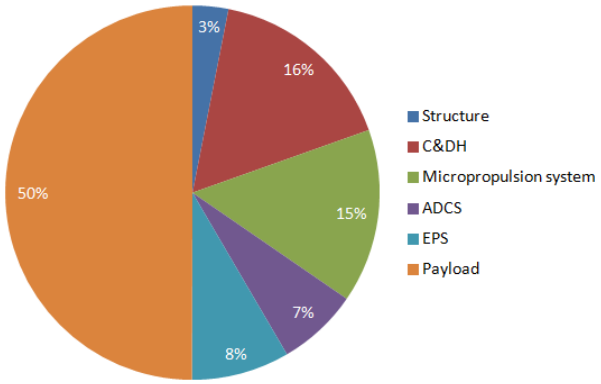

Figure 18.5: C^{3}EO subsystem cost, total cost with pl s/c = 0.2 M

Subsystem	DELFIN3XT	C^{3}EO
Structure	2	6.2
Data Handling	5	43.4
ADCS	3	14
EPS	36	18.5
Micropropulsion system	15	30
Total material cost 1 s/c	61	112.1

Table 18.3: Subsystem cost breakdown for DELFIN3XT and C^{3}EO in k EUR

The biggest cost difference is in the data handling subsystem. For DELFI-N3XT it consists of a low data rate VHF/UHF transceiver (3,000 EUR) an on-board Computer(1,000 EUR) and a S-band transmitter (1,000 EUR). The main reason for the difference between data handling subsystem of C^{3}EO and DELFI-N3XT mission is the high required throughput and the data rate for the C^{3}EO as explained in chapter 12.

Type	Cost [EUR]
Assembly, integration, testing	22,000
R and D	2,000,000
Launch for 250 kg	8,000,000
Total non recurring cost	10,022,000

Table 18.4: DELFIN3XT non-recurring costs

The R & D cost for the DELFI-N3XT mission is estimated like if this would be a commercial mission, when in facts it is a science mission. The total mission cost is estimated around 10.6 M EUR as compared to C^{3}EO with around 90 M EUR, as seen in table 18.1.

18.2.2 Subsystems- a comparison between the DELFIN3XT and C^{3}EO

The DELFIN3XT is comparable to the C^{3}EO satellites in terms of percentage-wise cost breakdown of the satellite material cost, as can be seen in figures 18.6a and 18.6b. It can be seen from the figures that only the cost for two subsystems differ significantly.

The cost for the EPS of the DELFI-N3XT is higher than for the C^{3}EO mission. This difference, shown in figure 18.6a, is explained by the cost of the solar cells being 25,000 EUR. These solar panels(amorphous silicon solar cells) are a prototype from Dutch space , have a high quality. The C^{3}EO mission makes use of conventional GaAS, thin-film solar cells and are cheaper.

Another difference is the cost of the ADCS. The ADCS cost of the DELFI-N3XT mission lower, whereas the required pointing accuracy is lower. The DELFI-N3XT mission has a pointing accuracy of 3°, whereas the ADCS of the C^{3}EO mission requires a 0.25° accuracy. The sun sensor of the DELFI-N3XT does not support such a high pointing accuracy, such that the decision is made to use a star tracker for the attitude determination. The high estimated cost of a nanosatellite star tracker (10,000 EUR) cause cost of the ADCS of the C^{3}EO being significantly higher than for the DELFI-N3XT.

For completeness the cost breakdown including payload is shown in figure 18.5.

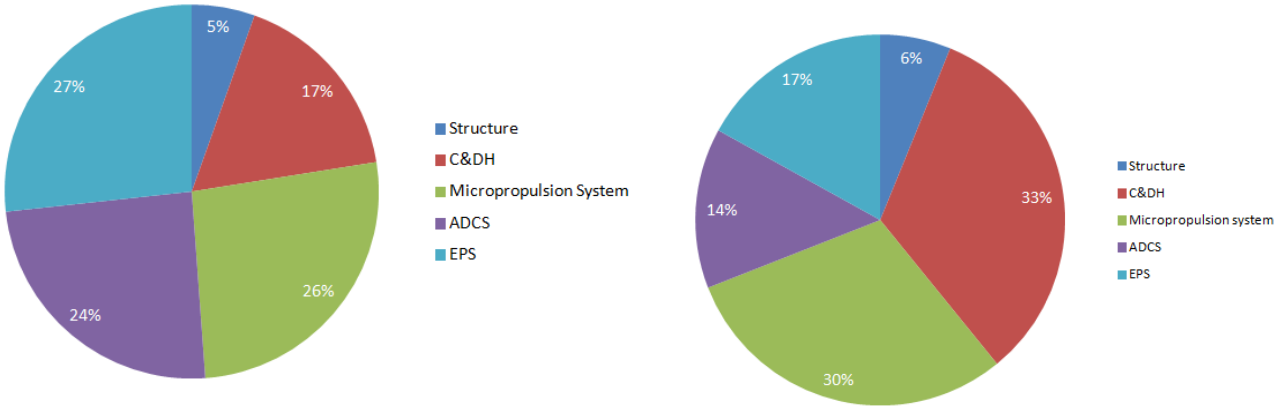

(a) DELFIN3XT subsystem cost, total cost s/c = 0.06 M EUR (b) C^{3}EO subsystem cost, total cost no pl s/c = 0.1 M EUR

Figure 18.6: Comparison on Subsystem Cost between Delfi N3XT and C^{3}EO

18.3 Return on Investment

It is assumed that the market volume of the product and hence the percentage of imaged surface actually sold is 2%.[72] This value is taken from the market volume of RapidEye.

18.3.1 Market share

For any business it is important to estimate the market share. The global market revenue for commercial satellite imaging market was valued at USD 1,240 million in 2011[73]. It is expected to reach an estimated value of USD 3,764.66 million (2,860.6 M EUR) in 2018, growing at a CAGR of 20.3% from 2012 to 2018. Interestingly, the North American region holds the majority of the market share in the commercial satellite imaging market.

Non direct competitors like GeoEye and DigitalGlobe represent approximately 75 % of this market, and 2/3 of their revenue is tied to the U.S. government. In case of C^{3}EO, the market share is computed by the percentage that the revenue of C^{3}EO generates over 1 year (200 M EUR) of the global market for commercial satellite imaging(2861 M EUR).Hence the achievable market share that C^{3}EO can achieve is **7%**.

18.3.2 RapidEye a direct competitor

In order to understand the true benefit of the C^{3}EO mission, existing missions are analysed. The RapidEye constellation referred in chapter 3 as direct competitor[72] gives a good overview in terms of relative cost comparisons. In table 18.5 hard values are compared to see if the market of RapidEye is taken by C^{3}EO and if all parameters for C^{3}EO are realistic values. The ground station cost of RapidEye is considerably higher because all stations are manned; C^{3}EO mainly uses automatic stations. Quite a significant number is the maximum image capacity per 24 hrs (chapter 5) of C^{3}EO, which ultimately leads to the impressive revenue generated.

Parameter	Unit	C^{3}EO	RapidEye
Total mission cost	M EUR	90	196
Cost per satellite	M EUR	0.2	5.3
# satellites	-	88	5
Launch cost	M EUR	13	11
Ground segment cost	M EUR	2.55	36
1 year operation cost	M EUR	3.75	3.5
1 year expected revenue	M EUR	200	28
Data price	EUR/km^2	0.1	0.95
Total surface area of the Earth	M km^2	510	510
Daily imaged Earth surface area	M km^2	273	4
Average daily duty cycle	%	17	0.78
Expected imaged area to be sold daily	M km^2	5.5	0.08

Table 18.5: RapidEye and C^{3}EO

The 24 hrs image capacity A_{24hrs} is defined by the temporal resolution, which is one week for the ANT-2 RCC carrying satellites and one day for the ARCTIC and ANT-2 TMA platforms. This results in equation 18.5, which shows how much total area per day is imaged. In this calculation A_{EARTH} is taken twice into account for the ARCTIC and ANT-2 TMA carrying satellites, whereas $(A_{EARTH}/7)$ is the contribution of the ANT-2 RCC satellites. Again 25% results from the duty cycle.

$$A_{24hrs} = (A_{EARTH} + A_{EARTH} + (A_{EARTH}/7)) \cdot 0.25 \tag{18.5}$$

The conclusion is, that because of the maximum image capacity of C^{3}EO(273 M km^2) as compared to RapidEye(4 M km^2) and lower total mission cost it is shown that C^{3}EO is a much more cost effective mission than RapidEye.

18.3.3 Break even chart

The data cost is given as EUR price per km^2. Is is validated with the amount of data, that RapidEye generates. As mentioned before the total km^2 sold(data volume) are 2% of the Surface imaged and 25% of this km^2 is only used because of the duty cycle and an overlap factor of 1.1 included.

Cost of goods sold (cogs) are the direct costs attributable to the production of the goods sold by a company. This amount includes the cost of the materials used in creating the good together with the direct labour costs used to produce the good. Cogs here equals the total mission cost for 2 years inclusive the recurring cost of operations for 2 years[74] is referred to as cost of goods sold. It is assumed that the data volume per day sold is constant and it is not accounted for market or customer changes.

The revenue(R) is given by the price P per km^2(fixed) of 0.1 EUR per km^2, multiplied with the total amount of km^2 sold $S(t_{life})$ (fixed) times the time vector(variable).For clarity, it should be noted, that the total surface area $S(t_{life})$ imaged is a function of the design lifetime t_{life} and hence is a fixed amount, dictated by the 2 years design lifetime. The value of $S(t_{life})$ is equal to $4.4165 \cdot 10^9$ km^2.

The time vector t ranges from 0:0.5:2.5 years. Hence the total amount of data sold is always a fraction of the amount of data generated over 2 years, reaching the maximum amount exactly at the time equal to 2 years at the end of lifetime.

$$R = P \cdot S(t_{life}) \cdot t \tag{18.6}$$

The Gross profit(GP), equation 18.7, is a company's residual profit after selling a product or service and deducting the cost associated.

$$GP = R - Cogs(t) \tag{18.7}$$

In section 18.1.1 these values are generated. In which $C_{nonrec_{wl}}$ is represented by the equation 18.8. The values for $C_{nonrec_{wl}}$ and C_{oper} are 82.3 M EUR and 6.6 M EUR, respectively.

$$Cogs(t) = C_{nonrec_{wl}} + C_{oper} \cdot t \tag{18.8}$$

With the help of equation 18.6 a break-even chart is generated, which has been done for a customer price of 0.1 EUR/km^2 and is found in figure 18.7. It is seen that for this image price the mission breaks even after 5 months, where the COGS precisely equals the revenue. From this point on, profit is made.

The very competitive price of 0.1 EUR per km^2 is possible because of the large amount of data generated by the constellation and reasonable low start-up costs of around 90 M EUR (table 18.1) compared to 196 M EUR of the RapidEye mission.

Image cost iterations

Some remarks should be made about the computation of the average image price of 0.1 EUR per km^2. Given the case that the km^2 would be calculated per e.g 5 years than the image price could further decrease because of the increased amount of data generated.It is seen, after 2 years the profit generated is 300 M EUR.

Note that all image prices used are below the image price of 0.95 EUR per km^2 of the competitor RapidEye. Also, if the price is increase to 0.2 EUR then break even is just after start-up of the company and break even point would shift to the left see figure 18.9. Hence the break even time decreases to 2.4 months. However with the price of 0.1 EUR a broader market is addressed and more data will be sold because of the relatively cheap data price, hence the price is not increased. With an image price of 0.02 EUR the break even time is after 2.4 years as shown in figure 18.8 and since the mission is 2 years this price is not an option.

18.3.4 Data cost for the three platforms

There should be a difference in price for the different images that all cameras produce, based on the value of the surface area imaged. The goal is to have an average of 0.1 EUR per km^2 cost per image in order to break even before 1 year as seen in figure 18.7. The image prices for the RCC camera should be a fraction higher, because of the less data generated per year and much higher resolution. The TMA and ARCTIC data should be sold at an approximately equal cost.

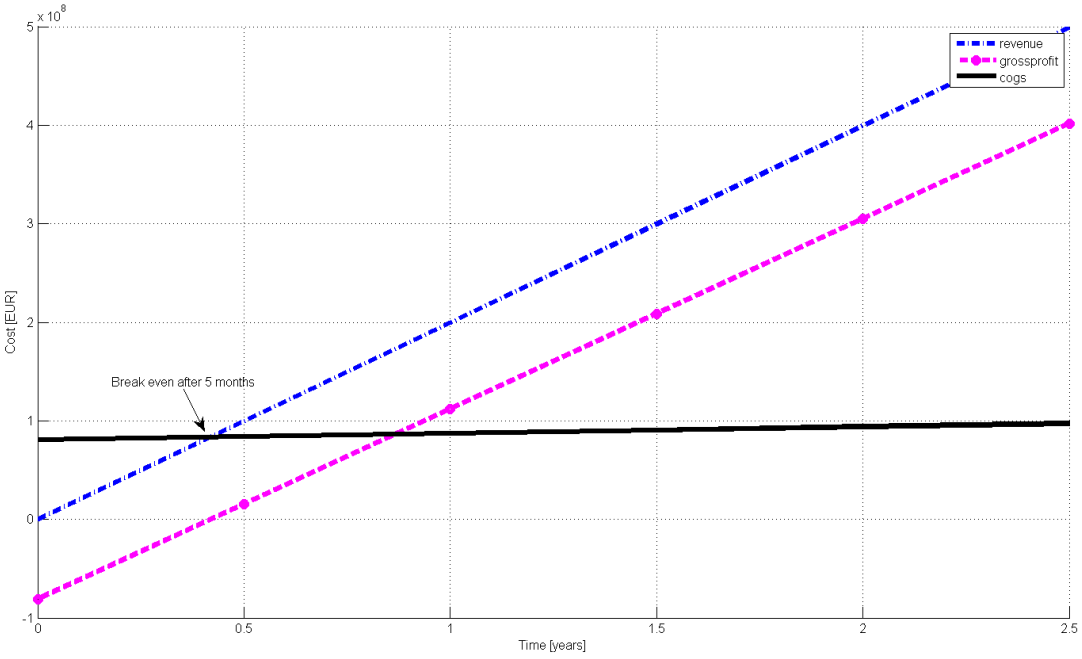

Figure 18.7: Break even time for Image average price of 0.1 EUR

Calculation of camera specific image cost

The total imaged area per camera constellation for a lifetime of 2 years A_{camera} $[km^2]$ is computed for each camera layer (excl.duty cycle), after which they are added up to the total surface area imaged A_{all}. Th number of orbits n_{orbits} is computed for two years. The area that is contained in one image is give by A_{image}. The number of images taken per orbit are n_{images}.

The imaged area per platform type, $\%_{Images}$, is computed as a fraction of the total imaged surface area in 2 years. The areas given are for the total constellation unless specifically specified for only one camera platform. The values used for the calculations are shown in table 18.6 .

The total surface area imaged for each camera layer A_{camera} e.g for the RCC-camera layer A_{RCC} is computed by:

$$A_{RCC} = n_{orbits} \cdot n_{images} \cdot A_{image} \tag{18.9}$$

$$A_{all} = A_{RCC} + A_{TMA} + A_{ARCTIC} \tag{18.10}$$

For example for the RCC camera:

$$\%_{Images} = \frac{A_{RCC}}{A_{all}} \tag{18.11}$$

These fractions per camera are multiplied with the individual prices per image per km^2 and several EUR prices per camera have been iterated over, until the average price P_{avg} is equal to 0.1 EUR.

$$P_{avg} = 0.1 = \%_{Images} \cdot P_{TMA/RCC/ARCTIC} \tag{18.12}$$

$$P_{avg} = 0.1 = (0.529 \cdot P_{TMA}) + (0.085 \cdot P_{RCC}) + (0.385 \cdot P_{ARCTIC}) \tag{18.13}$$

The km^2 are added to 100 percent and the km^2 per camera($km^2 cam$) are computed as fractions of 100 percent. The lowest fraction is multiplied with the highest price as seen in equation 18.13 and the result of the multiplications of the fraction of the images per camera times the price needs to be equal to the average price of 10 cents. Furthermore it should be noted, that the duty cycle is excluded, since only relative percentages of surface area imaged matter per camera and the overlap factor used is 1.1.

The calculation sequence results in an image data price of 0.2 EUR for an image made by the ANT-2 RCC camera, 0.1 EUR for an image made by an ANT-2 TMA camera and 0.1 EUR for an image made by an ARCTIC camera. The images made by the ANT-2 RCC camera are the most expensive, which is reasonable as they have the highest resolution.

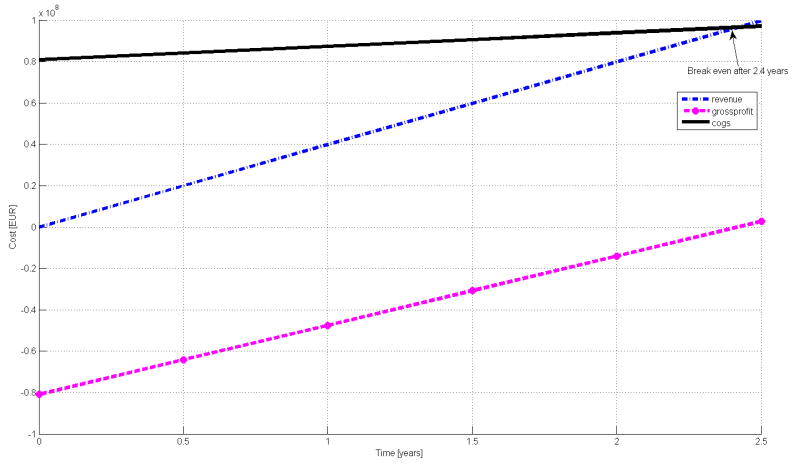

Figure 18.8: Break even time for Image average price of 0.02 EUR

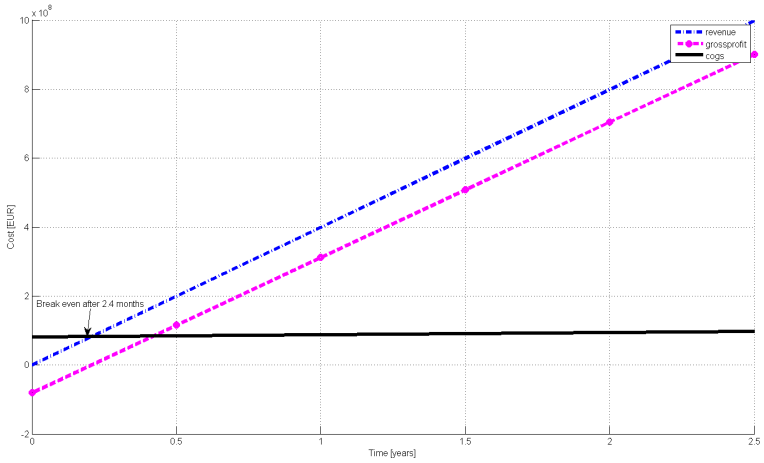

Figure 18.9: Break even time for Image average price of 0.2 EUR

18.3.5 Return on Investment

The return on investment (ROI) is the gross profit (GP) made on the sale of a security or other asset divided by the amount of investment (cogs), expressed as an annual percentage rate. This ratio is an indication of the profitability of the business.

$$ROI = \frac{GP}{cogs} \tag{18.14}$$

The ROI for 1 year is 20% and for 2 years cumulative around **130%**. This is an indication that the business is incredibly profitable in a short amount of time.

18.3.6 Recommendations

It is recommended to increase the lifetime of the mission, to enlarge the return of investment. As the sensor and storage lifetime is restricting the satellite lifetime at the moment, it is recommended to increase their lifetime by, for example, radiation hardening them.

Furthermore, since this mission is a constellation and subsystem parts are bought in large amounts, it means that cost could decrease because of mass producing the satellites. However, at this stage this is not accounted for in the cost calculation, so it is recommended to change this in any further studies.

It is also recommended to further study the percentage of the goods that is being sold. In this stage of the cost analysis the percentage is determined to be 2%, however if more than 2% can be sold, an increase in profit can be achieved.

Parameter		Unit	RCC	ARCTIC	TMA
Camera specs					
	Resolution	m/pix	4	55	25
Constellation specs					
	Design lifetime	$years$	2	2	2
	Orbit height	km	288	443	500
	Swadth width	km	8.84	38.6	51.1
	No of images per day	-	$1.91 \cdot 10^6$	$7.03 \cdot 10^5$	$3.54 \cdot 10^5$
	No of Orbits in 2 years	-	$1.167 \cdot 10^4$	$1.12 \cdot 10^4$	$1.113 \cdot 10^4$
	Area of camera image A_{camera}	km^2	78.2	959.37	2621.4
	Revisit time	hrs	$24 \cdot 7$	24	24
	% Images	$\%_{Images}$	8.5	38.5	52.9
Image price camera specific		EUR	**0.2**	**0.1**	**0.1**

Table 18.6: TMA, RCC and ARCTIC image cost data input (excl. duty cycle)

Chapter 19 | Conclusion & Recommendations

In this chapter the conclusion and recommendations are presented in sections 19.1 and 19.2 respectively. Furthermore suggestions on how the platforms work together are presented in section 19.2.

19.1 Conclusion

The goal of this DSE assignment was to develop a competitive constellation for disaster and environmental monitoring using the ANT and ARCTIC instruments as cornerstones. In order to find out what could make the constellation competitive, a market and application survey is performed in chapter 3 which findings resulted in the following market need statement:

"Produce images for environmental and disaster monitoring using a low-cost solution equipped with ARCTIC and/or ANT-2 cameras at a low altitude to achieve high spatial resolution."

From the market survey it becomes apparent that a high temporal resolution and a high spatial resolution is required to make the constellation competitive. With these requirements in mind, the constellation is designed. The constellation design features three segments; 24 ANT-2 RCC at 288 km, 27 ANT-2 TMA at 500 km both in sun-synchronous orbit and 37 ARCTIC in a 443 km polar orbit. This results in high resolution visual images with a weekly revisit time and mid resolution visual and infrared images with a daily revisit time.

The amount of data generated by the ANT-2 and ARCTIC instruments is unprecedented for nanosatellites. Special attention was put in the communication segment which resulted in an innovative s-band transmitter on the satellites combined with a distributed network of eight ground stations, including two commercial ones. The three segments of the constellation are launched in three separate launches on the Shtil 2.1 launch vehicle avoiding complex plane change manoeuvres. Due to the low altitude drag and torque compensation proved to be a challenge. This challenge is met by a specially design ADCS system featuring four reaction wheels and magneto-torques. Furthermore the drag and injection inaccuracies are compensated by micro machined electro spray thrusters.

With this three segments the constellation has full Earth coverage in the infrared and near complete coverage in the visual spectrum serving a multitude of applications. During the design of all subsystems, it became apparent that with the use of novel components, the concept is feasible from a technical perspective. The cost analysis proved that the average image price would be 0.1 EUR/km^2, which is almost one order of magnitude smaller than the image price of the nearest competitor Rapid Eye, who has an image price of 0.95 EUR/km^2.

The constellation offers capabilities comparable to competing systems for a fraction of the price. Employing the low cost solutions offered by nanosatellites the constellations proves to be very competitive in price, flexibility and operations. This DSE assignment proved to be a promising base for the development of a nanosatellite Earth observation constellation.

19.2 Recommendations

During the design process several possible points of improvement are discovered that are out of scope of the DSE. In this section recommendations for these improvements are discussed.

Operational lifetime extension

In the process of setting up the constellation large investments are needed. Setting up the ground segment and buying space on launch vehicles are accompanied by high cost. These investments need to be earned back in the relative short operational lifetime of two years. Extending the operational lifetime will significantly lower the cost per image, but at the same time it will require the usage of radiation tolerant components. This will induce extra cost on the constellation. Future research should focus on finding an optimum between component cost and operational lifetime.

Spectrum extension

Currently the constellation provides images in five bands; blue, green, red, near infrared (NIR) and thermal infrared (TIR). Extending the number of bands to include for example ultra violet (UV) will increase the number of applications and will enable for hyper spectral analysis. The inclusion of RADAR instruments gives rise to the possibility of using interferometry. Using RADAR interferometry high resolution digital elevation models (DEM) are produced. Co-registrating these models with the optical images also results in an increase in applications.

ARCTIC thermal system redesign

The current design of the ARCTIC instruments features a radiator surface that blocks communication when placed on a nanosatellite platform. To overcome this problem, a quick redesign is made during the DSE. This adaptation however is not sufficiently analysed. Furthermore, the ARCTIC carrying satellites need body mounted solar panels which change the thermal behaviour of the satellite. Further investigations on the redesign of the ARCTIC thermal control subsystem are therefore required.

Increase aperture size

A severe limitation of the instruments is the limited field of view caused by the small aperture size. The size of the aperture is limited by the CubeSat standard. However clustering multiple CubeSats together gives rise to the possibility of greatly increasing the aperture size. On the other hand this will also increase the spacecraft weight, complexity and cost. A future study should asses whether it is worth while to increase the aperture size.

Increase downlink capability

During the operational phase, the cameras have a limited duty cycle. This limitation is mainly caused on the limited downlink capabilities of the on-board transmitters. Further research should focus on optimising antennae, reducing power dissipation and the possibility of using higher frequency bands. In addition, increasing the number of ground station and/or increasing ground station antennae gains will improve the downlink capacities.

Simulation of the attitude control

The imaging mission highly limits the maximum allowed angular velocity of the satellites. However, it can only be checked if these limits are not exceeded if a simulation is made for the attitude control. From the simulation it must become clear how much of the disturbance torques are actually secular and cyclic, such that the sizing of the magneto torquer (which is used for momentum dumping) can be designed properly. The simulation must also point out the best way to detumble the satellite after ejection: the usage of reaction wheels, magneto torquers or the thruster system.

Investigation of zero momentum ACS by thrusters only

The MEMS thruster system that is used for the C^{3}EO can be used for full attitude control. In the C^{3}EO design it only accounts for the aerodynamic drag, but as the individual thrusters can be placed anywhere on the satellite, the system can be used very well for full attitude control. The relatively heavy reaction wheels and magneto torquers are then unnecessary.

Investigation of the satellite aerodynamics

It is hard to estimate the drag coefficient of the satellite. At the very high orbital velocities particles almost instantly come to an absolute standstill, but the amount of drag they cause cannot be studied very precise. In the disturbance torque estimation assumptions have been made for the center of pressure and the aerodynamic center. If a more precise location of these two points can be given, the disturbance torque calculations will become more accurate and the probability that the ACS is over-designed then decreases.

Solar cell types

For the ANT-2 RCC and TMA carrying satellites, it is decided to use thin film solar cells for power generation. Thin film solar cells are of lower cost than Triple Junction type cells. This however means that the solar array area is increased. This puts additional requirements on the solar panel deployment hinges. No considerations of these mechanisms are taken into account in the current design. Further investigations should be made to see if the benefit of having a lower solar panel price outweighs additional requirements of the hinge mechanisms.

Launch segment

In the current design three separate launches are used. This is to avoid high ΔV and complex plane change manoeuvres. The actual cost implications of this complexity is however not determined. Further analysis might prove that the extra cost of these manoeuvres is lower than the extra cost of separate launches.

Development Cost

The current outlook on return on investment is highly optimistic. It should however been noted that the estimations of cost are very rough. Effects like interest rate, insurance fees and additional competition are not taken into account. On the other hand, cost effects of buying components in bulk were hard to quantify and also not taken into account.

In order to come to a more realistic cost figure, a more detailed assessment is required in terms of a break down per camera. From this break down a more accurate estimation can be made on the image price per km^2, which will differ for each platform. In addition, the real duty cycle per camera should be taken into account as stated in section 3.3. This real duty cycle also influences the availability of the images.

Comparison with RapidEye

The comparison in revenue with RapidEye is mainly based on the image area. However, there is no comparison on the quality of the image in terms of signal to noise, bit depth and image size, since these values are not know for the RapidEye. The only comparison can be made on the ground sample distance, where C^{3}EO is better only in the visual waveband.

19.3 Constellation configurations

Placing a three-camera constellation is not the only possible approach to Earth observation. Although a three-camera constellation can be used in all the applications mentioned in this section, there is no single application that benefits from the collaboration of all three cameras.

As such, this constellation can be part of a business model to provide data to many different costumers, while the possibility of several constellation configurations can be used in a business model where the constellations are handed in to a single customer who then maintains the system, such as governments. The advantages of this approach lie in the ability to provide a constellation optimized to a specific application by using the cameras in collaboration with each other. It is clear that a modular approach to constellations has several scientific applications which can be used by governments as well as commercial applications where imagery can be sold to users.

Correlation of data can be used to make a much more detailed map of the area observed as well as provide foundations necessary to model the behaviour of certain phenomena. There are six additional constellations that cater to different needs and each is explained in the sections that follow.

19.3.1 RCC & TMA

This combination of cameras is targeted at land coverage, more specifically to forestry and agriculture. This is because both cameras possess the ability to monitor vegetation health by assessing the chlorophyll density. The TMA excels at producing imagery with a high temporal resolution, while the RCC provides high spatial resolution imagery. As such, the TMA can be used to monitor large scale logging, as well as fires with NIR, and the RCC can then take over when a more detailed map is needed.

This system works just as well with agriculture, where the TMA can be used to monitor large scale farming and the RCC can provide a more detailed assessment of crop health when needed. The disadvantage of this constellation is that both cameras are dependent on cloudless skies to obtain data, making it harder to provide imagery with the same time stamp if required.

19.3.2 RCC & ARCTIC

This constellation has both commercial as well as scientific uses, mainly related to oceanography. The RCC platform can be used to monitor coral population and extent, while the ARCTIC provides the temperature map for the same area with the same time stamp. With this, the correlation between sea surface temperature and coral populations can be studied.

A new and interesting use of these platforms is in the domain of ice monitoring in the north pole. With the rate at which the sea ice concentration is decreasing, the viability of shipping lanes in this area is increasing. The ARCTIC camera can provide a daily status update on the sea ice required by cargo ships attempting this route, while the RCC can provide a detailed view of the ice with a lower temporal resolution.

19.3.3 TMA & ARCTIC

The large swath widths of these platforms are ideal for forestry, namely by tracking the status of forests across the globe with the TMA to estimate chlorophyll density, as well as fire tracking with both cameras. Furthermore, with the ARCTIC camera it is then possible to study the effects tropical forest removal on soil temperature.

Secondly, this combination can be used for phytoplankton monitoring, such as algae blooms. The ARCTIC platform can provide a temperature map to model behaviour of these blooms, while the TMA can generate imagery to determine its size. The study of phytoplankton is extremely relevant due to its effects on fisheries as well as coastal pollution.

Lastly, such a constellation can also be used for volcano monitoring, as the ARCTIC platform can map the temperature of pyroclastic clouds as well as SO_2 concentrations while the TMA camera can be used to monitor volcanic ash with its NIR capabilities [75].

19.3.4 TMA

Constellations of a single platform can also be considered. These can be cost effective if the client is not interested in correlated data provided by two or more platforms. The strength of the TMA lies on its ability to track fires as well as forest health and algae blooms. A daily temporal resolution is easily achievable, but several passes over the same area may be required due to cloud cover.

19.3.5 RCC

The RCC platform has a wide range of applications, only limited by cost and temporal resolution due to its very small swath width. This system can be used to monitor crop health, assess damage after natural catastrophes with its high resolution imagery and coral extent mapping.

19.3.6 ARCTIC

The ARCTIC camera is a very versatile standalone version. A high temporal resolution is easily achievable with its swath width and low data volume. Furthermore, it is not limited by cloud cover nor eclipse time. Its applications range from polar cap monitoring which can be used to assess the viability of shipping routes, to global temperature mapping and volcano monitoring.

PART V

BIBLIOGRAPHY & APPENDICES

Bibliography

[1] *The Space economy at a Glance 2011, Executive summary* OECD Publishing, 22 July, 2011

[2] *Space economy at a glance 2011* OECD Publishing, 22 July, 2011

[3] Taylor Dinerman *The Space Review: Financial risk analysis for the space industry* New York City, US, June 16, 2008

[4] *Highlights of Obama's 2013 NASA Budget Proposal* http://www.space.com/14553-2013-nasa-budget-proposal-highlights.html

[5] *Value Chains and Market Segments of Downstream Value-Adding Sectors of Space Applications, ESA TEN-S/SL/1177 (2007)*

[6] Adam Keith, *Earth Observation: Emerging Markets, Partnerships Set to Fuel Global Growth*, Euroconsult, Montreal Office, 2011

[7] Josep Virgili and Peter C.E. Roberts *DMC-HD, a Very Low Earth Orbit high resolution small satellite*

[8] Wayne A. Shiroma et al. *CubeSats: A Bright Future for Nanosatellites*.Central European Journal of Engineering, Honolulu, USA : University of Hawaii, 2011

[9] D. Barnhart, T. Vladimirova, M.N. Sweeting, *System-on-a-Chip Design of Self-Powered Wireless Sensor Nodes for Hostile Environments*. Surrey, United Kingdom : Surrey University, 2007

[10] D. Barnhart, T. Vladimirova, A.M. Baker, M.N. Sweeting, *A low-cost femtosatellite to enable distributed space missions*, Acta Astronautica, 2009

[11] J. Dorsch, *Does Moore's Law still hold up?*, http://cse.yeditepe.edu.tr/ sgoren/spring2011/CSE221/ mooreslaw.pdf, last accessed on 21th November, 2012.

[12] J. Wiley & J. H. Wertz, *Space mission analysis and Design, 3rd ed*. California, USA : Microcosm Press, 1999

[13] R. Sandau, *International Study on Cost-Effective Earth Observation Missions*. Taylor & Francis, 2006

[14] Stephen S. Sung, *Retrodirective Antenna Technology for CubeSat Networks*. Honolulu, USA : University of Hawaii, 2003

[15] D. DePasquale, A.C. Charinia, *Analysis of the Earth-to-Orbit Launch Market for Nano and Microsatellites*

[16] Tatyana Suslova, *Russian Small Launchers Overview*, http://esamultimedia.esa.int/docs/EMO/SmallLaunchers.pdf, last accessed on 22th November 2012.

[17] Tanya Vladimirova, *Emergency Response Networks for Disaster Monitoring and Detection from Space*, Surrey, United Kingdom : Surrey University, 2009

[18] *GeoEye-1*, http://en.wikipedia.org/wiki/GeoEye-1, last accessed on 21th November 2012.

[19] M.S. Moran et al., *Opportunities and limitations for image-based remote sensing in precision crop management*, U.S. Water Conservation Laboratory, Phoenix, Arizona, 1997.

[20] *LULUCF under the Kyoto Protocol* http://unfccc.int/methods_and_science/lulucf/items/4129.php. Last accessed on 17-01-2013

[21] R. Bindschadler et al., *MONITORING ICE SHEET BEHAVIOR FROM SPACE*, American Geophysical Union, 1998.

[22] I. S. Robinson, *Measuring the Oceans from Space*, Mairdumont Gmbh & Co. Kg, Germany, 2004

[23] Z. Li et al, *Satellite-based detection of Canadian boreal forest ÂÕ res: development and application of the algorithm*, http://www.atmos.umd.edu/žli/PDF_papers/IJRS00_Fire1.pdf. Last accessed on 10-01-2013

[24] C. Hu et al., *Detection of natural oil slicks in the NW Gulf of Mexico using MODIS imagery*, American Geophysical Union, 2009.

[25] DMC Constellation, *http://www.dmcii.com/*, last accessed on 11 December 2012

[26] DMC3 Mission, http://www.sstl.co.uk/Missions/DMC3/DMC3/DMC3–The-Mission

[27] RapidEye company, http://www.rapideye.com/

[28] *Surrey satellite technology*. http://www.sst-us.com/, last accessed 12/18/2012

[29] Hans Kuiper, *Project Guide Design Synthesis Exercise: Space Cubesat Camera & Formations*, TU Delft, Delft 5 November 2012

[30] DSE 2011 Group 09, *Advanced Nano Telescope - A cornerstone solution in Earth observation*, TU Delft, Delft, 28 June 2011

[31] DSE 2012, *Advanced Remote-sensing Cubesat Thermal Infrared Camera*, TU Delft, Delft, 29 June 2012

[32] Arianespace - Services and Solutions, *Vega User Manual, Issue 3*, March 2006

[33] Arianespace - Services and Solutions, *Ariane 5 User Manual, Issue 5*, July 2011

[34] *ISIS - Innovative Solutions In Space* http://www.isispace.nl/brochures/ISIS_CubeSat%20Structures_Brochure_v.7.11.pdf

[35] Schott http://www.markoptics.com/files/Schott

[36] ISIS - Innovative Solutions In Space, *ISIPOD CubeSat Deployer*

[37] J. Wiley & J. H. Wertz, *Space Mission Engineering: The New SMAD*. California, USA : Microcosm Press, 2011

[38] *Clyde Space, CubeSat Shop* http://www.clyde-space.com/cubesat_shop accessed 14-01-2013

[39] *Nasa Science, How do Photovoltaics Work?, Gil Knier* http://science.nasa.gov/science-news/science-at-nasa/2002/solarcells/ accessed 14-01-2013

[40] Sun Shot, *SunShot Vision Study*,US Department of Energy, February 2012

[41] Martin A. Green, Keith Emery, Yoshihiro Hishikawa, Wilhelm Warta, Ewan D. Dunlop *Solar cell efficiency tables (version 40)*,PROGRESS IN PHOTOVOLTAICS: RESEARCH AND APPLICATIONS, June 2012

[42] Spectrolab, *29.5% NeXt Triple Junction (XTJ) Solar Cells*,Spectrolab, Boeing, 2012

[43] M.Raja Reddy *Space solar cells - trade off analysis* Solar Energy Materials & Solar Cells 77; 2003

[44] Robert D. Karam *Satellite Thermal Control for Systems Engineers* Progress in Astronautics and Aeronautics Volume 18, American Institute of Aeronautics and Astronautics,1998

[45] J. Bouwmeester et. al Technical Note Delfi N3xt, *ADCS- Control Torques*. 18/02/2009

[46] CA Bernal et al., *Releasing the cloud a deployment system for the QB 50*. 26th Annual Conference on small satellites missios

[47] J. Bouwmeester et. al Technical Note Delfi N3xt, *ADCS- Disturbance torques*. 07/04/2011

[48] without author, *Faulhaber, Miniature Drive Systems*, Product catalog 2010 -2011

[49] Gerry Webb, Eugene Motorny, Nina Pestmal, Oleg Sokolov Commercial Space Technologies Ltd. *THE MARKET FOR LAUNCHING SMALL SATELLITE IN RUSSIA, ITS PRESENT SITUATION AND LIKELY FUTURE TRENDS*, http://www.commercialspace.co.uk/, last accessed on 27 November 2012.

[50] STATE ROCKET CENTRE, 'Makeyev Design Bureau'-SPACE ROCKET COMPLEX SHTIL, USER'S GUIDE ISSUE 1.1 January, 2002

[51] J. Bouwmeester, *Concept study of a LEO constellation of nanosatellites for near real time optical remote sensing*. Delft, Netherlands : Delft University of Technology, 2011

[52] Daniel. L. Oltrogge & Kyle Leveque *An evaluation of CubeSat orbital decay*

[53] *NASA, Shape effects on drag* http://www.grc.nasa.gov/WWW/k-12/airplane/shaped.html

[54] *IADC Space Debris Mitigation Guidelines & Supporting Document* Inter Agency Space Debris Coordination Committee

[55] Busek Co. Inc., *Cubesat and Nanosat Propulsion Solutions*. Natick, MA, USA

[56] Jochen Schein, Andrew Gerhan, Filip Rysanek and Mahadevan Krishnan, *Vacuum Arc Thruster for CubeSat Propulsion*. USA

[57] François Martel,Paulo Lozano and Louis Perna, *Miniature ion electrospray thrusters and performance tests on CubeSats*

[58] F. Martel, L. Perna, P. Lozano *Ion electrospray thruster assemblies for CubeSats*

[59] Gomspace, *NanoMind A712C Datasheet*.

[60] Stellenbosch University, *NanoMind A712C Datasheet*.

[61] Clyde Space Ltd., *CubeSat Mission Interface Computer*

[62] Guoxia Yu, Tanya Vladimirova, Martin N. Sweeting, *Image compression systems on board satellites*. Acta Astronautica 64 (2009) 988 âĂŞ 1005.

[63] Turan S. Tuli, et al., *Low Cost Ground Station Design for Nanosatellite Missions*, Space Flight Laboratory, Toronto

[64] *United states frequency allocations* http://www.ntia.doc.gov/files/ntia/publications/2003-allochrt.pdf. Last accessed on 14-01-2013.

[65] S. R. Tsitas et al., *6U CubeSat design for Earth observation with 6.5m GSD, five spectral bands and 14Mbps downlink*, 2010

[66] Kongsberg, *Kongsberg Satellite Services* http://ksat.no/node/73

[67] *Panoramic Tools Graphical User Interface* http://www.ptgui.com accessed 14-01-2013

[68] *Investopedia, Overhead* http://www.investopedia.com/terms/o/overhead.asp#axzz2HwYKswn9 accessed 14-01-2013

[69] Dr. Paul Graf,UT-Austin *Nasa cost estimating module v.1.0.*Draft NASA Cost EstimatorâĂŹs Handbook 2004

[70] Gerry Webb, Eugene Motorny, Nina Pestmal, Oleg Sokolov *THE MARKET FOR LAUNCHING SMALL SATELLITE IN RUSSIA, ITS PRESENT SITUATION AND LIKELY FUTURE TRENDS* Commercial Space Technologies Ltd

[71] Liam P. Sarsfield *Small Spacecraft for Space and Earth Science*. RAND Critical Technologies Institute; 1998

[72] Colin Doughan *Business Case for a CubeSat-based Earth Imaging Constellation* http://spacebusinessblog.blogspot.nl/2011/05/business-case-for-cubesat-based-earth.html accessed 13-01-2013

[73] *Commercial Satellite Imaging Market - Global Industry Size, Market Share, Trends Analysis, And Forecast, 2012 - 2018* http://www.transparencymarketresearch.com/commercial-satellite-imaging-market.html accessed 13-01-2013

[74] *Investopedia, Cost Of Goods Sold - COGS* http://www.investopedia.com/terms/c/cogs.asp#axzz2GpM2d8iI accessed 14-01-2013

[75] K. Kinoshita et al, *Ground and Satellite Monitoring of Volcanic Aerosols in Visible and Infrared Bands*. The CEReS International Symposium on Remote Sensing, Chiba, Japan, 16-17 December 2003.

Chapter A | ADCS requirements

In this section it is explained how the requirements for the maximum allowed angular velocity are derived.

As a basis for these calculations, equations A.1-A.4 are used [31], p 64, in which it is assumed that $d = \frac{1}{2} \cdot w_{pix}$ is the maximum allowed movement of the ground view.

$$\alpha_{xy_{max}} = \frac{1}{2} \cdot \alpha_{pix} = atan(\frac{d}{h_{sat}}) = atan(\frac{\frac{1}{2} \cdot w_{pix}}{h_{sat}}) \tag{A.1}$$

$$\Omega_{xy_{max}} = \frac{\alpha_{xy_{max}}}{t_i} \tag{A.2}$$

$$\alpha_{z_{max}} = atan(\frac{d}{2 \cdot \pi \cdot R}) = atan(\frac{\frac{1}{2} \cdot w_{pix}}{2\pi R}) \tag{A.3}$$

$$\Omega_{z_{max}} = \frac{\alpha_{z_{max}}}{t_i} \tag{A.4}$$

Here, w_{pix} is the effective pixel width, h_{sat} the height of the satellite's orbit, t_i the integration time and R the radius of a circle that exactly fits the square field of view as shown in fig (A.1)

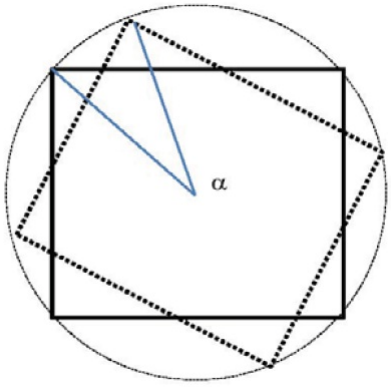

Figure A.1: Visualization of the field of view rotation when the satellite rotate around its z-axis.[31] p. 65

The results for this equation can be used when the satellite is rotated over one of its axis. However, as the satellite can rotate over its three body-axis, the engineers of the ARCTIC design made a worst-case scenario simulation. In this simulation the maximum shift of the view is calculated. Hence, $\frac{1}{2} \cdot w_{pix}$ is not the maximum allowed shift, as for the worst case the shift canbe higher or lower. A rotation of the field of view over three axis is visualized by figure (A.2), in which the lower left point is displaced the most.

As the code of the simulation was not known, backwards engineering has been applied to calculate the value x, y and z that are taken $\frac{1}{2}$ in eq. A.1-A.4. The inputs (design characteristics of the ARCTIC) and the outputs (x, y and z) are given in table A.1. With the use of the values x, y and z the values for $\Omega_{x,y,z}$ for the ARCTIC and ANT-2 cameras in the C^{3}EO can be calculated. The input variables and the results are given in table (A.2). An example of the calculation for the maximum angular velocity around the x-axis for the ANT-2 is given in equation (A.5,A.6).

$$\alpha_{x_{max}} = atan(\frac{x \cdot w_{pix}}{h_{sat}}) = atan(\frac{0.1921 \cdot 2.59}{288 \cdot 10^3}) = 1.73 \cdot 10^{-6} rad \tag{A.5}$$

$$\Omega_{xy_{max}} = \frac{\alpha_{xy_{max}}}{t_i} = \frac{1.73 \cdot 10^{-6}}{1 \cdot 10^{-3}} = 0.0017 rad/s = 0.1^{\circ}/s \tag{A.6}$$

After that the maximum angular rotation for the ARCTIC C^{3}EO design can be calculated and using the same values for x, y and z the maximum allowed rotational velocities for the ANT-2 carrying satellite can be calculated.

Inputs			Outputs		
Parameter	**Unit**	**Value**	**Parameter**	**Unit**	**Value**
w_{pix}	m	65.59	x	-	0.1921
h_{sat}	km	500	y	-	0.3842
t_i	s	$0.84{\cdot}10^{-3}$	z	-	0.4236
R	km	26.32			
$\Omega_{x_{max}}$	rad/s	0.03			
$\Omega_{y_{max}}$	rad/s	0.06			
$\Omega_{z_{max}}$	rad/s	0.20			

Table A.1: Inputs and outputs for the calculation of x, y and z

Inputs				Outputs			
Parameter	**Unit**	**ARCTIC**	**ANT**	**Parameter**	**Unit**	**ARCTIC**	**ANT**
w_{pix}	km	52.30	2.59	Ω_x	$^\circ/s$	1.55	0.10
h_{sat}	km	443	288	Ω_y	$^\circ/s$	3.09	0.20
t_i	s	$0.84{\cdot}10^{-3}$	$1{\cdot}10^{-3}$	Ω_z	$^\circ/s$	11.54	0.05
R	km	20.92	24.17				

Table A.2: Inputs and outputs of calculation of $\Omega_{x,y,z}$ for the satellites

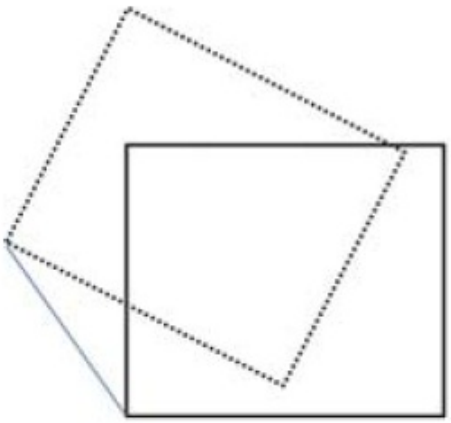

Figure A.2: Visualisation of a worst case rotated field of view.[31] p. 65

Chapter B | Validation of disturbance torques

It is important that the calculations made for the disturbance torques are correct, as the flywheel design depends on it. Therefore, results are checked with the disturbance torque calculations of DELFI-N3XT. In tableB.1 the results can be seen. Below, an explanation of the differences is presented.

Disturbance type	Unit	Values for C^3EO	Values for DELFI-N3xt
Aerodynamic drag torque	Nm	$1.16 \cdot 10^{-5}$	$2.87 \cdot 10^{-7}$
Aerodynamic drag angular momentum storage	Nms	0.063 (one orbit)	$8.39 \cdot 10^{-4}$ ($\frac{1}{2}$ orbit)
Solar pressure torque	Nm	$1.01 \cdot 10^{-8}$	$4.92 \cdot 10^{-8}$
Solar pressure angular momentum storage	Nms	$5.47 \cdot 10^{-5}$ (one orbit)	$1.42 \cdot 10^{-4}$ ($\frac{1}{2}$ orbit)
Magnetic disturbance torque	Nm	$2.86 \cdot 10^{-7}$	$2.34 \cdot 10^{-7}$
Magnetic disturbance angular momentum storage	Nms	$3.73 \cdot 10^{-5}$ ($\frac{1}{2}$ orbit)	$3.34 \cdot 10^{-4}$ ($\frac{1}{4}$ orbit)
Gravity gradient torque	Nm	$1.41 \cdot 10^{-8}$	$6.49 \cdot 10^{-8}$
Gravity gradient angular momentum storage	Nms	$3.83 \cdot 10^{-5}$ ($\frac{1}{2}$ orbit)	$9.42 \cdot 10^{-5}$ ($\frac{1}{4}$ orbit)

Table B.1: Disturbance torques and required angular momentum storage for the ANT-2 RCC carrying satellite

Difference in aerodynamic drag torque

The aerodynamic drag shows the largest difference with the DELFI-N3XT disturbance torque calculations. However, this result is expected, as it is well-known that atmospheric drag causes the satellite to de-orbit if it is placed in LEO. If the calculations for satellites are done for an orbit height of 600 km, which is the orbit height of the DELFI-N3XT, the resulting torque is $3.22 \cdot 10^{-9}$. The difference between the two values is caused by using another ram area and another atmospheric density. The calculations for the DELFI-N3XT mission accounts for the worst case atmospheric density and the model made for the C^3EO does not.

Solar pressure

It can be seen that the calculations for the solar pressure torque are in the same order of magnitude. The difference for the calculation of the maximum required angular momentum storage is caused by the fact that the C^3EO accounts for solar pressure build-up over a whole orbital period. The reaction wheels of the DELFI-N3XT accounts for a maximum torque build-up over half a period, which would mean that they need to offload their reaction wheels twice every period if a maximum disturbance occurs.

Magnetic disturbance torque

The worst case disturbance torque due to the interference of the satellites' magnetic field with the Earth magnetic field are in the same order of magnitude. The difference in maximum required angular momentum storage is (again) caused by the choice that has been made for the satellites to be able to store this torque for longer than the DELFI-N3XT does.

Gravity gradient torque

The gravity gradient torque is for both missions in the same order of magnitude, as well as the required angular momentum storage. It can be seen that there is a difference in the required angular momentum storage, which is caused by the design choice to be able to store the maximum disturbance torque for a longer period.

Chapter C | Attitude control methods and their capabilities

For spacecraft, the attitude control can be done by several type of attitude control systems[12], p 359. For all of these systems listed in table C.1, the feasibility is checked for the C^{3}EO mission. In the study it is concluded that only two options are feasible: zero momentum with three reaction wheels or with thrusters.

Type	**Accuracy** [°]	**Reason to conclude non-feasibility**
Gravity gradient	±5 (2- axis)	accuracy range too low
Gravity gradient and momentum bias wheel	±5 (3- axis)	accuracy range too low
Passive magnetic	±5 (2- axis)	accuracy range too low
Pure spin stabilization	±0.1 to ±1 (2-axis)	imaging mission requires non-spinning satellite
Dual spin stabilization	±0.1 to ±1 (2-axis)	imaging mission requires non-spinning satellite
Bias momentum (1 wheel)	±0.1 to ±1	three axis stabilization is required
Zero momentum (thruster only)	±0.001 to ±1	feasible, although available propellant systems form a restriction
Zero momentum (3 wheels)	±0.001 to ±1	feasible. magnetotorquer or thrusters are needed for momentum dumping

Table C.1: Attitude control types and their feasibility for the C^{3}EO mission

Chapter D | ADCS MATLAB simulation algorithm

The simulation that has been written for the attitude control is a conceptual software tool to determine if the satellite is stable and if the satellite can meet the requirements that are set on the ADCS. In this section it is explained how the simulation works and what assumptions are made.

D.1 Inputs of the simulation

The inputs of the program are the initial values for the attitude of the spacecraft $\theta[rad]$ and the initial angular velocities $dot\theta[rad/s]$.

D.2 simulation of the disturbance torques

The disturbance torques that are used for the simulation are taken as a function of the attitude of the satellite.

First, a function creates a vector which represents the latitude of the satellite at time instance t. This function will be used as an input of the magnetic disturbance torque, which now can be determined using equation D.1 and D.2.

$$T_{m_x} = D \times B = D \cdot Bsin(\frac{\pi}{2} - latitude - \theta_y) \tag{D.1}$$

$$T_{m_y} = D \times B = D \cdot Bsin(\frac{\pi}{2} - latitude - \theta_x) \tag{D.2}$$

The gravity gradient disturbance torque can also be dependent on the attitude of the S/C

$$T_{g_x} = \frac{3\mu}{2R}|I_z - I_{xy}|sin(2\theta_y) \tag{D.3}$$

$$T_{g_y} = \frac{3\mu}{2R}|I_z - I_{xy}|sin(2\theta_x) \tag{D.4}$$

Now the aerodynamic torques have to be made dependent on attitude. To do so, the satellite is modelled as three panels: the panel representing top/bottom of the satellite, the panel representing the sides of the panel, including the solar panels and the panel representing the front and back of the satellite.

The main approach to determine the forces in x,y and z-direction for all of the three panels is as follows:

It is assumed that due to the flow of particles 'around' the three plates, a force normal to their surface is experienced. The pressure coefficient, which determines the magnitude and direction of the force, can be calculated using the the plate theory, expressed by equation D.5

$$C_p = 2.3 \cdot sin(\alpha_{plate}) \tag{D.5}$$

In which α_{plate} is the angle of attack of the plate. For plate 1, 2 and 3 these angles are given by the displaced angle around body x, z and y respectively. Of course if the satellite suffers an attitude change, the normal vector on the three plates has components in three directions, which can be calculated using a 3-2-1 rotation transformation matrix. Now the forces in three directions can be calculated using equation D.6.

$$[F_a] = C_p \cdot \frac{1}{2}\rho {V_{sat}}^2 A_{side} * [TF] * [n] \tag{D.6}$$

In which$[F_a]$ is the aerodynamic force matrix (3 by 1), [TF] is the 3-2-1 transformation matrix (3 by 3) and [n] is the normal vector on the plate (3 by 1).

Having calculated the aerodynamic forces in three directions of all the plates, they can be summed and used to calculate the torques around all three axis, using the equation D.7

$$\begin{bmatrix} Ta_x \\ Ta_y \\ Ta_z \end{bmatrix} = \begin{bmatrix} 0 & Ca_z - Cg_z & Ca_y - Cg_y \\ -(Ca_z - Cg_z) & 0 & -(Ca_x - Cg_x) \\ -(Cg_y - Cg_y) & -(Ca_x - Cg_x) & 0 \end{bmatrix} \begin{bmatrix} Fa_{x_{total}} \\ Fa_{y_{total}} \\ Fa_{z_{total}} \end{bmatrix} \tag{D.7}$$

A similar approach can be used for the solar radiation pressure, but it is important to note that it is assumed that the solar radiation pressure only causes a torque in the y-direction of the satellite. The disturbance torques are added up around each of the body axis.

D.3 Spacecraft dynamics

The spacecraft dynamics that are used are for a nadir pointing satellite, in which it is assumed that the cross-moments of inertia are negligible and that the attitude deviations are small. This results in the following set of differential equations.

$$\begin{bmatrix} I_{xx}\ddot{\theta_x} \\ I_{yy}\ddot{\theta_y} \\ I_{zz}\ddot{\theta_z} \end{bmatrix} = \begin{bmatrix} 0 & 0 & \omega_0(I_{zz}-I_{yy}) \\ 0 & 0 & 0 \\ \omega_0(I_{yy}-I_{zz}) & 0 & 0 \end{bmatrix} \begin{bmatrix} \dot{\theta_x} \\ \dot{\theta_y} \\ \dot{\theta_z} \end{bmatrix} + \begin{bmatrix} T_{x_disturbance} \\ T_{y_disturbance} \\ T_{z_disturbance} \end{bmatrix} - \begin{bmatrix} T_{x_control} \\ T_{y_control} \\ T_{z_control} \end{bmatrix} \tag{D.8}$$

In this equation $\ddot{\theta}$ are angular acceleration in rad/s^2 and $\dot{\theta}$ the angular velocity in rad/s. ω_0 is the mean motion of the spacecraft, the constant angular velocity the satellite has in orbit, in rad/s.

D.4 Control Torque of reaction wheel

In equation D.8, it can be seen that the angular acceleration of the satellite depends on the control torque of the actuators. In the simulation this control torque is simulated by the use of PD-control. This means that the control torque depends on the attitude and the angular velocity that is measured by the sensors. The simulation doesn't take sensor inaccuracies into account. The control torque now can be expressed by equation D.9.

$$\begin{bmatrix} T_{x_control} \\ T_{y_control} \\ T_{z_control} \end{bmatrix} = \begin{bmatrix} K_{p_x} & 0 & 0 \\ 0 & K_{p_y} & 0 \\ 0 & 0 & K_{p_z} \end{bmatrix} \begin{bmatrix} \theta_x \\ \theta_y \\ \theta_z \end{bmatrix} + \begin{bmatrix} K_{d_x} & 0 & 0 \\ 0 & K_{d_y} & 0 \\ 0 & 0 & K_{d_z} \end{bmatrix} \begin{bmatrix} \dot{\theta_x} \\ \dot{\theta_y} \\ \dot{\theta_z} \end{bmatrix} \tag{D.9}$$

With the help of this equation and the moment of inertia of the flywheel the angular accelerations and velocities of the flywheel can be calculated. It is incorporated in the program that the torque the flywheel delivers can never be larger than 0.16 mNm. The program gives a warning when the flywheel is spinning at its maximum angular velocity, such that is is known that the flywheel needs to be desaturated.

D.5 algorithm of the simulation

The simulation makes use of a very large 'for' loop. This loop runs from time instance zero to a desired ending time, with steps that can be predefined. It must be noted that if the time-steps or the desired simulation time is too small/large respectively, Matlab takes a very long time to do the calculations. A time-step of 1 s and an ending time of 5500 s (which is approximately equal to one orbital period) is recommended.

Within the loop the calculations for disturbance torques, control torques and accelerations, velocities and attitude are done. The disturbance torques are calculated for each time instance based on the calculated attitude of the former loop iteration. The same accounts for the control torque. At the end of an iteration all the torques are summed and with the help of the S/C dynamic equations the resulting acceleration is calculated.

With the help of the initial inputs for angular velocity, the angular velocity at any iteration can be calculated. If the subscript i expresses the current loop, the angular velocity in loop i can be expressed by equation D.10.

$$\dot{\theta}_{i+1} = \ddot{\theta}_{i+1} * dt + \dot{\theta}_i \tag{D.10}$$

In which $\ddot{\theta}_{i+1}$ is the angular velocity that was calculated with the help of S/C dynamics and dt is the time-step of the iteration.

After a similar equation is used for the calculation of the attitude, the loop starts over again. The loop starts with the expression $i = i + 1$, such that the calculations of the disturbance torques are based on the attitudes that were calculated in the former loop.

D.6 Outputs of the program

The program has several outputs. The main outputs of the simulation are the displacement angles, angular velocities and angular acceleration of the satellites. Graphs of these values are plotted versus the simulated time period and are shown together in one figure.

The second outputs of the program are the torques acting on the satellite: the disturbance torques and the control torques. These torques are plotted against simulated time period and are shown together in one figure.

The third output of the simulation are the control characteristics: the angular acceleration and the angular velocity of the flywheel. These graphs are, again, plotted against the simulated time period and are shown together in one figure.

Chapter E | Satellite mass budget

RCC Mass Budget							
Subsystem	**Amount**	**Unit Mass (g)**	**Current best estimate (g)**	**Contigency**	**Allocated mass (g)**	**% total mass**
ADCS			623,30	0,30	810,29	14,53
reaction wheels	3	57,00	171,00	0,30	222,30	3,99
3-axis magnetotorquer assembly	1	130,00	130,00	0,30	169,00	3,03
PCB and support	1	150,00	150,00	0,30	195,00	3,50
3-axis magnetometer assembly	1	15,00	15,00	0,30	19,50	0,35
faulhaber motor	3	1,10	3,30	0,30	4,29	0,08
3-axis MEMS gyro	1	10,00	10,00	0,30	13,00	0,23
Star tracker STELLA	1	120,00	120,00	0,30	156,00	2,80
3-axis linear accelerometer	1	24,00	24,00	0,30	31,20	0,56
Data Handling			497,00	0,00	497,00	8,91
S-band patch antenna	1	60,00	60,00	0,00	60,00	1,08
Telemetry antenna	1	100,00	100,00	0,00	100,00	1,79
Transceiver	1	85,00	85,00	0,00	85,00	1,52
S-band transmitter	1	200,00	200,00	0,00	200,00	3,59
Data storage	1	2,00	2,00	0,00	2,00	0,04
OnBoard Computer	1	50,00	50,00	0,00	50,00	0,90
EPS - Electrical power system			640,00	0,08	707,00	12,68
Solar Panels	3	100,00	300,00	0,20	360,00	6,46
Battery	2	100,00	200,00	0,00	200,00	3,59
Circuitboard	1	140,00	140,00	0,05	147,00	2,64
Mechanical System			100,00	0,15	115,00	2,06
Solar panel deployment hinges	2	50,00	100,00	0,15	115,00	2,06
Payload			1650,00	0,20	1980,00	35,51
ANT-2 TMA	0	1650,00	0,00	0,20	0,00	0,00
ANT-2 RCC	1	1650,00	1650,00	0,20	1980,00	35,51
Structural Subsystem			780,00	0,05	819,00	14,69
2U CubeSat structure	2	390,00	780,00	0,05	819,00	14,69
Thermal Control			40,00	0,50	60,00	1,08
Thermal tape	1	40,00	40,00	0,50	60,00	1,08
Cables			90,00	0,15	103,50	1,86
Connectors	18	5,00	90,00	0,15	103,50	1,86
Propulsion system			363,00	0,29	484,50	8,69
ES Microthruster system	1	200,00	200,00	0,20	240,00	4,30
Propellant Mass	1	163,00	163,00	0,50	244,50	4,38
Total Unit Mass (g)		**0,00**	**4783,30**	**0,17**	**5576,29**	**100,00**
Total RCC mass (kg)	**N. Sats**	**24,00**	**114,80**		**133,83**	

Figure E.1: ANT-2 RCC Mass budget

TMA Mass Budget						
Subsystem	**Amount**	**Unit Mass (g)**	**Current best estimate (g)**	**Contigency**	**Allocated mass (g)**	**% total mass**
ADCS			623,30	0,30	810,29	14,86
reaction wheels	3	57,00	171,00	0,30	222,30	4,08
3-axis magnetotorquer assembly	1	130,00	130,00	0,30	169,00	3,10
ADCS PCB	1	150,00	150,00	0,30	195,00	3,58
3-axis magnetometer assembly	1	15,00	15,00	0,30	19,50	0,36
faulhaber motor	3	1,10	3,30	0,30	4,29	0,08
3-axis MEMS gyro	1	10,00	10,00	0,30	13,00	0,24
Star tracker STELLA	1	120,00	120,00	0,30	156,00	2,86
3-axis linear accelerometer	1	24,00	24,00	0,30	31,20	0,57
Data Handling			447,00	0,00	447,00	8,20
S-band patch antenna	1	60,00	60,00	0,00	60,00	1,10
Telemetry antenna	1	100,00	100,00	0,00	100,00	1,83
Transceiver	1	85,00	85,00	0,00	85,00	1,56
S-band transmitter	1	200,00	200,00	0,00	200,00	3,67
Data storage	1	2,00	2,00	0,00	2,00	0,04
EPS - Electrical power system			640,00	0,08	707,00	12,97
Solar Panels	3	100,00	300,00	0,20	360,00	6,60
Battery	2	100,00	200,00	0,00	200,00	3,67
Circuitboard	1	140,00	140,00	0,05	147,00	2,70
Mechanical System			100,00	0,15	115,00	2,11
Solar panel deployment hinges	2	50,00	100,00	0,15	115,00	2,11
Payload			1650,00	0,20	1980,00	36,32
ANT-2 TMA	1	1650,00	1650,00	0,20	1980,00	36,32
ANT-2 RCC	0	1650,00	0,00	0,20	0,00	0,00
Structural Subsystem			780,00	0,05	819,00	15,02
2U CubeSat structure	2	390,00	780,00	0,05	819,00	15,02
Thermal Control			40,00	0,50	60,00	1,10
Thermal tape	1	40,00	40,00	0,50	60,00	1,10
Cables			90,00	0,15	103,50	1,90
Connectors	18	5,00	90,00	0,15	103,50	1,90
Propulsion system			280,00	0,29	360,00	6,60
ES Microthruster system	1	200,00	200,00	0,20	240,00	4,40
Propellant Mass	1	80,00	80,00	0,50	120,00	2,20
Total Unit Mass (g)		**0,00**	**4700,30**	**0,16**	**5451,79**	**100,00**
Constellation mass (kg)	**N. Sats**	**27,00**	**126,91**		**147,20**	

Figure E.2: ANT-2 MA Mass budget

ARCTIC Mass Budget						
Subsystem	**Amount**	**Unit Mass (g)**	**Current best estimate (g)**	**Contigency**	**Allocated mass (g)**	**% total mass**
ADCS			623,30	0,30	810,29	13,85
reaction wheels	3	57,00	171,00	0,30	222,30	3,80
3-axis magnetotorquer assembly	1	130,00	130,00	0,30	169,00	2,89
ADCS PCB	1	150,00	150,00	0,30	195,00	3,33
3-axis magnetometer assembly	1	15,00	15,00	0,30	19,50	0,33
faulhaber motor	3	1,10	3,30	0,30	4,29	0,07
3-axis MEMS gyro	1	10,00	10,00	0,30	13,00	0,22
Star tracker STELLA	1	120,00	120,00	0,30	156,00	2,67
3-axis linear accelerometer	1	24,00	24,00	0,30	31,20	0,53
Data Handling			447,00	0,00	447,00	7,64
S-band patch antenna	1	60,00	60,00	0,00	60,00	1,03
Telemetry antenna	1	100,00	100,00	0,00	100,00	1,71
Transceiver	1	85,00	85,00	0,00	85,00	1,45
S-band transmitter	1	200,00	200,00	0,00	200,00	3,42
Data storage	1	2,00	2,00	0,00	2,00	0,03
EPS - Electrical power system			940,00	0,07	1060,00	18,12
Solar Panels	3	200,00	600,00	0,20	720,00	12,31
Battery	2	100,00	200,00	0,00	200,00	3,42
Circuitboard	1	140,00	140,00	0,00	140,00	2,39
Mechanical System			150,00	0,20	180,00	3,08
Solar panel deployment hinges	3	50,00	150,00	0,20	180,00	3,08
Payload			1664,00	0,20	1664,00	28,45
ANT-2 TMA	0	1650,00	0,00	0,20	0,00	0,00
ANT-2 RCC	0	1650,00	0,00	0,20	0,00	0,00
ARCTIC	1	1664,00	1664,00		1664,00	28,45
Structural Subsystem			780,00	0,10	858,00	14,67
2U CubeSat structure	2	390,00	780,00	0,10	858,00	14,67
Thermal Control			250,00	0,35	312,00	5,33
Thermal tape	1	40,00	40,00	0,50	60,00	1,03
Thermal umbrella	1	210,00	210,00	0,20	252,00	4,31
Cables			90,00	0,20	108,00	1,85
Connectors	18	5,00	90,00	0,20	108,00	1,85
Propulsion system			280,00	0,27	360,00	6,15
ES Microthruster system	1	200,00	200,00	0,20	240,00	4,10
Propellant Mass	1	80,00	80,00	0,50	120,00	2,05
Total Unit Mass (g)		**0,00**	**5274,30**	**0,11**	**5849,29**	**100,00**
Constellation mass (kg)	**N. Sats**	**37,00**	**195,15**		**216,42**	

Figure E.3: ANT-2 ARCTIC Mass budget

Chapter F | RCC and TMA assembly drawings

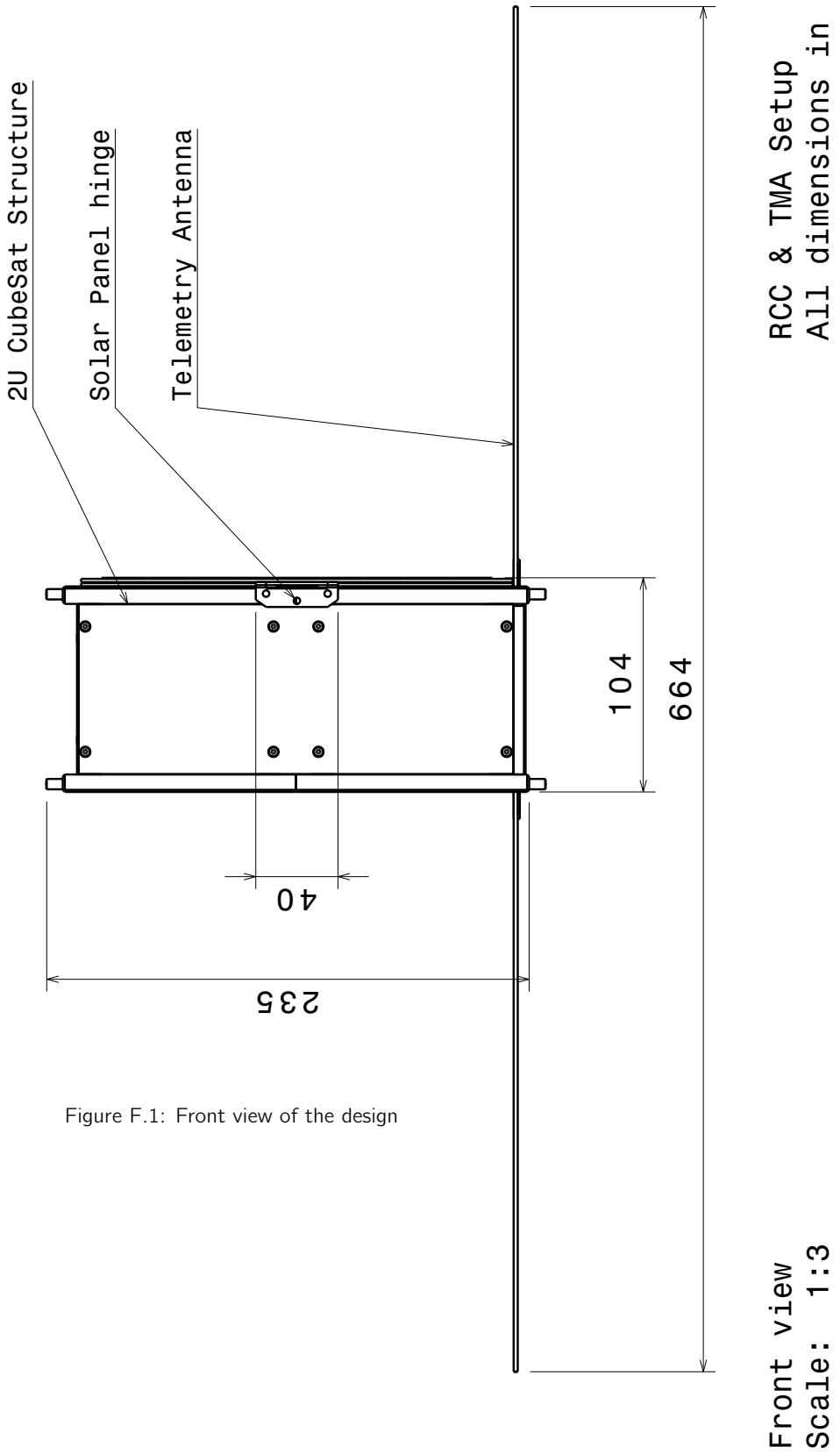

Figure F.1: Front view of the design

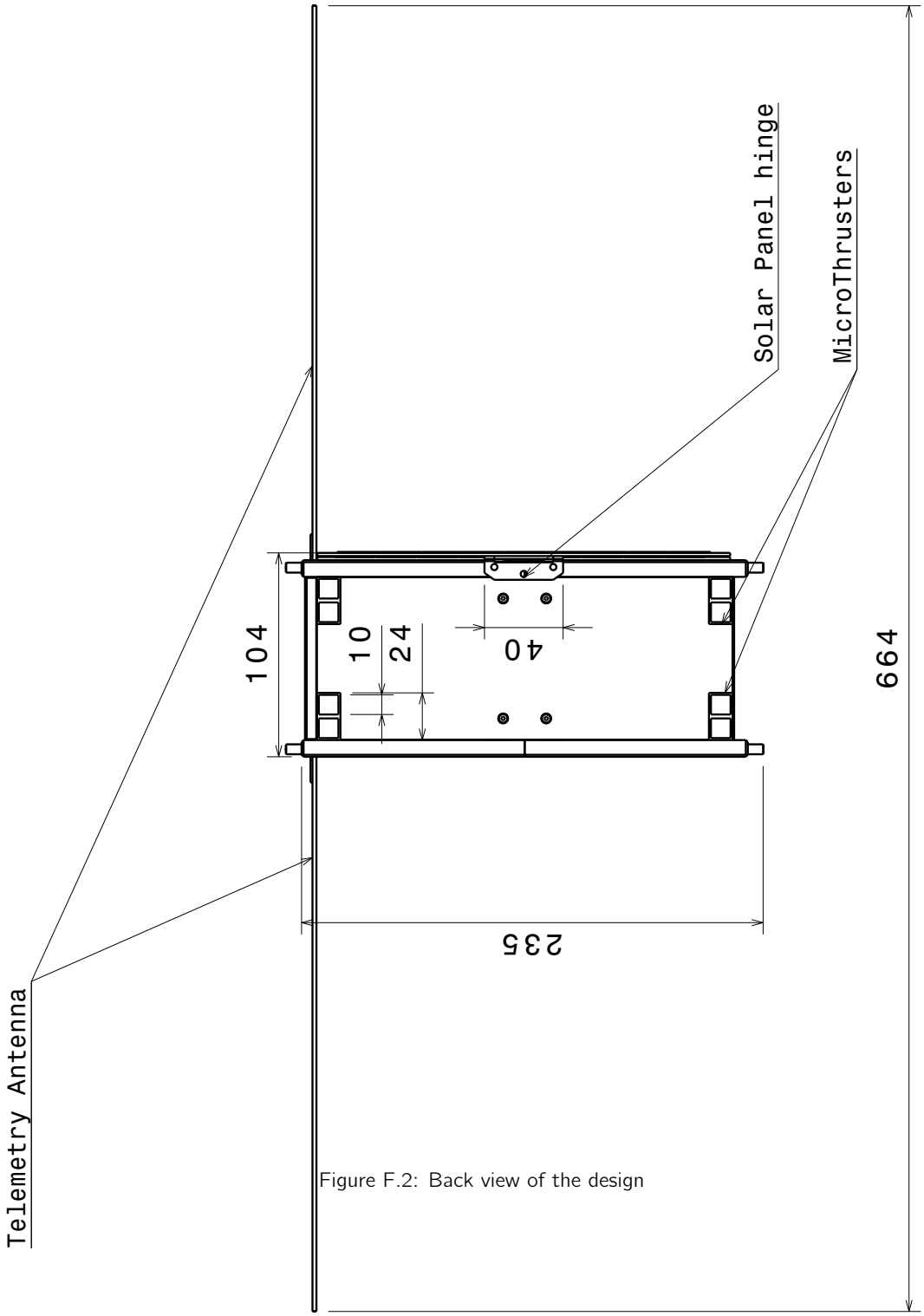

Figure F.2: Back view of the design

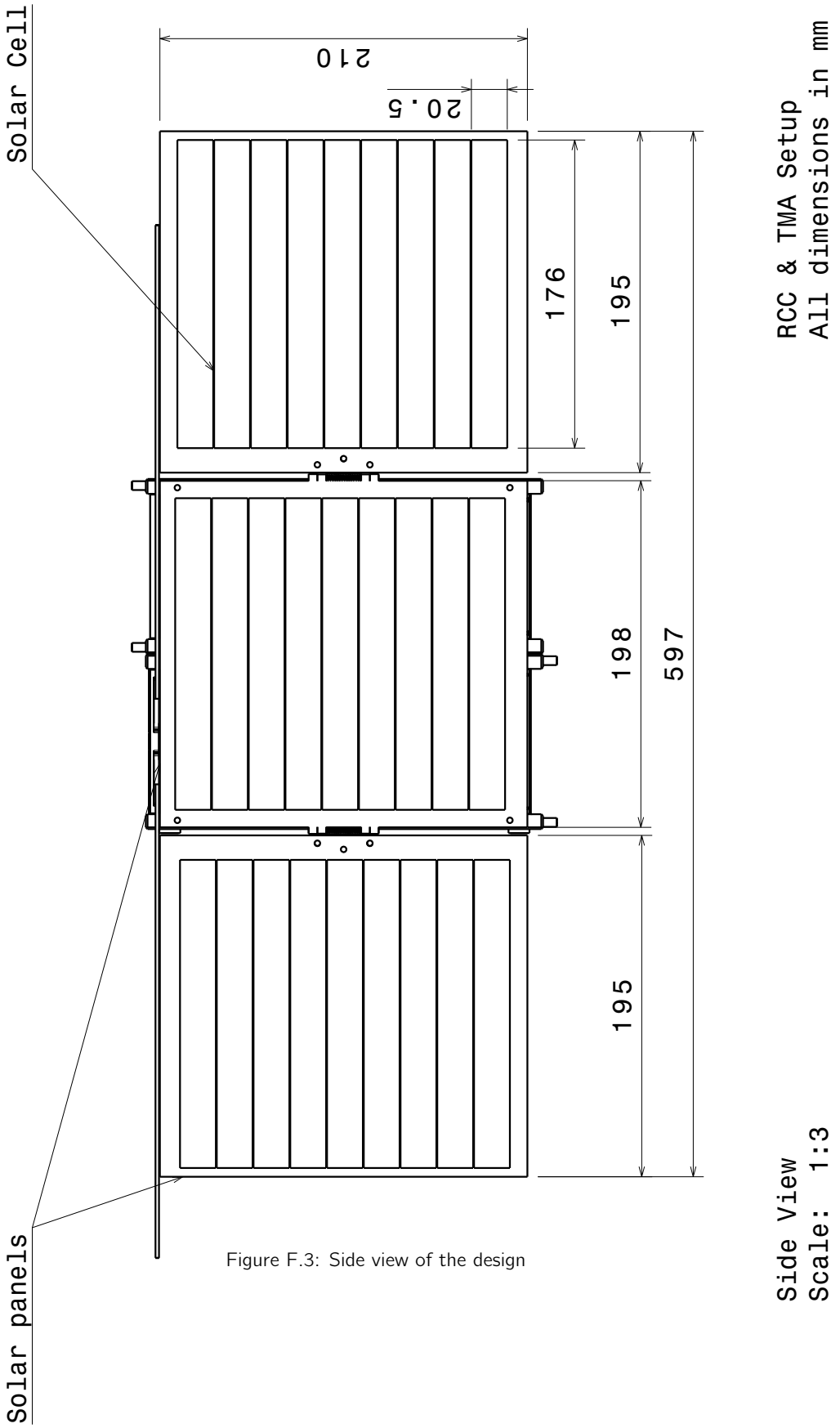

Figure F.3: Side view of the design

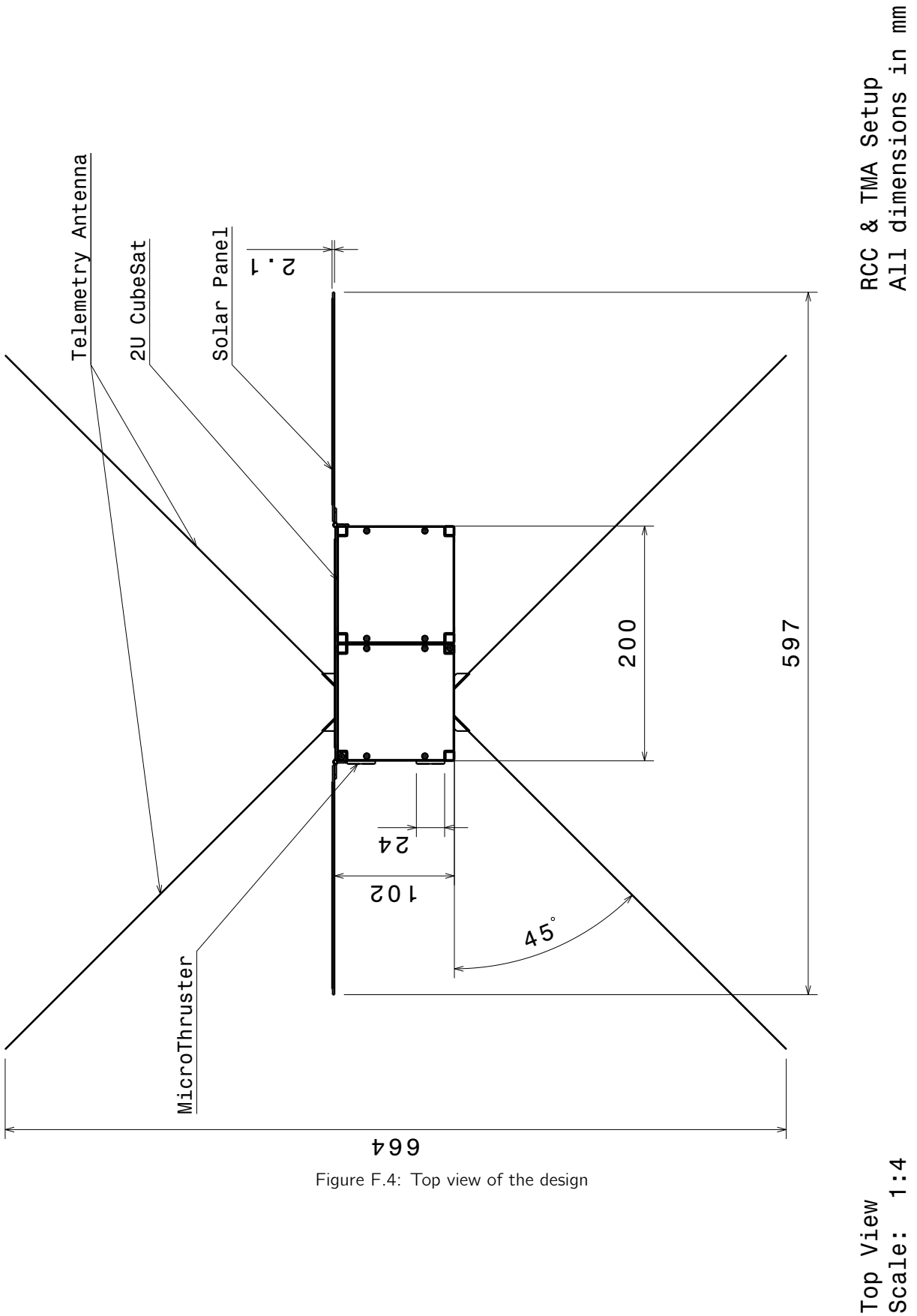

Figure F.4: Top view of the design

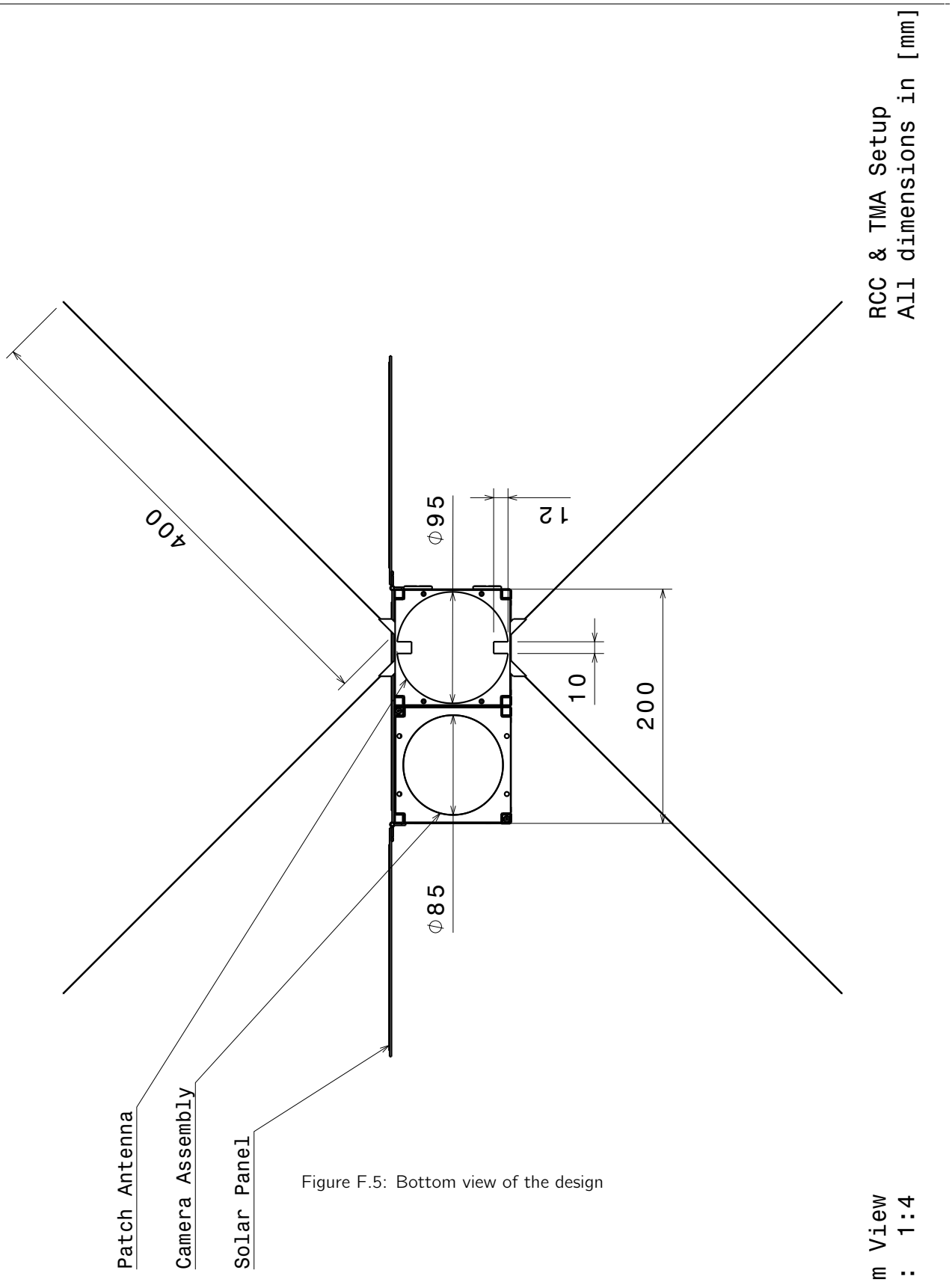

Figure F.5: Bottom view of the design